Temporal and Spatial Regulation of Rho GTPase Activity and Specificity

Inaugural-Dissertation

to obtain the academic degree

Doctor rerum naturalium

(Dr. rer. nat.)

submitted to

the Department of Biology, Chemistry and Pharmacy

of Freie Universität Berlin

by

Paul Markus Müller

from

Rottweil, Germany

2017

Paul Markus Müller:
Temporal and Spatial Regulation of Rho GTPase Activity and Specificity
Inaugural-Dissertation

Supervision:	Dr. Oliver Rocks
Institution:	Max Delbrück Center for Molecular Medicine in the Helmholtz Association, Berlin, Germany
Time period:	March 2012 to November 2017
1st Reviewer:	Dr. Oliver Rocks Spatio-temporal Control of Rho GTPase Signaling Max Delbrück Center for Molecular Medicine Berlin, Germany
2nd Reviewer:	Prof. Dr. Volker Haucke Department Molecular Pharmacology and Cell Biology Leibniz-Forschungsinstitut für Molekulare Pharmakologie Berlin, Germany
Date of defense:	March 13, 2018

Contents

List of Figures

List of Tables

List of Abbreviations

ARP2/3	Actin-related protein-2/3
BSA	Bovine serum albumin
cDNA	Complementary DNA
CRIB	Cdc42/Rac1 interactive binding
DH	Dbl-homology
DHR1	Dock-homology region-1
DHR2	Dock-homology region-2
DNA	Deoxyribonucleic acid
DOCK	Dedicator of cytokinesis
EGFR	Epidermal growth factor receptor
ELMO	Engulfment and cell motility protein
FCS	Fetal calf serum
FLAP	Fluorescence loss after photoactivation
FOV	Field of view
FRAP	Fluorescence recovery after photobleaching
FRET	Förster resonance energy transfer
FWHM	full width at half maximum
GAP	GTPase activating protein
GDI	Guanine nucleotide dissociation inhibitor
GDP	Guanosine diphosphate
GEF	Guanine nucleotide exchange factor
GPCR	G protein-coupled receptor
GPI	Glycosylphosphatidylinositol
GTP	Guanosine triphosphate
GTPase	Guanine nucleotide-binding protein
HVR	Hypervariable region
IAC	Integrin-based adhesion complex
LIMK	LIM kinase
mDia	Mammalian diaphanous protein
mEGFP	monomeric enhanced green fluorescent protein
miRFP670	monomeric infrared fluorescent protein 670
MLC	Myosin light chain

mPAGFP ..... monomeric photoactivatable green fluorescent protein
PAK ..... p21-activated kinase
PBD ..... p21-binding domain
PBR ..... Polybasic region
PCR ..... Polymerase chain reaction
PH ..... Pleckstrin-homology
PI(3)K ..... Phosphatidylinositol-(4,5)-bisphosphate 3-kinase
$PI(3,4,5)P_3$ ..... Phosphatidylinositol-(3,4,5)-trisphosphate
$PI(4,5)P_2$ ..... Phosphatidylinositol-(4,5)-bisphosphate
PKA ..... Protein kinase A
PKN1 ..... Serine/threonine protein kinase N1
RBD ..... Rho binding domain
RhoGAP ..... Rho GTPase activating protein
RhoGDI ..... Rho guanine nucleotide dissociation inhibitor
RhoGEF ..... Rho guanine nucleotide exchange factor
ROCK ..... Rho kinase
ROI ..... Region of interest
ROS ..... Reactive oxygen species
RTK ..... Receptor tyrosine kinase
SDS ..... Sodium dodecyl sulfate
SH2 ..... Src-homology 2
SH3 ..... Src-homology 3
shRNA ..... Short hairpin ribonucleic acid
SNR ..... Signal-to-noise ratio
SPT ..... Single particle tracking
TIRF ..... Total internal reflection fluorescence
TMD ..... Transmembrane domain
TMR ..... Tetramethylrhodamine
WASP ..... Wiskott-Aldrich syndrome protein
WAVE ..... WASP-family verprolin-homologous

1 Abstract

Rho GTPases are central signalling nodes in pathways that regulate cytoskeletal dynamics and control complex cellular functions such as cell adhesion, cell migration, and cell division. Rho GTPases are molecular switches: They exist in an active GTP-bound state and an inactive GDP-bound state. The transition between these states relies on the activating Rho guanine nucleotide exchange factors (RhoGEFs) and the inactivating Rho GTPase activating proteins (RhoGAPs). The number of signalling pathways up- and downstream of Rho GTPases is multitudinous and so is the large number of GAPs and GEFs, reflecting the diversity of physiological processes that involve Rho GTPase signalling. The human genome encodes as many as 150 of these regulatory proteins. Rho guanine nucleotide dissociation inhibitors (RhoGDIs) add an additional layer of regulation to the localisation and activity of Rho GTPases. They bind to and stabilise Rho GTPases and thus create a soluble cytosolic pool of inactive Rho proteins.

Understanding the substrate specificity of the RhoGEFs and RhoGAPs is important in order to link them to their downstream signalling pathways. However, this has never been investigated in a systematic manner and is yet unknown for many GAPs and GEFs. I employed a previously assembled complete expression library of all full length RhoGEFs and RhoGAPs to systematically describe their activity towards any of the three paradigm Rho GTPases RhoA, Rac1 and Cdc42. For this purpose, I established a novel automated microscopic live cell RhoGEF and RhoGAP assay, based on second generation FRET biosensors for RhoA, Rac1, and Cdc42. The sensitivity of the assay was significantly enhanced by the modulation of cellular RhoGDI levels. I could show that the assay is very robust and suited to visualize subtle activity changes within living cells. I found that RhoGEFs have mostly exclusive activity, whereas RhoGAPs can have both exclusive and promiscuous activity. Furthermore, by applying semiquantitative image analysis I could demonstrate that autoinhibition is a common mechanism by which RhoGEFs and RhoGAPs are regulated in cells.

I furthermore performed a family-wide analysis of RhoGEF and RhoGAP localisation at focal adhesions and identified as many as 37 of them residing at these structures. Subsequent correlation of their substrate specificity suggests a key role of Rac1 in the regulation focal adhesion dynamics.

Along with activity, also the membrane association of Rho GTPases is tightly regulated. However, RhoGDI-mediated shuttling between membranes and rapid diffusion of Rho GTPases within membranes intuitively counteract spatially confined Rho signals and how Rho activity is locally initiated, maintained and terminated is not known. I analysed features that control the subcellular localisation of Rho GTPases and established the dynamic nature of Rho GTPase membrane residence. I could demonstrate that this dynamic membrane interaction is not primarily caused by RhoGDI but rather due to rapid lateral diffusion. In order to more precisely decipher the spatio-temporal signalling framework of Rho GTPases at the plasma membrane, I advanced the establishment of a single molecule tracking approach for Rho proteins. This assay can be used in future work to systematically investigate factors that regulate the spatial concentration of Rho GTPase activity.

Altogether, my study provides a systemic framework to place the Rho GTPases RhoA, Rac1, and Cdc42 into the complex network of up- and downstream signalling pathways and thus a basis for a better understanding of the spatio-temporal regulation of Rho GTPase signalling.

Zusammenfassung

Rho GTPasen sind zentrale Signalproteine in einem komplexen und weitreichenden Netzwerk intrazellulärer Signalwege, welche durch Organisation und Umbau des Zytoskeletts unter anderem Zellmigration, Zelladhäsion und Zellteilung kontrollieren. Als molekulare Schalter können Rho-Proteine einen aktiven GTP-gebundenen und einen inaktiven GDP-gebundenen Zustand einnehmen. Die Aktivierung der Rho GTPasen erfolgt durch GTP-Austauschfaktoren (GEFs), die Inaktivierung durch GTPase-aktivierende Proteine (GAPs). Entsprechend der Vielzahl der Signalwege, die durch Rho GTPasen kontrolliert werden, sind auch die regulatorischen RhoGEFs und RhoGAPs zahlreich, was die Komplexität der physiologischen Prozesse wider spiegelt, die durch Rho-Proteine reguliert werden. Das humane Genom enthält 150 dieser Rho-Regulatorproteine. Zusätzlich werden Rho GTPasen durch Guaninnukleotid-Dissoziations-Inhibitoren (RhoGDIs) reguliert. Diese binden an die posttranslationale Lipidmodifikation der Rho GTPasen und versetzen diese dadurch in einen löslichen Zustand, wodurch ein inaktiver zytosolischer Fundus an Rho GTPasen geschaffen wird.

Das Verständnis um die Substratspezifität von RhoGEFs und RhoGAPs ist unerlässlich, um diese in nachfolgende Signalwege einordnen zu können. Die Substratspezifität wurde jedoch noch nie umfassend und systematisch untersucht und ist für viele der RhoGEFs und RhoGAPs gänzlich unbekannt. Ich habe auf der Grundlage einer zuvor generierten Expressionsbibliothek systematisch die Aktivität aller RhoGEFs und RhoGAPs gegenüber jeder der drei wichtigen Rho GTPasen RhoA, Rac1 und Cdc42 untersucht. Zu diesem Zweck habe ich mithilfe der neuesten FRET Biosensoren für RhoA, Rac1 und Cdc42 eine neue, automatisierbare und auf Mikroskopie basierende Methode entwickelt. Die Sensitivität dieses Assays wurde zusätzlich, durch die gezielte Veränderung der RhoGDI Expressionslevel, signifikant gesteigert. Ich konnte darüber hinaus zeigen, dass der Assay zuverlässig selbst kleinste Aktivitätsveränderungen in lebenden Zellen wiedergeben kann. Dadurch konnte ich feststellen, dass RhoGEFs größtenteils Aktivität gegenüber einzelnen Rho GTPasen haben, wohingegen RhoGAPs sowohl Aktivität gegenüber einzelnen, als auch mehreren Rho GTPasen haben. Eine semiquantitative Analyse der Aktivitäten einiger RhoGEFs und RhoGAPs zeigte, dass die meisten dieser Regulatoren in Zellen autoinhibitorischen Regulationsmechanismen unterliegen.

Außerdem habe ich die gesamte Familie der RhoGEFs und RhoGAPs auf ihre Lokalisation an Fokalen Adhäsionen untersucht, wodurch ich 37 dieser Proteine identifiziert habe, die dort lokalisieren. Eine anschließende Korrelation mit der Substratspezifität hat ergeben, dass Rac1 vermutlich eine Schlüsselfunktion für die Regulation der Fokalen Adhäsionen hat.

Neben der Aktivität ist auch die Membranassoziation von Rho GTPasen genauestens reguliert. Der Transport von Rho GTPasen durch RhoGDI zwischen zellulären Membranen und ihre schnelle laterale Diffusion an Membranen widerspricht jedoch intuitiv einer räumlich begrenzten Anreicherung von Rho Aktivitäten. Wie daher die Signaltransduktion von Rho GTPasen lokal initiiert, aufrecht erhalten und wieder beendet wird, ist nicht bekannt. Ich habe hier Strukturelemente untersucht, die die subzelluläre Lokalisation von Rho GTPasen steuern und festgestellt, dass Rho GTPasen sehr dynamisch an Membranen binden. Ich konnte darüber hinaus zeigen, dass diese dynamische Membraninteraktion nicht primär RhoGDI geschuldet ist, sondern eher durch schnelle laterale Diffusion zustande kommt. Um die zeitliche und räumliche Kontrolle der Prozesse, die der Rho Signaltransduktion an Membranen zugrunde liegen, präzise auftrennen zu können, habe ich die Entwicklung einer Einzelmolekülmikroskopie Methode für Rho-Proteine vorangetrieben. Mit dieser Methode wird das Ziel verfolgt werden systematisch nach Faktoren zu suchen, durch welche die räumliche Anreicherung von aktiven Rho GTPasen gewährleistet werden kann.

Mit dieser Studie habe ich systembiologisch relevante Informationen erarbeitet, durch die sich die Rho GTPasen RhoA, Rac1 und Cdc42 in dem weitgefächerten und hochkomplexen Netzwerk ihrer Signalwege platzieren lassen und habe dadurch eine wichtige Grundlage zum Verständnis der zeitlichen und räumlichen Regulation der Rho Signaltransduktion gelegt.

2 Introduction

2.1 The Rho GTPase family

The Rho family of small GTPases is embedded in a complex network of signalling pathways that controls fundamental processes common to all eukaryotic cells, including morphogenesis, movement, polarity, and cell division. The number of proteins that either regulate or are regulated by direct interaction with members of the Rho GTPase family is multitudinous and comprises over one percent of the genes in the human genome. Underlying this biological complexity is a simple biochemical principle: Rho GTPases are central molecular switches integrating information from multiple input pathways and relaying them into just as many output interactions. Considering the diversity of the connected signalling network, the positioning of Rho GTPases as central signalling hubs within that network allows them to control countless information paths and their spatio-temporal translation into distinct biological responses.

2.1.1 Rho GTPase proteins - a family of small GTPases

GTPases are molecular switches whose function is based on a simple biochemical principle to control complex cellular processes. They cycle between two stable conformational states: They are turned on by binding guanosine triphosphate (GTP) and off by GTP hydrolysis to guanosine diphosphate (GDP). The active GTP-bound GTPase can bind target proteins and transduce signals until it returns to the inactive state by GTP hydrolysis. This GTP switch has evolved early in evolution and is present in all kingdoms. Regulatory G-proteins (also known as guanine nucleotide-binding proteins, hereafter referred to as GTPases) are the most prominent members of GTPase switches. They can be divided in two families: The heterotrimeric G proteins and the Ras GTPase superfamily of small GTPases. The Ras superfamily is composed of more than 150 members and consists of 5 main families, classified by their phylogenetic relationship and cellular function: Ras GTPases, Rab GTPases, Arf GTPases, Ran GTPases, and Rho GTPases (Figure 2.1). These protein families have central functional implications in cell proliferation, membrane trafficking, vesicular transport, nuclear transport, and cytoskeletal dynamics, respectively (Takai *et al.*, 2001).

The mutationally activated and transforming Ras genes were discovered as first and thus name-giving members of this superfamily in the early 1980s. Shortly after, the first human genes of the Rho family were identified in 1985 (Madaule and Axel, 1985), followed by 2 Rac genes and the Cdc42 gene (Didsbury *et al.*, 1989; Munemitsu *et al.*, 1990). This, eventually, gave rise to the identification of the 20 members of the Rho GTPase family which are known to date in humans (Wennerberg and Der, 2004; Boureux *et al.*, 2007; Heasman and Ridley, 2008). These 20 Rho proteins are functionally divided into 12 classical and 8 atypical proteins (Figure 2.1). The classical Rho GTPases are characterised by their biochemical property to act as typical molecular switches. The atypical Rho GTPases do not operate through the classical cycle of activation and inactivation but are predominantly GTP-bound. Their availability and thus activity is rather differently controlled, for example by gene expression, protein stability and phosphorylation (Chardin, 2006; Aspenström *et al.*, 2007). Furthermore, the members of the Rho GTPase family can be phylogenetically clustered into 8 subfamilies (Figure 2.1). The fact that Rho, Rac and Cdc42 are conserved in all metazoan species and ubiquitously expressed in mammals demonstrates their pivotal role among the Rho GTPases.

2.1.2 Mechanisms of Rho GTPase signalling

Rho GTPases, as all small GTPases, are usually 20-25 kDa in size. They consist of a G-domain and a C-terminal hypervariable region (HVR). The G-domain is highly conserved across all GTPases, whereas the HVR is highly variable, as the name suggests. The G-domain contains a guanine nucleotide binding site with high nano- to picomolar affinity for GDP and GTP and two small regions, called switch I and switch II of 6 and 8 amino acids in length, respectively, which undergo large conformational changes between the GDP and GTP bound states (Vetter, 2014). The HVR is 13 to 21 amino acids long in classical Rho GTPases and comprises a polybasic stretch of positively charged amino acids and a terminal CAAX motif which undergoes prenylation and further posttranslational modification. The HVR is responsible for subcellular targeting of Rho GTPases to membranes, where they exert their signalling function (posttranslational modification of Rho GTPases and its implication of Rho GTPase targeting are discussed in section 2.4.1).

As molecular switches, Rho GTPases cycle between an “active” GTP-bound and an “inactive” GDP-bound state and do not typically carry any specific enzymatic or catalytic activity. Although GTP hydrolysis is the only catalytic activity of Rho GTPases, the actual reaction rate is in fact very slow (Zhang *et al.*, 1998). For that reason, the transi-

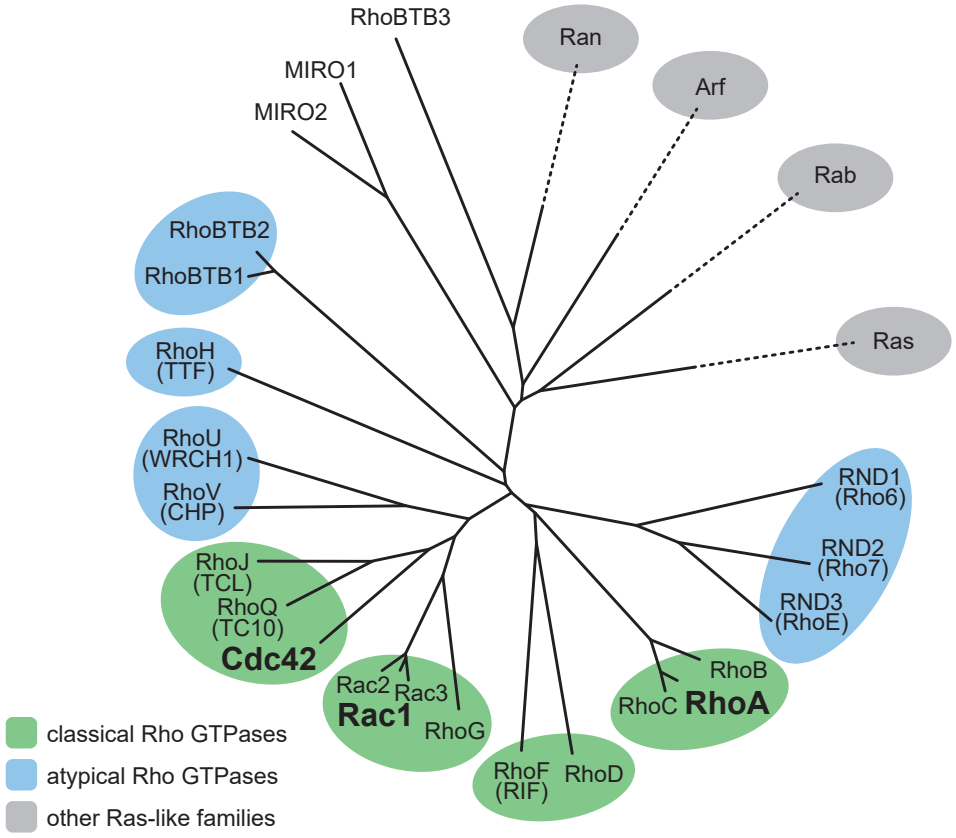

Figure 2.1 Phylogenetic structure of the human Rho GTPase family. An unrooted phylogenetic tree of Rho GTPases and other Ras-like subfamilies (highlighted in grey) based on alignments of the G-domains. The Rho family can be divided into 8 subfamilies. The classical Rho subfamilies (highlighted in green) comprise the 4 subfamilies: Rho, Rac, Cdc42, and RhoD/RhoF with the pivotal GTPases RhoA, Rac1 and Cdc42 (highlighted in bold). The atypical Rho subfamilies (highlighted in blue) include the subfamilies of RND, RhoBTB, RhoU and RhoV and RhoH. MIRO proteins rather constitute a distinct Ras superfamily than a Rho subfamily. RhoBTB3 is branched outside the Rho family. Different common names are figured into brackets under the Uniprot nomenclature. The dashed lines do not represent the real genetic distance of the Ras subfamilies Ras, Rab, Arf and Ran. Figure modified from Boureux *et al.* (2007).

tion between the GTP- and GDP-bound states requires the activity of guanine nucleotide exchange factors (GEFs) and GTPase-activating proteins (GAPs). GEFs induce the exchange of GDP for GTP and thus activate the GTPase, GAPs stimulate the hydrolysis reaction of GTP to GDP, which leads to inactivation of the GTPase (Figure 2.2) (the biochemical mechanism of the reactions catalysed by GEFs and GAPs is discussed in the sections 2.2.2 and 2.2.4). Upon activation, the Rho GTPase undergoes a conformational change allowing it to transduce signals to downstream effector proteins. The switch I and switch II regions of GTPases are the responsible structural features that allow the effector proteins to bind to active GTPases. The conformation of these regions differs strongly between GTP- and GDP-loaded state of the GTPase and is also described as loaded spring mechanism. In the GDP-bound conformation the flexibility of the switch I and II regions is high and the spring is released. Upon GTP binding, and thus activation of the GTPase, the γ-phosphate binds to and stabilises the switch I and II region in a closed loaded spring conformation. This mechanism is conserved in all small GTPases (Vetter and Wittinghofer, 2001). Thus, the switch regions are the unique structural feature that encodes the GTPase activity state. Consequently, this implicates that essentially all interfaces between GTPases and their interactors such as effector proteins, RhoGEFs, and RhoGAPs involve at least in part the switch I and switch II regions (Vetter and Wittinghofer, 2001).

A third class of proteins, the guanine nucleotide dissociation inhibitors (GDIs), account for an additional layer of regulation to Rho GTPase signalling. RhoGDIs engulf the prenyl moiety of Rho GTPases and solubilise the otherwise membrane targeted Rho GTPases in the cytosol. RhoGDIs thus serve as negative regulators of Rho GTPase activity, by withdrawing them from the signalling competent pool of Rho GTPases at membranes (Figure 2.2)(the mechanisms of regulation of Rho GTPase activity by RhoGDIs is described in detail in section 2.2.6).

2.1.3 Functional implications of Rho GTPase signalling

Rho GTPases are central signalling nodes in pathways that regulate cytoskeletal and cell adhesion dynamics. The members of the Rho GTPase family are assigned individual roles in this signalling network with specific morphogenic output. The direct effect of Rho GTPase activity on actin-mediated cellular morphogenesis was shown for the first time by Anne Ridley and Allan Hall in two seminal back-to-back publications (Ridley and Hall, 1992; Ridley *et al.*, 1992). In this work, the authors could show that the morphogenic effects of RhoA differ from those of Rac1. When microinjected into starved Swiss 3T3 cells RhoA induced the formation of stress fibers and focal adhesions, whereas Rac1 induced membrane ruffling and the formation of lamellipodia. Furthermore, they could

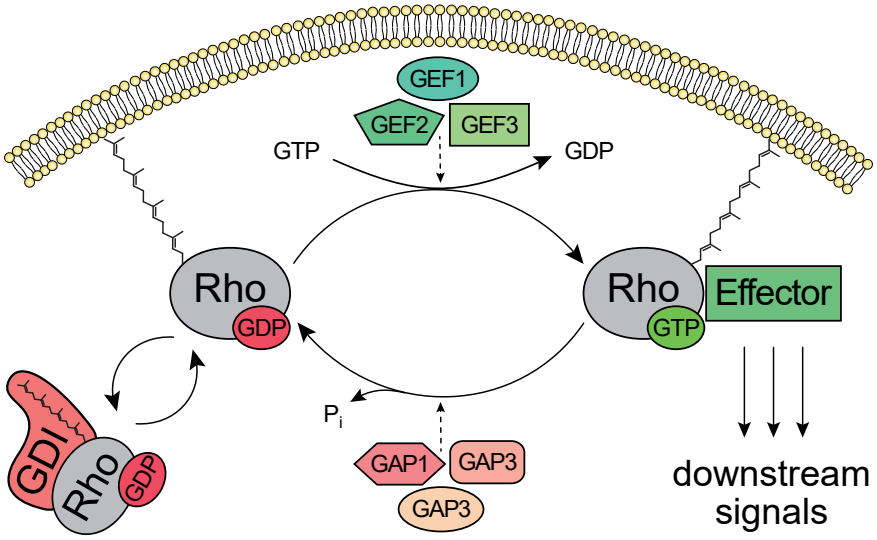

Figure 2.2 Rho GTPase GDP-GTP cycle and GDI-mediated membrane targeting-desorption cycle. Rho GTPases are molecular switches. The classical Rho GTPases cycle between an active GTP-bound and an active GDP-bound state. The transition between these states is regulated by GEF and GAP proteins. Active Rho GTPases transduce signals through effector proteins at the plasma membrane. GDIs extract Rho GTPases from the membrane and sequester them in an inactive cytosolic complex.

show that RhoA and Rac1 are essential components in the signal transduction of growth factor-induced morphogenic events. Shortly after, also Cdc42 was assigned an individual role the regulation of cellular morphogenesis, by showing that it promotes the formation of filopodia (Nobes and Hall, 1995; Kozma *et al.*, 1995). Together, these studies laid the foundation for the understanding of how Rho GTPases drive cellular morphogenic events on the example of cell migration. An early model of cell migration is based on broad gradients of Rho GTPase activity along the front-rear axis throughout the cell (Wehrle-Haller and Imhof, 2003). At the cell front high activities of Rac1 and Cdc42 induce actin polymerisation, pushing the cell front forward by formation of lamellipodia and filopodia. At the same time, high RhoA activity in the rear of the cell increases actin-myosin contractility and thus causes retraction of the cell tail (Etienne-Manneville and Hall, 2002).

Today, Rho GTPases have been implicated in the control of virtually all cellular processes that are driven by cytoskeletal dynamics such as cell polarity, cell-cell and cell-substrate adhesion, vesicle trafficking, endo- and exocytosis, as well as cytokinesis (Jaffe and Hall, 2005). In this way, they regulate physiological processes such as collective cell migration, chemotaxis, axon guidance, neuronal development, and also gene expression (Heasman and Ridley, 2008). Deregulation of Rho GTPase signalling is associated with

various kinds of diseases and developmental abnormalities and contributes to malignant transformation, neurological defects, and immunological diseases (Vega and Ridley, 2008; Pai *et al.*, 2010; DeGeer and Lamarche-Vane, 2013; Stankiewicz and Linseman, 2014).

The downstream signalling pathways of Rho GTPases show a remarkable complexity, only for RhoA, Rac1 and Cdc42 over 100 effector proteins have been identified, many of which are directly or indirectly involved in actin organisation (Etienne-Manneville and Hall, 2002; Dvorsky and Ahmadian, 2004). For example, Cdc42 drives actin polymerisation in filopodia through the Wiskott-Aldrich syndrome protein (WASP or N-WASP), which activates the actin-related protein-2/3 (ARP2/3) complex (Jaffe and Hall, 2005). ARP2/3 acts as an actin nucleator and actin branching factor. Cdc42 and Rac1 can both activate the serine-threonine p21-activated kinases (PAK), which then promote actin turnover and polymerisation via LIM kinase (LIMK) and inhibition of the actin regulator cofilin (Spiering and Hodgson, 2011). Moreover, Rac1 drives actin polymerisation in lamellipodia through WASP-family verprolin-homologous (WAVE) proteins and ARP2/3 (Campellone and Welch, 2010). Rho kinases (ROCK) are key effectors of RhoA and have multiple substrates. ROCK inhibits myosin light chain (MLC) phosphatase, which results in increased phosphorylation of MLC, promoting actin filament cross-linking activity of myosin and eventually release of contractile forces of stress fibers (Bishop and Hall, 2000). Furthermore, like Rac1 and Cdc42, also RhoA inhibits cofilin, through ROCK and LIMK, stabilising actin-myosin filaments. Importantly, proteins of the mammalian diaphanous protein family (mDia) formins are effector proteins of all tree Rho GTPases, RhoA, Rac1, and Cdc42 and drive unbranched actin polymerisation (Lammers *et al.*, 2008).

Many of the functions of RhoA, Rac1, and Cdc42 are mediated through overlapping effector pathways. Still, individual members of the Rho GTPase family have distinct cytoskeletal phenotypes, which suggests that their activity requires precise regulation by RhoGEFs and RhoGAPs in space and time, in order to translate their activity into specific morphogenic events.

2.2 Regulators of Rho GTPase activity

2.2.1 The Dbl-homology and DOCK families of RhoGEFs

RhoGEFs are activators of Rho GTPase signalling. They activate Rho GTPases by stimulating the release of GDP to allow binding of GTP. In metazoans two classes of RhoGEFs exist: The Dbl family RhoGEFs and the DOCK family RhoGEFs. RhoGEFs of the Dbl family share a catalytic Dbl-homology (DH) domain of approximately 200-residues, fol-

lowed in almost all cases by an adjacent regulatory pleckstrin-homology (PH) domain (Figure 2.3). The function of the regulatory PH domain is multitudinous and includes autoinhibition, participation in the GTPase-binding interface and assistance in GDP-GTP exchange reaction, membrane anchorage and allosteric regulation of GEF activity by phospholipid sensation, as well as protein-protein interaction to up- and downstream binding partners (Rossman *et al.*, 2005; Cherfils and Zeghouf, 2013). In humans, about 70 DH domain containing proteins have been identified (Rossman *et al.*, 2005; Jaiswal *et al.*, 2013). Dbl family RhoGEFs have a large variety of additional functional domains which are thought to mediate cross-talk between Rho GTPases and diverse other signalling pathways. The DOCK family RhoGEFs are characterised by two highly conserved regions, the Dock-homology region-1 and -2 (DHR1 and DHR2), the latter of which is the catalytically active domain (Laurin and Côté, 2014). The DHR1 domain of DOCK1, DOCK2, and most likely other DOCK family members mediates phosphatidylinositol(3,4,5)-trisphosphate-dependent ($PI(3,4,5)P_3$) recruitment to the plasma membrane. The DOCK family of RhoGEFs comprises 11 members in humans (Cook *et al.*, 2013). Based on sequence similarity, DOCK family RhoGEFs can be further subdivided into four DOCK subfamilies A, B, C, and D (Figure 2.3).

2.2.2 Mechanism of RhoGEF-stimulated exchange reaction

GEFs accelerate the guanine nucleotide exchange reaction of small GTPases by several orders of magnitude (Vetter and Wittinghofer, 2001). RhoGEFs respond to diverse extracellular stimuli and relay this information to Rho GTPase signalling pathways by catalysing the exchange of the nucleotide within Rho GTPases. RhoGEFs first bind with low affinity to the GDP-bound GTPase and induce dissociation of GDP from this complex. This leads to the formation of a high affinity intermediate and stabilises the Rho GTPase in a nucleotide- and Mg^{2+}-free state (Cherfils and Chardin, 1999). Thereupon, GTP is preferentially loaded into Rho GTPases because its cellular concentration by far exceeds that of GDP (Cherfils and Zeghouf, 2013; Rossman *et al.*, 2005). This eventually reduces the affinity of the GEF-GTPase complex and displaces the RhoGEF, yielding the active form of the GTPase.

2.2.3 RhoGAP proteins

Up to 70 proteins containing a conserved 150-residue RhoGAP domain are predicted to be encoded in the human genome (Tcherkezian and Lamarche-Vane, 2007). Rho GTPases are inactivated by RhoGAPs which contain a unique RhoGAP catalytic domain. Similar to RhoGEFs, also RhoGAPs are highly variable multidomain proteins, suggesting that

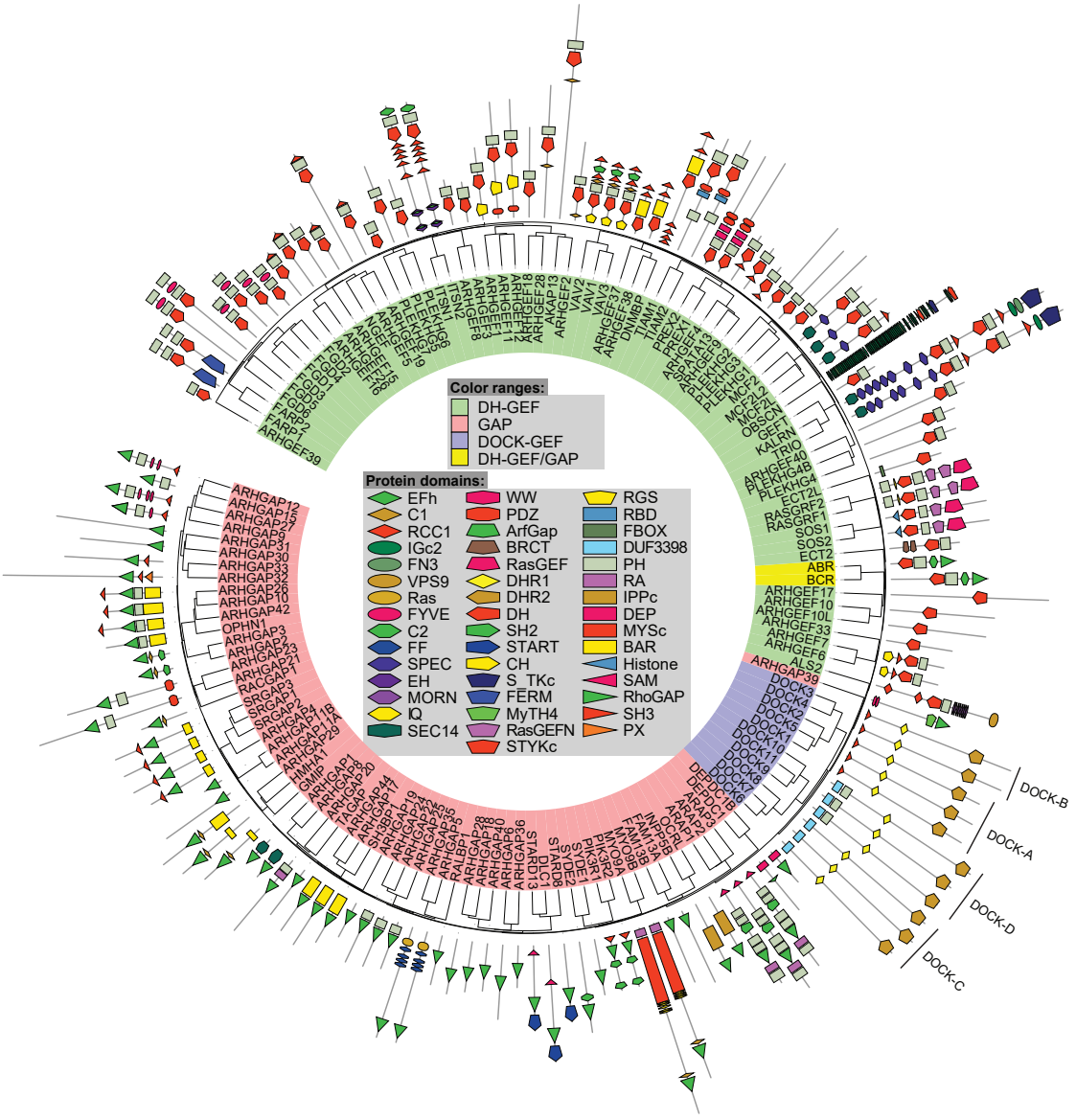

Figure 2.3 Modular domain architecture of the human RhoGEF and RhoGAP proteins. Phylogenetic tree of all human RhoGEF and RhoGAP proteins. RhoGEFs can be divided in DH-GEF family and DOCK-GEF family members. The DOCK-GEF family can be further subclassified into DOCK-A, DOCK-B, DOCK-C, and DOCK-D subfamilies. Two proteins have dual DH-GEF and GAP function. The multidomain architecture of RhoGEFs and RhoGAPs encodes information for context-specific regulation of Rho GTPase activity. Thereby they provide scaffolding and subcellular targeting information to embed Rho GTPase signalling in the variety of up- and downstream signalling pathways. Figure kindly provided by Oliver Rocks.

RhoGAPs can control biological responses via individual Rho GTPase proteins and thus contribute to the formation of context-specific Rho signals.

2.2.4 Mechanism of RhoGAP-stimulated GTP hydrolysis

Rho GTPases, as most small GTPases, have a very low intrinsic GTPase activity. This activity does not match the time scale of cellular functions. Thus, Rho GTPases require the assistance of RhoGAPs, which stimulate the GTPase activity by several orders of magnitude (Bos *et al.*, 2007). The mechanism by which RhoGAPs stimulate GTPase activity involves an arginine residue (arginine finger) that is conserved in all functional RhoGAPs. This arginine residue induces the transition state of the GTP γ-phosphate hydrolysis reaction by stabilising negative charges of the GTP β- and γ-phosphate. Furthermore, the arginine finger assists the glutamine 61 residue (Rac1 and Cdc42 numbering) in the activation of a water molecule for the nucleophilic attack to the γ-phosphate. As the affinity of RhoGAPs to active GTP-bound Rho GTPases is higher than for the GDP-bound inactive state, the GTPase is released once GTP is hydrolysed to GDP and inorganic phosphate (Cherfils and Zeghouf, 2013; Tcherkezian and Lamarche-Vane, 2007).

2.2.5 Regulation of RhoGEF and RhoGAP activity

Most if not all RhoGEFs and RhoGAPs are not constitutively active in cells, but they are specifically activated upon chemical and physical stimuli through all kinds of receptors, causing spatio-temporally controlled activation and inactivation of Rho signalling pathways (Buchsbaum, 2007). The domain architecture of both, RhoGEFs and RhoGAPs outside their catalytic domains is highly diverse and is believed to be key to regulation of their activity (Figure 2.3). However, due to the versatility of the RhoGEF and RhoGAP domain architecture, the regulation of their activity is not subject to a universal mechanism. Still, some common regulatory principles have emerged, such as autoinhibition, phosphorylation, protein-protein interaction, subcellular localisation, as well as stimulus dependent recruitment.

Several RhoGEFs and RhoGAPs have been shown to be regulated by their N- or C-terminal region. It is hypothesised that by intramolecular binding the RhoGEFs and RhoGAPs take a “closed” conformation, and thereby hinder the Rho GTPase from accessing the catalytic domain. Then, they become activated by a specific signalling cue that triggers the release of intramolecular binding, thus allowing access to the Rho GTPase. This functional mechanism can thus translate upstream signalling information in a spatially and temporally confined manner. Important examples for autoregulated RhoGEFs are MCF2 (Ron *et al.*, 1989), ITSN1 (Tsyba *et al.*, 2011), Vav1 (Yu *et al.*, 2010), SOS1

(Nimnual *et al.*, 1998), and DOCK-GEFs of the DOCK-A and DOCK-B families (Grimsley *et al.*, 2004; Lu *et al.*, 2005; Hanawa-Suetsugu *et al.*, 2012). Autoinhibition has, amongst others, also been found to regulate the activity of the chimaerin RhoGAPs CHN1 and CHN2 (Colón-González *et al.*, 2008; Canagarajah *et al.*, 2004). Furthermore, ARHGAP1 and the GRAF/oligophrenin subfamily member RhoGAPs are suggested to be regulated by autoinhibition (Cherfils and Zeghouf, 2013). The mechanisms underlying the regulation of these examples are explained in more detail in the following paragraph.

Release of autoinhibition can be mediated by protein-protein interaction, by phosphorylation, or by second messenger binding. The interaction of Engulfment and cell motility proteins (ELMO) with DOCK-GEFs is a prominent example for protein-protein interaction-mediated release of autoinhibition. In DOCK1 and DOCK2 and probably also other members of the DOCK-A and DOCK-B families, the N-terminal Src-homology 3 (SH3) domain directly binds to the catalytic DHR2 domain and thereby blocks nucleotide exchange. Binding of ELMO proteins to the SH3 domain of DOCK1 and DOCK2 have been shown to release intramolecular binding and stimulate RhoGEF activity (Lu *et al.*, 2004, 2005). Similar mechanisms of autoinhibition have been suggested for DOCK3 and DOCK4 (Grimsley *et al.*, 2004; Hiramoto *et al.*, 2006). Furthermore, ELMO2 serves as a scaffold for DOCK1 at cadherin-based cell-cell adhesions and thus combines subcellular localisation with local activation of DOCK1 (Toret *et al.*, 2014). ITSN1 and SOS1 are other examples of protein-protein interaction-mediated release of autoinhibition. For instance, Rac-GEF activity of SOS1 is unmasked by formation of a trimeric Eps8-Abi1-SOS1 complex in a p85- and PI(3,4,5)P_3-dependent manner (Innocenti *et al.*, 2003). Autoinhibition of ITSN1 by intramolecular binding of an SH3 domain to the DH domain is relieved by binding of this SH3 domain to the polyproline region of N-WASP and probably other yet unknown factors (Hussain *et al.*, 2001; Zamanian and Kelly, 2003; Pechstein *et al.*, 2010).

Autoinhibition of VAV1 is released by phosphorylation. The DH-PH tandem domain of VAV1 forms a close structure with its neighbouring SH3, an acidic region and a Zn-containing domain. Sequential phosphorylation of three tyrosine residues gradually opens up the structure, allowing access of Rho GTPases to the DH domain (Yu *et al.*, 2010).

CHN2 activation involves the binding to phospholipids and the second messenger diacylglycerol. The activity of the RhoGAP domain of CHN2 is sterically inhibited by compact folding of the RhoGAP domain, a C1 domain and a Src-homology 2 (SH2) domain and insertion of an N-terminal peptide into the active site of the RhoGAP domain. Binding of the C1 domain to phospholipids and diacylglycerol displaces the N-terminal peptide and releases the autoinhibitory effect (Canagarajah *et al.*, 2004).

Subcellular localisation is another important determinant of RhoGEF and RhoGAP activity. For example, ARHGEF25 localises to the plasma membrane by palmitoylation where it activates RhoA (Aittaleb *et al.*, 2011). Mislocalisation of ARHGEF25 to the Golgi complex or mitochondria has been shown to result in inefficient RhoA activation, whereas artificial recruitment of cytosolic ARHGAP25 to the plasma membrane has been shown to be sufficient for RhoA activation (van Unen *et al.*, 2015). Thus, plasma membrane localisation and recruitment might be a common principle of regulation of RhoGEF and RhoGAP activity. Almost all RhoGEFs and many RhoGAPs contain lipid interaction domains, such as PH domains, DHR1 domains, BAR domains, FERM domains, FYVE domains, C2 domains, or PX domains (Figure 2.3) (Bernards and Settleman, 2004; Bos *et al.*, 2007; Tcherkezian and Lamarche-Vane, 2007; Laurin and Côté, 2014). Most of these domains specifically recognise certain phospholipid species (Hamada *et al.*, 2000; Krauss and Haucke, 2007; Lemmon, 2008; Namekata *et al.*, 2014). Therefore, these domains might direct RhoGEFs and RhoGAPs to specific subdomains of the plasma membrane in response to both G protein-coupled receptor signalling (GPCR) and receptor tyrosine kinase (RTK) signalling. For example, local pools of PI(3,4,5)P_3 levels are regulated downstream of RTKs and GPCRs by class IA phosphatidylinositol-(4,5)-bisphosphate 3-kinases (PI(3)K) and downstream of GPCRs by class IB PI3Ks via heterotrimeric G protein G$\beta\gamma$ subunit (Liu *et al.*, 2009). Furthermore, phosphatidylinositol-(4,5)-bisphosphate (PI(4,5)P_2), PI(3,4,5)P_3, and other phospholipids are generally supposed not to be randomly distributed in cells, but to be organized in confined regions, called lipid rafts, that may laterally organize and control specific signalling functions (Lingwood and Simons, 2010; Wang and Richards, 2012). Additionally, BAR domains, which recognise membrane curvature, might recruit RhoGEFs and RhoGAPs to specific membrane topologies (Itoh and De Camilli, 2006; Lemmon, 2008).

Few examples are known for inhibitory interactions and modifications of RhoGEFs and RhoGAPs. DOCK6, for example, is inhibited by AKT-dependent serine-phosphorylation, and a phosphomimetic mutation of this residue showed no RhoGEF activity (Miyamoto *et al.*, 2013). Furthermore, LRCH1 has been shown to inhibit GEF activity of DOCK8 towards Cdc42 by competing with Cdc42 for interaction with DOCK8 (Xu *et al.*, 2017).

Together, the regulation of the activity of RhoGEFs and RhoGAPs by posttranslational modifications, the formation of specific protein complexes, and subcellular localisation assure precise spatio-temporally controlled activation of Rho GTPases upon distinct stimulations.

2.2.6 RhoGDIs

Besides GEFs and GAPs, Rho GTPase subfamily members associate with a third class of proteins regulating their activity: the guanine nucleotide dissociation inhibitors (GDIs). GDIs have been identified for Rho and Rab families of small GTPases, however, for Ras GTPases the GDI-like solubilising factor PDEδ has been described to be essential for correct subcellular localisation and spatial organisation (Chandra *et al.*, 2012; Schmick *et al.*, 2014).

Despite the diversity in the family of Rho proteins, there are only three genes encoding Rho GTPase-specific RhoGDIs in mammals (DerMardirossian and Bokoch, 2005). RhoGDI1 (also known as RhoGDIα) is the best-characterised RhoGDI. It is ubiquitously expressed at high levels and it interacts with most of the Rho GTPases, including RhoA, RhoC, Rac1, Rac2, and Cdc42 (Fukumoto *et al.*, 1990; Leonard *et al.*, 1992; Boulter *et al.*, 2010). RhoGDI2 (also known as RhoGDIβ) is mostly expressed in hematopoetic cells and binds Rho GTPases with lower affinity than RhoGDI1 (Platko *et al.*, 1995). RhoGDI3 (also known as RhoGDIγ) is mainly expressed in brain and pancreas. It is targeted to intracellular membranes and vesicles by a unique N-terminal extension and predominantly binds to RhoB and RhoG (Adra *et al.*, 1997; DerMardirossian and Bokoch, 2005). Therefore, RhoGDI1[1] takes a central role in the regulation of Rho GTPases.

RhoGDI comprises two domains, a C-terminal geranylgeranyl binding domain and a smaller N-terminal domain which binds to the switch I and switch II regions of Rho GTPases (Hoffman *et al.*, 2000). The central regulatory function of all RhoGDI proteins is the stable binding of Rho GTPases by engulfment of the prenyl moiety in a hydrophobic pocket. This way, RhoGDI solubilises the otherwise membrane bound Rho GTPases and exerts its obvious and name giving function, the inhibition of Rho GTPase nucleotide exchange (Ueda *et al.*, 1990). More precisely, RhoGDI binding prevents activation by RhoGEFs and inactivation by RhoGAPs by blocking access to the switch regions of the GTPases with its N-terminal domain. Taken together, RhoGDI exerts three central biological functions: Firstly, it negatively regulates the activity of Rho GTPases by binding to and shielding Rho GTPases from activation by RhoGEFs (Dovas and Couchman, 2005). Secondly, it acts as a chaperone, solubilising and stabilising a cytosolic reservoir of Rho GTPases. In the absence of RhoGDI, Rho GTPases are rapidly degraded in a proteasome-dependent manner due to a destabilising effect of the isoprenylation (Boulter *et al.*, 2010; Hancock and Hall, 1993). Thirdly, RhoGDI generates a cytosolic pool of Rho

[1] for convenience RhoGDI1 will simply be referred to as RhoGDI throughout this work

GTPases which accounts for 90-95 % of cellular Rho GTPases allowing rapid availability and translocation of Rho GTPases at cellular membranes (Garcia-Mata *et al.*, 2011).

Whereas the above mentioned RhoGDI functions have been thoroughly established over the last decade, many aspects of the role of RhoGDI in Rho GTPase signalling are still not clear. For example, whether RhoGDI is required for shuttling of Rho GTPases between cellular membranes is still controversial. It has been shown by Richard Cerione and colleagues that RhoGDI binding-deficient Cdc42 accumulated and mislocalised at perinuclear membranes instead of at the plasma membrane. They also demonstrated that RhoGDI interaction was required for Cdc42-mediated cell transformation (Lin *et al.*, 2003). Contrary to this, Amy Wilson-Delfosse and colleagues showed that RhoGDI interaction was dispensable for Cdc42-mediated actin reorganisation and filopodia formation and that RhoGDI binding-deficient Cdc42 was still accumulated at the plasma membrane (Gibson and Wilson-Delfosse, 2001; Gibson *et al.*, 2004).

Furthermore, whether or not RhoGDI also binds active GTP-bound Rho GTPases and if this is relevant in a biological context is still a matter of debate. In principle, RhoGDI binds to GDP and GTP loaded RhoA and Rac1 equally well *in vitro* (Hancock and Hall, 1993). However, in the presence of membranes the extraction of GDP-bound Cdc42 by RhoGDI was favoured over the extraction of GTP-bound Cdc42 by RhoGDI (Johnson *et al.*, 2009). This preference for inactive Rho GTPases is in line with biochemical studies on RhoA suggesting that the affinity of RhoGDI towards inactive RhoA is in the picomolar range whereas the affinity towards active RhoA is 500-fold lower in the nanomolar range (Tnimov *et al.*, 2012). Another factor that has been shown to regulate the affinity of Rho GTPases towards RhoGDI is phosphorylation. Specifically, it was found that phosphorylation within the HVR of Rho GTPases increases the affinity of the RhoGDI-Rho GTPase complex (Forget *et al.*, 2002; Garcia-Mata *et al.*, 2011). However, if the individual affinities of RhoGDI towards the Rho GTPase family members are equal or if RhoGDI preferentially binds to certain members is not known.

A general GDI displacement factor that initiates the release of the GTPase from RhoGDI, similar to PRA-1 for Rab GTPases, has not yet been identified for Rho GTPases (Sivars *et al.*, 2003). However, phosphorylation of different residues of RhoGDI can promote dissociation of the RhoGDI-Rho GTPase complex (Garcia-Mata *et al.*, 2011). This has also been shown to happen in a Rho GTPase type specific manner. For example, phosphorylation of RhoGDI by PAK1 has been shown to dissociate Rac1-RhoGDI complex, but did not impair the capacity of RhoGDI to bind to RhoA or Cdc42 (DerMardirossian *et al.*, 2004). It was furthermore suggested that Rac1-RhoGDI displacement at membranes requires PI(3,4,5)P_3 and subsequent activation by a RhoGEF to stably translocate Rac1 to membranes (Ugolev *et al.*, 2008). Moreover, context-specific RhoGDI displacement activ-

ity has been shown for ezrin/radixin/moesin proteins and the p75 neurotropin receptor which both initiated the specific release of RhoA (Takahashi *et al.*, 1997; Yamashita and Tohyama, 2003). Taken together, the prevalent model in literature suggests that general RhoGDI displacement factors do not exist but that rather a context-specific combination of factors is required to induce the release of Rho GTPases from the RhoGDI followed by anchoring of the Rho GTPase to the membrane.

2.3 RhoGEF and RhoGAP substrate specificity

RhoGEF and RhoGAP activities towards Rho GTPases are multiplexed and control the context-specific outcome of the complex biochemical Rho signalling network. It is therefore essential to know the substrate GTPase of RhoGEFs and RhoGAPs in order to link them to their downstream signalling pathways.

2.3.1 Structural determinants of RhoGEF and RhoGAP substrate specificity

Very little is known about structural determinants of RhoGEF and RhoGAP substrate specificity and common principles of its regulation have not yet been identified. In general, substrate specificities were only determined by individual studies on single or small groups of RhoGEFs and RhoGAPs.

However, several studies have tried to identify amino acid fingerprints which determine the substrate specificity of RhoGEFs and RhoGAPs. Indeed, for individual RhoGEFs such as ARHGEF12, ITSN1, and TIAM1 selectivity determining residues have been identified (Snyder *et al.*, 2002; Worthylake *et al.*, 2000). A study that compared available structures and substrate specificity of 14 isolated DH-PH tandem domains, the catalytically active domains of Dbl family RhoGEFs, identified that residues for RhoA, Rac1, and Cdc42 specificity are located within conserved interaction sites of DH-GEFs and that their interaction partners on Rho GTPases are almost exclusively restricted to the switch regions (Jaiswal *et al.*, 2013). In line with this, mutational studies have shown that the substrate specificity can be changed by manipulating individual fingerprint amino acids. Exchange of selectivity determining residues on ITSN1 or on Cdc42 and Rac1 could switch the ITSN1 substrate from Cdc42 to Rac1 (Snyder *et al.*, 2002; Karnoub *et al.*, 2001).

A recent study on sequence-structure-function relationship between RhoGAPs and Rho GTPases failed to identify conserved specificity determining fingerprint residues in the RhoGAP domain. The isolated GAP domains of 10 different RhoGAPs showed low selectivity towards individual Rho GTPase members although conserved interaction regions could be identified in the switch regions of Rho GTPases and on RhoGAPs (Amin *et al.*, 2016).

Also, particular RhoGEFs and RhoGAPs have been reported to change their substrate specificity upon a certain stimulus. For example RACGAP1, which has initially been described to have GAP activity towards Rac1 and Cdc42 (Touré *et al.*, 1998), can be functionally converted to a RhoA specific GAP through phosphorylation by Aurora kinase B (Minoshima *et al.*, 2003). Furthermore, it has been shown, that NGEF can have GEF activity towards RhoA, Rac1, Cdc42 in a phosphorylation-dependent manner. Activation of the fibroblast growth factor receptor and the Eph receptor A4 complex increased the nucleotide exchange activity of NGEF towards RhoA without changing the activity for Rac1 or Cdc42 (Zhang *et al.*, 2007).

To what extent other factors such as localised subcellular recruitment, activation by protein and lipid interactions, and posttranslational modifications of RhoGEFs and RhoGAPs also contribute to substrate specificity in a biological context is not known. However, it has been shown for the Ras GTPase family member KRas that its localisation in membranes is organised in micro- and nanodomains by selective interaction of the HVR with specific phospholipid species (Zhou *et al.*, 2017). This spatial organisation has furthermore been shown to be important for proper KRas signalling output. It is therefore imaginable that GTPases are locally concentrated or depleted in nanoenvironments of the plasma membrane which might control the effective substrate specificity of GEFs and GAPs by the availability of the substrate.

2.3.2 Experimental investigation of RhoGEF and RhoGAP substrate specificity

Biochemical and cell biological assays to directly measure the substrate-specific activity of RhoGEFs and RhoGAPs are essential tools, in order to link their function to downstream signalling contexts. Several *in vitro* and *in vivo* methods have been established over the last decades to accomplish that task.

2.3.2.1 *In vitro* RhoGEF and RhoGAP assays

In vitro RhoGEF activity assays are based on the detection of the GDP-GTP exchange reaction. This can be done in two ways: Either by means of radioactively labelled nucleotides or by fluorescent nucleotide analogues which spectroscopically differ when in their unbound and GTPase-bound states. The use of radioactively labelled nucleotides allows the detection of both the release of GDP and the incorporation of GTP (Hart *et al.*, 1991; Zheng *et al.*, 1995) and can be used to measure kinetics on the minutes time scale. Fluorescent nucleotide analogues are usually used to detect their incorporation into GTPases, as their fluorescence increases dramatically when they become bound in the nucleotide

binding pocket of a GTPase (John *et al.*, 1990; Leonard *et al.*, 1994). This method allows the measurement of fast, seconds and subseconds time scale kinetics by means of sopped-flow devices. However, one caveat here is that the fluorescent moiety of the nucleotide analogue can affect the effective hydrolysis rates (Mazhab-Jafari *et al.*, 2010).

In vitro RhoGAP assays are based on the detection of the GTP hydrolysis reaction. They can detect the release of inorganic phosphate either by radioactive labelling (Self and Hall, 1995) or by colorimetric detection of the inorganic phosphate, or, alternatively, they detect the change in GTP versus GDP concentrations, for example by HPLC (Eberth and Ahmadian, 2009; Paul *et al.*, 2017). More recently, an assay has been developed that spectroscopically senses conformational changes of Rho GTPase during GTP hydrolysis by means of fluorescent nucleotide analogues (Eberth *et al.*, 2005; Amin *et al.*, 2016).

Both the *in vitro* RhoGEF and RhoGAP assays are tools to study the biochemical kinetics and efficiency of Rho GTPase activation and inactivation. These assays are typically performed using recombinant isolated catalytic domains of RhoGEFs and RhoGAPs and have been extensively used to gain insights into the mechanisms and kinetics of substrate recognition, GEF and GAP catalysis, and intrinsic GTPase reaction (Jaiswal *et al.*, 2013; Amin *et al.*, 2016; Eberth *et al.*, 2005; Ahmadian *et al.*, 1999).

2.3.2.2 *In vivo* RhoGEF and RhoGAP assays

In vivo assays to detect RhoGEF and RhoGAP activity are based on the detection of changes in total GTP-bound Rho protein levels in the presence or absence of the regulators. These assays take advantage of the high affinity of Rho GTPase binding domains of effector proteins to active Rho GTPases. Binding domains in effector proteins specifically recognize the active, GTP-bound form of the upstream Rho GTPase. Experimentally, this is implemented by pull-down assays, where effector Rho binding domains serve as baits to bind active Rho GTPases from cell lysates and the GTP-bound Rho protein levels in the cell lysates are considered to resemble activity levels in the living cell. The amount of active Rho GTPases is then measured relative to the total amount of Rho GTPases by subsequent Western blot or enzyme-linked immunosorbent assay-based (ELISA) assays (Ren and Schwartz, 2000; Benard and Bokoch, 2002).

A frequently used effector domain for the detection of active Rac1 and Cdc42 is the N-terminal region of PAK. This region, referred to as the CRIB (Cdc42/Rac1 interactive binding domain) or PBD (p21-binding domain), has a minimal core sequence of 16 amino acids required for GTPase binding. Binding affinities of the PAK1 PBD reach down to 20 nM depending on the length of the peptide encompassing the minimal PBD domain (Thompson *et al.*, 1998). A homologous CRIB domain with Cdc42 selectivity is found in

WASP (Abdul-Manan *et al.*, 1999; Hemsath *et al.*, 2005). Rhotekin, a scaffold protein that is located downstream of Rho signalling, is frequently used to detect active RhoA, RhoB and RhoC (Reid *et al.*, 1996; Ren *et al.*, 1999). Furthermore, the N-terminal Rho binding domain (RBD) of the serine/threonine protein kinase N1 (PKN1) binds to RhoA in a GTP-bound-selective manner (Amano *et al.*, 1996; Flynn *et al.*, 1998).

2.3.2.3 Biosensors of Rho GTPase activity

Biosensors of Rho GTPase activity also take advantage of the interaction of active Rho GTPases with Rho GTPase binding domains of their effector proteins (Pertz, 2010). The most minimalist biosensor of Rho activity is a simple fusion of such an effector Rho GTPase binding domain to a fluorescent protein. This strategy has been used to study Rho GTPase activity patterns in *Xenopus laevis* oocytes and early embryos (Benink and Bement, 2005; Bement *et al.*, 2005). However, most effector domains often bind to multiple Rho GTPases and thus do not report specific Rho protein activities. To overcome this problem Förster resonance energy transfer (FRET)-based sensors have been engineered (Donnelly *et al.*, 2014).

FRET is a non-radiative energy transfer process between two compatible fluorophores, the efficiency of which mainly depends on, firstly, the spectral overlap of the donor fluorophore emission spectrum and the acceptor fluorophore absorption spectrum, secondly, the relative orientation of donor and acceptor dipole moments, and thirdly, distance between the donor and the acceptor fluorophores (Förster, 1948). What makes FRET a particularly valuable tool in cell biology, is its sensitivity to the relative distance of the two fluorophores in the range below 10 nm and their dipole orientations (Pietraszewska-Bogiel and Gadella, 2011).

Rho GTPase activity biosensors take advantage of FRET by detecting the change in distance and dipole orientation upon binding of the effector domain to the active Rho GTPase which results in an increase in FRET efficiency. Different uni- and bimolecular FRET-based Rho biosensors have been developed, with different advantages and disadvantages, according to the requirements of the application (Pertz, 2010; Donnelly *et al.*, 2014). The use of unimolecular FRET-probes facilitates FRET quantification, because FRET donor and acceptor fluorophores are fused together with the Rho GTPase and the effector Rho GTPase binding domain within a single protein chain, allowing ratiometric analysis. Recently, the performance of unimolecular FRET-probes has been systematically improved for RhoA (Fritz *et al.*, 2013; van Unen *et al.*, 2015), Rac1 (Moshfegh *et al.*, 2014; Fritz *et al.*, 2015), and Cdc42 (Hanna *et al.*, 2014; Martin *et al.*, 2016), enabling visualisation of Rho GTPase activity at high subcellular resolution in living cells. Importantly,

only the use of biosensors allows the detection of Rho GTPase activity in living cells, all other "*in vivo*" assays require cell lysis prior to detection of active Rho GTPase levels.

2.4 Rho GTPase signalling is precisely controlled in space and time

Different Rho family members control different cellular processes. Meanwhile, multiple pools of a given Rho GTPase can operate simultaneously in different signalling contexts, for example at the front or rear of a migrating cell or at cells junctions. Moreover, Rho GTPases can also crosstalk with each other, altogether resulting in a complex interplay of signalling networks (Guilluy *et al.*, 2011*a*). Thus, the activity of Rho GTPases is precisely controlled in space and time by their regulators in order to ensure specificity in the biological outcome.

2.4.1 Subcellular localisation and targeting of Rho GTPases

Membranes are believed to serve as signalling platforms for Rho GTPases. In order to target Rho proteins to membranes, the C-terminal CAAX motif within the HVR undergoes extensive posttranslational modification (Mitin *et al.*, 2012). The recognition of the tetrapeptide CAAX motif initiates the serial modification (**C** is the cysteine that is prenylated, **A** is any aliphatic amino acid, and X is the terminal amino acid that dictates prenyltransferase specificity). RhoA, Rac1, and Cdc42 are recognised by geranylgeranyltransferase type I which attaches a geranylgeranyl moiety to the thiol group of the CAAX cysteine. Then, the C-terminal tripeptide (AAX) is proteolytically cleaved from the carboxyl terminus by the Ras-converting enzyme 1 endoprotease. Finally, the C-terminal cysteine undergoes carboxymethylation by the protein-S-isoprenylcysteine-O-methyltransferase. Together, these modifications increase the hydrophobicity of the C-terminus and enable membrane association (McTaggart, 2006) .

Targeting of prenylated small GTPases to the plasma membrane can be regulated by additional palmitoylation or by a cluster of positively charged amino acids, termed polybasic region (PBR) within the HVR (Rocks *et al.*, 2006, 2010; Schmick *et al.*, 2014). Most Rho GTPases, especially RhoA, Rac1, and Cdc42 contain a C-terminal PBR. Rac1 localisation coincides with cellular phosphatidylserine distribution (Yeung *et al.*, 2008) and binding of Rac1 to the plasma membrane has been shown to be dependent on PI(3,4,5)P_3 and PI(4,5)P_2 (Heo *et al.*, 2006). Furthermore, the number of positive charges within the PBR correlated with the endomembrane to plasma membrane partitioning (Yeung *et al.*, 2008). This indicates that the distribution of PBR-containing small GTPases between

endomembranes and the plasma membrane is, at least in part, thermodynamically driven by an electrostatic binding mechanism between the positively charged PBR and negatively charged membrane lipids in the plasma membrane.

Intriguingly, targeting by the HVR might even account for signalling function of Rho GTPases. It was shown that signalling specificity of Rac1 and Rac2, which share more than 90 % overall sequence identity, can be exchanged by swapping their HVR (Filippi *et al.*, 2004). The importance of the HVR in Rho GTPase signalling function is further supported by the finding that RhoA and RhoC, which also share extraordinary sequence similarity within their G-domain (Ridley, 2013), have very distinct roles in cell morphology and cell migration (Vega *et al.*, 2011). In contrast, another study showed that differential binding of RhoA and RhoC to effector proteins can indeed depend on changes of single amino acids within the Rho GTPase G-domain, suggesting that variations in signalling do not only depend on the HVR-dependent distinct localisation (Kitzing *et al.*, 2010).

Of course, protein-protein interaction might also add to the subcellular localisation of Rho GTPases. However, whereas the role of RhoGDI in the regulation of Rho GTPase localisation has been addressed by several studies (Michaelson *et al.*, 2001; DerMardirossian and Bokoch, 2005; Garcia-Mata *et al.*, 2011), a potential contribution of upstream regulators, RhoGEFs, RhoGAPs and downstream effector proteins is only poorly investigated.

Taken together, the subcellular localisation of Rho GTPases is, to a great extent, controlled by their HVR. However, whether the HVR is responsible for functional differences between Rho family members is not fully understood.

2.4.2 Spatio-temporal Rho GTPase signalling patterns

The relevance of the temporal and spatial dimensions of Rho GTPase signalling have emerged only within the last few years, by means of improved biosensors and live cell imaging techniques. Recent studies highlighted that Rho GTPase activity is precisely regulated in micrometre space and on a tens of seconds to minutes time scale during cellular actin-based morphological reorganisation such as random and directed migration (Pertz *et al.*, 2006; Machacek *et al.*, 2009; Zawistowski *et al.*, 2013; Hanna *et al.*, 2014; Fritz *et al.*, 2015; Martin *et al.*, 2016), phagocytosis and macropinocytosis (Hoppe and Swanson, 2004; Yoshida *et al.*, 2009; Zawistowski *et al.*, 2013; Hanna *et al.*, 2014), cytokinesis (Bement *et al.*, 2005), invadopodia formation (Bravo-Cordero *et al.*, 2011), and axon growth cone protrusion and collapse (Fritz *et al.*, 2013). The differential organization of the activity of the Rho GTPases RhoA, Rac1, Cdc42, and others in well-defined time frames and confined zones is a common observation in all of these studies. Presumably, RhoGEFs and RhoGAPs, as direct regulators of Rho GTPase activity, are key to the formation of

these spatio-temporal microdomains of Rho GTPase activity. It is conceivable that the information contributing to the spatio-temporal signalling specificity is encoded within the multidomain architecture of the RhoGEFs and RhoGAPs. The fact that the regulators by far outnumber the Rho GTPases underscores their requirement for precise context-specific regulation of Rho GTPase activity in a multitude of biological processes.

2.4.3 Local regulation of Rho GTPase signalling by RhoGDI, RhoGEFs, and RhoGAPs

The use of recently developed improved FRET-based biosensors has enabled researchers to investigate how spatially confined Rho signalling networks are formed and orchestrated by RhoGEFs and RhoGAPs. Some of these recent investigations are summarised in the following paragraph.

The formation of cell-cell contacts is mediated through adherens junctions by formation of cadherin-based structures linking the cells to each other (Weber *et al.*, 2011). W. James Nelson and colleagues showed that the RhoGEF DOCK1 was recruited in an ELMO2-dependent manner to early cell-cell contact sites, where they locally activate Rac1 and, probably by a secondary mechanism, inactivate RhoA. In the absence of DOCK1 or ELMO2 the formation of E-cadherin-based cell-cell contact sites was slowed down (Toret *et al.*, 2014). This suggested that DOCK1 together with ELMO2 has a very specific but transient function in the regulation of Rho GTPase activities during cell-cell contact formation.

The ability of cancer cells to invade and metastasise is correlated with their ability to degrade extracellular matrix components by formation of specialised cell protrusions, called invadopodia (Murphy and Courtneidge, 2011). Louis Hodgson and colleagues reported that invadopodia have low levels of Rac1 activity. In turn, an increase of Rac1 activity levels was responsible for invadopodia disassembly. This increase was linked to TRIO RhoGEF activity, and invadopodia lifetime was extended in the absence of TRIO (Moshfegh *et al.*, 2014).

Furthermore, RhoA levels have been shown to be locally elevated at the cleavage furrow during cytokinesis in *Xenopus laevis* (Bement *et al.*, 2005). Restriction of RhoA activity has been shown recently to be controlled by MgcRacGAP (RACGAP1 in humans), which localised at the ingressing cytokinetic furrows (Breznau *et al.*, 2015). The common principle that emerges from all of these studies is that activities of RhoGEFs and RhoGAPs are precisely regulated and localised in order to shape transient Rho GTPase activity pools that dynamically regulate cellular morphogenesis.

Besides RhoGEFs and RhoGAPs, RhoGDI has also been implicated in the regulation of

morphogenic events by locally controlled interaction with Rho GTPases. The interaction of RhoA with RhoGDI has been shown to be synchronised with lamellipodia protrusion in protein kinase A (PKA)-dependent manner (Tkachenko *et al.*, 2011). The activity of PKA and RhoA in migrating cells correlated both temporally and spatially as visualised by activity biosensors for RhoA and PKA. RhoA activation led to protrusion of the leading edge, where PKA activation closely followed. This activation was proposed to be via mechanical stimulation due to the formation of adhesions within the protrusion. PKA is then thought to phosphorylate RhoA at serine 188, thereby promoting RhoGDI-mediated membrane displacement by increasing RhoA-RhoGDI affinity. This eventually led to inhibition of RhoA and termination of protrusion and in turn adhesions, forming a self-inhibiting feedback loop. This is an intriguing example of how RhoGDI is involved in the formation and regulation of spatio-temporally controlled RhoA activity patterns.

The examples above show that all three classes of Rho regulators critically contribute to the formation of local Rho GTPase activity pools and resulting morphogenic events. However, only for a few specific Rho GTPase signalling contexts the function of regulators has been directly linked to localised Rho GTPase signalling output. Many examples remain to be investigated to substantiate this hypothesis as a general principle of Rho GTPase signalling. The dynamic maturation and the disassembly of integrin-based adhesion complexes (also known as focal adhesions) is another example of such cellular signalling contexts controlled by a complex regulator-Rho GTPase signalling network, which I discuss in the following section.

2.4.4 Rho GTPase signalling at focal adhesions

Integrin-family proteins are single-pass transmembrane proteins that form a mechanical link between the extracellular matrix substrate and intracellular actin bundles. Furthermore, integrins function as receptors which permit cells to sense chemical, physical and geometrical properties of the extracellular matrix (Geiger and Bershadsky, 2002; Geiger *et al.*, 2009). Importantly, they exhibit bidirectional signalling (Hynes, 2002). On the one hand, signals from within the cell can change the affinity of integrins for extracellular ligands, on the other hand, integrin engagement with extracellular matrix proteins initiates recruitment of intracellular signalling proteins, adapter proteins and components of the cytoskeletal machinery, eventually leading to the formation of micrometre-scale adhesion sites. These integrin-based adhesion sites can then develop into different integrin-based adhesion complexes (IACs) mostly referred to as focal complexes, focal adhesions, fibrillar adhesions, podosomes and invadopodia (Geiger *et al.*, 2001; Huttenlocher and Horwitz, 2011). These classes of IACs are however dynamic and can transform into each other.

Accordingly, there is often a continuum between focal complexes, focal adhesions, and fibrillar adhesions and these three classes of IACs mark different stages of IAC maturation (Geiger *et al.*, 2001, 2009).

The dual functionality of integrins, mechanical linkage and environmental sensing, makes IACs a key signalling hub in cell migration and cell-substrate adhesion, but also in cell survival and differentiation (Hynes, 2002). The complex multimolecular network of the integrin-based adhesion proteome has been reported to involve more than 200 core components (Winograd-Katz *et al.*, 2014; Zaidel-Bar and Geiger, 2010; Zaidel-Bar *et al.*, 2007). In a recent meta-analysis, based on quantitative cross-linking proteomics approaches, the number of proteins involved in context-dependent integrin adhesion complexes add up to even more than 2,400 proteins (Horton *et al.*, 2015). Functional protein families found in the integrin adhesion network comprise adaptor proteins, actin and actin regulating proteins, GTPases, GEFs and GAPs, protein kinases and phosphatases, lipid kinases and phosphatases, and other types of proteins.

Rho GTPases serve as functional switches in the signal transduction downstream of IACs. This involves RhoGEFs and RhoGAPs, which have been shown to bind to adaptor proteins of IACs where they locally activate or deactivate Rho GTPases in the vicinity of adhesion sites. Different Rho GTPase activities have been shown to correlate with different stages of IAC maturation. It is generally accepted that early adhesion IACs for example at the leading edge of a migrating cell corresponds to local high levels of Rac1 and Cdc42 activity, thus driving actin polymerisation and actin branching. Meanwhile, towards the cell rear, RhoA activity levels gradually increase whereas Rac1 activity diminishes resulting in maturation of IACs to focal adhesion and fibrillar adhesions. These serve as anchor points for stress fibers allowing actomyosin contractility and cell rear retraction. However, RhoA activity has also been shown recently to be required at the cell front as well (Pertz *et al.*, 2006; Machacek *et al.*, 2009; Ridley, 2015). Some examples of the functional interplay of integrins, Rho GTPases and its regulators to create such Rho GTPase activities as required for maturation of IACs have been studied in the past decade. To date, ARHGEF6, ARHGEF7, DOCK180, TRIO, VAV-family Rho GEFs and TIAM1 have been linked to local activation of Rac1 and Cdc42 at early adhesion sites, whereas ARHGAP35 has been shown to inactivate RhoA in the same context. ARHGEF28, ARHGEF1 and ARHGEF12 together with ARHGAP24 and RACGAP1 are potential candidates involved in the switch to RhoA activation and Rac1 inactivation, respectively, during focal adhesion maturation (van Buul *et al.*, 2014; Lawson and Burridge, 2014).

IACs are key functional structures in cell migration and cell adhesion and as such also target of Rho GTPase signalling. However, effects of Rho GTPase activity that directly

drive IACs assembly and disassembly have not yet been described. Instead, effects of Rho GTPases on IACs dynamics are believed to result from regulatory effects on the actin cytoskeleton anchored to IACs, such as mechanical tension by RhoA-stimulated actomyosin contractility of stress fibers (Kaverina *et al.*, 2002; Burridge and Guilluy, 2016).

Taken together, by combining receptor and mechanical anchoring function, IACs form a highly complex signalling network. The fact that IACs are dynamic structures which continuously turn-over and convert into different subtypes further explains the requirement of a complex regulatory network comprising numerous proteins. Rho GTPases are at the core of these regulatory networks by transducing many of the incoming signals. However, the number of RhoGEFs and RhoGAPs that have been linked to integrin-mediated signalling is relatively small and probably underestimated at the moment.

3 Objective

Rho signalling occurs in confined cellular environments on a tens of seconds time scale and in micrometre space. Thus, Rho GTPase activity requires precise spatio-temporal control. RhoGEFs and RhoGAPs play a key role in the formation of such microenvironments. To date about 80 human RhoGEFs and 70 human RhoGAPs have been identified, many of which are only poorly characterized. Prerequisite for a systems-level understanding how these proteins impart specificity on Rho signalling is a comprehensive analysis of their enzymatic function and localisation. Another critical determinant of Rho GTPase signalling function is their reversible membrane association which is dictated by their lipid anchors and controlled by RhoGDI proteins. However, a dynamic membrane interaction would counteract spatially confined signalling. Thus, yet unrecognised mechanisms must exist to ensure precise Rho signalling in space and time. Their investigation in living cells requires novel approaches since the kinetics of Rho GTPase membrane association are not accessible with classical biochemical methods.

3.1 Comprehensive *in vivo* analysis of RhoGEF and RhoGAP substrate specificity and focal adhesion localisation

Major aim of my work was to complement a large scale screen of the interactome, cellular distribution and overexpression phenotypes of all mammalian RhoGAPs and RhoGEFs with a comprehensive screen for their substrate specificities and their localisation on focal adhesions. Current literature about RhoGEF and RhoGAP substrate specificity is incomplete and, moreover, considerably inconsistent. Importantly, the substrate specificity of RhoGEFs and RhoGAPs has never been investigated in a comprehensive and systematic manner. Instead, existing data is only available from hundreds of different studies employing different techniques and divergent experimental standards.

Here I aim to establish a screening compatible assay to systematically describe the substrate specificity of 141 RhoGEFs and RhoGAPs towards the three paradigm Rho GTPases RhoA, Rac1 and Cdc42 under standardised experimental conditions. I will furthermore perform a family-wide analysis of RhoGEF and RhoGAP localisation at focal adhesions, a central hub for Rho GTPase signalling. The combination of these two data

sets will allow me to analyse localisation-function relationships of the Rho regulators in order to identify Rho GTPases that are of particular importance in the regulation of focal adhesion dynamics. My study will complement a large scale data set about the interactome, subcellular localisations and overexpression phenotypes of all human RhoGAP and RhoGEF proteins in the lab. Together, this work will help to place the regulators into their functional context and provide a reference resource and a framework for future targeted studies to dissect the complexity of spatio-temporal control of Rho GTPase signalling.

3.2 Investigation of factors that regulate spatial and temporal specificity of Rho GTPase signalling

How exactly local Rho GTPase signalling on membranes is initiated, maintained and terminated is still unknown. Another goal of my thesis is to investigate factors that regulate spatial restriction and temporal persistence of Rho GTPase localisation and activity. Therefore, I aim to analyse intrinsic features of Rho proteins that determine their subcellular partitioning. I will furthermore study the impact of these features on membrane binding stability and establish the dynamic nature of Rho GTPase membrane residence. Moreover, I will evaluate the influence of RhoGDI on Rho protein localisation, membrane binding, and activity. Lastly, I will advance the establishment of a single molecule assay to precisely monitor and resolve the complex processes involved in Rho GTPase membrane interaction dynamics and its regulation in the future.

4 Materials and Methods

4.1 Molecular biology

4.1.1 Media, buffers, and solutions

Table 4.1 Molecular biology: Media, buffers, and solutions.

Media
LB medium 10 g/l bacto-tryptone, 5 g/l yeast extract, 5 g/l NaCl
LB agar plates 15 g/l agar, 10 g/l bacto-tryptone, 5 g/l yeast extract, 5 g/l NaCl, supplemented with 100 μg/ml ampicillin or 50 μg/ml kanamycin
Sucrose agar plates 15 g/l agar, 7 g/l sucrose, 10 g/l bacto-tryptone, 5 g/l yeast extract, 5 g/l NaCl, supplemented with 30 μg/ml chloramphenicol
Buffers and solutions
BSA (10x) 1 mg/ml, 1:20 dilution of BSA, Molecular Biology Grade (New England Biolabs, USA)
Optimized Cre recombinase buffer (10x) 50 mM Tris-HCl, 33 mM NaCl, 10 mM $MgCl_2$, 10 mM spermidine, pH 7.9
Orange G DNA loading buffer (6x) 50 % (v/v) glycerol, 25 mM EDTA, 5 g/l Orange G
TAE 40 mM Tris, 20 mM acetic acid, 1 mM EDTA, pH 8

4.1.2 Expression plasmids and oligonucleotides

Lists of expression plasmids and oligonucleotides are attached in the Appendix (Appendix Table 7.2 and Appendix Table 7.3).

4.1.3 Molecular cloning

In this work, mammalian expression plasmids were generated by means of the Creator recombination system, by In-Fusion enzyme-based cloning, or by classical restriction-ligation-based molecular cloning. Inserts for ligation were generated by restriction digestion of existing vectors, by polymerase chain reaction (PCR), or by oligonucleotide annealing. pEGFP-C1-derived (Clontech Laboratories, USA) vectors pmCitrine-C1, pmCherry-C1, pmPAGFP-C1, pmiRFP670-C1, and SNAP-C1 were used as destination vectors for In-Fusion enzyme-based and classical restriction-ligation-based molecular cloning. Point mutations were introduced by PCR-based site directed mutagenesis. All of these methods are explained in the following sections.

4.1.3.1 Creator recombination

The expression library of N-terminally labelled cDNAs of RhoGEFs and RhoGAPs was cloned into a modified Creator recombination system (Colwill *et al.*, 2006). The Creator system uses Cre-recombinase-mediated *loxP* site-specific recombination to shuttle a gene of interest, that is flanked by *loxP* sequences, from a donor vector into a destination expression vector with one *loxP* sequence. The *loxP* sequence consist of an 8 bp long asymmetric core sequence flanked by two 13 bp palindromic sequences (Sternberg *et al.*, 1981). The asymmetric sequence defines the directionality of insertion and ensures the correct orientation of the gene of interest in the acceptor vector. The acceptor vectors contained open reading frames for mCherry or mCitrine followed by a splice donor site and the *loxP* sequence. The donor vectors contained the RhoGEF and RhoGAP cDNA with an upstream splice acceptor site flanked by *loxP* sequences. After recombination splice donor and splice acceptor form an intron in the expression vector that is removed from the pre-mRNA upon transfection and transcription in mammalian cells. Additionally, RhoGEF and RhoGAP cDNAs were directly flanked by AscI and PacI restriction sites upstream and downstream, respectively, to facilitate restriction/ligation cloning and analytical restriction digests.

The Creator recombination reaction was performed as previously described (Colwill *et al.*, 2006). Briefly, the following components of the reaction were mixed and incubated for 15 min at room temperature:

Creator recombination reaction	
Component	**Amount**
Donor vector	500 ng
Acceptor vector	500 ng
BSA (10x)	1 μl
Optimized Cre recombinase buffer (10x)	1 μl
Cre enzyme	0.5 μl
Nuclease free H_2O	fill to 10 μl

After recombination Cre recombinase was heat-inactivated for 10 min at 70 °C followed by 2 min incubation on ice. 5 μl of the reaction were transformed into chemically competent DH5α bacteria as described below (see 4.1.3.8) and plated on sucrose agar plates with 30 μg/ml chloramphenicol to select correctly recombined clones by a positive/negative selection. Colonies were picked and DNA was amplified as described below (see 4.1.3.9). Purified DNA was digested with the restriction enzymes AscI and PacI (New England Biolabs, USA) for 1 h at 37 °C and correct recombination was routinely controlled by agarose gel electrophoresis as described below (see 4.1.3.6). Donor clones with cDNAs for the RhoGEFs and RhoGAPs, as well as mCherry and mCitrine acceptor vectors used in this study were previously cloned by Oliver Rocks or gifts from the Tony Pawson lab, SLRI, Mount Sinai Hospital, Toronto. The recombinase protein Cre was a kind gift of the Tony Pawson lab. All Creator recombination cloning was done with the help of Marlies Grieben, Lennart Brandenburg, Juliane Rademacher, and Lisa Keller.

4.1.3.2 Polymerase chain reaction

Polymerase chain reaction (PCR) was used to amplify specific sequences of DNA for further application in In-Fusion enzyme-based and restriction-ligation-based molecular cloning. Furthermore, PCR was used for site-directed mutagenesis of expression vectors as described below (see 4.1.3.11). PCR reactions were performed using Phusion High-Fidelity DNA Polymerase (New England Biolabs, USA). Reactions were prepared on ice as follows:

PCR reaction	
Component	**Amount**
5x Phusion GC or HF buffer	10 μl
dNTP mix (10 mM)	1 μl
Forward primer (10 μM)	2.5 μl
Reverse primer (10 μM)	2.5 μl
Template DNA (10-100 pg/μl)	2.5 μl
DMSO (if required)	1 μl
Phusion DNA Polymerase	0.5 μl
Nuclease free H_2O	fill to 50 μl

Reactions were performed in a mastercycler gradient (Eppendorf, Germany). PCR cycling parameters were set as follows:

PCR cycling parameters			
Step	**Temperature**	**Time**	**repeats**
Initial DNA denaturation	98 °C	3 min	1x
DNA denaturation	98 °C	10 s	35x
DNA-primer annealing	65-72 °C[1]	20 s	
DNA extension	72 °C	30 s per 1 kb	
Final extension	72 °C	10 min	1x

PCR products were controlled by agarose gel electrophoresis as described below (see 4.1.3.6) with 5 μl of the reaction. PCR products were purified using the GeneJET PCR Purification Kit (Thermo Fisher Scientific, USA). If required, PCR products were then digested with the respective restriction enzymes and again purified with the GeneJET PCR Purification Kit to remove the end fragments.

4.1.3.3 In-Fusion enzyme-based cloning

The In-Fusion enzyme (Clontech Laboratories, USA) reaction is based on recombination of homologous DNA ends. The In-Fusion enzyme joins any two pieces of DNA that have 15 bp of identity at their ends (Zhu *et al.*, 2007). Therefore, this technique is independent of defined restriction sites and allows recombination in DNA sequences that lack these sites. Target vector DNA was linearised by restriction digestion or by long range PCR, while donor vector DNA was linearised by PCR using overhanging primers to generate

[1] DNA-primer annealing temperature was calculated for each primer pair individually using the New England Biolabs Tm Calculator at www.neb.com

the homologous DNA ends. Reactions were carried out using the In-Fusion HD cloning kit (Clontech Laboratories, USA) according to manufacturer's instructions. 5 μl of the reaction were used for transformation of 100 μl chemically competent bacteria as described below (see 4.1.3.8).

4.1.3.4 DNA restriction digestion

Restriction enzymes were used from New England Biolabs (USA). Restriction digestion reactions were performed according to the manufacturer's instructions. Where required, the 5' phosphate of the DNA fragments was removed by Antarctic Phosphatase (New England Biolabs, USA).

4.1.3.5 Oligonucleotide annealing

5' phosphorylated custom oligonucleotides for the generation of small DNA inserts for cloning were purchased from Sigma-Aldrich (USA). Oligonucleotides were mixed at a final concentration of 1 μM in 1x NEBuffer2.1 (New England Biolabs, USA), heated to 95 °C for 5 min in a beaker filled with 1 l water and slowly cooled to room temperature over the time period of several hours. Annealed oligonucleotides were directly used for further ligation reactions.

4.1.3.6 Agarose gel electrophoresis

Agarose gel electrophoresis was used to separate DNA fragments by size, either for analytic purposes or for purification of DNA fragments for cloning purposes. Gels were prepared by dissolving 1 % (w/v) agarose in TAE buffer by heating. The warm agarose solution was poured into an electrophoresis chamber (BioRad, USA) and solidified by cooling to room temperature. DNA samples were loaded in Orange G DNA loading buffer and the DNA separation in the gels was run in TAE buffer by applying 100 V until sufficient separation was reached, estimated by the Orange G band marking a size of 50 bp. Gels were incubated in a 25 μg/ml Ethidium bromide bath for 10 min before imaging in a UV-light transilluminator. Size of DNA fragments was estimated relative to a 1 kb DNA Ladder marker (New England Biolabs, USA) that was run in parallel. For extraction of DNA fragments from the gel, the DNA was excised with a scalpel and purified using the GeneJET Gel Extraction Kit (Thermo Fisher Scientific, USA) according to the manufacturer's protocol.

4.1.3.7 DNA ligation

For ligation reactions 50 ng restriction enzyme digested and gel purified vector backbone DNA were incubated with insert DNA at a molar ratio between 1:3 to 1:5 with 2 µl 10x T4 DNA Ligase buffer and 1 µl T4 DNA Ligase (New England BioLabs, USA) in a final reaction volume of 20 µl. Ligation was incubated for 1 h at room temperature and 5 µl of the reaction were subsequently transformed into chemically competent *E. coli* as described below (see 4.1.3.8).

4.1.3.8 Transformation of *E. coli*

The heat-shock transformation method was used to introduce exogenous plasmid DNA into *E. coli* bacteria. 100 µl chemically competent DH5α *E. coli* were thawed on ice and 5 µl of plasmid or reaction to be transformed were added and carefully mixed. Bacteria were incubated for 20 min on ice and then heat-shocked for 1 min at 42 °C in a water bath. Bacteria were cooled on ice for 5 min before addition of 500 µl LB medium containing 20 mM glucose. Bacteria were incubated with shaking for 1 h at 37 °C and then centrifuged for 1 min at 6000 g. Supernatant was removed except for 100 µl and bacterial pellet was resuspended and plated on LB agar plates with the required antibiotic. Plates were incubated to form colonies overnight at 37 °C.

4.1.3.9 Amplification of plasmid DNA in *E. coli* and plasmid DNA extraction

Bacterial cultures were inoculated with individual colonies from agar plates or with bacteria from glycerol socks (see 4.1.3.10). Depending on the required amount of plasmid DNA, bacteria were grown in 7 ml or 100 ml LB medium overnight at 37 °C while shaking. Plasmid DNA was purified from pelleted bacteria using the ZR Plasmid Miniprep Classic kit (Zymo Research, USA) for 7 ml cultures or the PureLink HiPure Plasmid Midiprep Kit (Thermo Fisher Scientific, USA) for 100 ml cultures according to manufacturer's instructions. DNA concentrations were measured using a NanoDrop 1000 (PeqLab, Germany).

4.1.3.10 Glycerol stock preparation

For long-term storage of transformed bacteria 700 µl bacteria culture grown in LB medium overnight were mixed with 300 µl glycerol, thoroughly vortexed and immediately placed at -80 °C.

4.1.3.11 Site-directed mutagenesis

Point mutations were created by PCR-based site-directed mutagenesis using the QuikChange II XL kit (Agilent Technologies, USA) following manufacturer's instructions. After the PCR reaction the DNA was incubated with the restriction enzyme DpnI, which specifically digests the methylated bacterial template DNA, leaving only unmethylated mutant DNA for following transformation.

4.2 Cell culture

4.2.1 Cell culture media, reagents, and materials

Table 4.2 Cell culture: Media and buffers, reagents and additives, consumables.

Media and buffers	
Dulbecco's Modified Eagle Medium (DMEM)	Thermo Fisher Scientific, USA
Dulbecco's Phosphate-Buffered Saline (DPBS)	PAN Biotech, Germany
Fetal calf serum (FCS)	Biochrom, Germany
FluoroBrite DMEM	Thermo Fisher Scientific, USA
Gey's Balanced Salt Solution, w: 2.27 g/l $NaHCO_3$	PAN Biotech, Germany
Ham's F12, w/o: Phenol red, w: 1.176 g/l $NaHCO_3$	PAN Biotech, Germany
Reagents and additives	
Penicillin-Streptomycin, 10,000 U/ml	Thermo Fisher Scientific, USA
Blasticidin	PAA Laboratories, Germany
Puromycin dihydrochloride	Sigma-Aldrich, USA
Trypsin 0.25 % / EDTA 0.02 %	PAN Biotech, Germany
Versene EDTA Solution	Thermo Fisher Scientific, USA
FuGENE HD Transfection Reagent	Promega, USA
Lipofectamine 3000 Reagent	Thermo Fisher Scientific, USA
Polyethylenimine (PEI), linear, MW 25,000	Polysciences, USA
Poly-L-lysine, MW 150,000-300,000	Sigma-Aldrich, USA
Consumables	
Glass bottom culture dish, 35 mm, #1.5 coverslip	MatTek, USA
96-well μ-plate, no. 1.5 polymer coverslip, ibiTreat	ibidi, Germany
Cell culture dishes, 10 cm, 14.5 cm, CELLSTAR	Greiner Bio-One, Germany
Multiwell culture plates, CELLSTAR	Greiner Bio-One, Germany

4.2.2 Cell lines

All cell lines were routinely cultured at 37 °C in the presence of 5 % CO_2 in a standard cell culture incubator with humidification system. Cells were kept in cell culture dishes and passaged every 2-3 days. For passaging, cells were washed once with DPBS, incubated with Trypsin/EDTA, followed by resuspension in the cell culture medium and replating. All cell lines were routinely cultured in DMEM medium supplemented with 10 % FCS and 100 U/ml Penicillin-Streptomycin unless otherwise stated.

Table 4.3 Eukaryotic cell lines.

Cell line	ATCC number/Source
COS-7	ATCC number: CRL-1651
HEK293T	ATCC number: CRL-3216
HeLa	ATCC number: CCL-2
HeLa Tet-On	HeLa-EM2 cell line (Weidenfeld *et al.*, 2009)

4.2.3 DNA Transfection

4.2.3.1 Transfection of HEK293T cells

HEK293T cells for the FRET-based Rho GTPase activity assay were cultured in microscopic 96-well plates and kept in a custom-made humidity chamber inside a standard cell culture incubator with humidification system (Walzl *et al.*, 2012)[2]. 96-well plates were previously coated with 5 μg/well poly-L-lysine (200 μl) for 20 min, washed twice with DPBS and dried for at least 2 h. Cells were seeded in 250 μl FluoroBrite DMEM supplemented with 10 % FCS and 100 U/ml Penicillin-Streptomycin at a density of 5.5×10^4 cells per well and allowed to adhere over night. Before the transfection medium was replaced with fresh medium. For the RhoGEF activity screen, cells were transfected with 40 ng FRET sensor, 80 ng RhoGDI or mCherry control, and 280 ng RhoGEF or mCherry control. For the RhoGAP activity screen, cells were transfected with 30 ng FRET sensor and 270 ng RhoGAP or mCherry control. DNA was mixed with PEI transfection reagent (1 mg/ml, pH 7) at a ratio of 1:3 (DNA [μg] : PEI [μl]), incubated for 20 min, and thoroughly mixed by repeated pipetting before added drop wise to the cells. One day after transfection the medium was replaced with 300 μl FluoroBrite DMEM supplemented with 1 % FCS. Cells were subjected to imaging 48 h post transfection.

4.2.3.2 Transfection of HeLa and HEK293T cells

HeLa or HEK293T cells were seeded on cell culture dishes one day before transfection. FuGENE HD transfection reagent was used at a ratio of 1:3 (DNA [μg] : FuGENE HD [μl]). DNA and FuGENE HD were each pre-diluted in serum-free medium, then mixed, and incubated for 10 min before adding dropwise to cells. HeLa cells were transfected 16-20 h before the experiments.

[2] incubation in the custom-made humidity chamber was critical in order to minimise the edge effect and ensure consistent cell growth throughout the 96-well plate

4.2.3.3 Reverse transfection of COS-7 cells

COS-7 cells were transfected with Lipofectamine 3000 reagent at a ratio 1:2.5:2.5 (DNA [μg] : P3000 reagent [μl] : Lipofectamine 3000 [μl]). DNA was pre-mixed with serum-free medium and P3000 reagent and Lipofectamine 3000 was pre-mixed with serum-free medium beforehand. Both mixtures were combined and incubated for 5 min. Then cells, which were previously detached, were added to the transfection mix and incubated for 10 min in the incubator while gently inverting every 1 min. Cells were then seeded on 35 mm glass bottom culture dishes and allowed to adhere for 16-20 h before replacing the medium with FluoroBrite DMEM supplemented with 1 % FCS and performing TIRF microscopy.

4.2.4 Generation of stable cell lines by lentiviral gene delivery

4.2.4.1 Generation of stable shRNA-mediated RhoGDI knockdown HEK293T cell lines

Table 4.4 Target sequences and oligonucleotides for generation of RhoGDI shRNAs. shRNA1 targets the 3' untranslated region (3'UTR) of the RhoGDI mRNA, shRNA2 targets the coding sequence (CDS) of the RhoGDI mRNA.

shRNA1
target sequence 3'UTR:
CGTCTAACCATGATGCCTTAA
oligonucleotide forward:
CCGGCGTCTAACCATGATGCCTTAACTCGAGTTAAGGCATCATGGTTAGACGTTTTTG
oligonucleotide reverse:
AATTCAAAAACGTCTAACCATGATGCCTTAACTCGAGTTAAGGCATCATGGTTAGACG
shRNA2
target sequence CDS:
CAAGATTGACAAGACTGACTA
oligonucleotide forward:
CCGGCAAGATTGACAAGACTGACTACTCGAGTAGTCAGTCTTGTCAATCTTGTTTTTG
oligonucleotide reverse:
AATTCAAAAACAAGATTGACAAGACTGACTACTCGAGTAGTCAGTCTTGTCAATCTTG

Cloning of shRNA oligonucleotides into the pLKO.1 vector and production of lentiviral particles in HEK293T cells was done according to the protocol "Addgene Plasmid 10878. Protocol Version 1.0. December 2006" (available at: www.addgene.org/tools/protocols/plko/) and based on sequences identified by the the RNAi consortium (Moffat *et al.*, 2006). Briefly, the five target sequences suggested by the RNAi consortium were previously analysed by Oliver Rocks and two sequences were identified which yielded good knockdown

deficiency (Table 4.4). Oligonucleotides for each shRNA were annealed and cloned into pLKO.1 by AgeI and EcoRI restriction digestion. For the generation of a control virus, the pLKO.1 plasmid contained a 1.9 kb stuffer sequence in place of the shRNA oligonucleotide. The shRNA vectors were then transfected into HEK293T cells together with the psPAX2 packaging plasmid and the pCMV-VSVG envelope plasmid as described (see 4.2.3.2). One day after transfection the medium was replaced with fresh medium, two days after transfection the medium containing the lentiviral particles was harvested. HEK293T cells were then infected with 100 μl lentiviral particle containing medium per 4×10^5 cells and selected for transduced cells 24 h post infection with 2 μg/ml puromycin. HEK293T shRNA2 RhoGDI knockdown cells were used for the RhoGAP substrate specificity screen and RhoGAP activity FRET experiments.

4.2.4.2 Generation of a stable mCherry-paxillin COS-7 cell line

Lentiviral particles for the generation of the UbC promoter controlled mCherry-paxillin COS-7 cell line were kindly provided by Alexander Löwer. COS-7 cells were infected with lentiviral particles and selected for transduced cells 24 h post infection with 15 μg/ml blasticidin. Furthermore, mCherry positive cells were enriched by fluorescence-activated cell sorting (FACS).

4.3 Biochemistry

4.3.1 Buffers, solutions, and antibodies

Table 4.5 Biochemisty: Buffers and solutions.

Buffers and solutions
DPBS++ Dulbecco's Phosphate-Buffered Saline, w: calcium and magnesium (PAN Biotech, Germany)
NP40 lysis buffer 1 % NP40, 50 mM Tris-HCL pH 8, 150 mM NaCl
SDS sample buffer (6x) 375 mM Tris-HCl pH 6.8, 300 mM DTT, 12 % SDS, 60 % glycerol, 0.06 % bromophenol blue, 20 % 2-mercaptoethanol
SDS running buffer 100 mM Tris, 100 mM mM Hepes, 0.1 % SDS, pH 8.3
Wet blot transfer buffer 25 mM Tris, 190 mM glycine, 20 % methanol, pH 8.3
TBS-T 25 mM Tris, 150 mM NaCl, 0.1 % Tween20, pH 7.4

Table 4.6 Antibodies for Western blot and immunoprecipitation.

Antibody	Species	Clone number, company	Working dilution
Primary antibodies			
GFP	Rabbit	ab290, abcam	1:10,000
RhoGDI	Rabbit	sc360, Santa Cruz	1:2000
Tubulin	Mouse	DM1a, Sigma-Aldrich	1:10,000
Secondary antibodies			
anti-mouse IgG HRP Conjugate	Goat	1706516, BioRad	1:10,000
anti-rabbit IgG HRP Conjugate	Goat	1706515, BioRad	1:10,000

4.3.2 Preparation of protein samples from cultured cells

Cell lysis was done to obtain cellular protein for immunoprecipitation of RhoGDI with RhoGDI binding-deficient mutant of Rho GTPases or direct Western blot analysis for RhoGDI knockdown analysis of shRNA-mediated knockdown HEK293T cells. HEK293T

cells were washed with ice cold DPBS++ and harvested by merely pipetting up and down in DPBS++ on ice, as they detach easily. Cells were then pelleted by centrifugation at 200 g for 5 min at 4 °C. HEK293T cell pellets were lysed in NP40 lysis buffer, with complete protease inhibitor cocktail (Roche, Switzerland) for 20 min on ice and carefully mixed by pipetting every 5 min. Cell lysates were then cleared by centrifugation at 18,000 g for 5 min at 4 °C. Cleared lysate supernatants were then transferred to fresh reaction tubes. Protein concentration was measured using the Precision Red Advanced Protein Assay (Cytoskeleton, USA) according to manufacturers instructions. Absorbance was measured at 600 nm.

4.3.3 Immunoprecipitation

HEK293T cells were transfected with Rho GTPase constructs at 80 % confluency and harvested as described above the following day. Cleared lysate samples were split, one half was kept for Western blot controls, the other half was added to 20 μl Protein G Sepharose bead suspension (Sigma-Aldrich, USA) coupled with 0.5 μl anti-GFP antibody (ab290, abcam, UK) and rotated for 1 h at 4 °C. Beads were washed three times in NP40 lysis buffer and protein was eluted with SDS sample buffer (2x) for 20 min at 37 °C. Eluate samples were again centrifuged at 800 g for 1 min at 4 °C and the supernatant was separated from the beads and boiled for 5 min at 95 °C. Lysate and eluate samples were analysed by Western blot.

4.3.4 Western blot

Samples were incubated for 5 min at 95 °C and centrifuged at 18,000 g for 1 min. They were then separated by SDS-polyacrylamide gel electrophoresis on a 12 % resolving gel with a 4 % stacking gel. Gels were run in SDS running buffer for the first 10 min at 80 V then at 150 V until proteins were sufficiently separated. Gels were transferred onto 0.45 μm Amersham Hybond ECL nitrocellulose (Amersham, UK) by using a wet blot transfer system (Bio-Rad Laboratories, USA) for 90 min at 100 V in Wet blot transfer buffer. Successful protein transfer onto the membrane was confirmed by Ponceau S staining (Sigma-Aldrich, USA). After washing with TBS-T, membranes were blocked with 5 % milk powder in TBS-T for 1 h. Membranes were incubated with the primary antibody for 1 h at room temperature, washed three times with TBS-T and incubated with the HRP-coupled secondary antibody for 1 h at room temperature. After washing three times for 5 min in TBS-T membranes were then incubated with LumiGLO Reagent Substrate (Cell Signaling Technology, USA) for 1 min. Super RX X-ray films (Fujifilm, Japan) were exposed for varying times and developed.

4.4 Microscopy

4.4.1 Sensitised emission FRET microscopy

Ratiometric sensitised emission FRET experiments were performed on a fully automated Olympus IX81 inverted epifluorescence microscope equipped with an UPLSAPO 10x/0.4 NA air objective, an MT20 150 W xenon arc burner (Olympus, Japan) light source with an excitation filter wheel, a motorised dichroic mirror turret, and an emission filter wheel. Furthermore, the microscope was equipped with a motorised programmable stage (Märzhäuser Wetzlar, Germany) and a near-infrared laser-based autofocus system that allowed automated image acquisition of 96-well plates. Images were acquired with a water-cooled EMCCD camera (ImageEM, Hamamatsu) at a 16-bit depth. A temperature-controlled incubation chamber maintained 37 °C, 5 % CO_2, and 60 % humidity during the experiments. The following combinations of excitation filters, dichroic mirrors and emission filters were used for the indicated image channels or fluorophores:

Channel/Fluorophore	Excitation filter	Dichroic mirror	Emission filter
Donor	430/25	zt442RDC	483/32
FRET-Acceptor	430/25	zt442RDC	542/27
Acceptor/mVenus	500/20	zt514RDC	542/27
mCherry	572/23	HC BS 593	623/24
miRFP670	640/30	R405/488/561/635	692/40

Illumination settings were kept constant for all measurements. Cells were imaged 48 h after transfection in FluoroBrite DMEM supplemented with 1 % FCS. Images of five fields of view per condition were recorded. Background images were taken from at least six untransfected wells.

4.4.2 TIRF microscopy

Total internal reflection fluorescence (TIRF) microscopy was performed at an Olympus IX81 microscope equipped with an APON 60x/1.49 NA oil immersion TIRF objective, an UAPON 150x/1.45 NA oil immersion TIRF objective, and a motorised 4-line TIRF condenser (cellTIRF, Olympus) to achieve TIRF illumination. Images were taken with a water-cooled EMCCD camera (ImageEM, Hamamatsu) at a 16-bit depth. mCitrine and mEGFP were excited with a 488 nm solid state laser. mCherry and tetramethylrhodamine (TMR) were excited with a 561 nm solid state laser. mEGFP fluorescence was filtered with a 525/50 bandpass emission filter, mCitrine fluorescence was filtered with a 542/27

bandpass emission filter, and mCherry and TMR fluorescence was filtered with a 617/73 bandpass emission filter.

4.4.2.1 FRAP of immobilised fluorophores

The immobilisation of antibodies on epoxysilan coated glass slides was confirmed by fluorescence recovery after photobleaching (FRAP) experiments. FRAP experiments were performed on a TIRF microscope as described above using an APON 60x/1.49 NA oil immersion TIRF objective. Imaging was performed in TIRF-illumination using 488 nm (20 mW) and 561 nm (150 mW) solid state lasers. Bleaching was performed in wide-field illumination with a half closed field aperture at maximum laser intensity, to only bleach a small region within the FOV. In order to reduce photobleaching to a minimum, imaging was performed at low frame rates.

Antibody immobilisation on epoxysilan coated glass slides

Epoxysilan coated glass slides were custom made by SCHOTT upon request (NEXERION Coverslip Epoxysilane Coating (E) #1.5 ∅30 mm, SCHOTT Technical Glass Solutions, Germany). Epoxysilan glass slides were marked at the surface with a small scratch using a diamond grinding pen (Carl Roth, Germany) to facilitate focussing at the microscope. Slides were then incubated with 20 μg/ml goat anti-rabbit IgG AlexaFluor488 or goat anti-rabbit IgG AlexaFluor555 antibodies diluted in PBS upside-down on parafilm for 1 h at room temperature, and blocked for 1 h at room temperature in 1 % bovine serum albumin in DPBS-T (DPBS++, 0.05 % (v/v) Tween20). Slides were washed and mounted in a microscopic mounting chamber POCmini-2 (PeCon, Germany) and kept in DPBS-T.

mEGFP immobilisation on anti-GFP coated glass slides

Epoxysilan glass slide decoration with anti-GFP antibodies (Table 4.7) was performed as described above. HEK293T cells were transfected with mEGFP and lysed as described in sections 4.2.3.1 and 4.3.2. Anti-GFP antibody decorated and blocked glass slides were then incubated with the cleared lysates for 1 h at room temperature, washed and mounted in a microscopic mounting chamber POCmini-2 (PeCon, Germany) and kept in DPBS-T.

4.4.2.2 TIRF microscopic observation of single fluorescent particles

For the single molecule imaging experiments, fluorescently labelled molecules located at the bottom cell membrane facing the coverslip were observed with an UAPON 150x/1.45 NA oil immersion TIRF lens. Time-lapse recordings for single particle tracking (SPT) or single fluorophore bleaching were imaged at 30 Hz with continuous illumination.

Table 4.7 Antibodies for GFP immobilisation on epoxysilan glass slides.

Antibody	Clone number, company	Working dilution
GFP Tag Polyclonal Antibody	A11122, Thermo Fisher Scientific	1:200
Anti-GFP antibody	ab290, abcam	1:200
Anti-GFP antibody	ab13970, abcam	1:500
Living Colors EGFP Monoclonal Antibody	632569, Clontech Laboratories	1:100

SPT of TMR-labelled proteins

HeLa Tet-On cells seeded in 12-well plates at a density of 3×10^5 cells/well were transfected as described above (see 4.2.3.2). Cells were labelled with 0.1 μM SNAP-Cell TMR-Star (New England Biolabs, USA) for 1 h, thoroughly washed with complete medium, detached by Trypsin/EDTA treatment, again washed and transferred into glycine-coated glass bottom culture dishes. Glass bottom culture dishes were coated with 2 M glycine for 1 h at room temperature to reduce TMR attachment to the glass surface (Klein *et al.*, 2011). Cells were allowed to adhere for 3 h before imaging.

Antibody immobilisation of TMR-labelled proteins

HeLa Tet-On cells were treated as described above with the difference that instead of Trypsin/EDTA treatment, cells were detached by the Trypsin-free Versene EDTA Solution (Thermo Fisher Scientific, USA) to avoid proteolytic degradation of extracellular mEGFP. Cells were transferred to anti-GFP antibody-decorated (A11122, Thermo Fisher Scientific, USA) epoxysilan glass slides mounted in a microscopic mounting chamber and allowed to adhere for 2 h before imaging.

4.4.2.3 TIRF microscopic observation of focal adhesions localisation

COS-7 cells were transfected as described above 15-20 h before imaging (see 4.2.3.3). The localisation of RhoGEFs and RhoGAPs at focal adhesions was observed with an APON 60x/1.49 NA oil immersion TIRF lens using both wide-field and TIRF illumination.

4.4.3 FLAP assay

HeLa cells subjected to fluorescence loss after photoactivation (FLAP) experiments were transfected one day before the experiment. FLAP experiments were carried out on a Olympus FV1000 inverted microscope equipped with a UPLSAPO 60x/1.3 NA silicon oil immersion lens and a temperature-controlled incubation chamber maintained at 37 °C and 5 % CO_2. mPAGFP was excited at 488 nm using multi-line Argon laser. Photoactivation of mPAGFP was achieved using a 405 nm diode laser. mCherry plasma membrane

marker was exited with a 559 nm diode laser. The microscope was equipped with a SIM scanning unit allowing simultaneous laser manipulation and imaging. The position for photoactivation was placed at the vertical region of the plasma membrane and a circular region of 1-1.5 μm diameter was photoactivated by a 1 ms laser pulse. Fluorophore emission of mPAGFP was detected at 500-545 nm and emission of mCherry was detected at 570-670 nm. Images were acquired with a frame rate of 35 ms.

4.4.4 Spinning disc confocal microscopy

Subcellular localisation of Rho GTPases and its mutants was assessed on a Nikon/Andor CSU-W1 spinning disk confocal microscope on an inverted Nikon Ti-E stand. The microscope was equipped with a 50 μm pinhole spinning disk and a borealis unit for uniform illumination, a CFI PlanApo λ 100x/1.45 NA oil immersion objective, an EMCCD camera (iXON 888, Andor), and a stage incubator to maintain 37 °C and 5 % CO_2 during imaging. The following excitation laser and emission filters were used for imaging: mCitrine: 514 nm laser with 559/34 emission filter; mCherry: 561 nm with 609/54 emission filter; miRFP670: 637 nm with 685/40 emission filter.

4.5 Image data analysis

4.5.1 Automated image analysis of FRET-based RhoGEF and RhoGAP activity screens

The data set of ratiometric sensitised emission FRET experiments comprised raw images of donor channel, FRET-acceptor channel, acceptor channel, mCherry channel, and - where required - miRFP670 channel. Additionally, background images for each channel were recorded. Processing of raw image data sets was performed with a self-written automated ImageJ script (Figure 4.1). First, average background images were generated from 30 to 60 background images. Raw images and average background images were smoothened by Gaussian filter convolution with a σ radius of 1 pixel. Raw images of all channels were background corrected by subtraction of average background images. Background corrected images were then sequentially thresholded in order to define the regions of interest (ROIs) that were used for further analysis. The acceptor channel images, the mCherry channel images, and where needed the miRFP670 channel images were thresholded in order to create ROIs that only include transfected cells. Furthermore, ROIs were generated in the donor and FRET-acceptor channels to exclude low intensity pixels. Generally, images were taken with low intensity excitation light to avoid saturation, however, for the purpose of certainty saturated pixels were excluded from the ROI before background correction. All ROIs were combined by logical "AND" operation therefore generating a final ROI that included cells which were transfected with all components and excluded saturated and low intensity pixels. FRET-ratio images were created within that final ROI by dividing the FRET-acceptor by the donor channel image on a pixel basis. The final ROI was then applied to measure the average intensity within the FRET-ratio image and images of the acceptor, mCherry, and miRFP670 channels. Also, the area of the ROI was measured.

4.5.2 FLAP analysis

The mean intensity within the photoactivated region was measured in ImageJ. The average baseline intensity before photoactivation was subtracted and the initial peak intensity after photoactivation was normalized to 1. The photobleaching rate was determined by equivalent experiments in fixed cells. Cells were fixed for 15 min in 4 % paraformaldehyde immediately before the experiment. The photobleaching time constant τ_{bleach} was determined by fitting a first order exponential decay function:

$$I(t) = I_0 \cdot e^{\left(\frac{-t}{\tau_{bleach}}\right)} + I_{\text{background}}$$

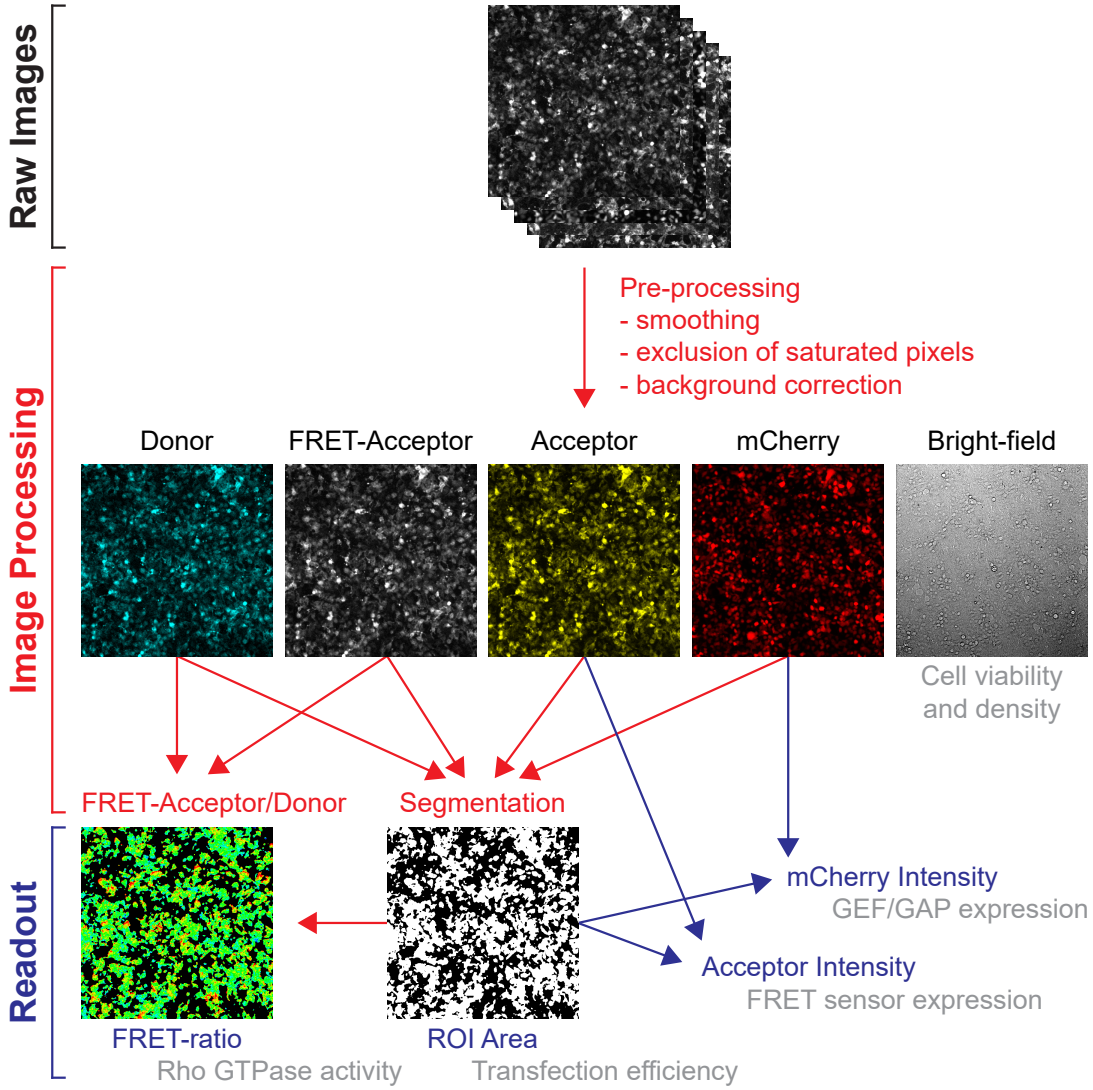

Figure 4.1 Image processing workflow of FRET-based RhoGEF and RhoGAP activity screen. Schematic workflow of automated data set processing of FRET-based RhoGEF and RhoGAP activity screen. Images were processed (red) to extract readout information (blue) about biologically relevant parameters (grey). Raw images were pre-processed and segmented to create a region of interest (ROI). Within that ROI the FRET-ratio image was generated and the average intensity of acceptor and mCherry channel were measured. FRET ratio served as a measure for relative Rho GTPase activity levels, the area of the ROI served as a readout for the transfection efficiency, and acceptor and mCherry intensity served as readout for FRET sensor and RhoGEF/RhoGAP expression levels. Where required, bright-field images were analysed for cell viability and cell density.

τ_{bleach} was then inserted as a correction parameter to fit the FLAP experiments with an exponential decay function of the n^{th}-order:

$$I(t) = I_1 \cdot e^{\left(\frac{-t}{\tau_1}\right)+\left(\frac{-t}{\tau_{bleach}}\right)} + I_2 \cdot e^{\left(\frac{-t}{\tau_2}\right)+\left(\frac{-t}{\tau_{bleach}}\right)} + ... + I_{\mathrm{n}} \cdot e^{\left(\frac{-t}{\tau_n}\right)+\left(\frac{-t}{\tau_{bleach}}\right)}$$

The lateral diffusion at the plasma membrane was assessed by plotting the full width at half maximum (FWHM) of the Gaussian distribution of the photoactivated mPAGFP intensity along the plasma membrane over time. Three consecutive images were averaged and the intensity was measured along the plasma membrane. Intensity profiles were analysed by Gaussian kernel regression using OriginPro software (OriginLab, USA). FWHM of the Gaussian kernel was plotted over time and analysed by fitting an exponential saturation function (negative exponential decay) also in OriginPro. Photobleaching and lateral diffusion in z dimension were assumed to occur homogeneously over the whole membrane and were thus ignored.

4.5.3 Single particle tracking

Single molecule time-lapse image series were obtained by TIRF microscopy with continuous illumination and 34 ms acquisition time for each image. Single particle trajectories were analysed using the "TrackMate" ImageJ plugin (Tinevez *et al.*, 2017), applying an automated particle tracking algorithm as described previously (Jaqaman *et al.*, 2008). Image segmentation to identify single molecules was achieved by fitting a Gaussian kernel to the point spread function of the diffraction-limited spots. The centroid position of the spot was tracked over time to generate trajectories of each detected spot. Based on single molecule trajectories, those molecules that underwent 2D motion were considered membrane bound and retained. Trajectories were colour coded by track duration and superimposed on the first image of the image series. Signal-to-noise ratio was calculated as described (Chenouard *et al.*, 2014).

$$SNR = \frac{I_{\mathrm{o}} - I_{\mathrm{b}}}{\sqrt{I_{\mathrm{o}}}}$$

with I_{o} denoting the peak particle intensity and I_{b} the mean background intensity

4.5.4 Line scan intensity plots

Line scans to determine fluorescence intensity profiles were generated using ImageJ software. The "plot profile" tool was used to create a graph of pixel intensity plotted over the distance along the line. To reduce noise, pixel intensity was averaged on a line width

of 3 pixels. For the Rho GTPase localisation studies the intensity was then normalized to the lowest and the highest intensity within the selection to highlight the subcellular distribution. For the localisation of Rho GTPases, RhoGEFs, and RhoGAPs on focal adhesions the intensity was normalized to the average intensity along the selection to maintain relative intensity proportions.

4.5.5 Colocalisation analysis

For the colocalisation analysis of FRET sensors and coexpressed RhoGAP the JACoP colocalisation analysis toolbox under ImageJ was used (Bolte and Cordelières, 2006). Images were taken as described above for the FRET screen (see 4.4.1). mVenus acceptor channel and mCherry channel images were background corrected and thresholded. Pearson's correlation coefficient r was calculated and Manders' coefficients M1 and M2 were calculated as the fraction of mCherry overlapping with mVenus acceptor (M1) and the fraction of mVenus acceptor overlapping with mCherry (M2).

4.6 Literature meta-analysis of RhoGEF and RhoGAP substrate specificities

Publications about RhoGEFs and RhoGAPs were identified using keyword search in UniProt and PubMed databases. Generally, all protein and gene names suggested by the UniProt database were used as keywords. The following data were extracted from publications: (1) the substrate specificity towards RhoA, Rac1, and Cdc42, (2) the applied method to determine the substrate specificity, (3) the use of full length or truncated versions of the regulators to determine the substrate specificity, (4) information about conditions that increased or decreased the activity of the regulators. Assays that detect Rho GTPase activity based on effector domain pull-down from cell lysates, based on FRET-biosensors, and based on Rho GDP/GTP thin-layer chromatography from cell lysates were classified as *in vivo* assays. Biochemical assays that directly measure the GDP/GTP exchange reaction or the hydrolysis reaction by radioactivity-based and spectroscopy-based methods with at least one recombinant protein source were classified as *in vitro* assays. The following pieces of information were categorised as indication for autoinhibitory control of RhoGEF and RhoGAP activity: Higher activity of a truncated version of a regulator compared to full length, proof of phosphorylation or kinase activity that increased regulator activity, increased regulator activity by protein-protein interaction or interaction with other components such as lipids or second messengers, and if regulator activity was higher in stimulated cells than in resting cells. The collected information about substrate specificity of RhoGEFs and RhoGAPs towards RhoA, Rac1, and Cdc42 by multiple publications was integrated to generate a silver standard and a gold standard list. Entries in the list were made for "activity" or "no activity". The requirements for an entry in the silver standard list were defined as the following: conform results from a minimum of 2 independent publications or methods, 3 conform results overruled one opposed result unless the 3 identical results were determined *in vivo* and the one opposed result was determined *in vitro* or the other way round. The requirements for an entry in the gold standard list were defined as follows: conform results from a minimum of 2 independent publications or methods covering one *in vivo* and one *in vitro* technique, 3 conform results overruled one opposed result if the net sum of activities still contained a minimum of one *in vivo* result.

4.7 Statistics

4.7.1 Precision and recall analysis

Precision and recall analysis is an approach to evaluate the performance of a method on the basis of known interactions (information from literature meta-analysis). An objective threshold that maximizes the precision and recall of the method, can then be applied to the population of uncharacterised interactions (RhoGEF and RhoGAP activity screens). Precision is a measure for the fraction of relevant instances among the retrieved instances, while recall is the fraction of relevant instances that have been retrieved over the total amount of relevant instances:

$$Precision = \frac{TP}{TP+FP}$$

$$Recall = \frac{TP}{TP+FN}$$

Here, these parameters were defined as: *TP*: activity in meta-analysis and activity in RhoGEF or RhoGAP screen; *FP*: no activity in meta-analysis but activity in RhoGEF or RhoGAP screen; *FN*: activity in meta-analysis but no activity in RhoGEF or RhoGAP screen. Precision and recall were plotted at different thresholds in order to visualise relationship between precision and recall for any given threshold. The objective threshold benchmark for the RhoGEF or RhoGAP activity screens was defined as highest possible recall and precision rate and read from the intersection of precision and recall curves. Precision and recall analysis was performed with the help of Evangelia Petsalaki (EMBL-EBI, Hinxton).

4.7.2 Correlation analysis

Correlation analysis between two readout parameters of the RhoGEF or RhoGAP activity screen data was performed by calculation of Pearson's correlation coefficient. Pearson's r retrieved from linear regression analysis of indicated plots using OriginPro software (OriginLab, USA). r = -0.3 to 0.3 was categorised as no correlation, r = 0.3 to 0.5 or r = -0.3 to -0.5 was categorised as low correlation, and r = 0.5 to 0.7 or r = -0.5 to -0.7 was categorised as moderate correlation (Mukaka, 2012).

4.7.3 Significance analysis

4.7.3.1 Student's t-tests

Statistical analysis between two sets of data was performed with unpaired Student's t-test. Generally, significance was defined as 95 % confidence level and significance levels were generally classified as *** $p < 0.001$, ** $p < 0.01$, * $p < 0.05$. Error bars in all graphs depict standard deviation.

4.7.3.2 Benjamini-Hochberg procedure

For the calculation of significance of the RhoGEF or RhoGAP activity screen data the Benjamini-Hochberg procedure was used as a multiple testing correction. p values were calculated by unpaired Student's t-test as described and ordered from lowest to highest. The global significance level α_{g} was set to 0.05 and the local α_{i} was defined as

$$\alpha_{\mathrm{i}} = \frac{\alpha_{\mathrm{g}}}{k} \cdot i$$

with $i = 1,...,k$ and $k =$ the total number of tests. Each p value got assigned its local α_{i} significance level and the null hypothesis was rejected for all $p \leq \alpha_{\mathrm{i}}$. The first $p > \alpha_{\mathrm{i}}$ marks the point from which on all null hypotheses are not rejected.

5 Results

5.1 Subcellular localisation of Rho GTPases and its regulation by RhoGDI

5.1.1 Rho GTPases bind to membranes through their hypervariable region

Rho GTPase activity at cellular membranes has been shown to be regulated in micrometre space on a seconds to minutes time scale during localised cytoskeletal signalling responses such as lamellipodia protrusion and retraction movements, invadopodia formation and phagocytosis (Hoppe and Swanson, 2004; Machacek *et al.*, 2009; Bravo-Cordero *et al.*, 2011; Martin *et al.*, 2016). However, how such spatially confined Rho GTPase activity pools are achieved and maintained is not known. I therefore first investigated signals that control Rho GTPase membrane targeting and the stability of Rho GTPase residence in confined membrane regions.

5.1.1.1 Overexpressed Rho GTPases localise in the cytosol and at membranes

Classical Rho GTPases consist of a conserved G-domain and a hypervariable region (HVR) (Figure 5.1A). The G-domain is responsible for guanine nucleotide binding and most protein-protein interactions, whereas the HVR which undergoes extensive posttranslational modification is responsible for RhoGDI and membrane binding. Membrane association of Rho GTPases is regulated by two main C-terminal signals: a geranylgeranyl lipid moiety and the adjacent polybasic region. These signals thermodynamically target the GTPases to membranes. To get an initial idea of where the canonical Rho GTPases RhoA, Rac1, and Cdc42 localise in cells, I overexpressed N-terminally fluorescent protein tagged versions of these three Rho GTPases in HeLa cells and assessed their subcellular localisation by confocal microscopy (Figure 5.1B). RhoA localised mostly in the cytosol, whereas Rac1 and Cdc42 resided both in the cytosol and on the plasma membrane, as evident from colocalisation with the plasma membrane marker mCherry-KRas-HVR (Hancock *et al.*, 1990, 1991). This construct comprises the HVR of KRas and is targeted to the plasma membrane by its farnesyl moiety and polybasic region in a PDEδ and Arl2-dependent manner (Schmick *et al.*, 2014).

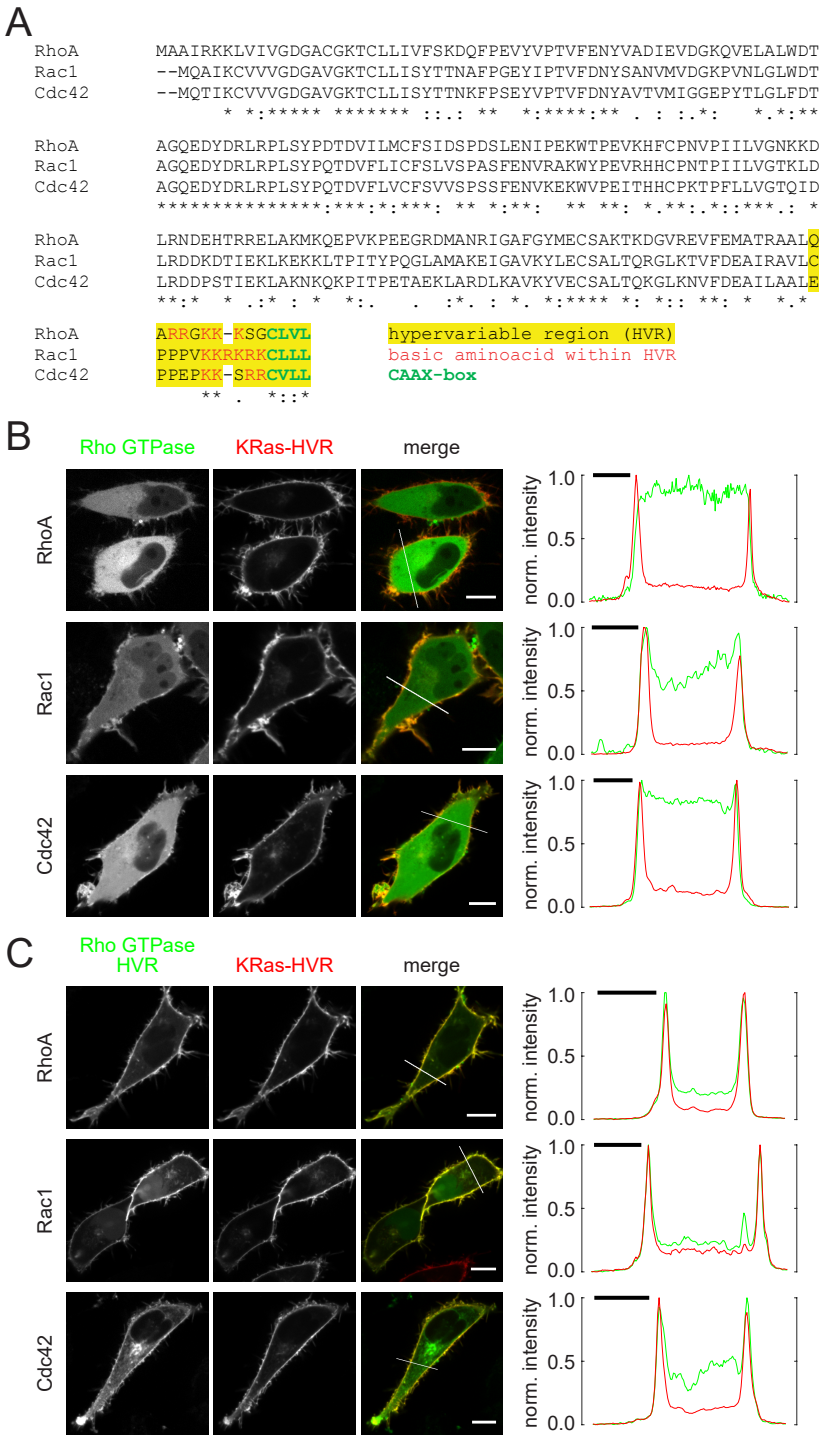

Figure 5.1 Overexpressed Rho GTPases localise in the cytosol and at membranes. (**A**) Sequence alignment of the amino acid sequence of the Rho GTPases RhoA, Rac1, and Cdc42. HVR is highlighted in yellow, basic amino acids within the HVR are marked in red, the CAAX-box is highlighted in green characters. Asterisks (*) mark conserved residues, colons (:) indicate conservation between residues of strongly similar properties, periods (.) indicate conservation between residues of weakly similar properties. (**B+C**) The full length Rho GTPases mCitrine-RhoA, mCitrine-Rac1, and mCitrine-Cdc42 (**B**) or truncations of Rho GTPases comprising the HVR mCitrine-RhoA-HVR, mCitrine-Rac1-HVR, and mCitrine-Cdc42-HVR (**C**) were overexpressed at low levels in HeLa cells together with mCherry-KRas-HVR as a plasma membrane marker. 16 h post transfection images were collected by live cell spinning disk confocal microscopy. Line scan fluorescence intensity profiles on the right show normalised intensities across the white line in the merged images. White scale bars in images: 10 μm. Black scale bars in graphs: 5 μm

5.1.1.2 Rho GTPases are targeted to membranes by their hypervariable region

In order to investigate intrinsic subcellular targeting signals encoded by the Rho GTPases RhoA, Rac1, and Cdc42, I created truncation constructs that just comprise their HVR. Interestingly, the information encoded in this short sequence was sufficient to target the constructs to the plasma membrane (Figure 5.1C). The HVR of Cdc42 was also enriched on perinuclear endomembranes, whereas RhoA and Rac1 only showed minor perinuclear localisation. In contrast to full length Rho GTPases, the HVR constructs did not accumulate in the cytosol. This is due to the fact that they can no longer bind to and become solubilised by RhoGDI (data not shown). However, the fact that RhoGDI- and PDEδ-binding deficient HVR constructs of Rho GTPases are enriched at the plasma membrane is interesting, since plasma membrane localisation of the farnesylated KRas-HVR has been shown to depend on binding to its GDI-like solubilising factor PDEδ (Chandra *et al.*, 2012; Schmick *et al.*, 2014).

5.1.1.3 Rho GTPase membrane binding stability is determined by their hypervariable region

To understand if Rho GTPases themselves provide membrane binding stability by their intrinsic membrane targeting signals on a time scale that is required for cell physiological processes, I initially applied a plasma membrane localised fluorescence loss after photoactivation (FLAP) approach. Here, a small fraction of photoactivatable green fluorescent protein (mPAGFP)-labelled Rho proteins (Patterson and Lippincott-Schwartz, 2002) is locally photoactivated at the plasma membrane in a 1 μm spot (Yokoe and Meyer, 1996). Spatial signal spread and signal loss are then recorded at high temporal resolution (Figure 5.2A and B). The signal decay of Rho GTPases could be best described by a third order exponential function, which indicates that multiple processes with different time constants contribute to the diffusion of Rho GTPases (Figure 5.2C). Interestingly, I could show that plasma membrane binding of Rho proteins is highly dynamic and that the half-life of confined membrane residence in this spatial scale is in the subsecond range. Importantly, the presence of the G-domain did not alter the half-life of membrane residence as the diffusion behaviour of full length Rho GTPases was indistinguishable from constructs that just comprise their HVR (Figure 5.2D). Together this raises the fundamental question of how localised Rho GTPase signalling is achieved and maintained over longer time scales in cells.

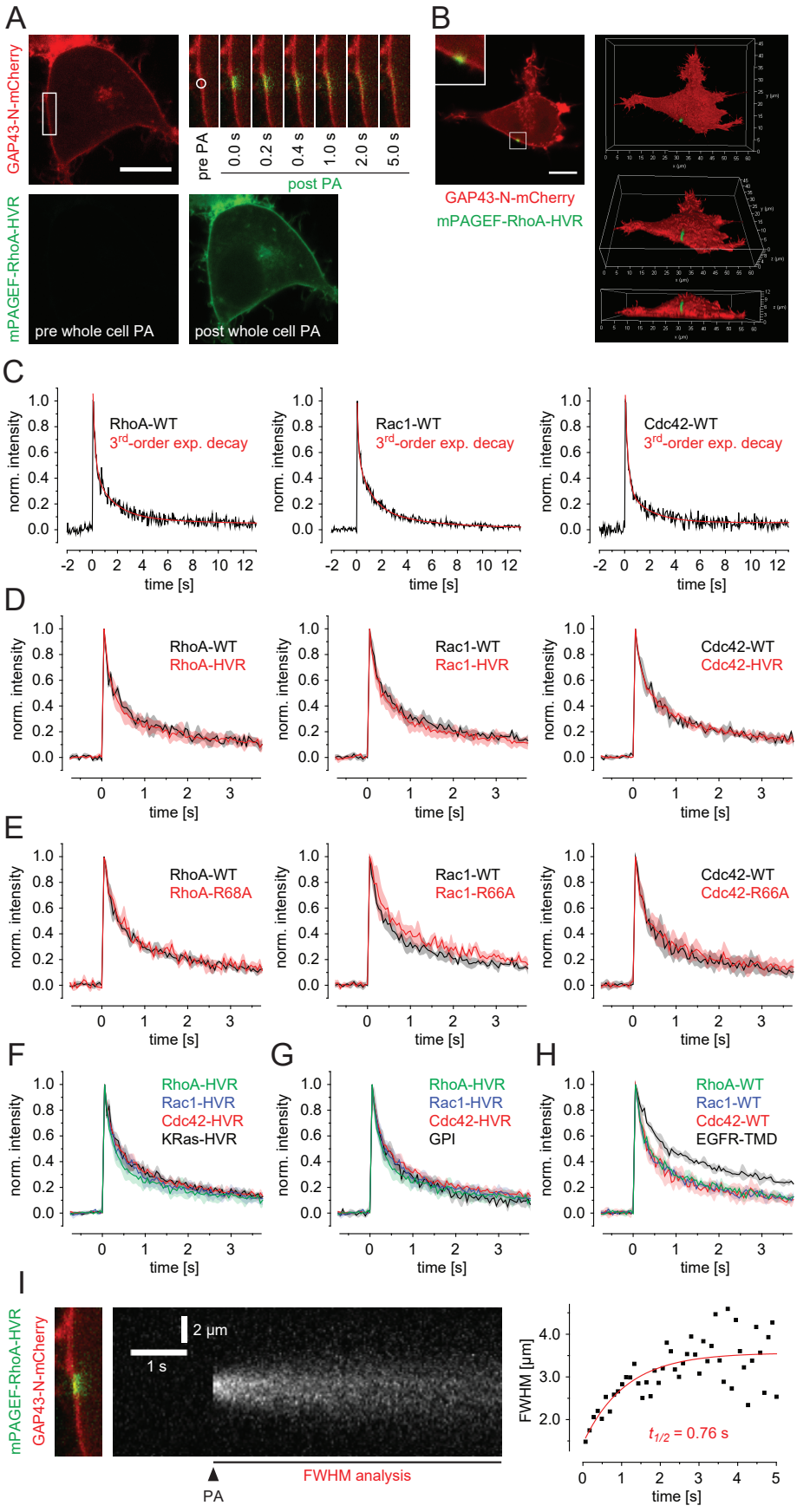

Figure 5.2 see next page

Figure 5.2 (continued) Investigation of Rho GTPase membrane binding stability by a localised FLAP assay. (**A**) mPAGFP-RhoA-HVR and a plasma membrane marker (GAP43-N-mCherry) were expressed in HeLa cells. Cells were subjected to FLAP by confocal microscopy. A small fraction of mPAGFP-RhoA-HVR was photoactivated (PA) in a 1 μm area by a short 405 nm laser pulse localised at the plasma membrane and its intensity decay was recorded over time. Region indicated by the white box is magnified on the right. Below the mPAGFP-RhoA-HVR signal is shown before and after photoactivation of the whole cell. (**B**) Same treatment as in (A), with the difference that cells were fixed before photoactivation of a 1 μm region at the plasma membrane. Image on the left shows a confocal slice of the central region of the cell. Image on the right shows cell surface representations of a 3D reconstruction from z-stacks through the whole cell from three different viewing angles. White scale bar: 10 μm. (**C**) Photoactivation of mPAGFP-RhoA, mPAGFP-Rac1, and mPAGFP-Cdc42 as in (A). Normalised intensity of the photoactivated area is shown over time. Timepoint of photoactivation was set to 0 s. Intensity values after photoactivation were fitted by a third order exponential decay function corrected for photobleaching. (**D-H**) FLAP experiments as in (A,C) of constructs as indicated in the graphs. Each curve shows average of n = 3 cells and standard deviation. (**I**) Same cell as in (A). On the left the photoactivation spot at the plasma membrane is shown. In the center a kymograph of the mPAGFP-RhoA-HVR intensity along the plasma membrane is shown before and after photoactivation (PA). Graph on the right shows plot of full width at half maximum (FWHM) of Gaussian fits of the mPAGFP intensity along the plasma membrane over time, to reduce noise of the intensity profile, three consecutive images were averaged for each Gaussian fit. Red line shows exponential saturation function fit and the corresponding half life.

5.1.2 RhoGDI is a major regulator of Rho GTPase localisation

Having confirmed the dynamic nature of Rho GTPase membrane residence, I further analysed the effect of RhoGDI on Rho GTPase localisation and its contribution to the short lived nature of Rho GTPase membrane residence time.

5.1.2.1 RhoGDI extracts Rho GTPases from membranes

RhoGDI has a strong and complex impact on Rho GTPase function, all based on its ability to bind and solubilise the GTPases. It balances the homeostasis of Rho signalling by indirectly affecting activity, folding and degradation, as well as Rho GTPase shuttling (Boulter *et al.*, 2010; Garcia-Mata *et al.*, 2011). In order to describe the effect of RhoGDI on the steady state localisation of Rho GTPases, I cooverexpressed RhoA, Rac1, and Cdc42 with and without RhoGDI in HeLa cells and observed their localisation relative to the plasma membrane marker KRas-HVR by confocal microscopy. I could show that all three Rho GTPases relocalised to the cytosol in the presence of excess RhoGDI (Figure 5.3). To control if this effect is direct, I used RhoGDI binding-deficient versions of the Rho

GTPases. The binding of arginine 66 (Rac1 and Cdc42 numbering) of the canonical switch II region of Rho GTPases to RhoGDI is an important feature of bridging and stabilising the two domains of RhoGDI. The guanidinium group of arginine forms 3 hydrogen bonds to residues within 2 different domains of RhoGDI and on top the aliphatic potion of arginine undergoes hydrophobic interactions with 3 residues from 2 different domains (Hoffman *et al.*, 2000). Therefore, arginine 66 (Rac1 and Cdc42 numbering) or 68 (RhoA numbering) is a key residue within the GTPase-RhoGDI interface. Mutations of this arginine residue to glutamate or alanine block the binding to RhoGDI (Gibson and Wilson-Delfosse, 2001; Lin *et al.*, 2003; Gandhi *et al.*, 2004). The Rho GTPase binding deficient mutants RhoA-R68A, Rac1-R66A and Cdc42-R66A localised on membranes and a cytosolic signal could not be detected when compared to wild type Rho GTPases (Figure 5.4A). As expected, the RhoGDI binding-deficient mutants RhoA-R68A, Rac1-R66A, and Cdc42-R66A were unable to get solubilised by three-fold excess RhoGDI (Figure 5.4B) and showed a similar localisation as wild type Rho GTPases in cells which were depleted of RhoGDI (data not shown). I further confirmed the inability of the Rho GTPase mutants RhoA-R68A, Rac1-R66A and Cdc42-R66A to bind to RhoGDI by co-immunoprecipitation (Appendix Figure 7.1). Together, these experiments show that the cytosolic pool of Rho GTPases depends on their binding to RhoGDI and that Rho GTPases reside at membranes in the absence of RhoGDI.

5.1.2.2 RhoGDI has no direct effect on Rho GTPase membrane binding stability

Given the important role of RhoGDI in solubilisation of Rho GTPases, I asked if and to what extent RhoGDI would contribute to the rapid signal loss as observed during FLAP experiments of Rho GTPases (see 5.1.1.3). However, the fact that the diffusion behaviour of a construct comprising only the HVR of Rho GTPases did not significantly differ from that of the full length Rho GTPases already indicated that RhoGDI does not actively contribute to membrane desorption of Rho GTPases (Figure 5.2D). By comparing the membrane localisation stability of wild type Rho GTPases to that of RhoGDI binding-deficient mutants, I could show that the half-life of membrane residence of the two did not differ for RhoA and Cdc42 and was only marginally prolonged for Rac1-R66A (Figure 5.2E). This suggests that RhoGDI-mediated membrane extraction is not the main reason for the rapid signal loss and that most likely RhoGDI does not actively extract Rho GTPases from membranes. However, the fast kinetic of Rho GTPase residence time in confined regions of the plasma membrane was most likely due to rapid lateral diffusion. This is supported by the fact that Rho GTPase diffusion at the plasma membrane was sim-

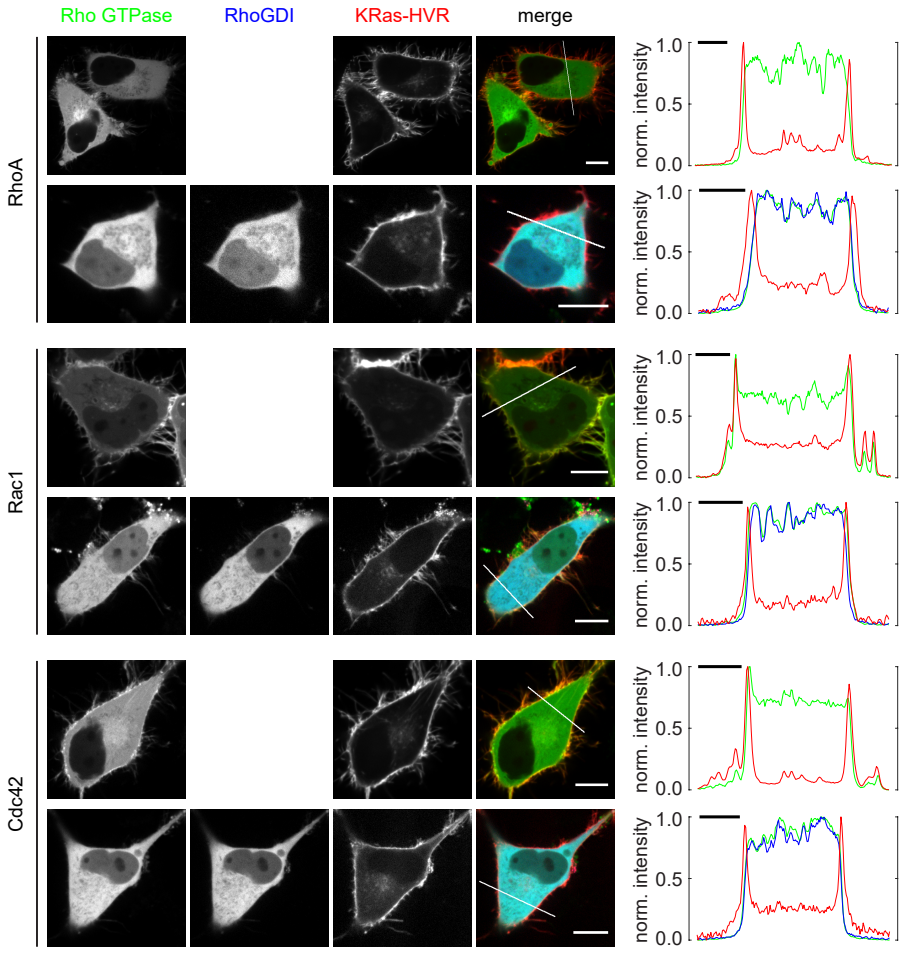

Figure 5.3 RhoGDI extracts Rho GTPases from membranes and colocalises with them in the cytosol. mCitrine-RhoA, mCitrine-Rac1, and mCitrine-Cdc42 were expressed at low levels with and without three-fold excess RhoGDI-mCherry in the presence of the plasma membrane marker miRFP670-KRas-HVR in HeLa cells. 16 h post transfection images were collected by live cell spinning disk confocal microscopy. Line scan fluorescence intensity profiles on the right show normalised intensities across the white lines in the merged images. White scale bars in images: 10 μm. Black scale bars in graphs: 5 μm

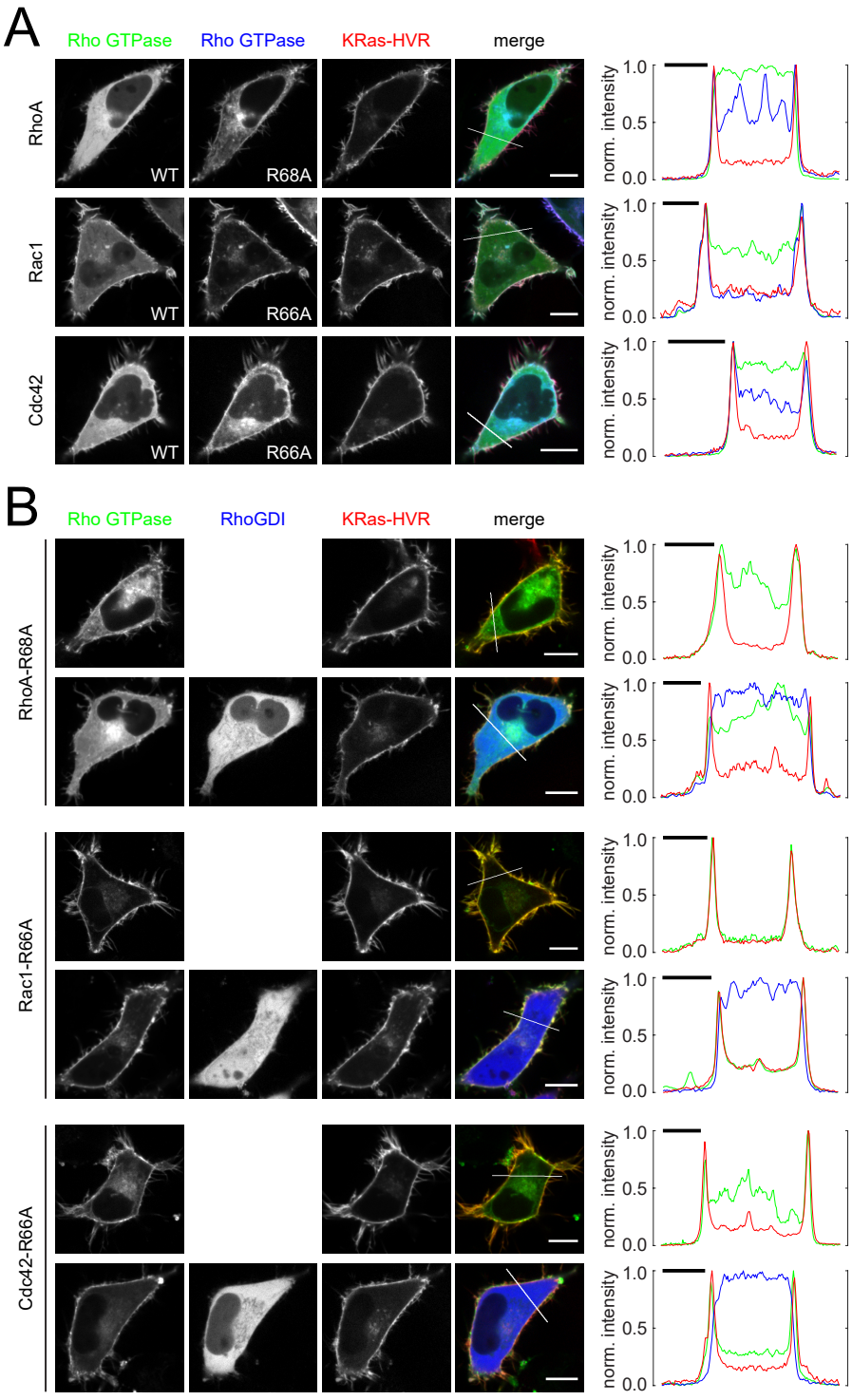

Figure 5.4 RhoGDI binding-deficient Rho GTPases localise at membranes. (**A**) mCitrine-RhoA, mCitrine-Rac1, and mCitrine-Cdc42 were expressed at low levels together with mCherry-RhoA-R68A, mCherry-Rac1-R66A, and mCherry-Cdc42-R66A in the presence of the plasma membrane marker miRFP670-KRas-HVR in HeLa cells. (**B**) mCitrine-RhoA-R68A, mCitrine-Rac1-R66A, and mCitrine-Cdc42-R66A were expressed at low levels with and without three-fold excess RhoGDI-mCherry in the presence of the plasma membrane marker miRFP670-KRas-HVR in HeLa cells. (**A**+**B**)16 h post transfection images were collected by live cell spinning disk confocal microscopy. Line scan fluorescence intensity profiles on the right show normalised intensities across the white line in the merged images. White scale bars in images: 10 μm. Black scale bars in graphs: 5 μm

ilar to other lipid-anchored probes, such as KRas-HVR and a glycosylphosphatidylinositol (GPI)-anchored probe (Sharma *et al.*, 2004) in the exoplasmic leaflet (Figure 5.2F and G) and faster than that of an artificial transmembrane construct comprising an epidermal-growth-factor-receptor transmembrane domain fused to mPAGFP (EGFR-TMD) (Figure 5.2H). Transmembrane domain-anchored proteins have been shown before to diffuse slower in the plasma membrane than lipid anchored proteins (Meder *et al.*, 2006). I could further confirm that lateral diffusion is rapid, by analysing the lateral spreading of the photoactivated fraction of probes along the plasma membrane. Therefore, the intensity distribution of the mPAGFP signal of RhoA-HVR along the plasma membrane was fitted to a Gaussian function and the full width at half maximum, a measure for the width of the Gaussian function, was plotted against the time. This analysis reviled a half life of 0.76 s (Figure 5.2I), indicating that the explanatory power and the interpretability of processes which have a slower kinetic than the rapid lateral of the FLAP assay is limited.

Together, I showed that local Rho protein pools at the plasma membrane dissipate over time by rapid lateral diffusion and other processes potentially involving membrane desorption. This indicates that Rho GTPase activity is during Rho signalling events concentrated by yet unknown mechanisms. The investigation of these processes by means of the FLAP assay is limited and requires sophisticated techniques.

5.1.3 Establishment of a Rho GTPase single molecule tracking approach

The above experiments suggest that the localisation of Rho GTPases to confined regions of the plasma membrane is not *per se* static as required for compartmentalised cell physiological processes, but instead subject to highly dynamic multidimensional processes (see 5.1.1.3). However, detailed kinetics of Rho protein membrane binding and diffusion and its control by RhoGEFs, RhoGAPs, RhoGDI and effector proteins cannot be further resolved by means of classical microscopic and biochemical techniques. These techniques are based on bulk protein analysis and thus monitor the sum of all individual underlying processes which limits their ability to segregate the kinetics of each of these processes. I therefore set out to establish an imaging approach to precisely monitor the membrane binding dynamics of Rho GTPases and its regulation in living cells without the need of protein overexpression.

Single particle tracking (SPT) is a highly sensitive fluorescence microscopy technique that provides information on the localisation of individual proteins in living cells, thereby

allowing a complete statistical characterization of the system under study. In the context of Rho GTPase membrane binding and residence, SPT is capable of visually resolving all relevant diffusion processes, namely lateral diffusion, immobilisation, and membrane dissociation, that otherwise cannot be segregated by any other currently available technique. I therefore aimed to establish a SPT assay that can be applied in the future to study Rho GTPase membrane binding dynamics and its regulation in detail.

Total internal reflection fluorescence (TIRF) microscopy is a camera-based microscopic technique that allows visualisation of fluorescent molecules at exceptional signal-to-noise ratio (SNR). This is achieved by creation of an evanescent wave along the glass-water interface by total internal reflection of the excitation light beam. The electric field of the evanescent wave decays exponentially from the interface, and thus penetrates to a depth of only approximately 100 nm into the water. Thereby, the evanescent wave selectively illuminates molecules that are within a thin volume near the glass-coverslip surface but not those that are deeper in solution. When cells are grown on the coverslip only molecules that reside at the lower plasma membrane or in very close proximity to the plasma membrane are excited. The exceptional signal-to-noise ratio of TIRF microscopy combined with highly sensitive scientific cameras allows the detection of individual fluorescent molecules.

SPT requires low concentrations of labelled protein in order to be able to distinguish individual molecules from each other when observed by diffraction limited light microscopy, such as TIRF microscopy. To this end, I employed the Tet-On tetracycline-controlled transcriptional activation system. In principle, this method is designed to reversibly turn on and off gene expression in the presence or absence of the antibiotic tetracycline or its derivative doxycycline (Gossen *et al.*, 1995). Here, I took advantage of the leakiness of the Tet-On promoter in the absence of the transcriptional activator to obtain minimal background expression levels of Rho protein probes as required for single molecule observation. At first, I compared background expression of first, second, and third generation of Tet-On promoters in the absence of doxycycline (Loew *et al.*, 2010). I found that the third generation Tet-On promoters yielded lowest expression levels of Rho GTPase probes which were ideal for single molecule observation in Tet-On HeLa cells (Weidenfeld *et al.*, 2009).

The purpose of SPT is to follow the motion of single molecules in space over time. These single molecule trajectories can then be analysed in order to extract quantitative information about their diffusion behaviour, such as modes of motion, heterogeneities in

the motion, diffusion coefficient and, in combination with TIRF microscopy, membrane residence time. The time duration of single molecule trajectories is ultimately limited by photobleaching of the fluorophore label which may not withstand long lasting illumination at high frequency. In order to faithfully report the membrane residence time of Rho GTPases, the SPT assay critically requires full control of photobleaching. This is crucial in order to be able to differentiate between Rho GTPase membrane dissociation and photobleaching events which both appear as disappearance of the single particle signal in TIRF microscopy. Genetically encoded fluorophores are highly susceptible to photobleaching and therefore not suitable for SPT on longer time scales. In order to be able to perform SPT on a time scale of tens of seconds I decided to use the SNAP-tag-based self labelling technique which allows site-specific labelling of cellular proteins in living cells with organic fluorescent dyes (Keppler *et al.*, 2003; Lukinavičius *et al.*, 2015). These dyes exhibit superior photostability and SNR compared to fluorescent proteins (Sun *et al.*, 2011; Toseland, 2013). This allows imaging with low laser power and short exposure times for long time periods.

However, as organic fluorescent dyes are still susceptible to photobleaching, although at low rates, I first established a system to precisely determine the photobleaching rates. In principle this can be accomplished *in vitro* by simply imaging single fluorophores that have settled on a glass coverslip. However, this way, the obtained photobleaching rates do not reflect the real *in vivo* situation. Photobleaching can be considered an irreversible loss of its ability to fluoresce due to photochemical modification of the dye. The main cause seems to involve photodynamic interactions between excited fluorophores and molecular oxygen or other intracellular components such as proteins and lipids (Diaspro *et al.*, 2006). As the number of photons emitted before a dye molecule is destroyed depends both on the nature of the dye molecule itself and on its environment, photobleaching inside cells can be considered to occur at substantially different rates than in the cell culture medium. Furthermore, variability in the photobleaching process has been demonstrated within individual cells (Benson *et al.*, 1985).

To precisely determine photobleaching rates of single molecules at the plasma membrane in the cellular environment, I established a method to immobilise the SNAP-fluorophore in living cells using an engineered transmembrane protein. To this end I immobilised an anti-GFP capture antibody by covalent linkage to epoxysilan coated glass slides. The antibody extracellularly binds the transmembrane protein at the lower plasma membrane of cells (Figure 5.5E). This “artificial receptor” was composed of an extracellular N-terminal mEGFP, a membrane spanning transmembrane domain of the epidermal-growth-factor-

receptor (EGFR-TMD) (Meder *et al.*, 2006) and a C-terminally fused intracellular SNAP-tag. I confirmed the functionality of the transmembrane protein and its ability to localise correctly in the plasma membrane by replacing the mEGFP with the pH sensitive GFP variant ecliptic pHluorin (e-pHluorin) (Miesenböck *et al.*, 1998). Fluorescence of e-pHluorin is still high in the endoplasmic reticulum and gets dimmer throughout the endocytic pathway as pH decreases (Paroutis *et al.*, 2004). Once it reaches the extracellular space with a physiological pH of 7.4 in the cell culture medium, its fluorescence is fully restored. By lowering the pH in the cell culture medium I could show that fluorescence of e-pHluorin was lost at the plasma membrane but conserved inside the cell. This confirmed the correct cotranslational insertion of this construct into the endoplasmic reticulum and its correct targeting to the plasma membrane (Appendix Figure 7.2A). Furthermore, I confirmed colocalisation of the mEGFP signal with the signal from the Tetramethylrhodamine (TMR) labelled SNAP-tag (Appendix Figure 7.2B). Subsequently, I studied the ability of the engineered transmembrane receptor to become immobilised by the extracellular capture antibody. I confirmed that antibody binding to epoxysilan coated glass slides was stable by fluorescence recovery after photobleaching (FRAP) experiments (Appendix Figure 7.3A). FRAP is a method to determine the kinetics of diffusion and to discriminate between mobile and immobile fractions of the labelled probe by quantifying the fluorescence recovery within a confined photobleached region (Ishikawa-Ankerhold *et al.*, 2012). The FRAP experiments showed that virtually all antibodies were immobile. Furthermore, out of four different anti-GFP antibodies I selected the one with the highest GFP labelling efficiency and immobilisation rate as determined by FRAP experiments (Appendix Figure 7.3B, two antibodies performed badly and are not shown). Next, I seeded HeLa Tet-On cells, which expressed the engineered transmembrane receptor by leaky expression, on anti-GFP decorated epoxysilan glass slides. Importantly, I could show that immobilisation of the receptor in these cells was stable on a time scale of minutes, as evident from exact congruence of the immobilised mEGFP signal over a time lag of 2 min (Figure 5.5A). When the SNAP-tag was labelled with a TMR substrate, I could correlate signals of mEGFP and SNAP-TMR from individual "artificial receptors" (Figure 5.5B). I could furthermore identify single molecule photobleaching steps of individual SNAP-TMR molecules in these cells (Figure 5.5C).

Eventually, a proof of principle tracking experiment with a TMR labelled SNAP-KRas-HVR construct revealed high quality tracks with remarkable SNR of 41.4 ± 16.3 (Figure 5.5D) given that a SNR of 4 has been shown to be a critical level (Cheezum *et al.*, 2001; Chenouard *et al.*, 2014).

Together, these experiments show that SPT by means of organic dyes is a promising approach to track Rho GTPases at the plasma membrane with high SNR and low exposure times. Together with the precise "artificial receptor" based photobleaching control this assay will enable long-time visualisation of Rho GTPase membrane interactions and membrane residence times, as well as their modulation by up- and downstream interactors. By detecting Rho GTPases at the single molecule instead of bulk protein level, I overcame the limitation of existing assays of not being able to dissect processes of Rho GTPase diffusion at the plasma membrane. I thus provides the groundwork for future studies to gain detailed insights into how Rho GTPase binding to the plasma membrane is regulated and organised.

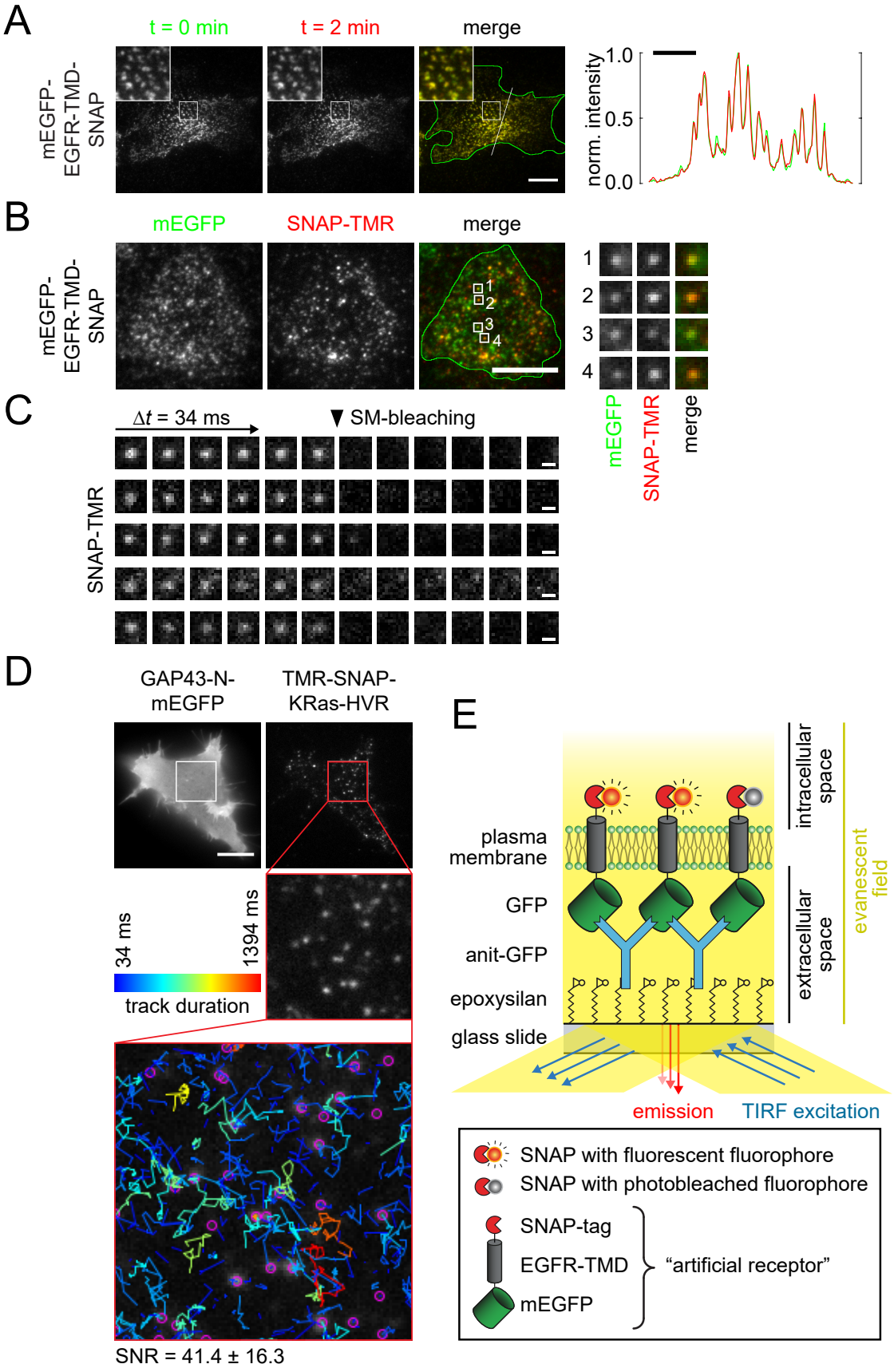

Figure 5.5 see next page

Figure 5.5 (continued) Establishment of a SPT assay with precise photobleaching control. (**A-C**) mEGFP-EGFR-TMD-SNAP was expressed in HeLa Tet-On cells by leaky expression. 16 h post transfection cells were transferred to anti-anti-GFP decorated epoxysilan glass slides and allowed to adhere for 4 h. Images were acquired by TIRF microscopy. (**A**) mEGFP images were acquired with a time interval of 2 min. Inset on the upper left of each image represents a three-fold magnification of the area indicated by the white box. Green line in merged image indicates cell outline. Line scan fluorescence intensity profiles on the right shows normalised intensities across the white line in the merged image. White scale bar in image: 10 μm. Black scale bar in graph: 5 μm (**B**) Before transfer on capture antibody decorated glass slides cells were labelled with 0.1 μM SNAP-Cell TMR-Star for 1 h. Green line in merged image indicates cell outline. Magnification of white boxes in the merged image are shown on the right. White scale bar: 10 μm. (**C**) Time courses of single molecule photobleaching from individual SNAP-TMR fluorophores from cell in (B). White scale bars: 500 nm. (**D**) SNAP-KRas-HVR was expressed in HeLa Tet-On cells by leaky expression together with the overexpressed plasma membrane and Golgi complex marker GAP43-N-mEGFP. Cells were labelled with 0.1 μM SNAP-Cell TMR-Star for 1 h. mEGFP image was collected by epifluorescence microscopy, TMR-SNAP-KRas-HVR images time course was acquired by TIRF microscopy with a frame rate of 30 Hz. Time course was subjected to SPT analysis and SNR was calculated for tracked particles. Single particle tracks are colour coded by track length as indicated by colour code bar. White scale bar: 10 μm. (**E**) Scheme of the fluorophore immobilisation assay inside living cells as applied for photobleaching control. Anti-GFP antibodies are covalently immobilised on epoxysilan coated glass slides. The "artificial receptor", composed of mEGFP, a EGF-receptor transmembrane domain (EGFR-TMD) and a SNAP-tag, immobilises the SNAP-tag labelling fluorophore inside the cell. The correlation of signals from mEGFP and labelled SNAP tags allows the precise determination of photobleaching events from individual molecules.

5.2 Systematic analysis of RhoGEF and RhoGAP activities

5.2.1 RhoGEF and RhoGAP expression library

In order to systematically analyse the localisation and activity of all mammalian RhoGEFs and RhoGAPs, we created an expression library of full length cDNAs of 141 RhoGEFs and RhoGAPs in the lab. The cDNA library was cloned into a modified Creator recombination system (Colwill *et al.*, 2006). This recombination system is based on the Cre recombinase from the bacteriophage P1 and its recognition sequence *loxP* (Sternberg *et al.*, 1981). This site-specific DNA recombination technology is well known for its application in conditional mutagenesis in mice but can also be used *in vitro* for rapid recombination and shuttling of cDNAs between vectors. Our library includes 64 potential Dbl family RhoGEFs, all 11 DOCK family RhoGEFs, 64 RhoGAP domain-containing proteins and 2 proteins with dual RhoGEF/RhoGAP function. In this work I used expression constructs of RhoGEFs and RhoGAPs, which were N-terminally tagged with mCitrine or mCherry[1] (Griesbeck *et al.*, 2001; Zacharias *et al.*, 2002; Shaner *et al.*, 2004). Expression and localisation of all constructs were confirmed by co-expression of mCitrine- and mCherry-labelled constructs and colocalisation analysis. Molecular cloning experiments were performed with support of Lennart Brandenburg, Marlies Grieben, and Juliane Rademacher.

5.2.2 Establishment of a screening-compatible FRET-based Rho GTPase activity assay

RhoGEFs and RhoGAPs critically contribute to context-specific regulation of Rho GTPase activity. They activate Rho GTPases in a stimulus-dependent, spatio-temporally-regulated and substrate-specific manner (Schmidt and Hall, 2002; Rossman *et al.*, 2005; Tcherkezian and Lamarche-Vane, 2007). However, the substrate specificity is not known for all RhoGEFs and RhoGAPs, and thus how they are linked to their downstream signalling pathways. Moreover, RhoGEF and RhoGAP substrate specificities have never been investigated in a systematic and comprehensive manner but is only known from individual studies using different methods and applying different experimental standards (see 5.2.3). Therefore, I set out to use our RhoGEF and RhoGAP expression library to systematically analyse the substrate specificity of all regulators towards the three canonical Rho GTPases RhoA, Rac1, and Cdc42.

Such a comprehensive analysis required a reliable and robust method. The method of choice would have to be quantitative, screening-compatible, and be able to cope with full length RhoGEFs and RhoGAPs at low cost of time and material. Established *in vitro*

[1] at the time of writing the mCherry- and mCitrine-tagged versions of DOCK1, DOCK10, DOCK11 and ARHGAP42 were not yet successfully cloned

approaches typically utilise labelled guanosine nucleotides to monitor either the GDP-GTP exchange reaction in the presence of a GEF or the GTP hydrolysis and release of the inorganic phosphate product in the presence of a GAP. *In vivo* methods are typically based on the "pull-down" principle. They rely on the selective isolation of active GTPases via their high affinity to effector proteins, followed by immunoassay-based quantification techniques. While these established assays operate well with small sample numbers, the requirements of the workflow in order to obtain consistent results would not allow processing of large sample numbers due to susceptibility to variations in GTP/GDP levels by intrinsic Rho GTPase hydrolysis rates. Furthermore, established methods to determine activity levels of Rho GTPases suffer from cost of time, requiring large amount of sample, as well as methodological inaccuracy and are therefore not suitable for high throughput screening formats. Therefore, at first I established an assay that fulfils these essential criteria.

In consideration of the stringent requirements, the measurement of Rho GTPase activity levels in living cells by means of FRET-biosensors was a promising approach to assess the substrate specificity of RhoGEFs and RhoGAPs in a high throughput compatible manner. The transfection of HEK293T cells in a 96-well format with high transfection efficiency was a prerequisite to standardise the conditions. Programmable automated live cell microscopy, EMCCD-camera-supported fast image acquisition and subsequent automated image analysis using self-written customised software scripts accelerated the throughput in order to cope with the large number of conditions and minimise sample-to-sample and day-to-day variations.

However, Rho GTPase FRET biosensors in general and in particular the second generation sensors RhoA-2G, Rac1-2G, and Cdc42-2G which I employed (Fritz *et al.*, 2013, 2015; Martin *et al.*, 2016) were not purposefully designed to reflect the Rho GTPase activity levels of large populations of cells, but rather to visualise the relative distribution of Rho GTPase activity within single cells. I thus first performed a comprehensive set of stringent control experiments to establish the suitability of the Rho GTPase FRET sensors for a microscopic assay in a high throughput live cell screening format. I thoroughly tested their reliability and I elaborated conditions for ideal performance of the biosensors.

5.2.2.1 FRET biosensors report all states of the Rho GTPase activity cycle

At first, I tested if the FRET biosensors can report all states of the Rho GTPase activity cycle (Figure 2.2) and their modulation by RhoGEFs, RhoGAPs and RhoGDIs in living cells. When expressed on its own, the activity level reported by the FRET sensor is high. This is because the endogenous cellular RhoGDI concentration is not sufficient to prevent sensor

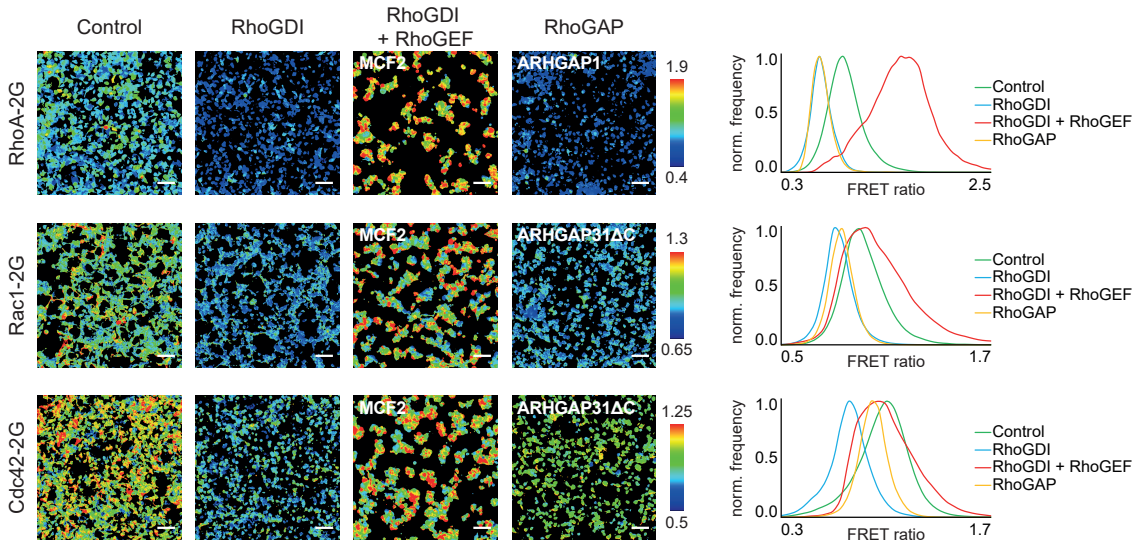

Figure 5.6 FRET biosensors report all states of the Rho GTPase activity cycle. RhoA-2G, Rac1-2G, and Cdc42-2G FRET sensors were transiently expressed in HEK293T cells together with mCherry (Control), RhoGDI or RhoGEFs and RhoGAPs as indicated. Low magnification microscopic images were taken in donor channel and FRET-acceptor channel. Images show the FRET ratio calculated as the ratio of background-corrected FRET-acceptor channel by donor channel images. Images were normalised to average FRET ratio of the control for each sensor and false colour coded according to the colour scale bar. Histograms on the right show the FRET ratio distribution of the images. Scale bars: 100 μm.

accumulation at membranes, where it is rapidly activated by endogenous RhoGEFs (Pertz *et al.*, 2006; Boulter *et al.*, 2010). Accordingly, FRET emission ratios of the FRET sensors could be reduced by coexpression of RhoGDI. Similarly, the coexpression of RhoGAPs, as exemplified by ARHGAP1 or a truncated constitutively active version of ARHGAP31 (Lamarche-Vane and Hall, 1998; Southgate *et al.*, 2011), efficiently decreased the FRET efficiency. In order to test the ability of the FRET sensors to respond to RhoGEFs, I first sequestered the sensor in the inactive RhoGDI bound conformation. Coexpression of the RhoGEF MCF2 (also known as Dbl) then activated all sensors, compared to the RhoGDI-bound basal activity (Figure 5.6). I could therefore confirm that the FRET sensors were able to run through all states of the Rho GTPase activation-inactivation cycle and report its modulation by the three main regulators RhoGEFs, RhoGAPs and RhoGDI.

5.2.2.2 Culture medium is a crucial determinant for sensitised emission FRET sensitivity

I next set out to optimise the sensitivity of the assay. The cell culture medium can have enormous influence on the background intensity and thus on the measurable intensity of the donor and FRET-acceptor channel. Phenol red free DMEM medium showed a substantial background intensity especially in the lower wavelength donor and FRET-

acceptor channel. This was most likely due to riboflavin, whose absorption and emission spectra exactly match the wavelength of the FRET-acceptor channel (Zhang *et al.*, 2012). The use of phenol red free Ham's F12 medium which contains more than 10 times less riboflavin in its formulation drastically reduced background levels. FluoroBrite DMEM medium further reduced background intensity, similar to Gey's balanced salt solution, which only contains salts and glucose. By using FluoroBrite DMEM medium and reducing FCS content to 1 % during imaging I could reduce background levels to a minimum while still preserving proper viability of the cells (Appendix Figure 7.4).

5.2.2.3 Cellular expression levels of cotransfected constructs correlate better when under control of the same promoter

The implementation of the FRET assay involves transfection of multiple plasmids with diverging ratios. Theoretically, one should consider that transcription abrogation and competition of promoters for transcription factors might downregulate the expression of individual plasmids and result in variations of expression levels (Manfred Gossen, personal communication) (Bacon and Sedegah, 2007). As ectopic RhoGEFs and RhoGAPs tend to express weakly I aimed to maximise the potential RhoGEF and RhoGAP activity by transfecting an excess of regulator plasmid over the FRET sensors. In order to analyse potential promoter crosstalk and to elaborate conditions of maximal sensitivity of the assay, I compared the expression of the FRET sensors under the control of different constitutive promoters. The promoter cassette of the immediate early gene of human cytomegalovirus (CMV) is a commonly used promoter to generate high levels of transient protein expression in mammalian cells (Boshart *et al.*, 1985). The Human elongation factor-1α (EF-1α) promoter is a constitutive promoter controlling the EF-1α gene (Kim *et al.*, 1990). This gene has a housekeeping function in all cells and is expressed at high levels. The human ubiquitin C (UbC) promoter controls the expression of the polyubiquitin C gene (Wiborg *et al.*, 1985) and is commonly used for moderate expression levels. I compared the expression levels of the FRET sensors under control of each of these three promoters in the presence of CMV promoter controlled RhoGAP or mCherry expression. The expression levels of the sensors under control of the CMV promoters in two different plasmid backbones were similar, the EF-1α promoter reached the highest expression levels and the UbC promoter controlled expression only reached about one half of the average expression levels of the EF-1α promoter as determined by mVenus intensity (Figure 5.7A). I therefore continued to analyse the ability of the EF-1α- and the CMV promoter-controlled Cdc42-2G FRET sensor constructs to become inactivated by mCherry-ARHGAP1 and ARHGAP31 (the Cdc42-2G sensor was analysed exemplarily for all FRET sensors). Surprisingly, RhoGAPs

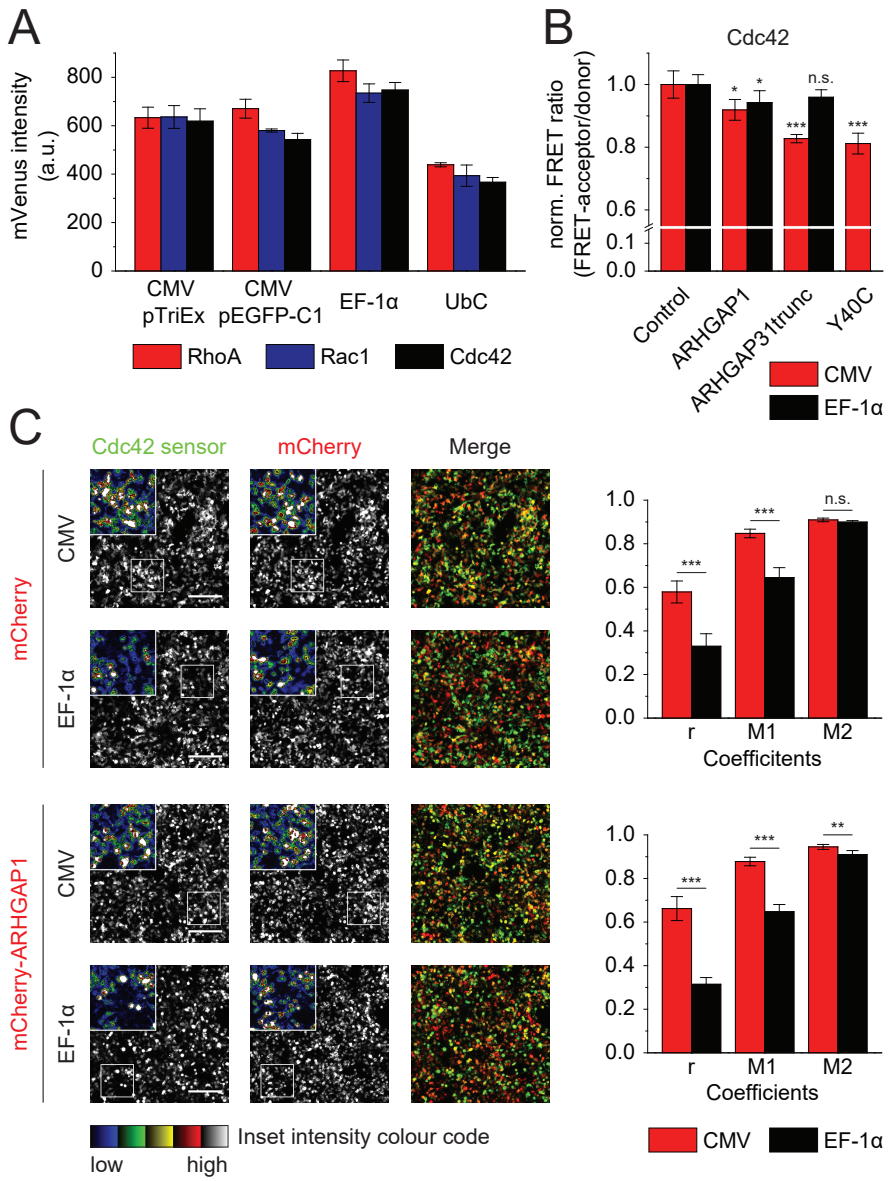

Figure 5.7 Promoter-dependent FRET sensor expression. FRET sensors were transiently expressed in HEK293T cells under control of CMV (in pTriEx and pcDNA3.1 backbones), EF-1α, and UbC promoters. (**A**) Sensor expression levels were assessed microscopically by measurement of background-corrected mVenus intensity. Mean and standard deviation of five fields of view are shown in bar graph. (**B**) Cdc42 FRET sensor was expressed from CMV pTriEx and EF-1α plasmids together with mCherry as control or mCherry-ARHGAP1 or a truncated constitutively active version of ARHGAP31. As low FRET control an inactive effector-binding deficient mutant of the FRET sensor (Y40C) was expressed. FRET ratio was calculated as FRET-acceptor channel intensity divided by donor channel intensity. FRET ratio was normalised to control. Mean and standard deviation of five fields of view are shown. (**C**) Cdc42 FRET sensor was expressed in HEK293T cells under control of CMV or EF-1α promoters together with mCherry as control or mCherry-ARHGAP1. Correlation of expression levels was analysed by colocalisation analysis. Pearson's coefficient (r) and Manders' coefficients (M1=fraction of mCherry overlapping with sensor, M2=fraction of sensor overlapping with mCherry) were determined for five fields of view, the average and standard deviation of which is shown in the diagrams on the right. Insets in images show two-fold magnification of the indicated boxed region, insets are false colour-coded as shown on the bottom to emphasise intensity levels. Scale bars: 200 μm. Significance levels were calculated by unpaired t-test against control or as indicated by lines: ***p<0.001, **p<0.01, *p<0.05, n.s.=not significant.

inactivated the Cdc42-2G FRET sensor more efficiently when the latter was expressed under control of the CMV promoter compared to the EF-1α promoter. Furthermore, the truncated version of ARHGAP31 was unable to inactivate the EF-1α-controlled Cdc42-2G FRET sensor but inactivated the CMV-controlled Cdc42-2G FRET sensor to a minimum, as defined by the FRET ratio of the effector binding-deficient mutant (Y40C) of the sensor (Figure 5.7B). To further investigate the reason for this discrepancy, I compared the correlation of the cellular sensor expression levels with the cotransfected mCherry-ARHGAP1 and mCherry expression levels. This was done in approximation by applying colocalisation analysis of microscopic low magnification images. Importantly, the cellular expression levels of sensor and RhoGAP or mCherry control correlated much better when expressed under the same promoter than under different promoters as evident from Pearson's and Manders' coefficients of colocalisation analysis (Figure 5.7C). Based on the above findings, I decided to employ the pTriEx backbone-based CMV-controlled FRET sensor expression plasmids for all further experiments.

5.2.2.4 Adjustment of RhoGDI levels increases the dynamic range of the FRET screen

In contrast to the first generation Raichu FRET sensors (Itoh *et al.*, 2002; Yoshizaki *et al.*, 2003), the reporters employed in this study have a preserved C-terminal HVR of the Rho GTPase and thus allow proper posttranslational modification and consequentially RhoGDI-binding to occur (Pertz, 2010). Therefore, overexpression of these Rho biosensors leads to saturation of endogenous RhoGDIs and results in accumulation of the reporter at membranes where they become activated by endogenous GEFs (Boulter *et al.*, 2010; Pertz *et al.*, 2006). The analysis of Rho activation by RhoGEFs therefore requires the adjustment of RhoGDI levels to restore low biosensor activity. I therefore set out to study the impact of RhoGDI on the activity levels of the FRET sensors.

I started with the cotransfection of increasing amounts of RhoGDI together with constant levels of FRET sensor. Expectedly, RhoGDI inactivated the FRET sensors in a dose-dependent manner. A RhoGDI:sensor vector ratio of 0.5 was already sufficient to significantly reduce the activity of all FRET sensors and when RhoGDI was four to five-fold overexpressed over the FRET sensors the FRET ratio reached a minimum (Figure 5.8). For the RhoGEF FRET screen I took advantage of this effect by mild coexpression of two-fold excess of RhoGDI over the sensor plasmids in order to restore low basal FRET sensor activity levels without overly saturating the system with RhoGDI.

I next hypothesised that the activity of Rho GTPases as measured by the FRET probes would increase in cells lacking RhoGDI. To this end I created stable shRNA-mediated

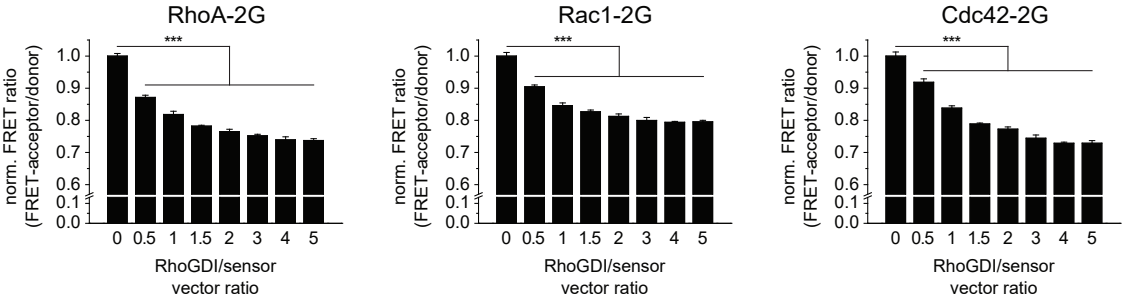

Figure 5.8 RhoGDI downregulates Rho GTPase activity. 5.5×10^4 HEK293T cells per well were transfected with 40 ng RhoA-2G, Rac1-2G and Cdc42-2G FRET sensor plasmid DNA and RhoGDI plasmid DNA at varying ratios in a 96-well format. DNA levels were filled to the same amount with mCherry plasmid DNA. FRET ratio was calculated as FRET-acceptor channel intensity divided by donor channel intensity. All data represent the mean of five fields of view for each condition, error bars indicate standard deviation. Significance levels were calculated by individual unpaired t-tests against control (RhoGDI/sensor vector ratio 0): ***$p<0.001$.

RhoGDI knockdown cell lines to measure Rho GTPase activity in the absence of RhoGDI. 5 shRNA sequences have previously been tested in the lab 2 of which successfully knocked down RhoGDI (Oliver Rocks, data not shown). I then used these two shRNA sequences (shRNA1 and shRNA2) to create stable RhoGDI knockdown cell lines by lentiviral transduction. Both shRNAs yielded superior knockdown efficiency (Appendix Figure 7.9). I then used these cell lines to measure the effect of RhoGDI depletion on Rho GTPase activity levels. Expectedly, the FRET ratios were elevated in the absence of RhoGDI compared to controls (Figure 5.9). I next tested if the use of RhoGDI knockdown cell lines for the RhoGAP screen would increase the dynamic range towards inactivation by potential RhoGAPs. Coexpression of RhoGAPs with FRET sensors in RhoGDI knockdown cell lines clearly showed, that the effect of RhoGAP-mediated Rho GTPase inactivation was more pronounced in the knockdown cell lines compared to control cell lines (Figure 5.10). Taken together, RhoGDI is a universal key-regulator of Rho GTPase activity in cells and the fine-tuning of its cellular expression levels allowed me to increase the sensitivity of the FRET-based Rho GTPase activity assay towards inactivation by RhoGAPs and activation by RhoGEFs.

5.2.2.5 FRET-based Rho GTPase activity assay - control experiments

In order to control the validity and robustness of the FRET-based Rho GTPase activity assay, I carefully tested the assay for potential sources of error and flaws in terms of consistency, variations in expression levels, or crosstalk with fluorophores or with the activity of endogenous Rho GTPases. Therefore, I performed a stringed set of control experiments which I will discuss in the following section.

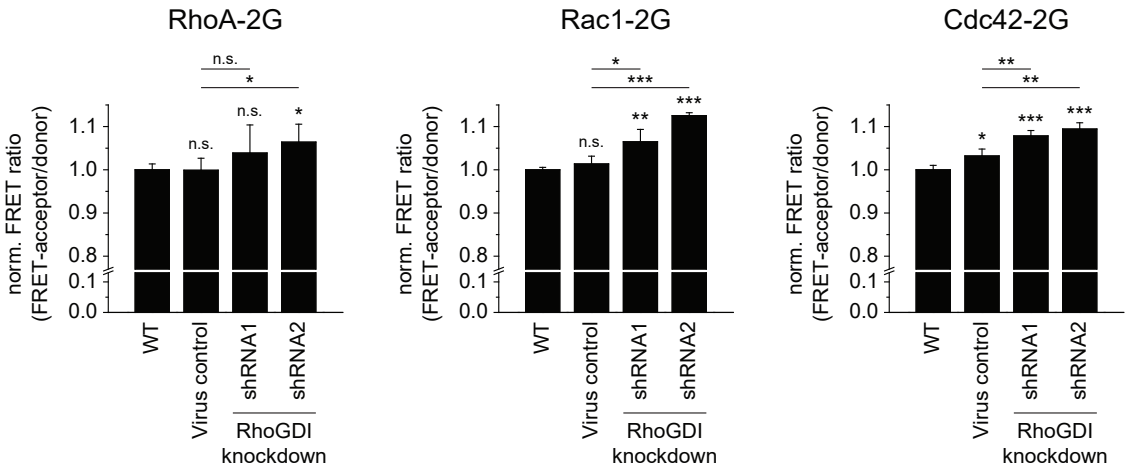

Figure 5.9 Rho GTPase activity increases in the absence of RhoGDI. HEK293T cells (WT), control virus treated HEK293T cells (control), and two stably virus-transduced shRNA-mediated RhoGDI knockdown HEK293T cell lines (shRNA1 and shRNA2) were transfected with RhoA-2G, Rac1-2G and Cdc42-2G FRET sensors. FRET ratio was calculated as FRET-acceptor channel intensity divided by donor channel intensity and normalised to WT. All data represent the mean of four different wells for each condition, error bars indicate standard deviation. Significance levels were calculated by unpaired t-tests against WT or as indicated by lines: ***p<0.001, **p<0.01, *p<0.05, n.s.=not significant.

Rho GTPase activity levels reported by FRET-sensors are highly consistent throughout 96-well plates

It is a commonly known phenomenon of multi-well plates that differential evaporation of water from outer to inner wells causes a parabolic pattern of cell growth over the plate. When 96-well plates were incubated in a standard cell culture incubator with humidification system, I observed a volume reduction by evaporation of approximately 20 μl in the edge wells, whereas in the centre wells the volume was unchanged. This was accompanied by a reduction of the cell growth rate in the edge wells, probably due to hyperosmotic stress, and also caused changes in the apparent FRET ratio of the sensors. By employment of a custom-made humidity chamber during culturing as described by Walzl *et al.* (2012) and daily medium changes I could reduce the evaporation-caused edge effect on 96-well plates to a minimum and substantially increase well-to-well consistency. FRET ratio measurements in neighbouring outer to inner wells of 96 well plates were consistent, as well as variations between wells that were recorded at the beginning and at the end of the measurement of a 96-well plate with a time difference of 45-90 min (Appendix Figure 7.5). These controls were regularly included in experiments in order to detect day-to-day variations in consistency.

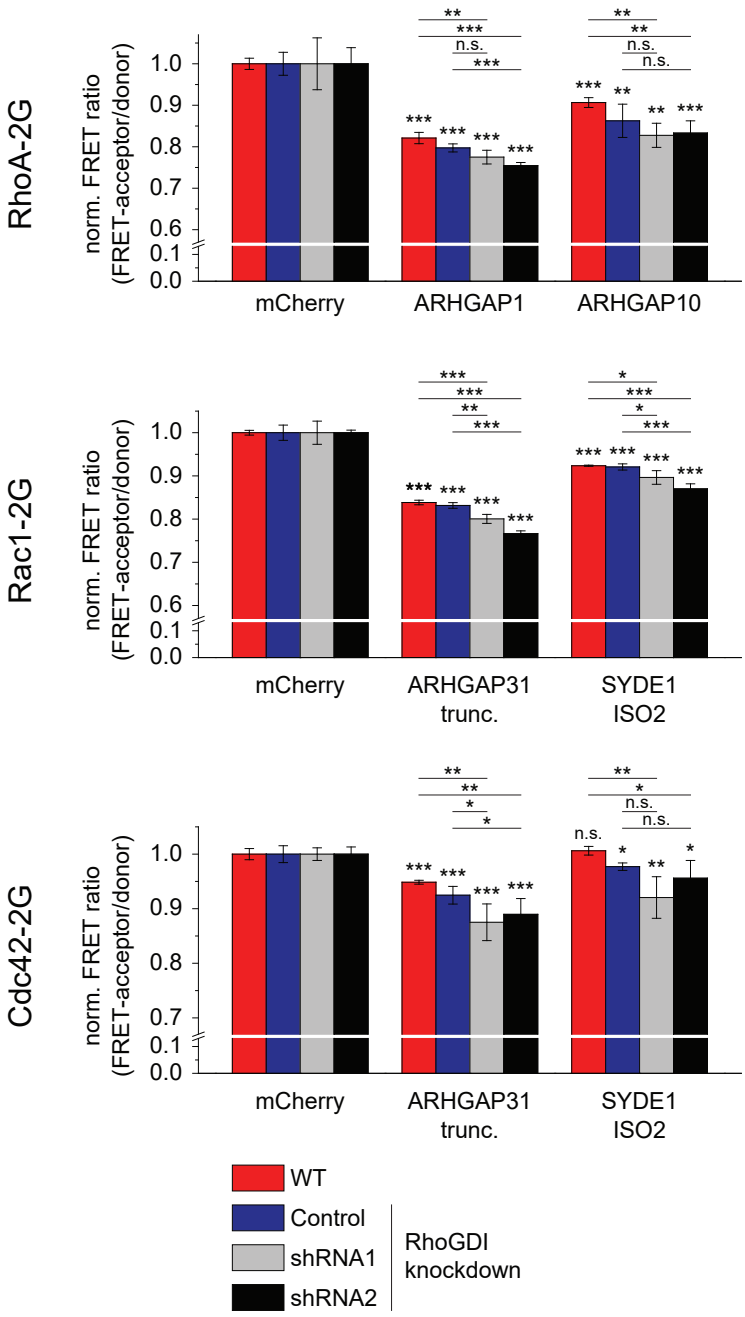

Figure 5.10 FRET response to RhoGAPs is more pronounced in RhoGDI knockdown cells. HEK293T cells (WT), pLKO.1 stuffer virus treated HEK293T cells (Virus control), and two stably virus-transduced shRNA-mediated RhoGDI knockdown HEK293T cell lines (shRNA1 and shRNA2) were transfected with RhoA-2G, Rac1-2G and Cdc42-2G FRET sensors together with RhoGAPs as indicated or with mCherry as control. FRET ratio was calculated as FRET-acceptor channel intensity divided by donor channel intensity and each cell line was normalised to its mCherry control. All data represent the mean of four different wells for each condition, error bars indicate standard deviation. Significance levels indicated on top of bars were calculated by unpaired t-tests against mCherry control. Significance levels indicated by lines were calculated by unpaired t-tests after data normalisation: ***p<0.001, **p<0.01, *p<0.05, n.s.=not significant.

FRET-based Rho GTPase activity assay is insensitive to variations in sensor expression levels

Depending on the expression levels of cotransfected RhoGEFs and RhoGAPs, I observed variations in the expression level of the sensor. Usually lower expression of RhoGEFs and RhoGAPs correlated with higher expression of the sensor and vice versa. In order to address this issue and the potential effects on the observed FRET ratio, I first compared the FRET ratios of different regions as defined by discrete sensor intensity levels. I observed that the FRET ratio was higher in regions of high sensor intensity than in regions of low sensor intensity (Appendix Figure 7.7). To analyse whether, and to what extent, variations in the expression of the biosensors affect their activity level, I expressed increasing amounts of FRET sensor and assessed the resulting average FRET ratio. Importantly, variations in the observed FRET ratio were minimal and did not significantly change across a broad range of reporter plasmid concentrations between 20 ng and 50 ng of sensor plasmid per well (Figure 5.11). This endorsed the use of 30 ng and 40 ng sensor plasmid for the RhoGAP and RhoGEF screen, respectively, and confirmed that the assay is resistant to technical and biological variability of sensor expression. Additionally, I routinely included a correlation analysis of FRET ratio and FRET sensor expression levels in the evaluation of the screening data to confirm the absence of a dependency of the two factors.

mCherry does not interfere with the FRET sensor fluorophore pair

The efficiency of FRET depends amongst others on the spectral overlap of the emission spectrum of the donor and the excitation spectrum of the acceptor fluorophore (Jares-Erijman and Jovin, 2003). Therefore, mCherry, which was tagged to the coexpressed RhoGEFs and RhoGAPs, can in principle also serve as a FRET acceptor fluorophore for mTFP1, although with a lower efficiency than mVenus. I performed control experiments formally to exclude that mCherry actually happens to form a FRET pair with mTFP1 in the FRET assay. Initially, I compared the FRET ratio of the sensors in the presence of excess mCherry to the FRET ratio in the presence of miRFP670, which should drastically reduce this potential fluorophore crosstalk. Moreover, to direct mCherry as a potential FRET acceptor more specifically to the close proximity of mTFP1, I compared the FRET ratio in the presence of excess unlabelled RhoGDI and in the presence of excess mCherry labelled RhoGDI. Direct binding of mCherry-labelled RhoGDI to the Rho GTPase moiety of the sensor, increases the probability of a potential FRET effect to occur. Additionally, RhoGDI stabilises Rho GTPases in their inactive state (see 5.2.2.4) which reduces intramolecular FRET of the sensor and by this increases the proportion of poten-

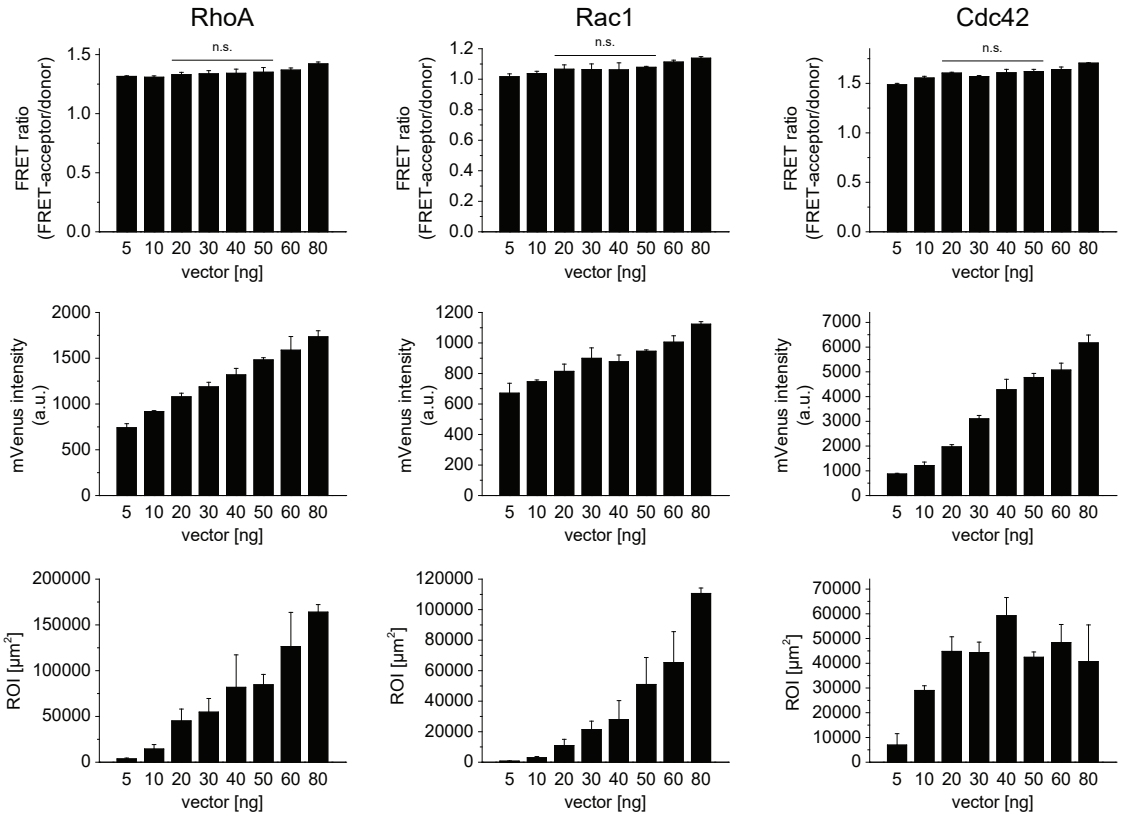

Figure 5.11 FRET ratio is stable across a wide range of sensor expression levels. HEK293T cells were transfected with increasing amounts of RhoA-2G, Rac1-2G and Cdc42-2G FRET sensor plasmid DNA. DNA levels were filled to the same amount with mCherry plasmid DNA. FRET ratio was calculated as FRET-acceptor channel intensity divided by donor channel intensity. mVenus intensity is shown in the middle and represents the sensor concentration within the region of interest. The area of the region of interest (ROI) as a measure for the number of cells that express the sensor is shown on the bottom. All data represent the mean of three independent wells for each condition, error bars indicate standard deviation. Significance levels were calculated by individual unpaired t-tests within all samples under the line: n.s.=not significant.

tial donor fluorophore for mCherry. However, none of these control experiments revealed any evidence for potential impact FRET interaction between mTFP1 and mCherry on the measured FRET ratio of the sensor (Appendix Figure 7.6).

Minimal RhoGEF or RhoGAP expression levels result in substantial changes in biosensor activity

Many RhoGEFs and RhoGAPs in the library are large multidomain proteins (Figure 2.3) and may thus theoretically express only at low levels when transfected in cells. I therefore addressed the question if, in principle, low levels of RhoGEFs and RhoGAPs are sufficient to significantly activate or inactivate Rho GTPases as determined by the FRET sensors. To this end I titrated increasing amounts of RhoGEFs and RhoGAPs and measured the FRET ratio and relative GEF and GAP expression levels by mCherry intensity. Already minimal amounts of mCherry-MCF2, a RhoGEF with specificity for RhoA, Rac1, and Cdc42, substantially activated all biosensors (Figure 5.12). However, Cdc42-2G required higher levels of MCF2 to consistently report activation. For RhoA-2G and Rac1-2G a sensor:RhoGDI:RhoGEF ratio of 1:2:0.375 significantly increased the FRET ratio, for Cdc42 a sensor:RhoGDI:RhoGEF ratio of 1:2:2 was necessary. Similarly, minimal amounts of mCherry-tagged ARHGAP1, a strong RhoA GAP, or ARHGAP22, a strong Rac1 and Cdc42 GAP, were sufficient to substantially inactivate the sensors (Figure 5.13). For all three GTPases a ratio of 1:0.5 sensor:RhoGAP was sufficient, again for Cdc42 higher levels were needed to consistently inactivate the sensor. This indicates that the FRET sensors are highly sensitive to low levels of active RhoGEFs and RhoGAPs and that the FRET sensors respond to the expression of RhoGEFs and RhoGAPs in a dose-dependent manner. Importantly, the sensitivity of the FRET assay towards RhoGEF and RhoGAP activity could be even further increased by additional thresholding of the mCherry channel in the data analysis to include only RhoGEF- or RhoGAP-positive cells in the analysed region of interest (Appendix Figure 7.8). Notably, judged by the respective mCherry intensities, the expression levels of the RhoGEFs and RhoGAPs in the final screens were always higher than the minimal expression levels that were required to detect a significant FRET ratio change in the above titration experiments. However, in order to maximise the effect of coexpressed RhoGEFs and RhoGAPs and to reliably detect also those with potentially lower activity, I overexpressed excess of RhoGEFs and RhoGAPs in the screens at a ratio of 1:2:7 sensor:RhoGDI:RhoGEF and 1:9 sensor:RhoGAP.

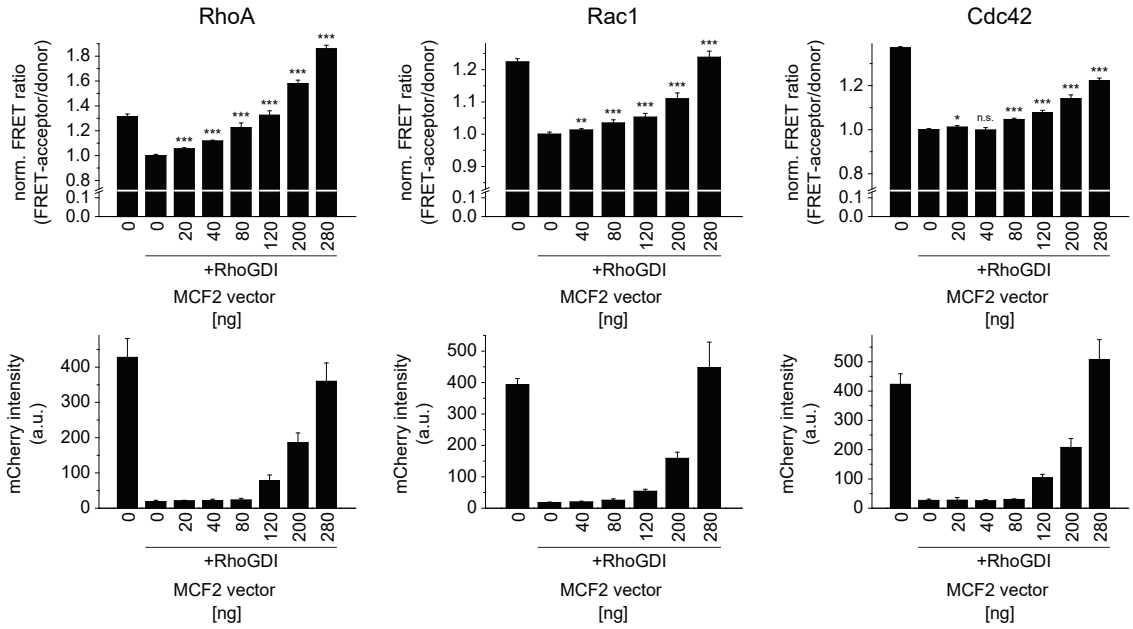

Figure 5.12 Minimal amounts of RhoGEFs are sufficient to activate Rho FRET sensors. 5.5×10^4 HEK293T cells per well were transfected in a 96-well format with 40 ng RhoA-2G, Rac1-2G and Cdc42-2G FRET sensor plasmid DNA together with increasing amounts the RhoGEF MCF2 plasmid DNA and 80 ng RhoGDI plasmid DNA where indicated, 80 ng mCherry were expressed where RhoGDI was absent. DNA levels were filled to the same amount with miRFP670 plasmid DNA. FRET ratio was calculated as FRET-acceptor channel intensity divided by donor channel intensity. FRET ratio was normalised to 0 ng MCF2+RhoGDI control. mCherry intensity is shown on the bottom and represents the relative RhoGEF concentration within the region of interest. All data represent the mean of five fields of view, error bars indicate standard deviation. Significance levels were calculated by unpaired t-tests versus 0 ng MCF2+RhoGDI: ***p<0.001, **p<0.01, *p<0.05, n.s.=not significant.

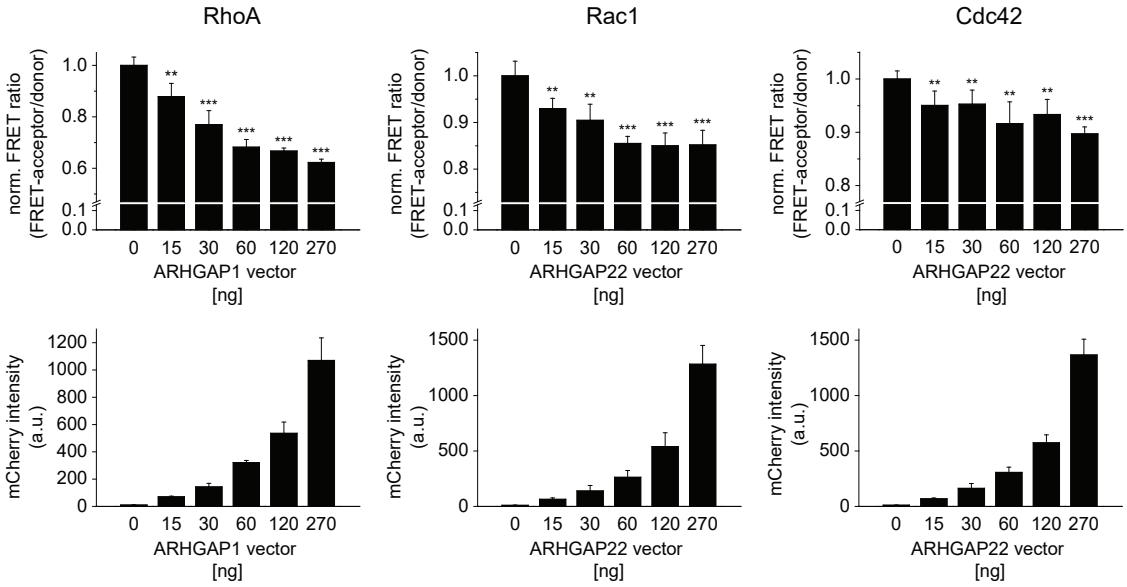

Figure 5.13 Minimal amounts of RhoGAPs are sufficient to inactivate Rho FRET sensors. 5.5×10^4 HEK293T RhoGDI knockdown cells per well of a 96-well plate were transfected with 30 ng RhoA-2G, Rac1-2G and Cdc42-2G FRET sensor plasmid DNA together with increasing amounts the RhoGAPs ARHGAP1 for RhoA and ARHGAP22 for Rac1 and Cdc42. DNA levels were filled to the same amount with miRFP670 plasmid DNA. FRET ratio was calculated as FRET-acceptor channel intensity divided by donor channel intensity. FRET ratio was normalised to 0 ng RhoGAP control. mCherry intensity is shown on the bottom and represents the relative RhoGAP concentration within the region of interest. All data represent the mean of five fields of view, error bars indicate standard deviation. Significance levels were calculated by unpaired t-tests versus 0 ng RhoGAP: ***p<0.001, **p<0.01.

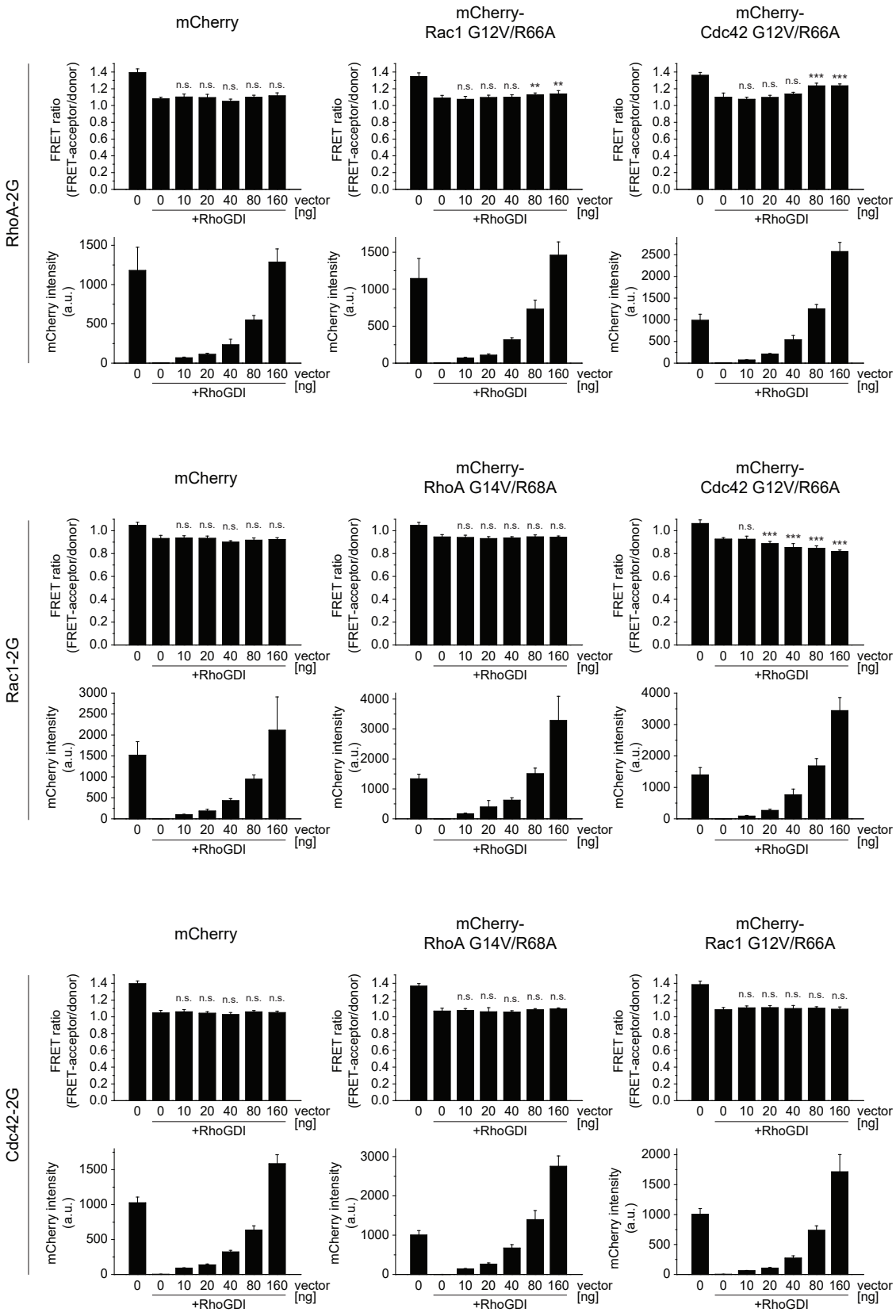

Figure 5.14 see next page

Figure 5.14 (continued) Crosstalk of active Rho GTPases to other family members. HEK293T cells were transfected with 40 ng RhoA-2G, Rac1-2G, and Cdc42-2G sensors together with increasing amounts of mCherry as control and mCherry-tagged constitutively active and RhoGDI binding-deficient versions of Rho GTPases. 80 ng RhoGDI was coexpressed where indicated, 80 ng mCherry were expressed where RhoGDI was absent. DNA levels were filled to the same amount with miRFP670 plasmid DNA. FRET ratio was calculated as FRET-acceptor channel intensity divided by donor channel intensity. mCherry intensity is shown below FRET ratios and represents the Rho GTPase concentration within the region of interest. For mCherry control one well with five fields of view were analysed, for mutant Rho GTPase transfected samples two wells with five fields of view each were analysed. Mean and standard deviation of all fields of view are given in the graphs. Significance levels were calculated by unpaired t-tests versus 0 ng vector +RhoGDI: ***p<0.001, **p<0.01, n.s.=not significant.

Rho GTPase activity crosstalk

RhoA, Rac1 and Cdc42 have been reported to mutually affect their activity. Antagonistic regulation has been suggested for RhoA and Rac1 (Sander *et al.*, 1999; Chauhan *et al.*, 2011) as well as for RhoA and Cdc42 (Yang *et al.*, 2016), whereas synergistic regulatory mechanisms are proposed for Rac1 and Cdc42 (Kurokawa *et al.*, 2004). Generally, the molecular basis for the reciprocal regulation is not well understood. However, context-specific examples of mutual Rho GTPase regulation have been described and involve reciprocal effector-mediated feedback loops which activate RhoGAPs and inactivate RhoGEFs. For example, Rac1 can inhibit RhoA through activation of NADPH oxidase and generation of reactive oxygen species (ROS) during membrane ruffling and cell spreading. ROS then inactivate low-molecular-weight protein tyrosine phosphatase through oxidation of the active sulfhydryl group in the catalytic pocket, which subsequently increases tyrosine phosphorylation and activation of ARHGAP35 and ultimately to inactivation of RhoA (Nimnual *et al.*, 2003). Furthermore, Alberts and colleagues suggest an example of Rac1-dependent inactivation of the RhoA GEF NET1 (Alberts *et al.*, 2005). They described a mechanism by which the Rac1 effector PAK1 phosphorylates and downregulates the activity of NET1 which results in reduced actin stress fiber formation. In turn, during amoeboid movement of tumor cells RhoA can inactivate Rac1 (and Cdc42) through activation of ARHGAP22, most likely via its effector ROCK to suppresses mesenchymal movement (Katsumi *et al.*, 2002; Sanz-Moreno *et al.*, 2008). RhoA also antagonizes Rac1 by promoting ROCK-mediated phosphorylation and thus stimulation of ARHGAP24, a GAP for Rac1 that localises to sites of membrane protrusion (Ohta *et al.*, 2006). This mechanism is involved in cellular polarity establishment by suppressing leading edge protrusion and promoting cell retraction. One more example how RhoA and Cdc42 activity is reciprocally regulated in an effector-independent manner by an ARHGEF11, ARHGEF12, and PLEKHG4B multi-RhoGEF complex downstream of GPCRs is currently investigated

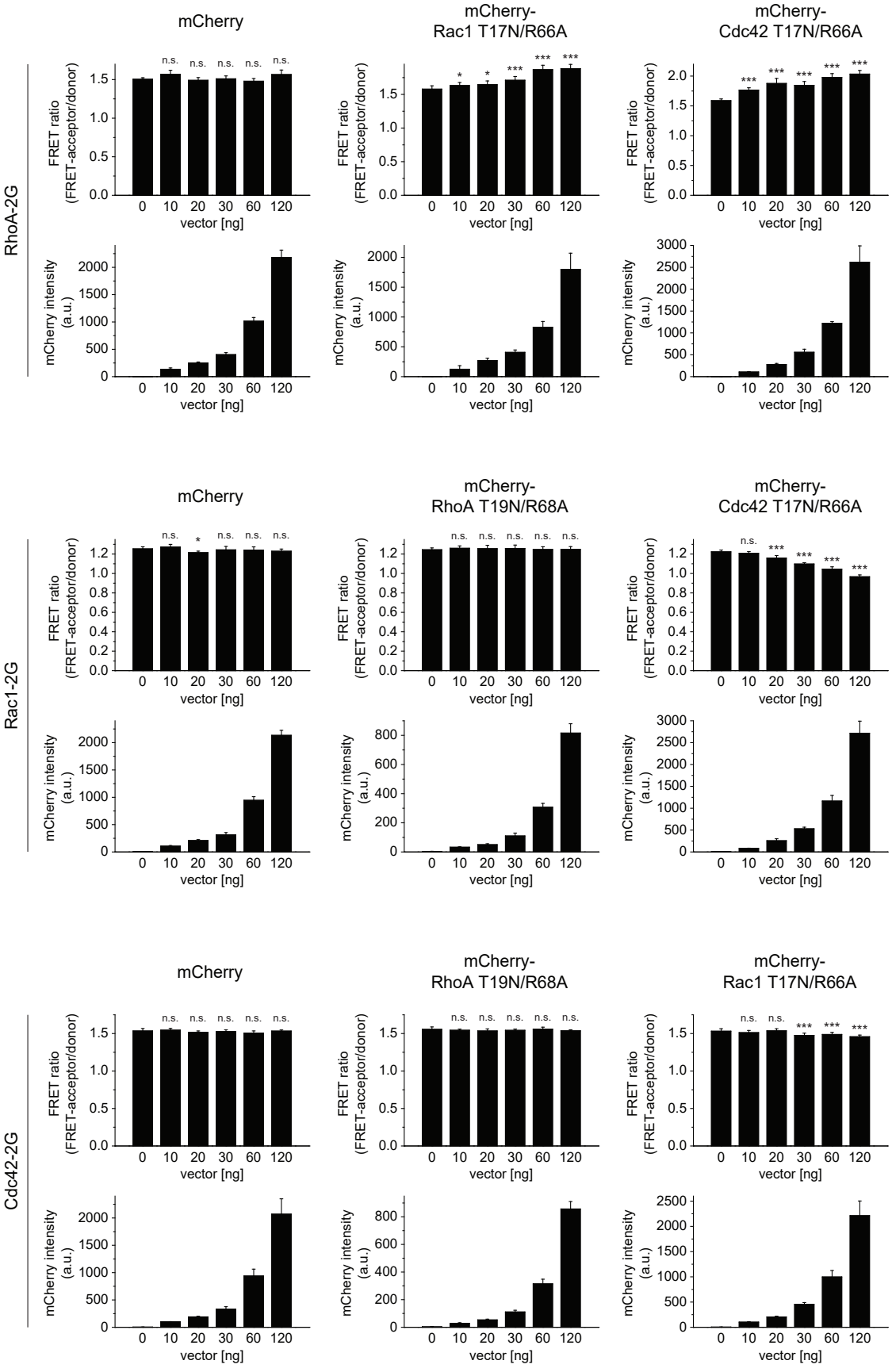

Figure 5.15 see next page

Figure 5.15 (continued) Crosstalk of inactive Rho GTPases to other family members. HEK293T RhoGDI knockdown cells were transfected with 30 ng RhoA-2G, Rac1-2G, and Cdc42-2G sensors together with increasing amounts of mCherry as control and mCherry-tagged dominant negative and RhoGDI binding-deficient versions of Rho GTPases. DNA levels were filled to the same amount with miRFP670 plasmid DNA. FRET ratio was calculated as FRET-acceptor channel intensity divided by donor channel intensity. mCherry intensity is shown below FRET ratios and represents the Rho GTPase concentration within the region of interest. For mCherry control one well with five fields of view were analysed, for mutant Rho GTPase transfected samples two wells with five fields of view each were analysed. Mean and standard deviation of all fields of view are given in the graphs. Significance levels were calculated by unpaired t-tests versus 0 ng vector: ***$p<0.001$, *$p<0.05$, n.s.=not significant.

in the lab (Rademacher et al. manuscript in preparation). Two mechanisms have been suggested how active Cdc42 can coactivate Rac1: A RhoGDI-dependent mechanism of Cdc42-mediated activation of Rac1 has been described by DerMardirossian and colleagues. They showed that active Cdc42 stimulates the release and thus the activation of Rac1 from RhoGDI in a PAK1-dependent manner (DerMardirossian *et al.*, 2004). Furthermore, ten Klooster *et al.* (2006) showed that active Cdc42 can stimulate the activation of Rac1 via PAK1 autophosphorylation, subsequent release and activation of ARHGEF7 (also known as β-Pix) which then activated Rac1.

Considering the mutual crossregulation of Rho GTPases within cells, I was wondering if and how activation and inactivation of endogenous RhoA, Rac1 and Cdc42 by exogenously expressed RhoGEFs and RhoGAPs can indirectly affect the activity levels of the Rho biosensors. Therefore, I coexpressed each FRET sensor with dominant negative or constitutively active mutant forms of one of the other two Rho GTPases in order to mimic high and low activities of endogenous Rho GTPases. However, changes in the well balanced expression levels of Rho GTPases and RhoGDI have been shown to result in altered activity levels of Rho GTPases (Boulter *et al.*, 2010; Garcia-Mata *et al.*, 2011). In order to not further perturb the RhoGDI-GTPase stoichiometry by coexpression of an additional dominant negative or constitutively active Rho protein besides the sensor, I employed RhoGDI binding-deficient double mutant forms. Indeed, high levels of constitutively active and RhoGDI binding-deficient Rac1-G12V/R66A and Cdc42-G12V/R66A activated the RhoA-2G FRET sensor and RhoGDI (Figure 5.14). Interestingly, Cdc42-G12V/R66A inactivated Rac1-2G at high expression levels, whereas active Rac1-G12V/R66A had no effect on Cdc42-2G. RhoA-G14V/R68A had no effect on the activity of Rac1-2G and Cdc42-2G.

This indicates, that strong Rac1 or Cdc42 specific RhoGEFs might lead to activation of RhoA by crosstalk between Rho GTPases. However, in the screen I identified RhoGEFs with exclusive high activity for Cdc42 (PLEKHG4B and SPATA13) or with exclusive high

activity for Rac1 (TIAM2) that did not affect the activity of the RhoA-2G biosensor (Figure 5.17). This suggests, that the Rho GTPase crosstalk is negligible in the context of the RhoGEF assay most probably because the GEFs cannot recapitulate the extreme perturbation of the system by the GTPase mutants expressed at high levels. I can, however, not exclude that in case of a RhoGEF with strong activity towards Cdc42 an additional weak Rac1 GEF activity may be missed in the screen.

Dominant negative and RhoGDI binding-deficient Rac1-T17N/R66A coinactivated Cdc42-2G at high expression levels, while it activated RhoA-2G. Similarly, dominant negative and RhoGDI-binding deficient Cdc42-T17N/R66A coinactivated Rac1 and activated RhoA. RhoA-T19N/R68A had no effect on the activity levels of Rac1-2G and Cdc42-2G. However, in the screen the Rac1 specific RhoGAPs ARHGAP15, ARHGAP9, CHN1, CHN2, and SH3BP1 did not inactivate Cdc42, again indicating that crosstalk from inactive Rac1 to Cdc42 is negligible in the context of the assay (Figure 5.18). However, the fact that I only identified one Cdc42 specific RhoGAP might also be accounted for by the crosstalk from inactive Cdc42 to Rac1. Furthermore, I cannot exclude that in case of a RhoGAP with strong activity towards Rac1 and Cdc42 an additional weak RhoA GAP activity may be missed in the screen.

Taken together, the extensive set of control experiments revealed that the assay was sensitive, robust, and reliable and thus ideally suited to be applied to systematic analysis of all RhoGEFs and RhoGAPs. Furthermore, by including controls I routinely confirmed and reassured the validity and the accuracy of the assay.

5.2.3 Meta-analysis of RhoGEF and RhoGAP substrate specificities

One way to validate the results of the FRET-based RhoGEF and RhoGAP substrate specificity screen is to compare them to published work. I therefore performed a comprehensive literature meta-analysis of existing data. As available protein-protein interaction databases such as UniProt, STRING, IntAct or BioGRID are either very incomplete or do not distinguish between enzyme-substrate interactions and other protein-protein interactions, I manually searched more than 2000 PubMed studies on RhoGEFs or RhoGAPs and extracted information from more than 450 publication. I collected information about the determined substrate specificities, the applied method, the use of full length or truncated versions of the regulators and, where available, information that suggest the involvement of autoinhibitory mechanisms controlling the catalytic activities.

In summary, I found that 11 % of all RhoGEFs and RhoGAPs were completely uncharacterised in terms their catalytic activity and a further 11 % were described incompletely. Furthermore, for 40 % of all RhoGEFs and RhoGAPs the activity towards at least one

GTPase was controversially reported in different publications. Therefore, I defined two sets of criteria to summarise and appraise the collected information which allowed me to create curated lists of certain RhoGEF and RhoGAP substrate specificities, termed gold and silver standard list (Tables 5.2 and 5.3). For the silver standard list activities had to be shown by a minimum of two independent publications or methods, for the gold standard list activities had to be shown by *in vivo* and *in vitro* methods. For conflicting data the net information still had to fulfil these criteria (see also 4.6). The gold standard list contains 18, 20, and 13 RhoGEFs with activity towards RhoA, Rac1, and Cdc42, respectively, and 15, 17, and 10 RhoGAPs with activity towards RhoA, Rac1, and Cdc42, respectively. The less stringent silver standard list contains 24, 25, and 18 RhoGEFs with activity towards RhoA, Rac1, and Cdc42, respectively, and 19, 20, and 14 RhoGAPs with activity towards RhoA, Rac1, and Cdc42, respectively (Figure 5.16). Thus, according to these criteria for only 28 % (silver standard) or 17 % (gold standard) of RhoGEFs and RhoGAPs the substrate specificity towards all three Rho GTPases RhoA, Rac1, and Cdc42 is well characterised. Moreover, the activity for 28 % (silver standard) or 43 % (gold standard) of RhoGEFs and RhoGAPs is unknown, uncertain or controversial. Furthermore, it appears that RhoGEFs and RhoGAPs mostly have either exclusive activity towards one GTPase, or the activity is only well described towards one Rho GTPase (Figure 5.16). Indeed, according to the silver and gold criteria the substrate specificity towards all three GTPases, RhoA, Rac1, and Cdc42, is only certain for 23 % (silver standard) or 9 % (gold standard) of RhoGEFs and for 12 % (silver standard) or 9 % (gold standard) of RhoGAPs . Altogether, the substrate specificity of RhoGEFs and RhoGAPs towards RhoA, Rac1, and Cdc42 is incomplete and largely not well studied. Discrepancies in substrate specificity can be attributed to the use of different experimental approaches and setups, underscoring the need for a comprehensive comparative analysis under standardised conditions.

5.2.4 Systematic family-wide FRET-based RhoGEF activity screen

In order to describe the activity of 66 potential Dbl-homology RhoGEFs (including ABR and BCR with dual RhoGEF/RhoGAP function) and 8 DOCK family RhoGEFs towards RhoA, Rac1 and Cdc42, I coexpressed each of the RhoGEFs as mCherry fusions together with RhoGDI and the respective Rho GTPase FRET sensor in HEK293T cells in a 96 well format. The cells were subjected to automated microscopic image acquisition and the images were subsequently processed and analysed by applying a self-written automated software implementation in order to extract the FRET ratio and other control parameters. Briefly, the images were background corrected and a region of interest was generated by thresholding, based on the acceptor and the mCherry channels. Furthermore, low inten-

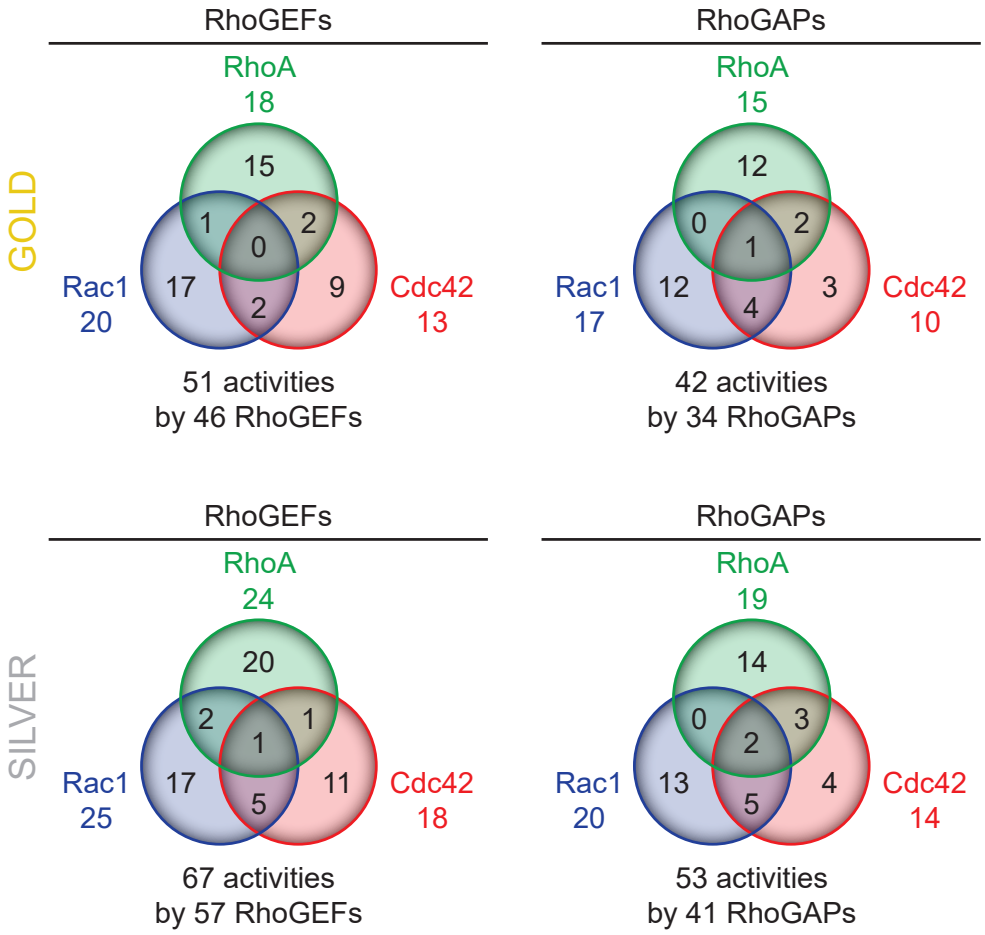

Figure 5.16 Venn diagrams of RhoGEF and RhoGAP substrate specificity meta-analysis. Venn diagrams show the numbers of RhoGEFs (left) and RhoGAPs (right) with single or multiple activities towards RhoA, Rac1, and Cdc42, as revealed by literature meta-analysis. Criteria of different stringency ("GOLD" and "SILVER") were applied to the data set in order to extract substrate specificities.

sity pixels in the donor and the FRET-acceptor images were excluded from the region of interest. The FRET ratio within the region of interest was calculated on a pixel-by-pixel basis by dividing the FRET-acceptor image by the donor image and eventually averaged for each image. Additionally, the average intensity was measured for each channel within the region of interest and the area of the region of interest was measured. The mCherry intensity served as a readout for successful RhoGEF expression. The results of three independent experiments were each normalised to controls and then averaged. In order to most precisely determine the control FRET ratio I included 4 identical controls in the measurements. To define the FRET ratio cut-off for identification of active RhoGEFs, I initially performed precision and recall analysis[2] based on the literature meta-analysis to obtain an objective benchmark for the cut-off. For the Rac1 and Cdc42 screens precision and recall analysis break-even point suggested a much lower threshold than for the RhoA screen (Appendix Figure 7.10). Therefore, the cut-off was defined as $2\,\sigma$ confidence level of the control for the Rac1 and Cdc42 screens and as $4\,\sigma$ confidence level of the control for the RhoA screen. Eventually, significance of candidates above the threshold were determined by the Benjamini-Hochberg procedure.

In total, I identified 29 RhoGEFs with activity towards RhoA, 20 RhoGEFs with activity towards Rac1 and 22 RhoGEFs with activity towards Cdc42 (Figure 5.17). 43 RhoGEFs exhibited activity towards at least one Rho GTPase, whereas 31 did not show any activity. 14 RhoGEFs had exclusive activity towards RhoA, 4 towards Rac1 and 7 towards Cdc42. In contrast to the results of the meta-analysis where RhoGEFs rarely had multiple substrates (Figure 5.16), I found 18 RhoGEFs with multiple activities, 3 towards RhoA and Rac1, 2 towards RhoA and Cdc42, 3 towards Rac1 and Cdc42 and 10 RhoGEFs had activity towards all 3 Rho GTPases (Figure 5.19). Furthermore, I found activity for 1 RhoGEF, PLEKHG4B, which has never been characterised before. Additionally, 22 out of these 71 active RhoGEF activities have not been described *in vivo* before (Figure 5.19).

In general, most of the well described RhoGEF subfamilies showed the expected substrate patterns. For example, the structurally related RhoGEF family of ARHGEF1, ARHGEF11 and ARHGEF12 showed exclusive activity towards RhoA, as anticipated. Furthermore, the RhoGEFs of the TIAM and the PREX family showed predominant Rac1 activity, as expected. The RhoGEFs of the ASEF family ARHGEF4, ARHGEF9 and SPATA13 were described to activate Cdc42, which I could also confirm in the screen. RhoGEFs of the FGD family showed predominant activity towards Cdc42, although I did not detect Cdc42 activity for all of the members. MCF2 (also known as DBL) and MCF2L (also known as DBS) showed activity towards all 3 Rho GTPases, as expected,

[2]Precision and recall analysis was performed together with Evangelia Petsalaki (EMBL-EBI, Hinxton)

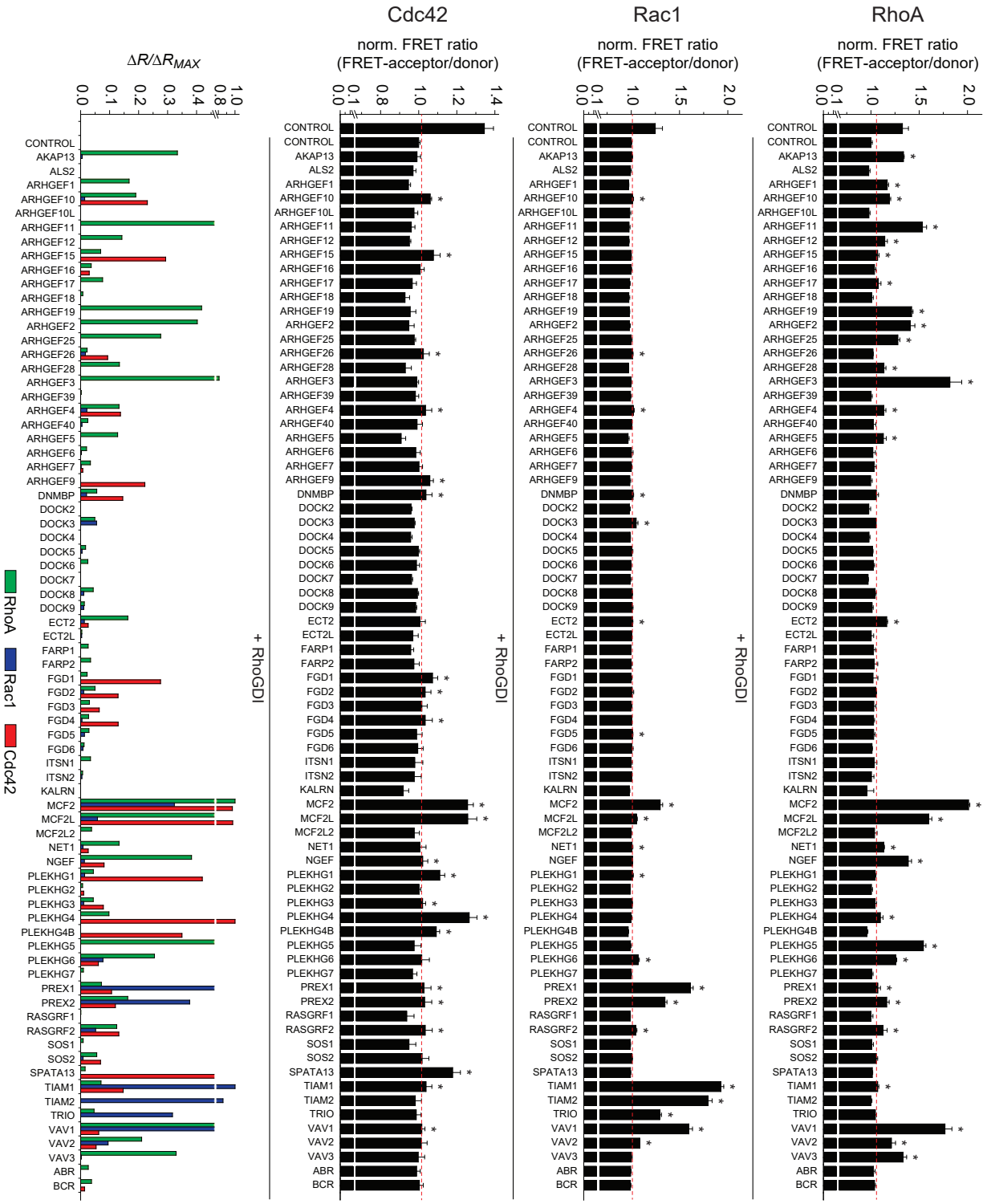

Figure 5.17 see next page

Figure 5.17 (continued) Systematic family-wide FRET-based RhoGEF activity screen. HEK293T cells were transfected with the mCherry-labelled RhoGEF cDNA expression library, the FRET sensors RhoA-2G, Rac1-2G, and Cdc42-2G and RhoGDI (where indicated) in a 96 well format. Controls were transfected with mCherry alone. 48 h after transfection cells were subjected to automated epifluorescent microscopic image acquisition. FRET ratio was calculated as FRET-acceptor channel intensity divided by donor channel intensity. For control+RhoGDI four wells were averaged per plate, all values were normalised to control+RhoGDI. Mean and standard deviation of three independent plates are given in the graphs. Dashed red line indicates threshold: 4σ of control+RhoGDI (1.05772) for RhoA, 2σ of control+RhoGDI (1.01172) for Rac1, 2σ of control+RhoGDI (1.01519) for Cdc42. Significance of values above the threshold was calculated by Student's t-test versus control+RhoGDI followed by Benjamini-Hochberg procedure, significant values are marked with an asterisk (*). Graph on the bottom shows quantification of RhoGEF activity and allows direct comparison of activities towards RhoA (green), Rac1 (blue), and Cdc42 (red). The change in FRET ratio compared to control+RhoGDI (ΔR) was normalised to the maximal FRET ratio change (ΔR_{MAX}).

whereas the homologous yet uncharacterised RhoGEF MCF2L2 had no activity. The VAV family RhoGEFs were mostly described as Rac1 specific RhoGEFs before. Surprisingly, only VAV1 and VAV2 showed activity towards Rac1, but all three of them showed activity towards RhoA and VAV1 showed a weak activity towards Cdc42, additionally.

However, for some RhoGEFs and even whole RhoGEF subfamilies I did not detect expected activities. Surprisingly, the RhoGEFs of the DOCK family, which are known to exert activity towards Rac1 and Cdc42, did not show activities in the screen, except for DOCK3. Furthermore, the intersectins ITSN1 and ITSN2, whose activity towards Cdc42 is very well established, also showed no activity in the screen. In the following sections (5.2.6 and 5.2.7) I was further validating the RhoGEF activity screen and investigating issues like autoinhibition and spatial exclusion.

5.2.5 Systematic family-wide FRET-based RhoGAP activity screen

In order to describe the activity of 65 proteins containing a RhoGAP domain (including ABR and BCR with dual RhoGEF/RhoGAP function) towards RhoA, Rac1 and Cdc42, I coexpressed mCherry fusions of the RhoGAP library together with one of the three biosensors in stable shRNA-mediated RhoGDI knockdown HEK293T cells in a 96 well format. The absence of RhoGDI increased the sensitivity of the assay towards inactivation by potential RhoGAPs as shown before (see 5.2.2.4 and Figure 5.10). The cells were subjected to automated microscopy and the data was analysed by automated image analysis. Three independent experiments were each normalized to 4 identical controls and then averaged. As for the RhoGEF activity screen, an objective cut-off benchmark for the identification of active RhoGAPs was defined by precision and recall analysis[3]based on the literature

[3]Precision and recall analysis was performed together with Evangelia Petsalaki (EMBL-EBI, Hinxton)

meta-analysis. The break-even point of precision and recall analysis suggested a less stringent threshold for the Cdc42 screen than for the Rac1 and RhoA screens. Therefore, the cut-off for the Cdc42 screen was defined as the $2\,\sigma$ confidence level of the control, whereas the for the RhoA and Rac1 screens the cut-off was defined as the 4σ confidence level of the control. Significance of candidates that matched the cut-off was determined by the Benjamini-Hochberg procedure.

Altogether, I detected 82 effective Rho GTPase-RhoGAP interactions from 50 RhoGAPs. 27 RhoGAPs had activity towards RhoA, 35 RhoGAPs towards Rac1 and 20 RhoGAPs towards Cdc42. 13 RhoGAPs had exclusive activity towards RhoA, 15 towards Rac1 and 1 towards Cdc42. 10 RhoGAPs had dual activity, 2 towards RhoA and Rac1, 1 towards RhoA and Cdc42 and 7 towards Rac1 and Cdc42. 11 RhoGAPs showed activity towards all 3 Rho GTPases (Figure 5.19). This relatively large number of RhoGAPs with multiple substrates was again surprising, as the meta-analysis suggested that RhoGAPs would mostly be specific towards one Rho GTPase (Figure 5.16). I identified 6 RhoGAPs exhibiting 12 activities whose activities were never investigated before. Moreover, 52 RhoGAP activities where not confirmed *in vivo* yet (Figure 5.19). Notably, I only identified one RhoGAP with exclusive substrate specificity for Cdc42 although 20 RhoGAPs exhibited Cdc42 GAP activity. Previously proposed Cdc42-specific RhoGAPs, such as ARHGEFAP17 and ARHGAP31 exhibited either no activity or also even more efficiently inactivated Rac1.

RhoGAP activities, that were well described before, largely matched the screen results. As expected, the RhoGAPs of the SRGAP family, SRGAP1, SRGAP2, SRGAP3, and ARHGAP4 (also known as SRGAP4), showed activity towards Rac1, throughout. SRGAP2 showed strong Cdc42 activity, additionally, and ARHGAP4 showed activity towards all 3 Rho GTPases. The two chimaerins CHN1 and CHN2 showed exclusive activity towards Rac1, as expected. The phylogenetically related RhoGAPs ARHGAP12, ARHGAP15, ARHGAP25 and ARHGAP9 also showed predominant activity towards Rac1. The homologous ARHGAP21 and ARHGAP23 showed activity towards RhoA, whereas the latter showed activity towards Rac1, additionally. The two RhoGAPs of the p190 family, ARHGAP35 and ARHGAP5, were catalytically active towards RhoA, as expected. The related RhoGAPs of the DLC family, STARD8 (DLC3), STARD13 (DLC2) and DLC1 RhoGAPs showed activity towards RhoA, as expected. However, out of these only STARD8 showed activity towards Cdc42. The RhoGAPs of the ARAP family showed activity towards Rac1 and Cdc42. Surprisingly, ARAP2, which lacks the catalytically essential arginine residue, also decreased Rho GTPase activities of RhoA, Rac1 , and Cdc42 in the screen. Furthermore, FAM13A, which also lacks the catalytically active arginine

residue, decreased the activity of Rac1 and Cdc42. All the other 5 arginine finger lacking RhoGAPs showed no activity, as well as the two GAP-like proteins PIK3R1 and PIK3R2, which lack conserved Rho GTPase binding residues and conserved amino acids around the arginine finger (Amin *et al.*, 2016).

5.2.6 Validation of family-wide analysis of RhoGEF and RhoGAP activities

5.2.6.1 FRET screen control parameter based quality control

In order to further validate the screen data by an additional quality analysis, I exploited and analysed parameters extracted from the screen raw data by automated image analysis, including expression levels of the RhoGEFs and RhoGAPs, expression levels of the FRET sensors and the area of the region of interest (as a measure for transfection efficiency and viability of the cells). I controlled potential interdependence between the FRET ratio obtained in the screen and parameters that were susceptible to biological and technical variability by calculation of Pearson's correlation coefficient r for the sum of all screen samples, by approximatively assuming linear relationship (Mukaka, 2012). I showed before that Rho GTPase activity as determined by FRET ratio correlates with intensity of FRET sensor (Appendix Figure 7.7). As the expression levels of the RhoGEFs and RhoGAPs varied, I first controlled if this would affect the expression levels of the FRET sensors and as a secondary effect the FRET-ratio. mVenus intensity of all screen samples plotted against mCherry intensity showed a low but consistent negative correlation throughout the RhoGEF and the RhoGAP screens (Appendix Figures 7.11A and 7.12A) indicating that samples with low RhoGEF or RhoGAP expression had higher levels of FRET sensor. However, this effect did not systematically affect obtained FRET-ratios as evident from absence of correlation between mVenus intensity and FRET-ratio as well as mCherry intensity and FRET-ratio (Appendix Figures 7.11B+C and 7.12B+C). Furthermore, this also confirmed the experiments which showed that already minimal amounts of active RhoGEFs and RhoGAPs are sufficient to significantly change the FRET-ratio (Figures 5.12 and 5.13). I next analysed if high FRET sensor expression or high RhoGEF or RhoGAP expression would have an effect on the cell viability as determined by the area of the region of interest. mVenus intensity negatively correlated with the area of transfected cells, especially for the RhoGEF screen, indicating that high levels of FRET sensors might be toxic to the cells (Appendix Figures 7.11D and 7.12D). High levels of RhoGEF and RhoGAP expression, however, did not negatively correlate with the area indicating that these are not toxic to the cells (Appendix Figures 7.11E and 7.12E). Conversely, the region of interest increased with higher levels of RhoGEFs and RhoGAPs, indicating that the RhoGEF and RhoGAP expression level is a critical and limiting factor of the region of

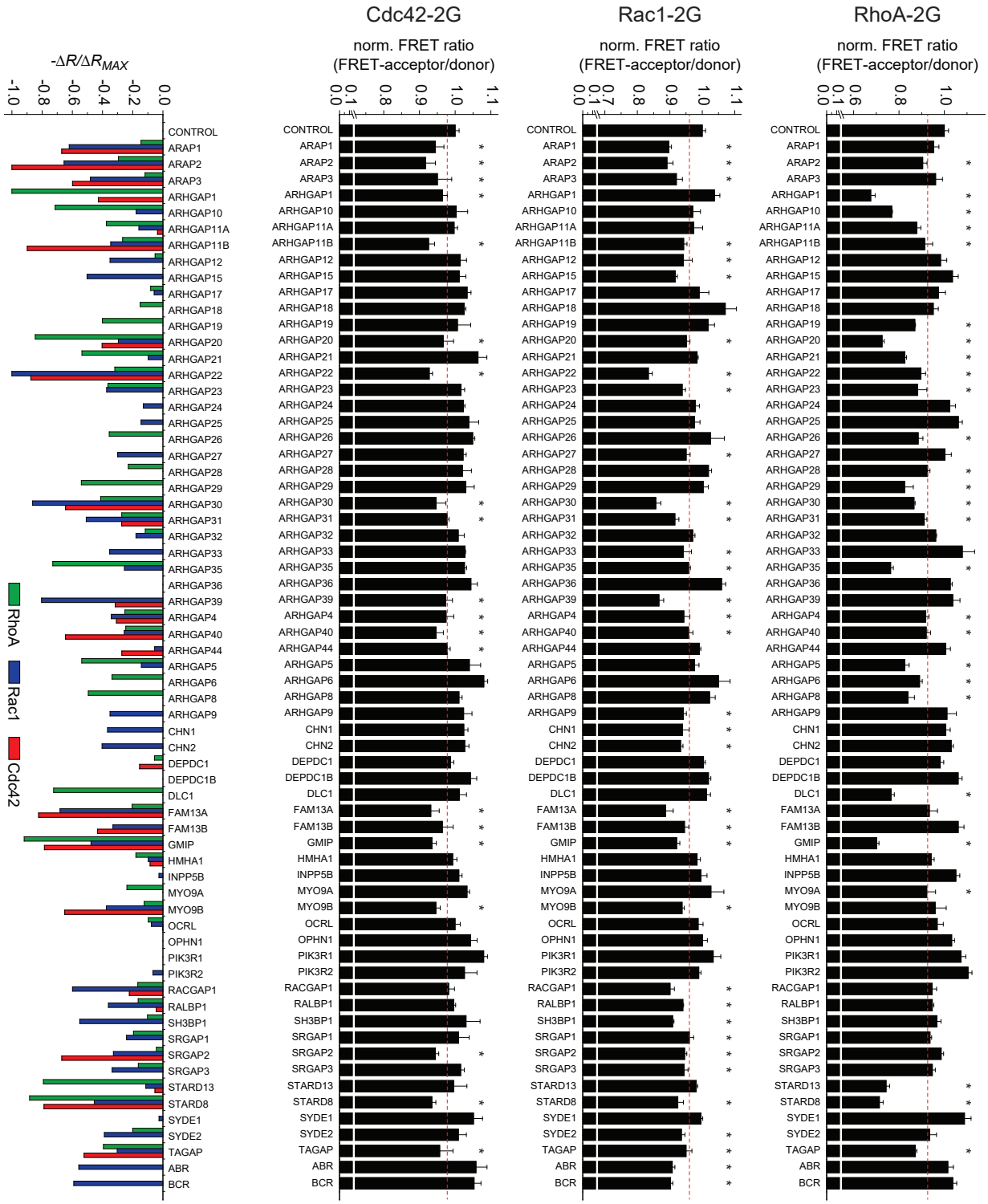

Figure 5.18 see next page

Figure 5.18 (continued) Systematic family-wide FRET-based RhoGAP activity screen. HEK293T RhoGDI knockdown cells were transfected with the mCherry-labelled RhoGAP cDNA expression library and the FRET sensors RhoA-2G, Rac1-2G, and Cdc42-2G in a 96 well format. Control was transfected with mCherry alone. 48 h after transfection cells were subjected to automated epifluorescent microscopic image acquisition. FRET ratio was calculated as FRET-acceptor channel intensity divided by donor channel intensity. For control four wells were averaged per plate, all values were normalised to control. Mean and standard deviation of three independent plates are given in the graphs. Dashed red line indicates threshold: 4σ of control+RhoGDI (0.9265) for RhoA, 4σ of control (0.9603) for Rac1, 2σ of control (0.9779) for Cdc42. Significance of values below the threshold was calculated by Student's t-test versus control followed by Benjamini-Hochberg procedure, significant values are marked with an asterisk (*). Graph on the bottom shows quantification of RhoGAP activity and allows direct comparison of activities towards RhoA (green), Rac1 (blue), and Cdc42 (red). The change in FRET ratio compared to control (ΔR) was normalised to the maximal FRET ratio change (ΔR_{MAX}).

interest. Importantly, the area of transfected cells showed no correlation with the obtained FRET-ratio (Appendix Figures 7.11F and 7.12F). Taken together, this additional quality analysis shows that the screening-scale FRET-based analysis of RhoGEF and RhoGAP activities was not susceptible to deviation by biological and technical sample variation and did not suffer from intrinsic systematic errors.

5.2.6.2 RhoGEF and RhoGAP activity is independent of their subcellular localisation

In parallel to the RhoGEF and RhoGAP substrate specificity screen, I and others in the lab performed a systematic analysis of the subcellular localisation of all 141 RhoGEFs and RhoGAPs (see section 5.3 "Systematic analysis of RhoGEF and RhoGAP localisation at focal adhesions" and data not shown). This localisation screen revealed that RhoGEFs and RhoGAPs inherently localise to distinct structures at steady state, decorating virtually all cellular compartments[4] . Rho GTPases reside at cellular membranes, including plasma membrane and endomembranes (Figure 5.1 and Figure 5.4). However, when inactive they are bound and solubilised in the cytosol by RhoGDI which shields them from getting activated by RhoGEFs. Importantly, Rho GTPase signalling is assumed to occur at the plasma membrane (Bustelo *et al.*, 2007; Ridley, 2011). I therefore analysed if the FRET sensors would not be accessible to some of the RhoGEFs and RhoGAPs due to spatial segregation. Notably, RhoGEFs and RhoGAPs from all different cellular structures and compartments successfully activated the FRET sensors and, more importantly, the sum of RhoGEFs and RhoGAPs that were active towards at least one Rho GTPase in the screen did not show a systematic difference in localisation proportions than RhoGEFs and

[4] confocal live-cell microscopy of transiently expressed mCitrine fusion of RhoGEFs and RhoGAPs was performed by Oliver Rocks, Cytochalasin D-induced actin co-aggregation assay was performed by Juliane Rademacher

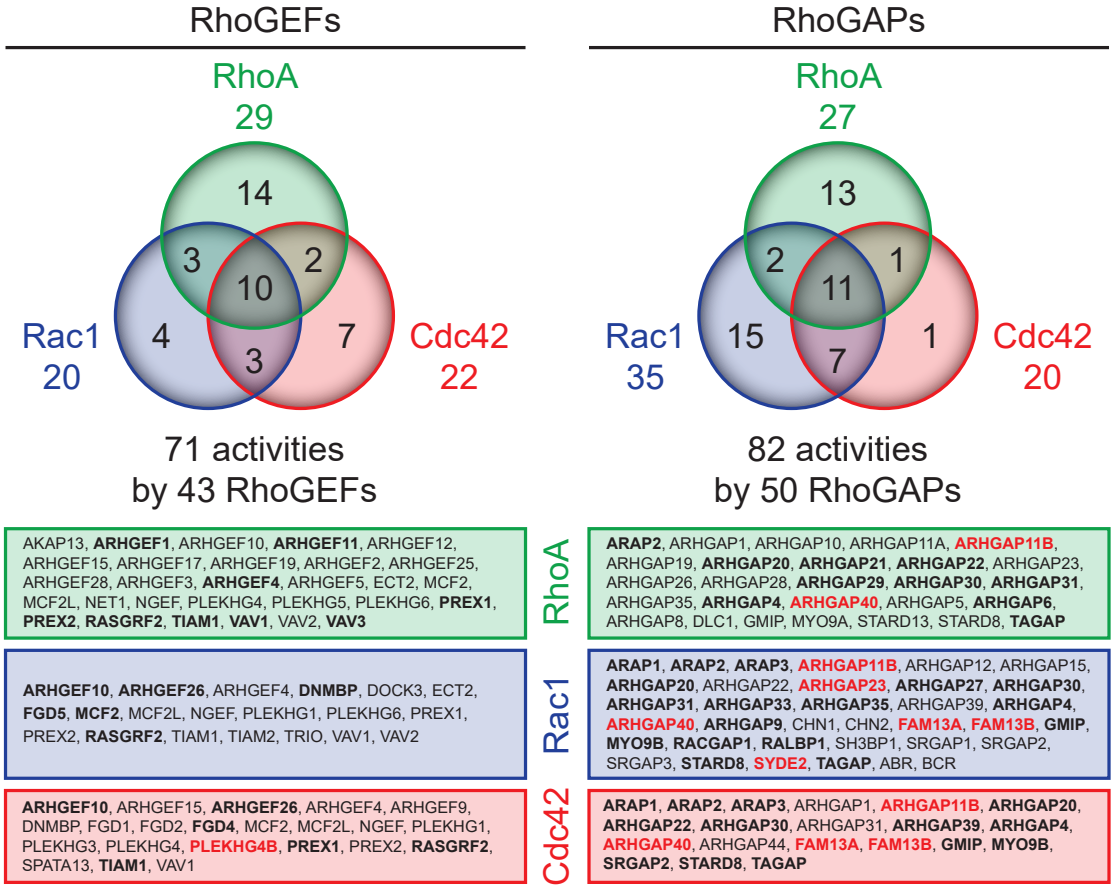

Figure 5.19 Venn diagrams of RhoGEF and RhoGAP substrate specificity screen results. Venn diagrams show the numbers of RhoGEFs and RhoGAPs with single or multiple activities towards RhoA, Rac1, and Cdc42, as revealed by systematic family-wide FRET-based substrate specificity analysis. Below the names of RhoGEFs and RhoGAPs with specificity towards RhoA (green box), Rac1 (blue box), and Cdc42 (red box) are given. RhoGEFs and RhoGAPs whose activity has been described for the first time are highlighted in red, those which were described for the first time *in vivo* are highlighted in bold.

RhoGAPs that were inactive in the screen (Appendix Figure 7.13). This indicates that spatial segregation did not have an influence on the ability as well as the efficiency of RhoGEFs or RhoGAPs to regulate the activity of the FRET sensors.

5.2.6.3 RhoGEF and RhoGAP activities identified in the substrate specificity screen are in agreement with known activities

To further control the validity and the sensitivity of the screen, I compared the RhoGEF and RhoGAP activities identified by the screen with the activities that were identified in the meta-analysis. There was an overall 84 %, 62 %, and 62 % agreement between the screen and the meta-analysis gold standard for RhoA, Rac1 and Cdc42, respectively. For the RhoGEF screen the agreement was 88 %, 62 %, and 77 % and for the RhoGAP screen 78 %, 63 %, and 41 % for RhoA, Rac1 and Cdc42, respectively. The values compared to the silver standard were very similar. I next took a closer look at the nature of the mismatches. In principle, most of the mismatches were "false negative"[5] results for which activity had been well described in literature, which I did not detect in the screen (12 %, 30 %, and 28 % for RhoA, Rac1 and Cdc42, respectively), only a minor part of the mismatches were due to "false positive" hits (7 %, 10 %, and 10 % for RhoA, Rac1 and Cdc42, respectively). The reason why I did not detect these activities could either be an insufficient sensitivity of the assay or regulation of RhoGEF and RhoGAP activity by autoinhibition which may not have been effective in *in vitro* assays in the literature (see 2.2.5 and 5.2.7). I therefore hypothesised that by use of full length constructs, as employed in the screen, autoinhibition of RhoGEF and RhoGAP activity would substantially contribute to the relatively large amount of "false negative" results. Therefore, I compared the information about autoinhibitory control from the meta-analysis with the "false negative" results and found that indeed for about two third of the "false negative" results autoinhibitory mechanism have been suggested before (Figure 5.20 and Appendix Figure 7.14). Taking this into account the screens showed a remarkably high agreement with previously described activities of RhoGEFs and RhoGAPs.

5.2.7 RhoGEF and RhoGAP activity is regulated by autoinhibition

The activity of many of the RhoGEFs and some of the RhoGAPs has been shown to be subject to autoinhibition or autoregulation (see 2.2.5). In the meta-analysis I found evidence for such regulation of activity for 41 RhoGEFs and 11 RhoGAPs (Table 5.2 and Table 5.3). I therefore set out to investigate if autoinhibition of activity applies to RhoGEFs and RhoGAPs as a common principle. To this end, I compared the activity

[5] although the results which did not match with those from the meta-analysis are not necessarily wrong, they will for the sake of convenience be referred to as "false positive" and "false negative"

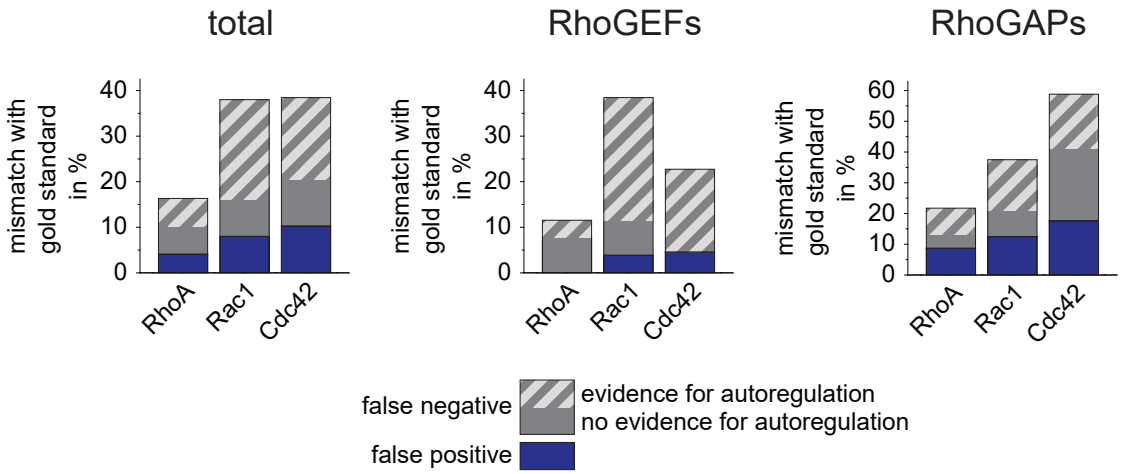

Figure 5.20 RhoGEF and RhoGAP activities identified by screen and by meta-analysis coincide well. RhoGEF and RhoGAP activities from the screen were compared to activities from the meta-analysis (in this figure results were compared to gold standard list, comparison to silver standard list is shown in Appendix Figure 7.14). Results are shown as % of total number of activities included in the gold standard list. "False positive" (blue) and "false negative" (grey) results of the FRET screen were defined with regard to gold standard list. "False negative" results are shown as sum of results for which autoinhibition of activity has been suggested (striped grey) and for which it has not been described yet (uniform grey). The combined results are shown on the left (total), the two graphs in the centre and on the right show the individual results of the RhoGEF screen and the RhoGAP screen.

of shorter isoforms of a subset of RhoGEFs and RhoGAPs, potentially lacking domains and regions responsible for autoinhibition, to the longest isoform in a semiquantitative manner (Table 5.1). Up to 95 % of human gene products have been estimated to undergo alternative splicing resulting in different protein isoforms of the same gene (Pan *et al.*, 2008) and this has been shown to have high impact on protein function in health and disease (Wang and Cooper, 2007; Stastna and Van Eyk, 2012). Expectedly, most of the RhoGEF and RhoGAP proteins have multiple isoforms arising from the same gene by alternative splicing or variable promoter usage. In the FRET screen I included by default the longest isoform of RhoGEFs and RhoGAPs (usually denoted as the canonical isoform). I hypothesised that isoform variations would also have impact on their activity and maybe even substrate specificity. Furthermore, I included truncated constructs of RhoGEFs and RhoGAPs which potentially lacked autoregulatory elements in the analysis (Table 5.1). I modified the analysis of the FRET-based Rho GTPase activity assay in order to be able to quantitatively assess the efficiency of the catalytic activity of RhoGEFs and RhoGAPs. By normalising the FRET ratio to the expression levels of the respective RhoGEF or RhoGAP by means of the mCherry intensity, I got a quantifiable measure, to which statistical analysis could be applied.

Strikingly, essentially all shorter isoforms or truncations of RhoGEFs that I tested

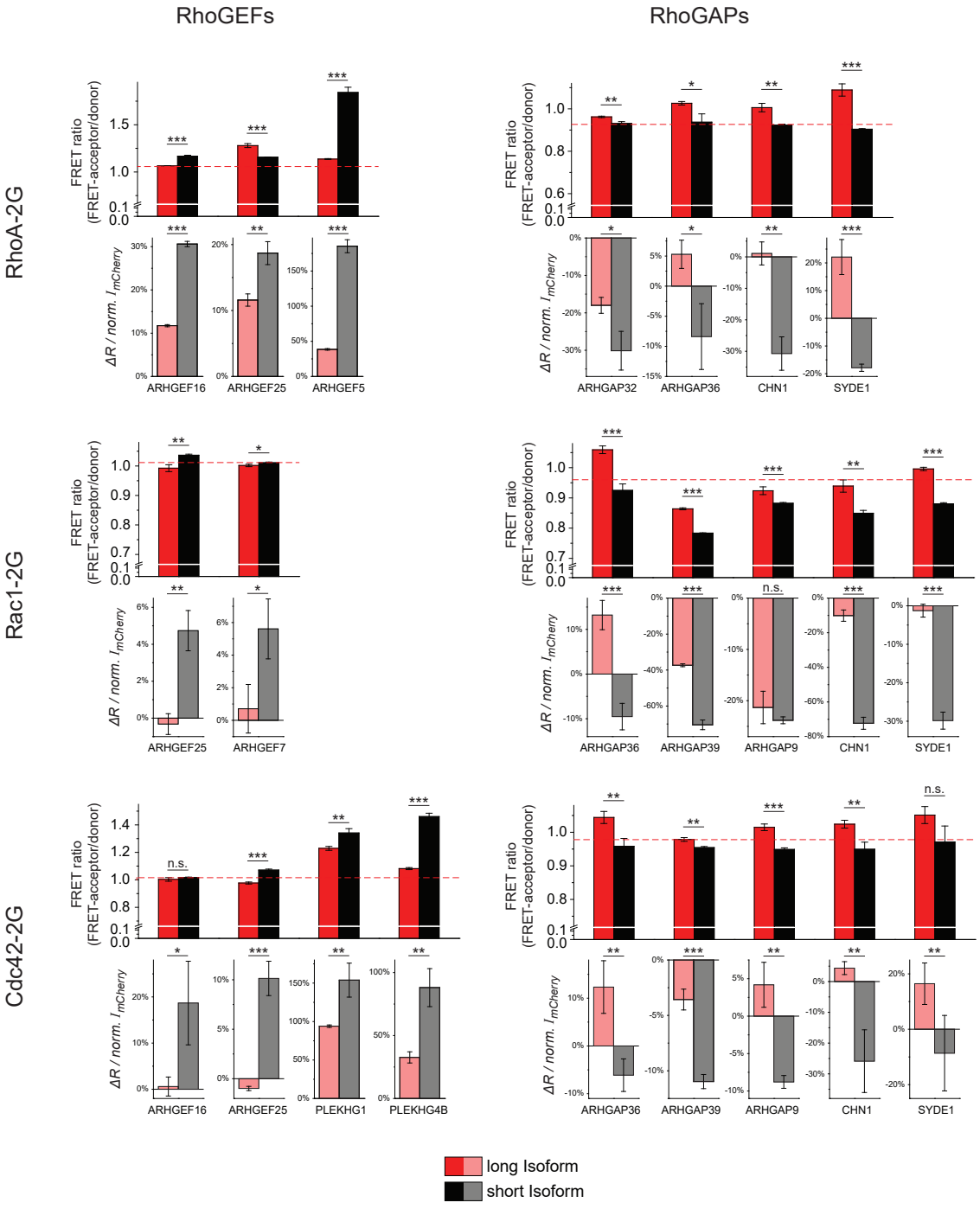

Figure 5.21 RhoGEF and RhoGAP activity is subject to autoinhibition. Full length canonical isoforms and shorter isoforms or truncations of RhoGEFs and RhoGAPs were expressed together with the FRET sensors as described in figure 5.17 and 5.18. The upper diagram for each sensor shows the FRET ratios calculated as FRET-acceptor channel intensity divided by donor channel intensity. The lower diagrams show the semiquantitative analysis, where each sample was normalised to its mCherry intensity (which was itself normalised to the mCherry intensity of the control). Values reflect arbitrary units. Diagrams show mean and standard deviation of three independent samples. Significance levels were calculated by unpaired t-tests as indicated: ***p<0.001, **p<0.01, *p<0.05, n.s.=not significant

showed a higher activity to at least one of the Rho GTPases compared to the long isoforms (Figure 5.21). For example ARHGEF16, which did not show any activity in the screen showed increased activity towards RhoA in its shorter isoform 2. Furthermore, the shorter canonical isoform 1 of ARHGEF25 showed increased activity towards all 3 Rho GTPases compared to the longer non-canonical isoform 3. ArhGEF5 has been shown to be autoinhibited by an N-terminal helical motif (Yohe *et al.*, 2007), accordingly, the isoform 2 which lacks an extensive N-terminal region showed a dramatic increase in activity towards RhoA compared to the canonical isoform 1. Whether or not ARHGEF6 and ARHGEF7 (also known as α-Pix and β-Pix) have a RhoGEF activity is still very controversial (Rosenberger and Kutsche, 2006). In the FRET screen both of these RhoGEFs did not show any activity (Figure 5.17). I compared the activity of the canonical isoform 4 of ARHGEF7 to isoform 1 which lacks an N-terminal Calponin-homology domain, responsible for actin binding. Isoform 1 showed a slightly but significantly increased activity towards Rac1. However, if this activity is relevant in a biological context would still need to be elucidated. PLEKHG1 and PLEKHG4B both showed activity towards Cdc42 in the screen. This activity could further be increased when parts of the C- or N-terminal region were missing.

Remarkably, also the shorter isoforms and truncations of RhoGAPs showed higher catalytic activity than their longer counterparts. Shorter versions of CHN1 and SYDE1 both showed a strong increase in GAP activity towards all 3 Rho GTPases. CHN1 which lacks an N-terminal SH2 domain in its short isoform α1 and thus potentially lacks a tyrosine phosphorylation-dependent autoinhibitory mechanism. Additionally, the short isoform might lack elements responsible for selectivity of the activity as isoform α2 only showed activity towards Rac1. A truncated version of ARHGAP39 lacking 2 N-terminal WW domains and a proline rich region also showed increased activity towards Rac1 and Cdc42 compared to the full length version. Interestingly, ARHGAP9, which only showed activity towards Rac1 in its full length version, also showed activity towards Cdc42 when the isoform 3 was expressed which lacked an N-terminal SH3 domain. This suggests that autoregulatory features might not only modulate the efficiency, but also the substrate selectivity of RhoGAPs.

Surprisingly, the short isoform 2 of ARHGAP36 showed increased "GAP" activity compared to the long isoform. This was unexpected because ARHGAP36 lacks the catalytic arginine residue, responsible for stimulation of the hydrolysis reaction of GTP. Nevertheless, RhoGAPs lacking the catalytic arginine residue have been shown to still bind Rho GTPases with high affinity (Graham *et al.*, 1999; Leonard *et al.*, 1998; Rowland *et al.*, 2011). Thus, they might still participate in regulation of Rho GTPase by binding to and thus stabilizing inactive Rho GTPases and thereby shifting the equilibrium of the Rho

GTPase activation and inactivation cycle.

Taken together, these experiments suggests that autoinhibition is a widespread mechanism for the regulation of activity and substrate selectivity of not only RhoGEFs, but also most RhoGAPs. Furthermore, isoform variations of RhoGEFs and RhoGAPs might add another layer of complexity to the regulation of context-specific Rho GTPase signalling, due to variations in activity as well as substrate selectivity of RhoGEF and RhoGAP activity.

Table 5.1 Isoforms of RhoGEFs and RhoGAPs employed for semiquantitative analysis of RhoGEF and RhoGAP activity. The canonical isoform is marked with an asterisk (*). Artificial truncations of the canonical isoform were used where indicated. AA = Amino acid, CH = Calponin-homology, PRR = Proline-rich region, PX = Phox, SH2 = Src-homology 2, SH3 = Src-homology 3.

RhoGEF /RhoGAP	Long isoform	Short isoform	Differences of the short from the long isoform and missing features
ARHGEF16	Isoform 1*	Isoform 2	AA 1-288 missing
ARHGEF25	Isoform 3	Isoform 1*	Alternative N-terminus 39 AA shorter
ARHGEF5	Isoform 1*	Isoform 2	AA 1-1078 missing
ARHGEF7	Isoform 4*	Isoform 1	AA 1-178 missing (CH domain), alternative C-terminus
PLEKHG1	Isoform 1*	Truncation	AA 433-1385 missing
PLEKHG4B	Isoform 1*	Truncation	AA 1-633 missing
ARHGAP32	Isoform 1*	Isoform 2	AA 1-349 missing (PX domain and SH3 domain)
ARHGAP36	Isoform 1*	Isoform 2	AA 2-32 missing
ARHGAP39	Isoform 1*	Truncation	AA 2-681 missing (2 WW domains and PRR)
ARHGAP9	Isoform 1*	Isoform 3	AA 1-184 missing (SH3 domain)
CHN1	Isoform α2*	Isoform α1	Alternative N-terminus 125 AA shorter (SH2 domain)
SYDE1	Isoform 1*	Isoform 2	AA 30-96 missing (part of PRR)

5.2.8 Rationally curated RhoGEF and RhoGAP substrate specificity

In contrast to studies that focus only on a single Rho regulator, the standardised screening approach allowed me to not only compare the catalytic efficiencies of all RhoGEFs or all

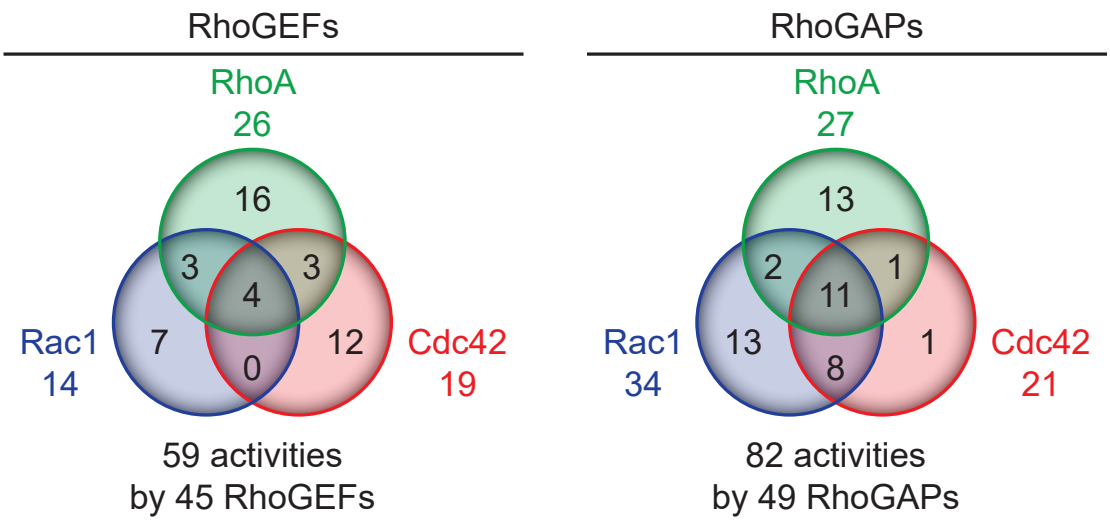

Figure 5.22 Venn diagrams of curated RhoGEF and RhoGAP substrate specificities. Venn diagrams show the numbers of RhoGEFs (left) and RhoGAPs (right) with single or multiple activities towards RhoA, Rac1, and Cdc42, as revealed by systematic family-wide FRET-based substrate specificity analysis and subsequent rational data filtering.

RhoGAPs with each other but also to directly relate the efficiencies of a given RhoGEF or RhoGAP towards the three Rho proteins. This enabled me to ultimately generate a curated specificity list in which I assigned a single major substrate to those regulators that exhibit a predominant activity for one GTPase and only minor additional activities towards other GTPases. Thereby, I rejected those activities which were probably not relevant in a biological context. To do so, I quantified the change in FRET ratio normalised to the maximal change observed in each screen (Figure 5.17 and 5.18). Based on these normalised RhoGEF and RhoGAP efficiencies, those with only 25 % or less efficiency compared to the main activity were neglected for each RhoGEF or RhoGAP (Table 5.2 and 5.3). Furthermore, results from the autoregulation analysis (see 5.2.7) were integrated to generate a rationally curated RhoGEF and RhoGAP substrate specificity list.

Notably, after this data processing step, the selectivity of RhoGEFs towards one Rho GTPase was largely restored. Only 10 out of 45 RhoGEFs had activities towards 2 or 3 Rho GTPases. However, RhoGAPs still maintained their relatively low selectivity. 22 out of 49 active RhoGAPs had multiple activities, 11 of them showed activity towards all 3 Rho GTPases (Figure 5.22). This suggests a functional model of Rho GTPase signalling where RhoGEFs precisely activate specific Rho GTPases in a context-specific manner, whereas RhoGAPs might function in two different ways, one to also inactivate Rho GTPases selectively in a context-specific manner, and the other, to more globally and less selectively inactivate Rho GTPases and thereby prevent subcellular signal leakage and unspecific accumulation of active Rho GTPases.

Table 5.2 RhoGEF substrate specificities from FRET-based screen and literature meta-analysis. Substrate specificities from screen data and curated screen data, as well as from silver and gold standard literature meta-analysis are shown, evidence for autoinhibitory regulation is listed.

	RhoGEF activity screen						Meta-analysis							
	Screen list			Curated list			Silver list			Gold list				
	RhoA	Rac1	Cdc42	RhoA	Rac1	Cdc42	RhoA	Rac1	Cdc42	RhoA	Rac1	Cdc42	Autoinhibition	Comment
AKAP13	+	-	-	+	-	-	+	-	-	+			+	
ALS2	-	-	-	-	-	-	-		-	-		-		
ARHGEF1	+	-	-	+	-	-	+	-	-				+	
ARHGEF10	+	+	+	+	-	+	+	-	-	+	-	-	+	
ARHGEF10L	-	-	-	-	-	-	+	-	-	+	-	-		
ARHGEF11	+	-	-	+	-	-	+	-	-				+	
ARHGEF12	+	-	-	+	-	-	+	-	-	+	-	-	+	
ARHGEF15	+	-	+	-	-	+	+						+	
ARHGEF16	-	-	-	+[1)]	-	-	-			-			+	1) only isoform 2 showed activity
ARHGEF17	+	-	-	+	-	-	+	-	-	+			+	
ARHGEF18	-	-	-	-	-	-	+		-	+		-		
ARHGEF19	+	-	-	+	-	-	+							
ARHGEF2	+	-	-	+	-	-	+	-	-	+	-	-		
ARHGEF25	+	-	-	+	+[1)]	+[1)]	+			+			+	1) only canonical isoform 1 showed activity
ARHGEF26	-	+	+	-	-	+								
ARHGEF28	+	-	-	+	-	-	+	-	-	+	-	-	+	
ARHGEF3	+	-	-	+	-	-	+			+				
ARHGEF39	-	-	-	-	-	-								
ARHGEF4	+	+	+	+	-	+	-		+			+	+	
ARHGEF40	-	-	-	-	-	-	+							
ARHGEF5	+	-	-	+	-	-	+	-	-	+	-	-	+	
ARHGEF6	-	-	-	-	-	-							+	
ARHGEF7	-	-	-	-	+[1)]	-		+					+	1) only isoform 1 showed activity
ARHGEF9	-	-	+	-	-	+	-	-	+	-	-	+		
DNMBP	-	+	+	-	-	+	-	-	+			+	+	
DOCK1	n.d.	n.d.	n.d.	n.d.	n.d.	n.d.	-	+	-	-	+	-	+	
DOCK10	n.d.	n.d.	n.d.	n.d.	n.d.	n.d.	-	+	+	-	+	+		
DOCK11	n.d.	n.d.	n.d.	n.d.	n.d.	n.d.	-	-	+	-	-	+	+	
DOCK2	-	-	-	-	-	-		+	-		+	-		
DOCK3	-	+	-	-	+	-		+	-		+	-	+	
DOCK4	-	-	-	-	-	-		+	-		+		+	
DOCK5	-	-	-	-	-	-							+	
DOCK6	-	-	-	-	-	-	-	+	+	-	+	+	+	
DOCK7	-	-	-	-	-	-	-	+		-	+			
DOCK8	-	-	-	-	-	-			+			+	+	
DOCK9	-	-	-	-	-	-	-	-	+	-	-	+	+	
ECT2	+	+	-	+	-	-		+			+		+	
ECT2L	-	-	-	-	-	-								
FARP1	-	-	-	-	-	-								
FARP2	-	-	-	-	-	-	-			-			+	
FGD1	-	-	+	-	-	+			+			+		
FGD2	-	-	+	-	-	+								
FGD3	-	-	-	-	-	-								
FGD4	-	-	+	-	-	+								
FGD5	-	+	-	-	+	-			+					
FGD6	-	-	-	-	-	-								
ITSN1	-	-	-	-	-	-	-	-	+			+	+	
ITSN2	-	-	-	-	-	-		-	+					
KALRN[1)]	-	-	-	-	-	-		+			+		+	1) two GEF domains
MCF2	+	+	+	+	+	+	+	+	+	+		+	+	
MCF2L	+	+	+	+	-	+	+		+	+		+	+	
MCF2L2	-	-	-	-	-	-								
NET1	+	-	-	+	-	-	+			+				
NGEF	+	+	+	+	-	-		+	+				+	
PLEKHG1	-	+	+	-	-	+								
PLEKHG2	-	-	-	-	-	-	-	+	+				+	
PLEKHG3	-	-	+	-	-	+		+	+					
PLEKHG4	+	-	+	-	-	+								
PLEKHG4B	-	-	+	-	-	+								
PLEKHG5	+	-	-	+	-	-	+			+				
PLEKHG6	+	+	-	+	+	-	+	-	-	+			+	
PLEKHG7	-	-	-	-	-	-								
PREX1	+	+	+	-	+	-	-	+			+		+	
PREX2	+	+	+	+	+	+		+			+		+	
RASGRF1	-	-	-	-	-	-	-	+	-		+		+	
RASGRF2	+	+	+	+	+	+								
SOS1	-	-	-	-	-	-		+			+		+	
SOS2	-	-	-	-	-	-								
SPATA13	-	-	+	-	-	+	-		+	-		+	+	
TIAM1	+	+	+	-	+	-		+			+		+	
TIAM2	-	+	-	-	+	-	-	+	-	-	+	-		
TRIO[1)]	-	+	-	-	+	-	+	+	-	+	+			1) two GEF domains
VAV1	+	+	+	+	+	-	+	+			+		+	
VAV2	+	+	-	+	+	-		+			+		+	
VAV3	+	-	-	+	-	-		+			+		+	
ABR[1)]	-	-	-	-	-	-								1) dual GEF and GAP function
BCR[1)]	-	-	-	-	-	-	+	+		+	+		+	1) dual GEF and GAP function

Table 5.3 RhoGAP substrate specificities from FRET-based screen and literature meta-analysis. Substrate specificities from screen data and curated screen data, as well as from silver and gold standard literature meta-analysis are shown, evidence for autoinhibitory regulation is listed.

	RhoGAP activity screen						Meta-analysis						Autoinhibition	Comment
	Screen list			Curated list			Silver list			Gold list				
	RhoA	Rac1	Cdc42	RhoA	Rac1	Cdc42	RhoA	Rac1	Cdc42	RhoA	Rac1	Cdc42		
ARAP1	-	+	+	-	+	+								
ARAP2[1]	+	+	+	-[1]	-[1]	-[1]	-	-	-	-	-	-		1) arginine finger missing
ARAP3	-	+	+	-	+	+	+	-	-	+			+	
ARHGAP1	+	-	+	+	-	+			+			+	+	
ARHGAP10	+	-	-	+	-	-	+	-	+	+	-	+		
ARHGAP11A	+	-	-	+	-	-								
ARHGAP11B	+	+	+	+	+	+								
ARHGAP12	-	+	-	-	+	-		+			+			
ARHGAP15	-	+	-	-	+	-		+			+			
ARHGAP17	-	-	-	-	-	-			+			+		
ARHGAP18	-	-	-	-	-	-		-	-					
ARHGAP19	+	-	-	+	-	-	+	-	-	+	-	-		
ARHGAP20	+	+	+	+	+	+	+						+	
ARHGAP21	+	-	-	+	-	-	+							
ARHGAP22	+	+	+	+	+	+	-	+	-	-	+	-		
ARHGAP23	+	+	-	+	+	-								
ARHGAP24	-	-	-	-	-	-	-	+	+	-	+	+	+	
ARHGAP25	-	-	-	-	-	-		+			+			
ARHGAP26	+	-	-	+	-	-	+			+				
ARHGAP27	-	+	-	-	+	-								
ARHGAP28	+	-	-	+	-	-								
ARHGAP29	+	-	-	+	-	-								
ARHGAP30	+	+	+	+	+	+	+							
ARHGAP31	+	+	+	+	+	+	-		+			+		
ARHGAP32	-	-	-	-	-	-		+	+		+	+	+	
ARHGAP33	-	+	-	-	+	-								
ARHGAP35	+	+	-	+	+	-	+			+				
ARHGAP36[1]	-	-	-	-[2]	-[2]	-[2]								1) arginine finger missing; 2) only isoform 2 showed "activity"
ARHGAP39	-	+	+	-	+	+		+			+			
ARHGAP4	+	+	+	+	+	+	+	+	+					
ARHGAP40	+	+	+	+	+	+								
ARHGAP42	n.d.	n.d.	n.d.	n.d.	n.d.	n.d.	+			+				
ARHGAP44	-	-	+	-	-	+		+	+		+	+		
ARHGAP5	+	-	-	+	-	-	+			+				
ARHGAP6	+	-	-	+	-	-								
ARHGAP8	+	-	-	+	-	-	+	-	-	+	-	-		
ARHGAP9	-	+	-	-	+	+[1]								1) only isoform 3 showed activity
CHN1	-	+	-	-	+	+[1]	-	+	-	-	+	-	+	1) only isoform α1 showed activity
CHN2	-	+	-	-	+	-	-	+	-	-	+	-	+	
DEPDC1[1]	-	-	-	-	-	-								1) arginine finger missing
DEPDC1B[1]	-	-	-	-	-	-		+						1) arginine finger missing
DLC1	+	-	-	+	-	-	+	-	+	+			+	
FAM13A	-	+	+	-	+	+								
FAM13B[1]	-	+	+	-	-[1]	-[1]								1) arginine finger missing
GMIP	+	+	+	+	+	+	+	-	-	+	-	-		
HMHA1	-	-	-	-	-	-		+			+		+	
INPP5B	-	-	-	-	-	-								
MYO9A	+	-	-	+	-	-	+			+				
MYO9B	-	+	+	-	+	+	+			+				
OCRL[1]	-	-	-	-	-	-	-	-	-					1) arginine finger missing
OPHN1	-	-	-	-	-	-	+	+	+	+	+	+	+	
PIK3R1[1]	-	-	-	-	-	-			-					1) lacks most GTPase binding residues
PIK3R2[1]	-	-	-	-	-	-								1) lacks most GTPase binding residues
RACGAP1	-	+	-	-	+	-		+	+					
RALBP1	-	+	-	-	+	-	-		+					
SH3BP1	-	+	-	-	+	-	-	+	+	-	+	+		
SRGAP1	-	+	-	-	+	-								
SRGAP2	-	+	+	-	+	+	-	+	-		+			
SRGAP3	-	+	-	-	+	-	-	+		-	+			
STARD13	+	-	-	+	-	-	+	-	+	+	-	+		
STARD8	+	+	+	+	+	+	+	-		+	-			
SYDE1	-	-	-	+[1]	+[1]	+[1]							+	1) only isoform 2 showed activity
SYDE2	-	+	-	-	+	-								
TAGAP	+	+	+	+	+	+								
ABR[1]	-	+	-	-	+	-	-	+		-	+			1) has dual GEF and GAP function
BCR[1]	-	+	-	-	+	-	-	+		-	+		+	1) has dual GEF and GAP function

5.3 Systematic analysis of RhoGEF and RhoGAP localisation at focal adhesions

Focal adhesions are integrin-based adhesion complexes (IACs) and as such key mechanistic and sensory components of cell adhesion and cell migration. Integrins act as receptors for extracellular signals and simultaneously as mechanical linkers between components of the extracellular matrix and intracellular actin fibers. Rho GTPases are important downstream regulators of integrins and translate incoming signals into actin polymerization and actin contractility, which in turn regulates adhesion dynamics. IACs are in constant turnover and mature into different subclasses correlating with activities of different Rho family members. Thus, focal adhesions serve as central signalling nodes where adhesion and cytoskeletal dynamics are orchestrated by Rho GTPases. It is therefore conceivable that RhoGEFs and RhoGAPs, at least transiently, localise at focal adhesions. To date only 10 RhoGEFs and RhoGAPs have been shown to reside on these structures and only 18 have been shown to be associated with focal adhesion signalling (Zaidel-Bar *et al.*, 2007; Winograd-Katz *et al.*, 2014). Given the complexity of the integrin signalling network and its role in the regulation of diverse physiological processes, I was hypothesising that the number of RhoGEFs and RhoGAPs residing at focal adhesions is underestimated. I therefore set out to systematically analyse the localisation of the Rho regulators on these structures by TIRF microscopy.

5.3.1 Establishment of a TIRF microscopic focal adhesion localisation assay

5.3.1.1 Establishment of a stable cell line to identify focal adhesions

In order to establish a system to systematically screen all RhoGEFs and RhoGAPs for steady state localisation at focal adhesions, I created stable cell lines that mildly overexpress mCherry-paxillin. Paxillin is a scaffolding protein, that recruits numerous regulatory and structural proteins to focal adhesions (Deakin and Turner, 2008). Therefore, paxillin is a common marker for focal adhesions. COS-7 and HeLa cell lines were stably transfected with mCherry-paxillin under control of a ubiquitin promoter, to ensure low expression levels, using lentiviral transduction. Then, cells were analysed for their ability to form focal adhesions as identified by mCherry-paxillin. When observed by TIRF microscopy, COS-7 cells, plated on uncoated glass slides, showed well-defined 1.5-6 μm long, ellipsoidal, elongated mCherry-paxillin-enriched structures between 18 h and 24 h after seeding (Appendix Figure 7.15). In contrast, compared to COS-7 cells, HeLa cells showed a less defined mCherry-paxillin distribution at the basal membrane when seeded on uncoated glass slides (Appendix Figure 7.15). The formation of peripheral focal adhesions

could be induced by growing HeLa cells on poly-D-lysine or fibronectin coated glass slides (Appendix Figure 7.15). However, the well-defined morphology and uniform distribution of focal adhesions in COS-7 cells made them ideally suited for a subsequent colocalisation screen with all RhoGEFs and RhoGAPs.

Focal adhesions appear as 2-5 μm ellipsoidal elongated structures which are, depending on the cell type, usually located in the cell periphery, but can also be found in more central regions of the cell. However, there is often a continuum between the different classes of IACs, which are focal complexes, focal adhesions and fibrillar adhesions. Many of the known scaffolding and signalling proteins have been identified in all of these structures (Geiger *et al.*, 2001; Parsons *et al.*, 2010). Furthermore, not all cell types exhibit the full range of adhesion structures. The fact, that both vinculin, a marker for focal complexes, and tensin, a marker for fibrillar adhesions, colocalise with paxillin (Figure 5.23) indicates that the structures I identified by mCherry-paxillin in COS-7 cells are not distinct adhesion classes but rather a continuum of IACs. However, for convenience, the structures identified by mCherry-paxillin will be referred to as focal adhesions.

5.3.1.2 Validation of a TIRF microscopic focal adhesion localisation assay

In order to control the validity of this colocalisation assay, I first set out to test the ability of control markers to colocalise with paxillin. Therefore, I used other known focal adhesion markers, actin filament markers, cytosolic markers and markers for the plasma membrane (Figure 5.23). The linker proteins vinculin, talin and tensin, which are involved in the connection between actin fibers and integrins, all colocalised with paxillin. The actin binding proteins zyxin, VASP and actinin also colocalised with paxillin. However, actinin, which has been shown to localise in the very proximal tip of focal adhesions (Kanchanawong *et al.*, 2010), showed a longitudinally shifted localisation. β-actin was weakly enriched in filamentous F-actin (polymerised actin fibers) structures, such as stress fibers, but mostly localised as cytosolic monomeric G-actin. Lifeact, which serves as a marker for F-actin, showed a partial overlap with paxillin and was, as expected, strongly shifted in the direction of the stress fiber. It is thus possible to distinguish actin associated proteins from focal adhesion localised proteins. Cytosolic mEGFP was not specifically enriched at focal adhesions, but sometimes showed higher intensities in the close surroundings of focal adhesions. This was also true for the plasma membrane marker KRas-HVR and the plasma membrane and endoplasmic reticulum marker EGFR-TMD. This can be explained by a a secondary effect of the cellular volume that is excited by the evanescent wave. In the area of focal adhesions the plasma membrane is closer to the substratum surface with a gap of only 10-15 nm (Medalia and Geiger, 2010). The amplitude of the evanescent wave of

the excitation light drops off exponentially with increasing distance from the glass/water interface. As a consequence, the relative cellular volume that is excited by the evanescent wave is larger in the area of the focal adhesion and its proximate surrounding and, additionally, the molecules closer to the glass/water interface are excited with higher intensity. However, in contrast to the well-defined morphology of the focal adhesion, this unspecific secondary effect could clearly be distinguished from actual focal adhesion localisation by its vast distribution around focal adhesions and its weak intensity contrast, as evidenced by intensity plots (Figure 5.23). Altogether, the identification of focal adhesions by means of mCherry-paxillin and the detection of potential focal adhesion localisation of coexpressed proteins by colocalisation with mCherry-paxillin using TIRF microscopy is a robust and valid method.

5.3.2 37 out of 141 RhoGEFs and RhoGAPs localise at focal adhesions

Table 5.4 RhoGEFs and RhoGAPs that localise at focal adhesions. Categorised list of RhoGEFs and RhoGAPs that colocalised with focal adhesions: Distinct colocalisation (Focal adhesion), specific enrichment in close proximity to focal adhesions with intensity minimum in the centre (Focal adhesion halo), apparent actin- or actinin-like localisation (Actin/Actinin).

Localisation Category	Count	RhoGEFs/RhoGAPs
Focal adhesion	15 RhoGEFs	ARHGEF6, ARHGEF7, ARHGEF19, ARHGEF39, DOCK3, DOCK5, ITSN1, ITSN2, KALRN, PLEKHG1, SOS1, SOS2, TRIO, VAV1, VAV3
	14 RhoGAPs	ARHGAP9, ARHGAP12, ARHGAP31, ARHGAP39, CHN2, DLC1, OCRL, PIK3R1, PIK3R2, SRGAP1, STARD8, STARD13, SYDE1, SYDE2
Focal adhesion "halo"	4 RhoGEFs	ARHGEF40, ECT2L, FARP2, MCF2
	4 RhoGAPs	ARAP2, ARHGAP22, ARHGAP23, SRGAP3
Actin/Actinin	5 RhoGEFs	FGD2, FGD4, PLEKHG2, PLEKHG3, PLEKHG6
	5 RhoGAPs	ARHGAP8, ARHGAP24, ARHGAP28, MYO9A, OPHN1

Having confirmed, that focal adhesion enrichment of a protein can be reliably detected by colocalisation with paxillin in COS-7 cells using TIRF microscopy, I overexpressed all

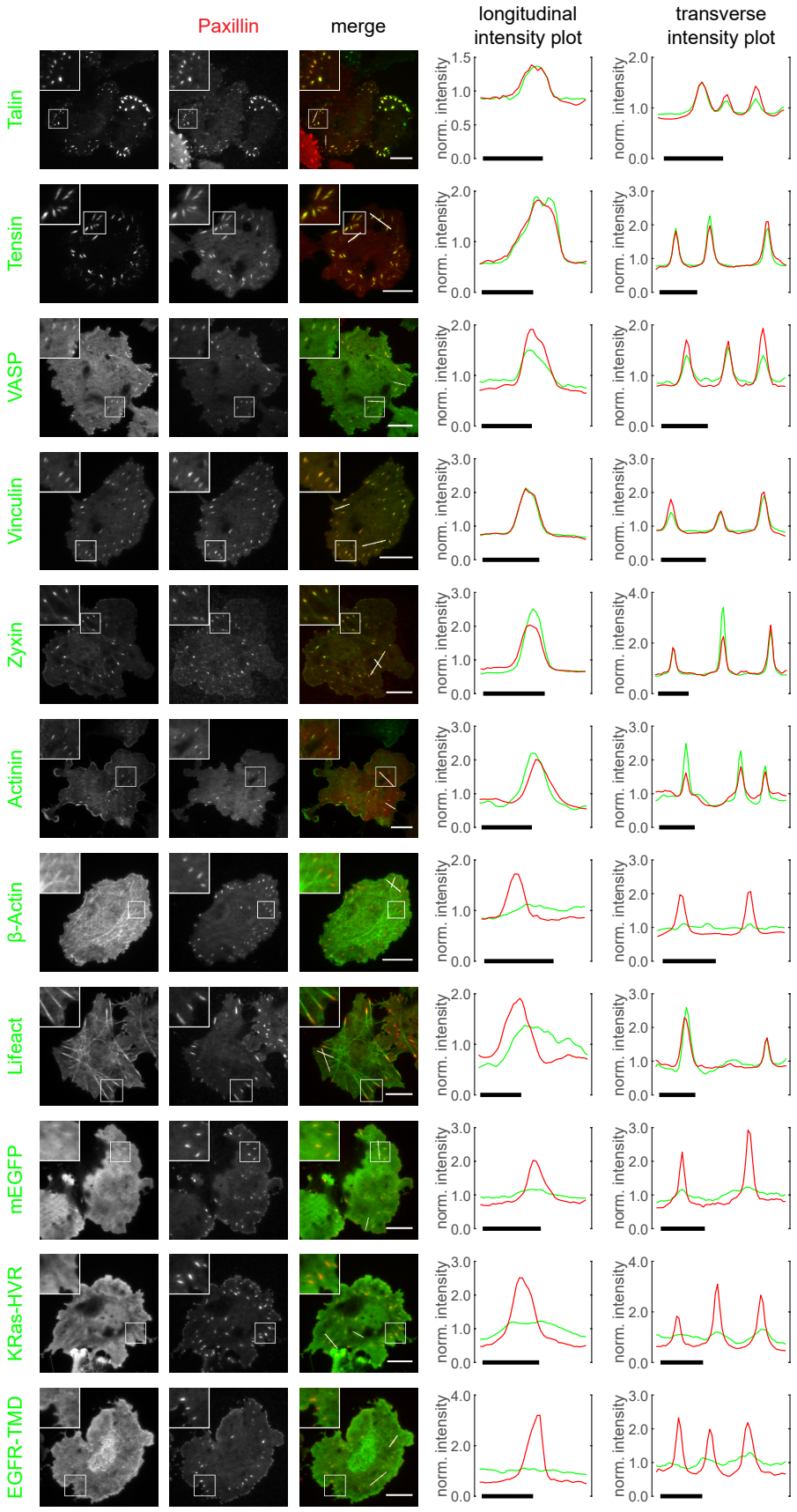

Figure 5.23 see next page

Figure 5.23 (continued) Localisation of control markers to focal adhesions. mCitrine-tagged control markers were expressed in COS-7 cells stably expressing mCherry-paxillin. Images were collected by live cell TIRF microscopy. Fluorescence intensity profiles of longitudinal and transverse sections through focal adhesions are shown on the right and indicated by white lines in the merged images. Intensity plots were normalised to the average intensity over the whole line to maintain relative intensity proportions. Insets on the upper left of each image represents an approximately two-fold magnification of the area indicated by a box. White scale bars in images: 20 μm. Black scale bars in graphs: 5 μm.

RhoGEFs and RhoGAPs in order to screen for steady state focal adhesion localisation. Surprisingly, I observed the clear enrichment of as many as 37 RhoGEFs and RhoGAPs at these structures. Out of these 29 showed a congruent localisation with paxillin as judged by longitudinal and transversal fluorescence intensity plots through the focal adhesions (Figures 5.24 and 5.25). Intriguingly, 4 RhoGEFs and 4 RhoGAPs showed a characteristic halo-like enrichment proximate to focal adhesions with a fluorescence intensity minimum at focal adhesions (Figure 5.26, Table 5.4). Additionally, I observed an intensity minimum at focal adhesions without specific surrounding enrichment for the RhoGEFs FARP1, MCF2L and MCF2L2. Furthermore, 10 RhoGEFs and RhoGAPs showed an actin- or actinin-like localisation (Appendix Figure 7.16, Table 5.4). ARAP3, PREX1, and PREX2 were slightly enriched on focal adhesions and require further investigation. Overexpression of the RhoGAPs ARHGAP10, ARHGAP23, MYO9A, MYO9B, and TAGAP led to complete depletion of focal adhesions. However, for ARHGAP23 and MYO9A GAP-deficient versions were available which lack the catalytically active "arginine finger". Cells expressing these GAP-deficient mutants ARHGAP23-R986K and MYO9A-R2098K showed normal focal adhesions. 84 RhoGEFs and RhoGAPs did not localise on focal adhesions.

5.3.3 Localisation of RhoGEFs and RhoGAPs at focal adhesions correlates with their substrate specificity

The activity of Rho GTPases, especially of RhoA and Rac1, has been shown to be precisely controlled downstream of integrin-mediated signalling during maturation and maintenance of focal adhesions (Lawson and Burridge, 2014). I therefore investigated if an enrichment of RhoGEFs and RhoGAPs with a certain substrate specificity towards one of the Rho GTPases RhoA, Rac1, and Cdc42 at focal adhesions would hint at a particular role of one of these Rho proteins in integrin-mediated signalling at focal adhesions. Interestingly, RhoGEF and RhoGAPs with activity towards Rac1 are overrepresented at focal adhesions. This was evident when all activities that were identified in the RhoGEF and RhoGAP activity screen were summarised, as well as when only RhoGEFs and RhoGAPs with exclusive activity were summarised (Figure 5.27A and Appendix Table 7.1). Importantly,

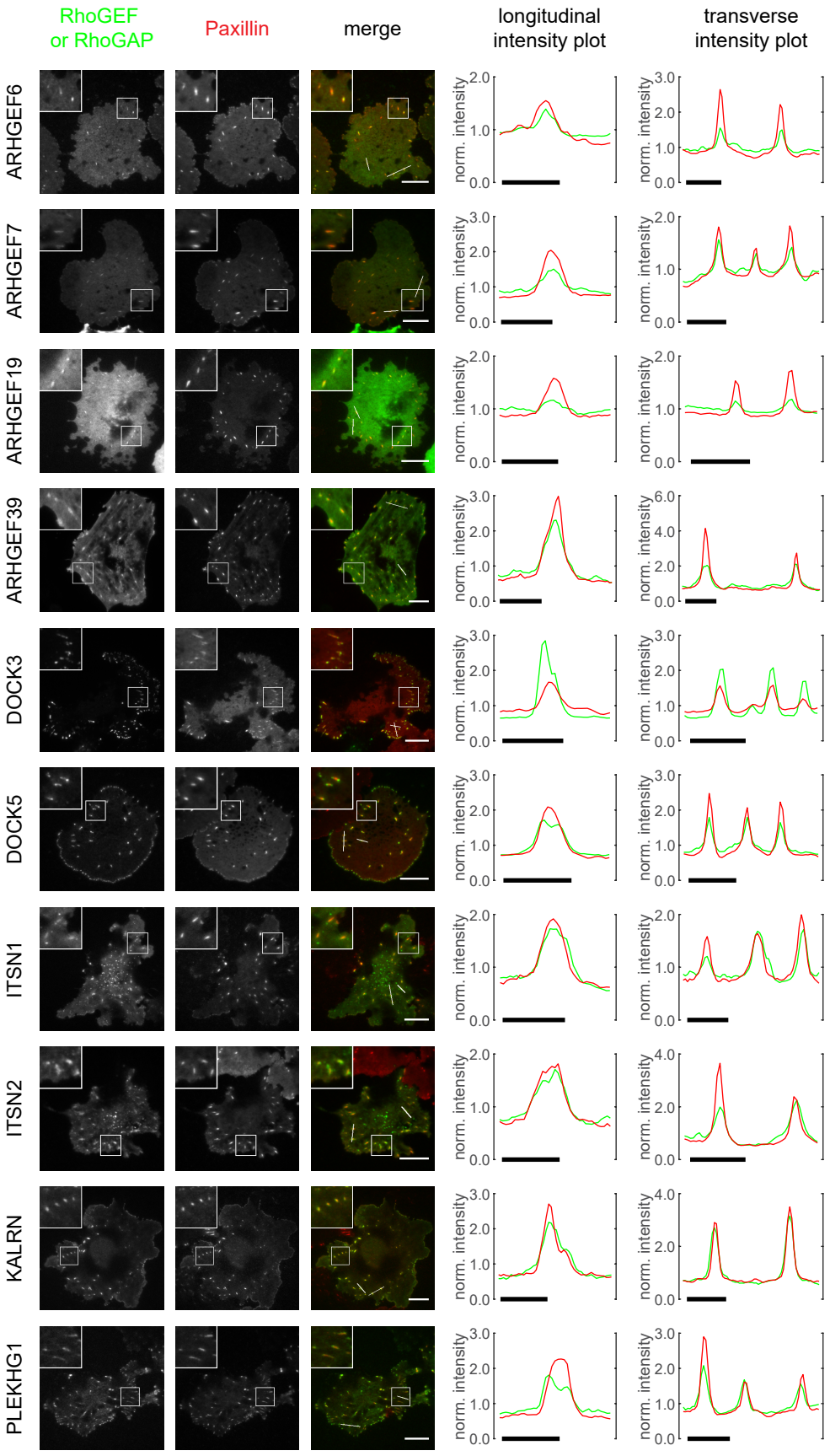

Figure 5.24 see next page

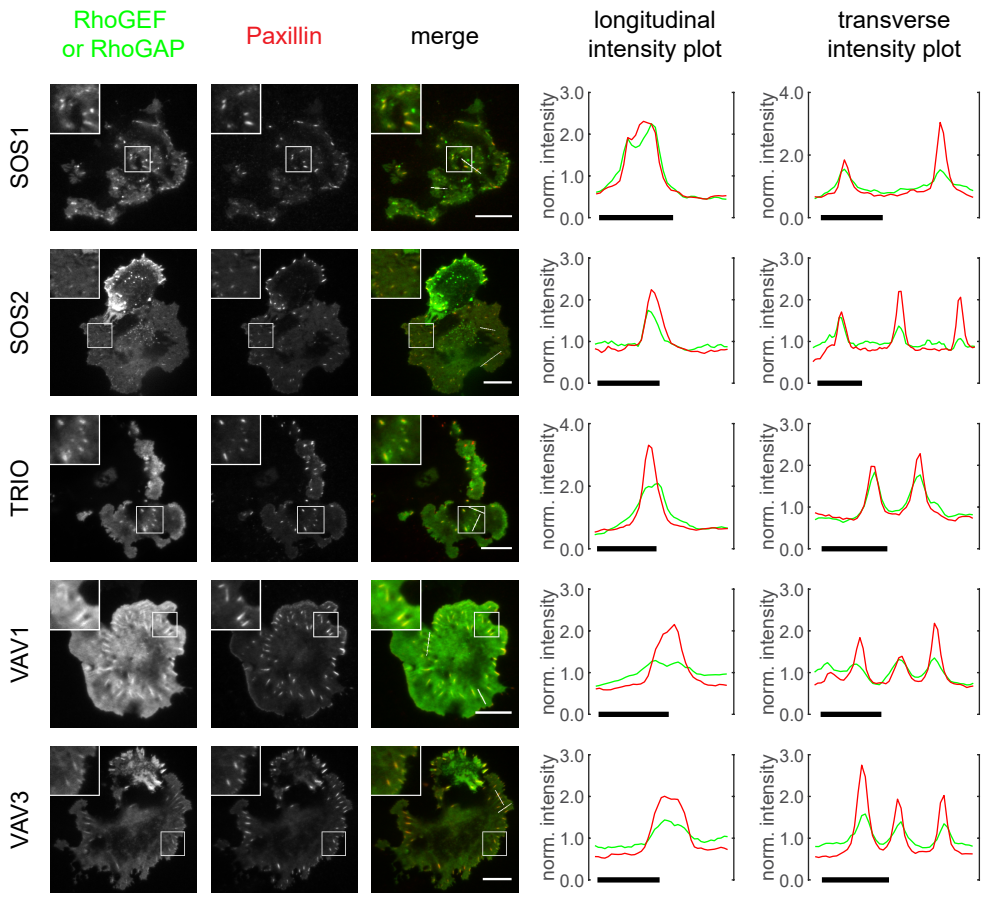

Figure 5.24 (continued) 15 RhoGEFs localise on focal adhesions. mCitrine-tagged RhoGEFs were expressed in COS-7 cells stably expressing mCherry-paxillin. Images were collected by live cell TIRF microscopy. Fluorescence intensity profiles of longitudinal and transverse sections through focal adhesions are shown on the right and indicated by white lines in the merged images. Intensity plots were normalised to the average intensity over the whole line to maintain relative intensity proportions. Insets on the upper left of each image represents an approximately two-fold magnification of the area indicated by a box. White scale bars in images: 20 μm. Black scale bars in graphs: 5 μm.

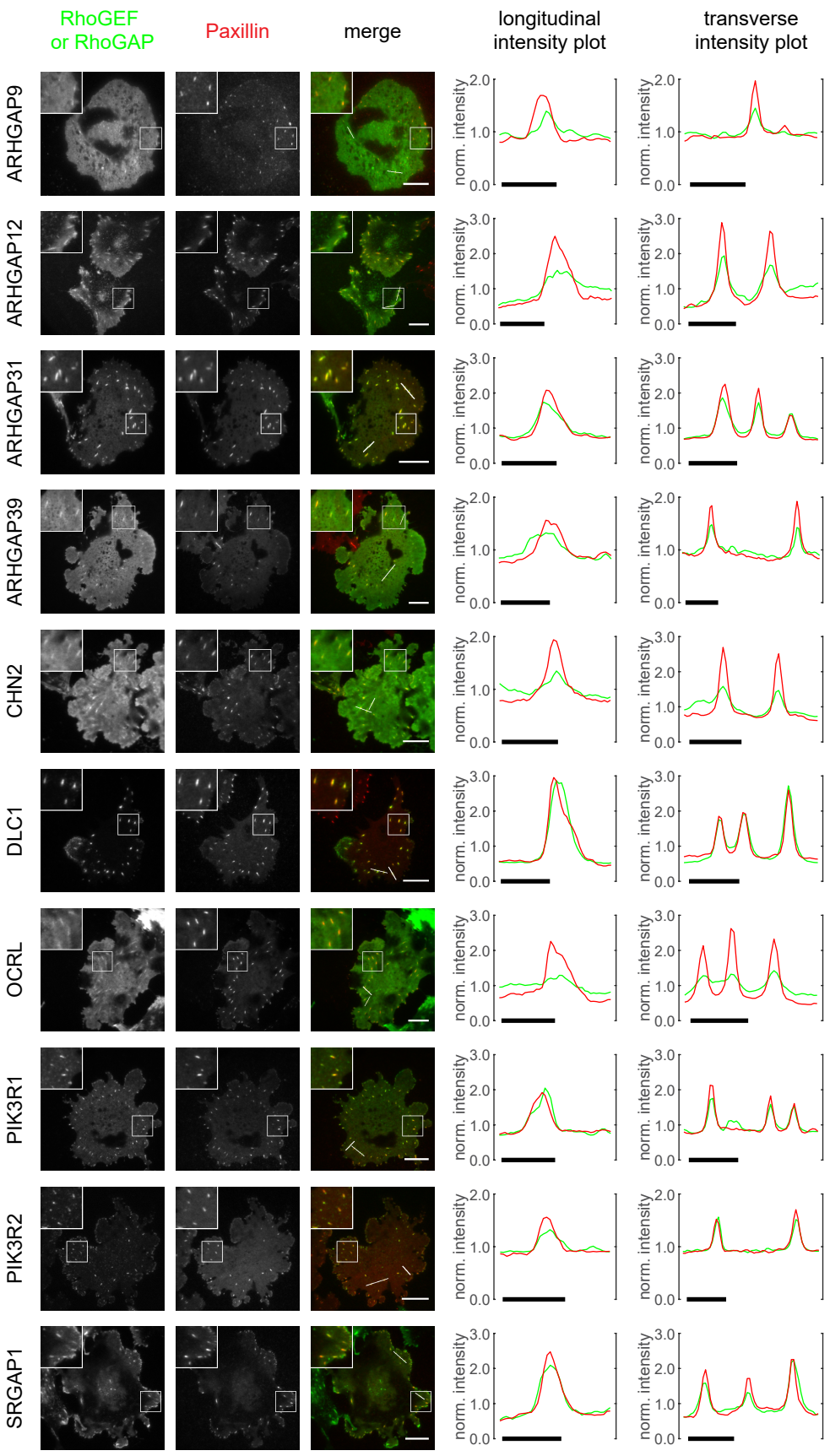

Figure 5.25 see next page

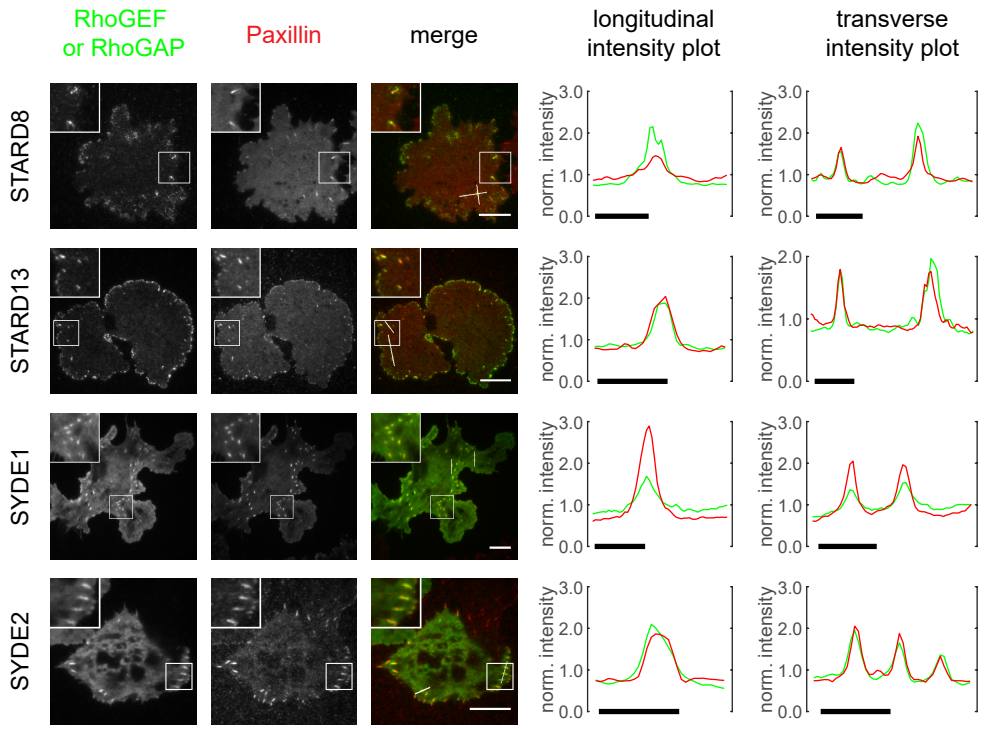

Figure 5.25 (continued) 14 RhoGAPs localise on focal adhesions. mCitrine-tagged RhoGAPs were expressed in COS-7 cells stably expressing mCherry-paxillin. Images were collected by live cell TIRF microscopy. Fluorescence intensity profiles of longitudinal and transverse sections through focal adhesions are shown on the right and indicated by white lines in the merged images. Intensity plots were normalised to the average intensity over the whole line to maintain relative intensity proportions. Insets on the upper left of each image represents an approximately two-fold magnification of the area indicated by a box. White scale bars in images: 20 μm. Black scale bars in graphs: 5 μm.

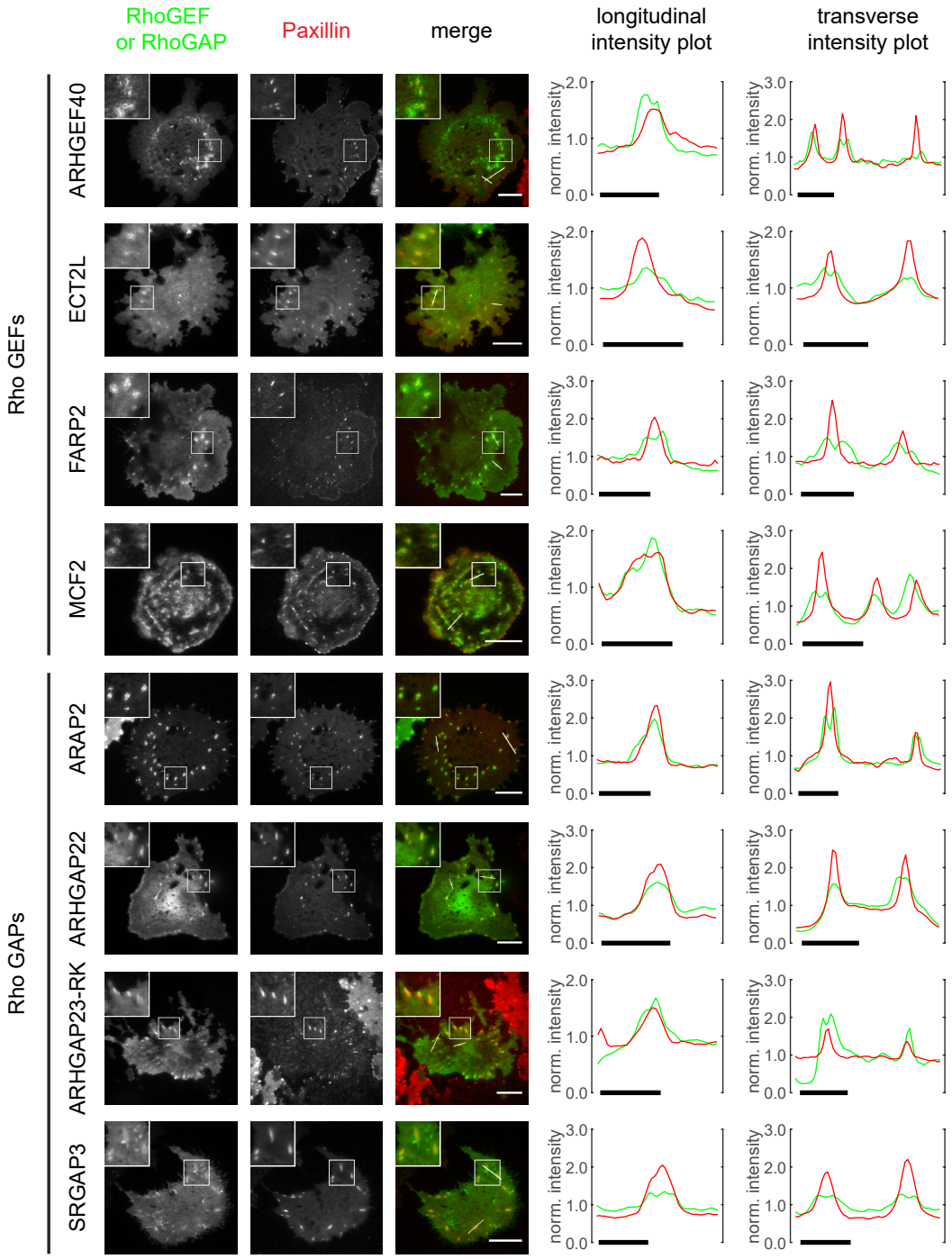

Figure 5.26 8 RhoGEFs and RhoGAPs localise in a focal adhesion "halo". mCitrine-tagged RhoGEFs and RhoGAPs were expressed in COS-7 cells stably expressing mCherry-paxillin. Images were collected by live cell TIRF microscopy. Fluorescence intensity profiles of longitudinal and transverse sections through focal adhesions are shown on the right and indicated by white lines in the merged images. Intensity plots were normalised to the average intensity over the whole line to maintain relative intensity proportions. Insets on the upper left of each image represents an approximately two-fold magnification of the area indicated by a box. White scale bars in images: 20 μm. Black scale bars in graphs: 5 μm.

the RhoGEF and RhoGAP activity meta-analysis results also strongly supported this tendency (Appendix Table 7.1). However, 15 out of 37 RhoGEFs and RhoGAPs that localised on focal adhesions did not show any activity in the activity screen and even more were not represented in the meta-analysis list. Therefore, further research is needed to elaborate this finding. Next, I analysed if Rho GTPases, which localised at cellular membranes and in the cytosol as I showed before (see 5.1.1), would themselves localise at focal adhesions. Strikingly, only overexpressed constitutively active Rac1 was found to be strongly enriched at focal adhesions (Figure 5.27B). RhoA and Cdc42 and any of their tested mutants did not localise at focal adhesions (Appendix Figure 7.17 and 7.18). Together, this suggests that Rac1 might play a central role in the maturation, maintenance and turnover of focal adhesions and that its activity requires precise control in this context.

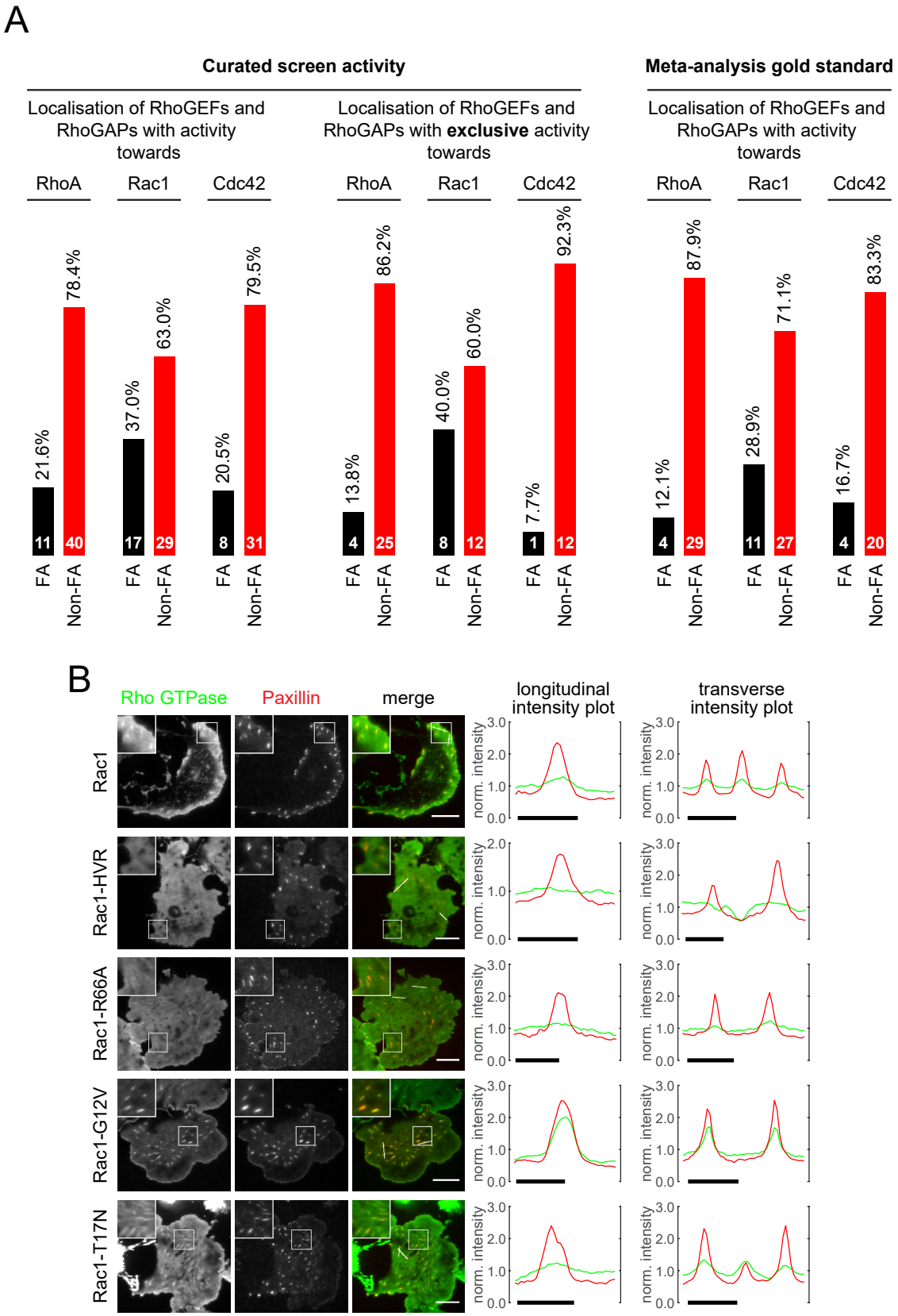

Figure 5.27 see next page

Figure 5.27 (continued) Rac1-specific RhoGEFs and RhoGAPs and constitutively active Rac1 localise at focal adhesions. (**A**) Correlation of RhoGEF and RhoGAP substrate specificities with focal adhesion localisation: Active RhoGEFs and RhoGAPs were divided into groups by focal adhesion localisation (FA and Non-FA) and by activity towards RhoA, Rac1, and Cdc42. On the left all active RhoGEFs and RhoGAPs from the curated screen list were considered, in the centre only RhoGEFs and RhoGAPs with exclusive activity from the curated screen list were considered, on the right all active RhoGEFs and RhoGAPs from the meta-analysis gold standard list were considered. Percentage is shown above the bars, total numbers are given in the bars. (**B**) mCitrine-tagged Rac1 and mutated versions of Rac1 were expressed in COS-7 cells stably expressing mCherry-paxillin. Images were collected by live cell TIRF microscopy. Fluorescence intensity profiles of longitudinal and transverse sections through focal adhesions are shown on the right and indicated by white lines in the merged images. Intensity plots were normalised to the average intensity over the whole line to maintain relative intensity proportions. Insets on the upper left of each image represents an approximately two-fold magnification of the area indicated by a box. White scale bars in images: 20 μm. Black scale bars in graphs: 5 μm.

6 Discussion

6.1 Rho GTPase localisation at membranes is dynamic

Membranes serve as signalling platforms for Rho GTPases. In living cells, signalling pathways are highly spatially organized, and often activating and deactivating enzymes differentially localise to distinct cellular structures. Activation signals are often generated at the plasma membrane by a confined activator and the localisation of antagonistic inactivators, for example in the cytosol, allows the restriction of active signalling molecules in close proximity to the activator (Kholodenko, 2009). This principle also applies to Rho GTPase signalling: active Rho GTPases stimulate actin polymerisation at the plasma membrane and thus drive the formation of lamellipodia, filopodia or regulate actin contractility (Spiering and Hodgson, 2011). However, how Rho GTPase activity is controlled within confined zones of the plasma membrane is not well understood. Furthermore, the membrane extraction of Rho GTPases by RhoGDI and lateral diffusion in theory counteract the formation of Rho activity microdomains. Therefore, I first analysed the mechanisms by which Rho GTPases are targeted to the plasma membrane and how RhoGDI regulates both Rho protein localisation and membrane binding stability.

6.1.1 Rho GTPase membrane targeting and its regulation by RhoGDI

The understanding of Rho GTPase localisation and its control by RhoGDI was an important prerequisite for the further experiments of my work. The principles of their interaction are known (Michaelson *et al.*, 2001; Garcia-Mata *et al.*, 2011), but imaging data is scarce and their interaction has not been thoroughly studied by microscopy. Therefore, I first set out to study the cellular localisation of Rho GTPases, their membrane targeting signals and the interaction of Rho proteins and their mutants with RhoGDI. When I overexpressed Rho GTPases in HeLa cells, RhoA showed no enrichment at the plasma membrane but was mostly localised in the cytosol, whereas Cdc42 and Rac1 were clearly enriched at the plasma membrane in addition to their cytosolic localisation (Figure 5.1B). This is in line with previous subcellular fractionation experiments, which showed that endogenous Rac1 and Cdc42 were equally partitioned between membranes and cytosol, whereas only 10 % of endogenous RhoA was localised at membranes and 90 percent localised in

the cytosol (Michaelson *et al.*, 2001). Rho GTPases are targeted to membranes by their HVR, and I could show that indeed, constructs comprising only the HVR of RhoA, Rac1, and Cdc42, localised mainly at the plasma membrane and Cdc42 additionally localised on endomembranes, especially in the perinuclear region (Figure 5.1C). Therefore, the cytosolic localisation of the full length Rho proteins was presumably due to their binding to RhoGDI. Indeed, I could show that RhoGDI binding-deficient mutants of RhoA, Rac1, and Cdc42 did not localise in the cytosol (Figure 5.4A) and could not be recruited to the cytosol in the presence of excess RhoGDI (Figure 5.4B). The fact, that excess RhoGDI completely withdrew wild type RhoA, Rac1, and Cdc42 from any cellular membrane and showed complete cytosolic colocalisation with the Rho proteins (Figure 5.3), further supports the role of RhoGDI as a key regulator of Rho GTPase localisation.

Unexpectedly, the localisation of the Rho HVR constructs and the RhoGDI binding-deficient mutants of the Rho proteins, both incapable of binding to RhoGDI, were not similar, especially for RhoA (Figure 5.1C and Figure 5.4A and B). This suggests that other factors might contribute to the localisation of Rho GTPases, probably via protein-protein or further protein-lipid interactions of the G-domain. It has been suggested for members of the Ras GTPase family that arginine residues located within the G-domain might additionally interact with negatively charged phospholipids and that this interaction might differentially regulate membrane affinity and conformation of GTP-bound and GDP-bound GTPases (Parker and Mattos, 2015). Similar mechanism might also regulate the localisation of Rho GTPases, but this has not been investigated, yet.

It is furthermore an interesting finding that HVR constructs and RhoGDI binding-deficient mutants of Rho GTPases are still enriched at the plasma membrane, because plasma membrane localisation of KRas has been shown to depend on binding to its GDI-like solubilising factor PDEδ (Chandra *et al.*, 2012). In the absence of PDEδ, KRas is entropically redistributed to endomembranes by endocytic vesicle transport and it was shown that PDEδ- and recycling endosome-mediated transport synergistically control the transport KRas to the plasma membrane (Schmick *et al.*, 2014). Geranylgeranylated proteins cannot become solubilised by PDEδ, which can therefore not compensate for a loss of RhoGDI binding (Chandra *et al.*, 2012). However, studies in *Saccharomyces cerevisiae*, where the RhoGDI1 homologue Rdi1 is conserved, showed that Cdc42 trafficking to the plasma membrane was controlled by two systems: a fast Rdi1-dependent pathway and a slower vesicle trafficking-based pathway. Consequently, deletion of Rdi1 had no obvious growth phenotype in *Saccharomyces cerevisiae* (Slaughter *et al.*, 2009). Vesicle mediated transport to the plasma membrane might therefore compensate for a loss of

RhoGDI and explain how Rho HVR constructs and the RhoGDI binding-deficient mutants of Rho GTPases reach the plasma membrane. This is further supported by the fact that RhoGDI1-knockout mice are viable and show a relatively mild phenotype (Togawa *et al.*, 1999; Shibata *et al.*, 2008). It will be interesting to investigate in the future if also in mammalian cells RhoGDI-mediated and vesicle-mediated trafficking of Rho GTPases between cellular membranes coexist and can compensate each other.

In addition to the geranylgeranyl modification, the GTPases RhoA, Rac1, and Cdc42 contain a PBR that also contributes to the regulation of their subcellular localisation. Prenylation of small GTPases promotes general membrane association of otherwise soluble proteins and additional targeting signals in the HVR, such as palmitoylation or PBRs, are required for a shift of the steady state localisation from endomembranes towards the plasma membrane (Roy *et al.*, 2000; Rocks *et al.*, 2006; Schmick *et al.*, 2014). It is assumed that small GTPases comprising a PBR in addition to the prenylation are thermodynamically enriched at the plasma membrane by electrostatic interaction with negatively charged phospholipids (Wright and Philips, 2006). It has been shown that four or less positive charges in the HVR are not sufficient to enrich prenylated probes at the plasma membrane, whereas probes with six or more positive net charges were strongly enriched at the plasma membrane (Yeung *et al.*, 2008). This possibly explains why the HVR region of Cdc42 localised more on endomembranes than RhoA and Rac1, because it only contains four basic amino acids, whereas RhoA and Rac1 contain five and six of them, respectively (Figure 5.1A). Interestingly, a recent study on KRas membrane targeting demonstrated, that the combination of amino acid sequence within the PBR and the prenyl group define a combinatorial code for selective lipid binding that targets KRas to phospholipid nanoclusters and is determines KRas signalling output (Zhou *et al.*, 2017). This suggests that the plasma membrane targeting mechanisms of prenylated proteins with a PBR is probably beyond simple electrostatics but control signalling by the formation of membrane nanodomains. Such mechanisms might also contribute to the localisation of Rho GTPases in the plasma membrane.

Together, the three Rho GTPases are targeted to the plasma membrane by their geranylgeranyl moiety and the PBR within the HVR. In addition, RhoGDI is an important regulator of the steady-state subcellular localisation of Rho GTPases and their availability at the plasma membrane. However, despite its important role in localisation, RhoGDI is dispensable for the transport of Rho GTPases to the plasma membrane.

6.1.2 Analysis of the dynamic Rho GTPase-membrane interaction requires sophisticated techniques

A central challenge in Rho GTPase biology is to understand how spatio-temporal signalling precision is achieved and maintained. Transient pools of Rho GTPase activity have been shown to be regulated in micrometre space and on a tens of seconds to minutes time scale during various actin-dependent morphological events. For example, during phagocytosis local activation of Rac1 and Cdc42 drive actin polymerisation in order to shape the phagosome. These pools of active Rac1 and Cdc42 are maintained for more than 5 min in a micrometre size area (Hoppe and Swanson, 2004).

Here, I showed that small populations of photolabelled mPAGFP-Rho GTPases at the plasma membrane in an approximately 1 μm area rapidly dissipated with a subsecond half life (Figure 5.2C). The signal decay could be best described by a third order exponential decay function, which indicates that at least 3 processes with different kinetics contribute to the diffusion of Rho GTPases at the membrane. Surprisingly, the kinetics of constructs comprising only the HVR of Rho GTPases and RhoGDI binding-deficient Rho mutants were not significantly different than those of the wild type proteins (Figure 5.2D). It can therefore be speculated that the fastest process in this setup is lateral diffusion, which is further supported by the fact that a KRas-HVR construct and a glycosylphosphatidylinositol (GPI)-anchored probe in the exoplasmic membrane leaflet showed the same diffusion behaviour (Figure 5.2F and G). I could confirm that lateral diffusion in the plasma membrane of RhoA-HVR was rapid, with a half life that matched the subsecond time scale of confined Rho GTPase membrane residence time (Figure 5.2I). Together, this indicates that Rho GTPases themselves do not have the ability to stably localise in confined region of the plasma membrane, but lateral diffusion and other yet unknown processes lead to their rapid dilution.

To investigate the question whether RhoGDI contributes to the rapid diffusion of Rho GTPases at the plasma membrane, I was also applying the localised FLAP assay. Here, I showed that RhoGDI binding-deficient versions of Rho proteins did not bind to membranes more stably, or only marginally more stable for Rac1, than wild type versions (Figure 5.2E). This suggest that RhoGDI does not actively extract Rho GTPases from membranes, but rather passively captures Rho proteins in the cytosol that dissociated of the membrane before. Indeed, kinetic studies of RhoGDI-mediated Rho protein membrane desorption by Richard Cerione and colleagues suggest a two step mechanism by which RhoGDI assists Rho GTPases to undergo the transition between a membrane-associated and a soluble cytosolic state. Initially, RhoGDI partially attaches to membrane bound

Rho GTPases with its regulatory arm, then, in the second step, the Rho GTPase dissociates off the membrane and the Rho GTPase-RhoGDI complex is formed by penetration of the geranylgeranyl lipid moiety into the hydrophobic pocket of RhoGDI (Nomanbhoy *et al.*, 1999). Out of these to binding steps, the first has been shown to happen preferentially to GTP-bound Rho GTPases, whereas the second was independent of the nucleotide state (Johnson *et al.*, 2009). Others have suggested a passive mechanism of membrane extraction which is driven by a series of Rho GTPase-RhoGDI complex conformations with gradually increasing affinities (Tnimov *et al.*, 2012). However, the ability of the FLAP assay to precisely describe the mechanism and the kinetics of RhoGDI-mediated Rho GTPase membrane desorption, as well as that of other potential regulators of Rho GTPase membrane binding is limited. This is for several reasons: Firstly, the assay visualises bulk protein. Therefore, the signal information integrates all individual processes that contribute to the signal decay. This limits the ability to reliably segregate the kinetics of each of these processes. Secondly, rapid signal loss by lateral diffusion with a half life of 0.76 s and a detectable photobleaching rate with a half life of 7.73 s might mask other processes with kinetics that might have similar time constants. And Thirdly, overexpression of the protein of interest oversaturates endogenous binding partners and might therefore increase the apparent mobility. Thus, the valid and reliable analysis of how Rho GTPase binding to membranes is controlled and thus how Rho GTPase activity is locally concentrated requires more sophisticated techniques that can experimentally resolve all underlying processes.

I therefore set out to establish an SPT assay to detect and track individual Rho GTPase proteins in the plasma membrane of living cells by means of TIRF microscopy in order to investigate Rho GTPase membrane residence time and its regulation. Single molecule imaging and SPT have been used to study complex systems and structures inside living cells such as membrane microdomain localisation and membrane mobility of Ras family members (Lommerse *et al.*, 2004, 2005, 2006), integrin nano-organisation inside focal adhesions by immobilisation and activation cycles (Rossier *et al.*, 2012; Shibata *et al.*, 2012), and the initiation of clathrin-coated pit assembly (Cocucci *et al.*, 2012). Particularly, single molecule techniques provide quantitative information and high statistical precision by providing four-dimensional localisation information in space and time on the level of individual molecules.

I employed the Tet-On tetracycline-controlled transcriptional activation system to ensure minimal expression levels of Rho GTPases which allowed subdiffraction localisation of individual probes (Figure 5.5D). This goes along with the additional advantage of avoid-

ing overexpression. The leaky promoter expression yielded approximately hundreds to thousands of copies per cell and thus can be assumed not to substantially add to the expression levels of endogenous Rho GTPases which have been estimated to be in the range of 3×10^5 to 2×10^6 copies per cell in mammalian cells (Schwanhäusser *et al.*, 2011) with varying relative ratios between RhoA, Rac1, and Cdc42 in different cell types (Michaelson *et al.*, 2001). Consequently, the well balanced equilibrium of Rho GTPase levels and its chaperone RhoGDI remains unaltered (Boulter *et al.*, 2010).

The choice of the fluorophore is a key determinant of the quality of SPT assays. The brightness of the fluorophore determines its SNR and therefore its subsequent reliable detection by computer algorithms and the photostability determines the time span of the trajectories. Organic dyes provide superior brightness and photostability compared to genetic fluorophores. In the last years, biocompatible rhodamine-based dyes have been rationally engineered in order to improve their brightness and photostability. Especially rhodamine and near-infrared silicon-rhodamine dyes and their azetidine derivatives are superior dyes for sophisticated single molecule imaging experiments (Lukinavičius *et al.*, 2013; Grimm *et al.*, 2015, 2017). The use of improved silicon-rhodamine derivatives will allow to establish conditions of minimal illumination power density and exposure times to further maximise the tracking time span of the assay. Here, I employed the SNAP-tag-based self labelling technique which allows covalent linkage of organic fluorophores. Using a TMR dye, I could track single molecules at extraordinary SNR (Figure 5.5D). However, all fluorescent dyes have a limited number of excitation and emission cycles they can run through (Diaspro *et al.*, 2006). Photobleaching of a single fluorescent particle appears as an abrupt loss of its signal (see Figure 5.5C for example). Just as photobleaching, the dissociation of a labelled Rho GTPase off the membrane, which marks the end of a single particle trajectory, is visualised as sudden disappearance of the single molecule signal, because the molecule leaves the evanescent field of the TIRF illumination. Accordingly, one has to also precisely know the photobleaching rate, in order to be able to measure the membrane residence time of Rho GTPases by means of an SPT assay. Therefore, I made an additional effort to establish a system to accurately measure the photobleaching rate. As photobleaching critically depends on the redox characteristics of the environment, especially the presence of ROS and oxygen, but also of intracellular organic molecules, it is necessary to determine the photobleaching rate in the same environment in which the experiment is conducted (Diaspro *et al.*, 2006; Benson *et al.*, 1985). To precisely measure photobleaching rates at the plasma membrane in living cells, I set up an assay to immobilise fluorophores at the intracellular leaflet of the basal plasma membrane (Figure 5.5A, B, and E) that I successfully used to identify single molecule bleaching events inside living

cells (Figure 5.5C). Together, I developed a tool to precisely monitor membrane binding dynamics of Rho GTPases, that overcomes methodological obstacles of established assays.

With the completion of the photobleaching control experiments the Rho GTPase SPT assay will be set up to unravel several fundamental questions of how Rho GTPase signalling is controlled at membranes. It will allow the accurate analysis of the Rho GTPase plasma membrane residence time. Tracking of individual Rho proteins will visualise the mobility of the Rho GTPases at the plasma membrane and provide insight into lateral diffusion and potential transient immobilisation. Subsequently, these parameters can be reassessed in the presence of regulatory and effector proteins or correlated with subcellular morphogenic events and Rho GTPase activity. The assay can be combined with the use of Rho activity biosensors to compare parameters of membrane binding in regions of high and low Rho activity. This will instantaneously provide insight into the mechanism by which Rho GTPase activity is spatially confined to membranes regions and ultimately help to answer the question how localised Rho signalling networks are orchestrated to give rise to complex morphodynamic cell behaviours.

The SPT assay will furthermore help to unravel the role of RhoGDI in Rho GTPase shuttling and delivery. For example, whether localised delivery of Rho GTPases by means of RhoGDI is required for proper signalling outcome is not known yet, and a general GDI displacement factor has so far not been identified. However, Rac1 has been shown to be delivered to preferentially to growing lamellipodia with high Rac1 activity (Das *et al.*, 2015) and others have shown that Rac1 is preferentially unloaded from RhoGDI at boundaries between raft and non-raft regions (Moissoglu *et al.*, 2014). Therefore, the assay could also be used to identify such preferential Rho "landing zones" in the plasma membrane. Finally, the approach will also allow the investigation of alternative RhoGDI-independent mechanisms of Rho GTPase delivery to the plasma membrane, which only have been shown to exist in *Saccharomyces cerevisiae* so far (Slaughter *et al.*, 2009).

6.2 Systematic family-wide analysis of RhoGEF and RhoGAP activities

RhoGEFs and RhoGAPs regulate the activity of Rho GTPases in a stimulus-dependent, spatio-temporally-regulated and substrate-specific manner (Schmidt and Hall, 2002; Rossman *et al.*, 2005; Tcherkezian and Lamarche-Vane, 2007). Given the complexity of RhoGEF and RhoGAP mediated spatio-temporal control of Rho signalling, the correct assignment of these enzymes to their cognate Rho GTPase family member substrates is key to properly link them to their downstream signalling pathways. I thus wanted to undertake a comprehensive screen of RhoGEF and RhoGAP substrate specificities towards the three paradigm Rho GTPases RhoA, Rac1, and Cdc42. A comprehensive literature meta-analysis of existing data about substrate specificities RhoGEFs and RhoGAPs was a prerequisite for the evaluation of the screening data. This meta-analysis revealed that the available information about RhoGEF and RhoGAP substrate specificities is incomplete, contains discrepancies due to different methods and variations in experimental setups, and has never been investigated in a systematic manner (see 5.2.3). A family-wide analysis required me to establish a screening-compatible assay. I therefore optimized a FRET biosensor-based approach which I confirmed to be robust, reliable and sufficiently sensitive.

6.2.1 A Rho GTPase-biosensor-based RhoGEF and RhoGAP activity assay

6.2.1.1 Advantages and disadvantages of existing techniques to assess RhoGEF and RhoGAP activities

Several *in vitro* and *in vivo* methods have been established in the past to determine the substrate specificity of RhoGEFs and RhoGAPs towards members of the Rho GTPase family (see 2.3.2). The choice of the appropriate assay is driven by the interest of the experimenter to describe the substrate specificity as the biochemical efficiency of the catalysed reaction or by their ultimate biological activity in a cellular environment. *In vitro* assays for RhoGEF and RhoGAP activities are valuable tools to precisely characterise the kinetics of their catalysed reaction. These approaches usually exhibit high biochemical accuracy at the cost of important regulatory elements of RhoGEF and RhoGAP activity. They not only require recombinant Rho GTPases, but also purified regulatory proteins and are thus not the method of choice to analyse full length RhoGEFs and RhoGAPs, which often exceed a size of 200 kDa. Therefore, *in vitro* assays mostly rely on the use of truncations comprising only the catalytic domains of the regulators, typically the DH-PH or DHR2 domain of RhoGEFs or the RhoGAP domain, respectively. However, by the use of such truncations one accepts the loss of regulatory elements of RhoGEF and RhoGAP

activity within their multidomain structure. Furthermore, *in vitro* assays measure the catalytic activity of the regulators outside their native biological context, and thus do not take into account any regulation by posttranslational modifications or protein-protein and protein-lipid interactions. Indeed, the substrate specificity of RhoGEFs and RhoGAPs has been shown to differ between *in vitro* and *in vivo* assays. For example, the RhoGEF PREX1 showed activity towards Rac1 and Cdc42 *in vitro* but high specificity only towards Rac1 in a pull-down assay (Welch *et al.*, 2002*a*). Similarly, the RhoGEF PLEKHG6 activated RhoA, RhoC, and Rac1 *in vitro*, but knockdown of PLEKHG6 in breast cancer cells only reduced the activity of RhoA and RhoC, but not of Rac1 (Wu *et al.*, 2009). This suggests, that regulatory mechanisms may exist in cells that contribute to the substrate specificity of RhoGEFs and likely also RhoGAPs.

Pull-down assays can be considered an *in vivo* method as they capture the Rho GTPase activity state of the living cell. Although being very sensitive, this method suffers from several limitations. The approach relies on the conservation of the Rho GTPase activity state. However, the assay is very sensitive to fast intrinsic GTP hydrolysis during cell lysis and sample processing. Therefore, this technique requires very rapid and standardised sample treatment. Especially the comparison of activity levels of different Rho family members is difficult, because intrinsic GTPase activities have been shown to differ between members of the Rho family (Zhang *et al.*, 1998). Furthermore, subsequent densiometric Western blot analysis is susceptible to signal variations between samples. Another disadvantage is the loss of spatial information of the localised Rho signal during cell lysis.

Taken together, these established assays are not screening compatible and thus did not meet the demands of a comprehensive analysis of RhoGEF and RhoGAP substrate specificity. The are time consuming, require large amount of sample, and are either incapable of use of full length proteins, or suffer from instability of the Rho GTPase activity state. Therefore, I established an assay that fulfilled these criteria.

6.2.1.2 Assessing RhoGEF and RhoGAP activities by a screening-scale FRET-based assay

The availability of highly sensitive ratiometric FRET biosensors with a large dynamic range was an essential prerequisite to determine RhoGEF and RhoGAP activities by means of automated fluorescence microscopy. I applied second generation FRET biosensors for RhoA, Rac1, and Cdc42 from Olivier Pertz and colleagues, which were systematically engineered by applying various circularly permutated fluorophore combinations in order to improve their performance (Fritz *et al.*, 2013, 2015; Martin *et al.*, 2016).

FRET biosensors to detect Rho GTPase activity levels in living cells offer important advantages that can be exploited for a screening-scale application. Firstly, they only require minimal sample sizes, allowing a multi-well-plate-based workflow. Secondly, as a live cell technique it does not require cell lysis and is therefore resistant to artefactual sample-to-sample variations in GTPase activity states arising from intrinsic GTP hydrolysis, especially when handling large sample numbers. Furthermore, it allows the investigation of full length regulators, an essential prerequisite to apply our full length RhoGEF and RhoGAP expression library. And lastly, the cell biological environment of RhoGEFs and RhoGAPs is preserved, providing regulatory factors such as posttranslational modification, subcellular localisation, protein-protein and protein-membrane interactions.

However, as the assay relies on overexpression of the involved components and thus interferes with the well balanced intracellular signalling network, I first performed a stringent set of control experiments to prove the suitability of the assay. I confirmed the responsiveness and the sensitiveness of the FRET sensors to minimal expression levels of all classes of regulators of Rho GTPase activity, namely RhoGDI, RhoGEFs, and RhoGAPs (Figure 5.6, Figure 5.8, Figure 5.9, Figure 5.12, Figure 5.13). Furthermore, I found that modulation of the expression levels of RhoGDI was required for the RhoGEF assay and increased the sensitivity of the RhoGAP assay. Importantly, the assay was robust against variations of sensor expression levels (Figure 5.11) and Rho activity levels reported by the sensors were consistent throughout 96-well plates (Appendix Figure 7.5).

It was essential for the validity of the assay to verify that crosstalk from endogenous RhoA, Rac1, and Cdc42 does not affect the activity levels of the biosensors. By coexpressing the FRET sensors of a given Rho GTPase with constitutively active mutants of the other two Rho GTPases, I mimicked the situation of a potential crosstalk by strong activation of an endogenous Rho GTPase (Figure 5.14) and by coexpression of the FRET sensors of a given Rho GTPase with dominant negative mutants of the other two Rho GTPases, I mimicked the situation of a potential crosstalk by strong inactivation of an endogenous Rho GTPase (Figure 5.15). I indeed found that active Rac1 and Cdc42 coactivated RhoA and active Cdc42 inhibited Rac1. However, in the screen I identified RhoGEFs with exclusive high activity for Rac1 (TIAM2) or with exclusive high activity for Cdc42 (SPATA13) that did not affect the activity of the RhoA biosensor. This led me to the conclusion that the Rho GTPase crosstalk is negligible in the context of a RhoGEF screen, most probably because the GEFs cannot recapitulate the extreme perturbation of the system by the GTPase mutants expressed at high levels. However, I cannot exclude that in case of a strong Cdc42 GEF an additional weak Rac1 GEF activity may be missed in the screen.

Dominant negative Rac1 coinactivated Cdc42 at high expression levels, while it activated RhoA. Similarly, dominant negative Cdc42 coinactivated Rac1 and activated RhoA. In the screen I found RhoGAPs with exclusive high activity for Rac1 (ARHGAP15, ARHGAP9, CHN1, CHN2, and SH3BP1) that did not coinactivate Cdc42, again suggesting that this crosstalk can be neglected. However, I cannot exclude that in case of a GAP with strong activity towards Rac1 or Cdc42 an additional weak RhoA GAP activity may be missed in the screen. Importantly, I only detected one GAP with exclusive Cdc42 GAP activity, ARHGAP44, which had relatively weak activity compared to other promiscuous Cdc42 GAPs. I can therefore not exclude that crosstalk from inactive Cdc42 to Rac1 is the reason for the detection of so few Cdc42 specific RhoGAPs. However, the mutual coinactivation of Rac1 and Cdc42 can alternatively also be explained by the mechanism of action of the dominant negative mutation. Dominant negative T17N (T19N for RhoA numbering) mutants of small Ras and Rho GTPase have a reduced affinity for guanine nucleotides (Lai *et al.*, 1993). GEFs have an high affinity for nucleotide-free GTPases, thereby stabilising the transition state of the GDP-GTP exchange reaction and the exchange reaction is the ended by binding of GTP and dissociation of the GTPase-GEF complex (Bos *et al.*, 2007). This guanine nucleotide-induced dissociation is slowed for the dominant negative mutants due to their reduced nucleotide affinity (Feig, 1999). Therefore, dominant negative Rho GTPases bind to RhoGEFs with high affinity and sequester the endogenous RhoGEFs by forming a non-functional dominant negative Rho GTPase-RhoGEF complex. This results in inhibition of other Rho GTPases by sequestering also RhoGEFs with promiscuous activity. Dominant negative mutants are therefore probably not appropriate constructs to be used in a control experiment. It is conceivable that the crosstalk by inactive endogenous Rho GTPase is less pronounced than the crosstalk by expression of exogenous dominant negative Rho GTPases.

Together, the measurement of RhoGEF and RhoGAP activities by means of FRET biosensors is sensitive, robust, and applicable in a screening format. The assay is suitable for the analysis of full length RhoGEF and RhoGAP expression constructs and allows to improve the sensitivity by specific modulation of RhoGDI levels. This made the assay ideally suited to systematically investigate the substrate specificity of all mammalian RhoGEFs and RhoGAPs.

6.2.2 Systematic and comprehensive analysis of RhoGEF and RhoGAP activities towards RhoA, Rac1, and Cdc42

A systematic analysis of the mammalian RhoGEF and RhoGAP enzymatic activities and substrate specificities under standardized conditions has been long awaited since currently available data is incomplete and considerably inconsistent due to the use of differing experimental setups. In this work used the FRET-based biosensor assay to analyse the substrate specificity of 74 candidate RhoGEFs and 65 candidate RhoGAPs towards the three canonical Rho GTPases RhoA, Rac1, and Cdc42.

Out of 74 candidate RhoGEFs in the screen, I identified 29 regulators with activity towards RhoA, 20 with activity towards Rac1, and 22 with activity towards Cdc42. Out of these, 25 showed exclusive activity towards one of the GTPases, whereas 18 had promiscuous activity (Figure 5.19). 31 RhoGEFs were inactive. The RhoGAP screen with 65 candidate RhoGAPs revealed 27 regulators that inactivated RhoA, 35 that inactivated Rac1, and 20 that inactivated Cdc42. 29 RhoGAPs showed exclusive activity towards on GTPase and 21 RhoGAPs were active towards two or three Rho GTPases (Figure 5.19). 15 RhoGAPs were inactive.

In general, the results of the screen were in good agreement with previously published work (Figure 5.20 and Appendix Figure 7.14). However, also discrepancies became apparent which likely result from differences between *in vitro* and *in vivo* experiments and illustrate the importance to distinguish between biochemical and biological activities. While the first reflect the rate constant of catalysis, typically of a recombinant truncated GEF or GAP domains, the latter analyse the full length regulators in their native cellular environment, thus taking into account their entire regulatory multidomain architecture that is subject to posttranslational modifications and protein-protein and protein-lipid interactions. The rate constant of *In vitro* assays thus do not directly relate to the biological activity of a given RhoGEF or RhoGAP *in vivo*. For example, two independent studies on ARHGAP32 compared the *in vitro* activity of GAP domain with the *in vivo* activity of the full length GAP. Both studies found that *in vitro* the GAP domain had strong catalytic activity towards RhoA, Rac1, and Cdc42, whereas *in vivo* pull-down assays showed very selective activity towards Rac1 and Cdc42 but no activity towards RhoA (Zhao *et al.*, 2003; Okabe *et al.*, 2003). Furthermore, a different study about ARHGAP8 detected the strongest activity towards Cdc42, a weaker but still significant activity towards RhoA, and no activity towards Rac1 by *in vitro* GTP hydrolysis assays. However, subsequent pull-down experiments only showed activity towards RhoA *in vivo*, but, surprisingly, no activity towards Cdc42 (Shang *et al.*, 2003). This suggests that both, the use of isolated catalytic domains and the absence of a cellular environment might strongly reduce

and change the substrate selectivity of RhoGEFs and RhoGAPs. It is therefore important do differ between biochemical activity and biological activity as many factors in the physiological environment of a RhoGEF or a RhoGAP might contribute to its substrate specificity. Also the catalytic efficiencies determined *in vitro* and *in vivo* cannot be directly correlated. This becomes obvious, when comparing the biochemically determined fold-activation, which allows the direct comparison of different regulator-substrate pairs, of the regulators towards RhoA, Rac1, and Cdc42 with the normalised activities of the RhoGEFs and RhoGAPs that I observed in the screen. In the thorough biochemical characterisation of a subset of RhoGEFs by Jaiswal *et al.* (2013), ARHGEF12 showed a more than 50,000-fold activation of the GDP-GTP exchange rate for RhoA *in vitro* whereas MCF2L only showed a 400-fold increase. Still in the screen the activity of MCF2L towards RhoA was by far higher than the activity of ARHGEF12. Furthermore, Jaiswal *et al.* showed a 50-fold activation of the exchange reaction for VAV2 towards RhoA *in vitro*, but a 5,000-fold activation towards Rac1. Still in the screen VAV2 showed a higher activity towards RhoA than towards Rac1. Also, TIAM1, which showed by far the strongest activation of Rac1 in the screen, however, only showed a 100-fold activation of the exchange reaction *in vitro* in the study of Jaiswal *et al.*. Moreover, the activity of PREX1 towards Rac1 in the screen was by far higher than towards Cdc42, still *in vitro* PREX1 showed the highest activity towards Cdc42.

Similar observations can be made when comparing *in vitro* activities of RhoGAPs as determined by Amin *et al.* (2016) with the *in vivo* activities observed in the screen. For example, the fold activation of the hydrolysis reaction by ARHGAP1 towards RhoA and Rac1 were similar, however, in the screen I did not detect any activity for Rac1, but ARHGAP1 was one of the strongest GAPs for RhoA. Furthermore, the two RhoGAPs STARD13 and STAR8 were in the study by Amin *et al.* classified as inefficient GAPs and their RhoGAP function was seriously questioned due to their low overall capability to stimulate GTP hydrolysis. Intriguingly, STRARD8 showed high activity towards all three Rho GTPases in the screen and STARD13 was a very strong RhoA GAP.

Together, this emphasises the importance of the investigation of RhoGEF and RhoGAP substrate specificities by both *in vivo* and *in vitro* assays. *In vitro* assays have the strong advantage that they detect the activity of GEFs and GAPs independent of stimuli and autoinhibitory mechanisms that potentially mask their activity. *In vivo* assays employing full length GEF and GAP constructs have a strong significance in order to confirm their biological activity in their native physiological environment implicating all their regulatory factors. However, this also suggests that those regulators that have been previously assigned an activity *in vitro* that was not detected in the screen need to be reevaluated and

more precisely investigated. Especially, RhoGEFs and RhoGAPs with high biochemical efficiency and low or no biological activity would be interesting candidates to further study in order to test for autoinhibitory regulation and to find stimuli that possibly release their activity.

6.2.3 RhoGEF and RhoGAP activity is subject to autoinhibition

The number of RhoGEFs and RhoGAPs that were reported to be inactive towards a certain Rho substrate in previous reports, but showed activity in the screen was small (Figure 5.20 and Appendix Figure 7.14). However, several Rho regulators did not exhibit any catalytic activity in the screen, in contrast to previous reports (Figure 5.20 and Appendix Figure 7.14). Out of 74 candidate RhoGEFs, 31 showed no activity and out of 65 candidate RhoGAPs 15 had no activity in the screens. At least 12 out of these inactive RhoGEFs and 6 out of the inactive RhoGAPs were expected to show activity according to the meta-analysis (Table 5.2 and Table 5.3). I was therefore analysing if autoinhibition could be an explanation for that. In principle only for a few RhoGEFs and RhoGAPs, the complete autoinhibitory mechanism is well described and characterised (see 2.2.5), however, in the meta-analysis I found evidence for autoinhibitory regulation of activity for 41 RhoGEFs and 11 RhoGAPs (Table 5.2 and Table 5.3). For example, studies in which a truncated version of a regulator showed a higher catalytic efficiency that the full length version hint at autoinhibitory regulation (Rümenapp *et al.*, 2002; Chikumi *et al.*, 2004; de Kreuk *et al.*, 2013). Other studies showed that phosphorylation or kinase activity increased regulator activity(Asiedu *et al.*, 2008; Justilien *et al.*, 2011), or regulator activity by was increased by protein-protein interaction or interaction with other components such as lipids or second messengers (Welch *et al.*, 2002*b*; Nishimura *et al.*, 2006; Koo *et al.*, 2007; Kurooka *et al.*, 2011). Furthermore, in some studies regulator activity only detectable in stimulated cells(Runne and Chen, 2013*a*).

I further experimentally investigated this by comparing the activity of short isoform versions or truncations, potentially lacking autoinhibitory elements, to full length versions for a subset of RhoGEFs and RhoGAPs. By semiquantitative analysis I found that for all tested isoforms, the activity of the shorter version or the truncation was significantly higher towards at least one of the Rho GTPase, compared to the activity of the longest isoform (Figure 5.21).

The activity of the short isoform 2 of ARHGEF16 showed a significant increase in activity towards RhoA, compared to the longer isoform 1 which showed no activity in the screen (Figure 5.17). ARHGEF16 has previously been identified as a canonical binding partner

of ELMO1, which is known for its function to recruit and activate DOCK-RhoGEFs (Laurin and Côté, 2014) (see 2.2.5). Furthermore, binding of ELMO1 to the very N-terminal region of the DH domain of ARHGEF16 has been shown to stimulate the activity of ARHGEF16 towards Rac1 (Lee *et al.*, 2014). The isoform 2 of ARHGEF16 completely lacks the N-terminal region in front of the DH domain compared to the canonical isoform 1, and might therefore lack an ELMO1 controlled autoinhibitory mechanism. However, if binding of ELMO1 to ARHGEF16 also affects its substrate specificity remains to be investigated. PLEKHG1 is only poorly investigated. However, PLEKHG2, which is closely related to PLEKHG1, has been shown to only exert RhoGEF activity in the presence of the heterotrimeric G protein $\beta\gamma$ subunit (Ueda *et al.*, 2008; Runne and Chen, 2013*b*). Therefore, similar regulatory mechanisms might also control the activity of PLEKHG1.

Autoinhibitory regulation of RhoGAP activities is generally not well studied. Here I could show that, similar to the RhoGEFs, all shorter isoforms of RhoGAPs that were studied showed a significant increase in their activity towards at least one Rho GTPase (Figure 5.21). The isoform α1 of CHN1 lacks an N-terminal region including an SH2 domain compared to the canonical isoform α2. I showed that the isoform α1 inactivated Rac1 more efficiently than the the longer isoform α2. This was in line with previous findings which showed that CHN1 lacking an N-terminal fraction showed higher activity towards Rac1, independently of the SH2 domain (Colón-González *et al.*, 2008). Interestingly, whereas isoform α2 was specific towards Rac1, isoform α1 showed activity towards all three Rho GTPases. This suggests that the N-terminal region of CHN1 might also regulate substrate specificity. Similarly, I could show that the isoform 2 of SYDE1, which lacked a part of the N-terminal proline rich region, showed activity towards all three Rho GTPases whereas the isoform 1 was inactive. This is in agreement with previous work, where the deletion of the whole N-terminal disordered region increased GAP activity of SYDE1 towards RhoA (Wentzel *et al.*, 2013).

Altogether, these findings demonstrate that shorter isoforms of RhoGEFs and RhoGAPs have a higher activity towards Rho GTPases than longer versions. However, the reason for this still needs to be further investigated. It can be assumed that at least some of the changes relate to autoinhibitory mechanism which lack or work less efficiently in the shorter isoforms. However, a different aspect might add an additional layer of complexity to the regulation of the catalytic efficiency of RhoGEFs and RhoGAPs and their isoforms: The catalytic rate constant of both GEF and GAP mediated reactions has been shown to be directly proportional to the association rate constant of the Rho GTPase with the RhoGEF or the RhoGAP, respectively (Jaiswal *et al.*, 2013; Amin *et al.*, 2016). This indicates that the formation of the transient GEF-Rho GTPase or GAP-Rho GTPase complex is the rate-limiting step of the catalysed reaction. Increased activity of shorter isoforms

of RhoGEFs and RhoGAPs might thus result from better accessibility of the catalytically active region by the Rho GTPase and sterical hindrance might reduce the activity of the longer isoforms. Therefore, to what extent this effect relates to direct intramolecular regulation mechanisms or arises from indirect sterical effects still needs to be investigated.

Together, these findings strongly suggest that autoinhibition is a more widespread mechanism to maintain RhoGEFs and RhoGAPs in a 'stand-by' low activity state which may allow precise release inhibition by context-specific upstream signals. The FRET-based screen emphasises the importance of the full length multidomain architecture of the RhoGEFs and RhoGAPs in the analysis of their substrate specificities as it can considerably affect the biological activity of the regulators in their native cellular environment. The abundance of autoinhibition, however, also requires further evaluation of the catalytic properties of those regulators that lacked activity in the FRET-based activity assay but were previously reported to be active. Especially, RhoGEFs and RhoGAPs with high biochemical efficiency and low or no biological activity will be interesting candidates for such investigation in order to detail the autoregulatory mechanisms and the corresponding stimuli to release their activity.

The DOCK family RhoGEFs would be interesting candidates for further investigation. Almost all of them have been shown to exert activity towards at least one Rho GTPase. Still they were largely inactive in the screen. The activity of members of the DOCK-A and DOCK-B families have been shown to be tightly regulated by ELMO proteins (Laurin2014). Although ELMO proteins have not been reported to regulate the activity of members of the DOCK-C and DOCK-D families, evidence exists that also these are regulated by different autoinhibitory mechanisms and feed forward loops (Lin *et al.*, 2006; Meller *et al.*, 2008; Mou *et al.*, 2012; Miyamoto *et al.*, 2013). Therefore, the use of isolated catalytically active DHR2-domains would be an initial experiment to investigate their substrate specificity. Clearly, the DOCK family RhoGEFs require further thorough analysis to establish their context-specific biological activities.

6.2.4 Not all RhoGEFs and RhoGAPs have exclusive substrate specificities

In the past, literature tended to functionally place RhoGEFs and RhoGAPs into single pathways in which they were assigned to control cytoskeletal processes via just one Rho GTPase. However, for example during PDGF-induced protrusion of lamellipodia in fibroblasts RhoA, Rac1 and Cdc42 have been shown to be simultaneously active at the lamellipodia edge (Martin *et al.*, 2016) and Rac1 and Cdc42 have been shown to be synchronously activated at the lamellipodia front during retraction movements of randomly migrating

cells (Machacek *et al.*, 2009). This shows that in principle signalling events exist that require simultaneous activation of different Rho GTPases within the same spatio-temporal niche. However, if these activity patterns are controlled by RhoGEFs and RhoGAPs with exclusive activities of by regulators with multiple activities has not been investigated yet.

The FRET screen revealed two classes of RhoGEFs and RhoGAPs: those with exclusive substrate selectivity for either RhoA, Rac1, or Cdc42, and those with activity towards two or even all three GTPases (Figure 5.19). The high number of promiscuous RhoGEFs and RhoGAPs is surprising and little is known about signalling contexts where RhoGEFs and RhoGAPs regulate the activity of multiple Rho GTPases which are not from the same subfamily.

As the RhoGEFs and RhoGAPs can be expected to express at equal levels in the individual screens for RhoA, Rac1, and Cdc42, the activity of a given RhoGEF or RhoGAP towards the three Rho GTPases can be semiquantitatively compared (Figure 5.17 and Figure 5.18). This allowed me to assign biologically relevant main activities to RhoGEFs and RhoGAPs with promiscuous specificity. Therefore, I excluded activities which were less than 25 % of the main activity in order to generate a curated specificity list (Figure 5.22, Table 5.2 and Table 5.3). This considerably reduced the number of RhoGEFs with multiple activities and suggests that most RhoGEFs indeed have a high substrate selectivity. However, the lack of selectivity for most RhoGAPs was not altered by the attempt to assign them main substrate activities which indicates that in contrast to RhoGEFs, many RhoGAPs lack exclusive substrate selectivity.

This is in line with biochemical characterisation of a subset of RhoGEFs and RhoGAPs by Mohammad R. Ahmadian and colleagues who found that rate constants for GDP/GTP exchange reactions of catalytic DH-PH domains of RhoGEFs are selectively high towards single Rho GTPases or subfamilies of Rho GTPases, whereas rate constants for GTP hydrolysis reactions by RhoGAP domains lacked such selectivity and were generally high or low towards all Rho GTPases (Jaiswal *et al.*, 2013; Amin *et al.*, 2016). The authors further identified regions and individual residues within DH-PH domains that were responsible for their substrate selectivity. However, such structural determinants of substrate selectivity could not be identified in the RhoGAP domains and it was speculated that RhoGAP substrate selectivity is probably not encoded in the RhoGAP domain itself, but rather in adjacent domains. This suggests that RhoGEFs in general have a higher selectivity towards single Rho GTPases than RhoGAPs and how RhoGAP substrate selectivity is controlled requires further structural investigation in the future.

Together, the tendency to assign individual substrate GTPases to the catalytic activity of RhoGEFs and RhoGAPs may in many cases oversimplify the biological function of the regulators. It has been shown that activities of Rho GTPases are well synchronised during cytoskeletal rearrangement processes and activities of different Rho family members coexist in the same spatio-temporal signalling niche (Machacek *et al.*, 2009; Martin *et al.*, 2016). For such scenarios it is conceivable that individual RhoGEFs and and especially RhoGAPs simultaneously regulate the activity of multiple Rho GTPases.

6.2.5 Outlook

In the future, it would be interesting to expand this assay to other Rho GTPase family members. Jaiswal *et al.* (2013) and colleagues suggested based on structural analysis that 15 of the Rho GTPase family members may be regulated by the conventional GTP-GDP cycle. For example, the highly homologous subfamily Rho GTPase members RhoA, RhoB, and RhoC have been assigned individual functions in cell migration by acting through different effector proteins, but if their activity is differentially regulated by RhoGEFs and RhoGAPs is poorly investigated (Vega *et al.*, 2011; Ridley, 2013; Zawistowski *et al.*, 2013). However, this would require FRET sensors for other Rho GTPases, which have to date only been established for RhoC and TC10, but are still missing for other Rho proteins (Zawistowski *et al.*, 2013; Kawase *et al.*, 2006). Though, the tool set that has been developed together with the systematic engineering of the RhoA-2G sensor, comprises vectors that allow the combination of different versions of circularly permutated donor and acceptor fluorophores, in order to systematically improve the dynamic range of FRET sensors. This will hopefully fuel the development of FRET sensors for other Rho GTPases in the near future.

6.3 Systematic analysis of RhoGEF and RhoGAP localisation at focal adhesions

6.3.1 An underestimated prevalence of focal adhesions associated RhoGEFs and RhoGAPs

Focal adhesions are an important signalling hub where Rho GTPases regulate the contractility of the actin cytoskeleton and its coupling with integrin-based adhesion complex (IACs) (Huveneers and Danen, 2009; Guilluy *et al.*, 2011*a*). Integrins function as receptors and mechanical linkers between extracellular matrix components and the actin cytoskeleton. RhoA, Rac1, and Cdc42 are assumed to have different and opposing roles during IAC maturation: initial adhesions requires low RhoA and high Rac1 and Cdc42 activities, to suppress actomyosin contractility and facilitate actin protrusion. Later, an inverted Rho GTPase activity profile drives the formation of stress fibers, to generate mechanical tension and alter the composition of the adhesion complexes (van Buul *et al.*, 2014; Lawson and Burridge, 2014). Given the complexity and the dynamic regulation of these macromolecular protein complexes, the number of Rho regulators that have been described to be implicated in these processes is seemingly small. I therefore systematically investigated the localisation of RhoGEFs and RhoGAPs at focal adhesions.

Since the enrichment of RhoGEFs and RhoGAPs on focal adhesions cannot be optimally resolved by confocal microscopy I used TIRF microscopy in COS-7 cells with a flat morphology to detect focal adhesion associated regulators. This way, I identified as many as 37 RhoGEFs and RhoGAPs to clearly localise at focal adhesions (Table 5.4). Out of these 29 completely colocalised with the adhesion marker paxillin (Figure 5.24 and Figure 5.25), while 8 were enriched in immediate proximity to focal adhesions (Figure 5.26). Among focal adhesion associated regulators were prominent proteins such as SOS1, CHN2, TRIO and VAV1 that have so far not been reported on this structure.

The interactome of IACs, referred to as the "adhesome", has been studied on a systems level using literature-based and proteomics-based approaches (Zaidel-Bar *et al.*, 2007; Winograd-Katz *et al.*, 2014; Horton *et al.*, 2015). The literature-based adhesome comprises a protein-protein interaction network of IACs with 150 core components and 82 associated components (www.adhesome.org)(Zaidel-Bar *et al.*, 2007; Winograd-Katz *et al.*, 2014). In this network 8[1] RhoGEFs and RhoGAPs are categorised as integral components and 10 RhoGEFs and RhoGAPs are listed as associated components of the IAC network. Out of these, I found 8 RhoGEFs and RhoGAPs that localised at focal adhesions (4 regulators

[1] 8 RhoGEFs and RhoGAPs including DOCK1 which was not available for my study

were categorised as integral components and 4 were categorised as associated components). However, 29 of the RhoGEFs and RhoGAPs were not associated with the IAC network before. Furthermore, for only 10 of the RhoGEFs and RhoGAPs I identified evidence exists in literature for localisation at focal adhesions (ARAP2 (Yoon *et al.*, 2006), ARHGAP31 (LaLonde *et al.*, 2006), ARHGAF6 (Manser *et al.*, 1998), ARHGEF7 (ten Klooster *et al.*, 2006), DLC1 (Kawai *et al.*, 2009*a*), DOCK5 (Frank *et al.*, 2017), PIK3R1 (Gillham *et al.*, 1999), SRGAP3 (Endris *et al.*, 2011), STARD8 (Kawai *et al.*, 2007), STARD13 (Kawai *et al.*, 2009*b*)). However, unlike shown before, I did not detect ARHGAP24 on focal adhesions, but on actin fibers (Lavelin and Geiger, 2005). Furthermore, ARHGAP35, ARHGEF28, and TIAM1 were reported before to localise on focal adhesion, which I did not detect (Tomar *et al.*, 2009; Lim *et al.*, 2008; Wang *et al.*, 2012). The number of RhoGEFs and RhoGAPs I identified at focal adhesions likely still underestimates the number that is involved in integrin-mediated Rho GTPase signalling, because the assay only examined unstimulated steady state localisation, while context-specific recruitment of RhoGEFs and RhoGAPs upon activation of adhesion signalling programs were not investigated in the screen. For example, integrin stimulation by mechanical force has been shown to recruit ARHGEF2 to focal adhesions by increased ERK-mediated phosphorylation (Guilluy *et al.*, 2011*b*). Furthermore, fibronectin ligand-induced IAC formation has been shown to recruit components of the focal adhesion interactome which are not detectable in the absence of the ligand (Horton *et al.*, 2015). It will therefore be interesting to further unravel context-specific recruitment of RhoGEFs and RhoGAPs in the presence of integrin ligands and during specific stages of IAC maturation.

The core components of the adhesome are prime candidates responsible for the local recruitment of the regulators by protein-protein interactions. A RhoGEF and RhoGAP interactome study by Oliver Rocks and colleagues in the lab identified such potential recruitment interactors: For example, ARHGAP12 may associate with focal adhesions via ASAP1/2, ARHGAP31 via talin, ARHGAP9 via ASAP1 or CRKL, and ARHGAP39 via PEAK1. The yet uncharacterised regulator ARHGAP39 interacts with the atypical kinase PEAK1/SGK269 which we also find on focal complexes. The interaction critically involves the second WW domain of ARHGAP39. An ARHGAP39 Y81A point mutation disrupting this WW domain both fails to co-immunoprecipitate with PEAK1 and to be recruited to focal adhesions (data not shown, manuscript in preparation). This suggests, that recruitment of RhoGEFs and RhoGAPs to focal adhesions is regulated by binding of protein-protein interaction domains within the GEF and GAP multidomain proteins to core components of IACs, probably, at least for some of them, in a stimulus-dependent manner.

6.3.2 RhoGEFs and RhoGAPs with activity towards Rac1 are overrepresented at focal adhesions

Above, I already highlighted the importance of differentially regulated Rho GTPase activities during IAC maturation. I was intrigued whether combining the two datasets, the systematic analysis of RhoGEF and RhoGAP substrate specificity and their localisation at focal adhesions, would allow me to identify unique roles of individual Rho GTPases. I found that RhoGEFs and RhoGAPs with activity towards Rac1 are overrepresented at focal adhesions compared to RhoA and Cdc42 (Figure 5.27A and Appendix Table 7.1). This was evident both when data from the substrate specificity screen or from the literature meta-analysis of specificities was taken into account. Moreover, I observed a strong enrichment of constitutively active Rac1 at focal adhesions , whereas wild type Rac1 and its dominant negative form were at least less enriched and the HVR of Rac1 was clearly absent from these structures(Figure 5.27B). Furthermore, RhoA or Cdc42 and any of their mutant forms were not enriched at focal adhesions. (Appendix Figure 7.17 and Appendix Figure 7.18).

Rac1 has been shown to directly bind to the SH3 domain of ARHGEF7 (also known as β-Pix) by a triple-proline motif within the HVR. ARHGEF7 is known to localise on focal adhesions, which I also observed, and its direct interaction was shown to be required for ARHGAP7-mediated activation of Rac1 (ten Klooster *et al.*, 2006). The authors of this study postulated that this interaction was independent of the activity state of Rac1 which is in contrast to another study where it was shown that active Rac1 is preferentially recruited to focal adhesions (Chang *et al.*, 2007). However, the fact that Rac1-HVR, which also comprises the triple-proline motif, was clearly not recruited to focal adhesions (Figure 5.27B) suggests that other additional mechanisms are required to recruit Rac1 to focal adhesions. It is conceivable that the recruitment is supported or alternatively regulated by an effector protein binding only the GTP-bound form of Rac1. PAK1, which is a known effector of Rac1 signalling, is a candidate protein which was also identified to localise on focal adhesions in the lab (Robert-William Welke, unpublished data).

Taken together, this suggests that Rac1 might play a unique role in the formation and turnover of focal complexes and thus has a particular requirement for precise control of its local GTPase activity. Moreover, the underestimated prevalence of focal adhesions associated RhoGEFs and RhoGAPs further underscores the importance of fine-tuned Rho signalling in the control of cell-matrix adhesion. Sill, the true functional implication of many of these regulators in the control of focal adhesion dynamics first needs to be

formally established. However, together with the substrate specificity data this will fuel and facilitate efforts to further deconvolute the different Rho GTPase dependent signalling responses during the adhesion complex maturation process.

6.4 A reaction-diffusion system-based model of Rho GTPase signalling

Rho GTPase signalling at the plasma membrane has for a long time been considered a static process. However, recent findings by others and work that I present in this thesis challenge this model. The fundamental question how spatially restricted Rho GTPase signalling is achieved and maintained has not been answered yet.

In this work, I showed that Rho GTPases do not stably reside in confined regions of the plasma membrane , but rapidly dissipate by diffusion (Figure 5.2). Therefore, mechanisms must exist that antagonise or prevent signal leakage of active Rho GTPases to other regions within of the cell. In principle, two different models of how Rho GTPase activity is locally concentrated and preserved are conceivable: Firstly, through immobilisation by protein-protein interactions with other locally tethered factors, such as scaffolding proteins, effector proteins, or other regulators. Or secondly, by a reaction-diffusion system with localised regions of Rho activation and inactivation.

Several facts argue against the first theory. Selective binding and recognition of active Rho GTPases is assumed to occur via the switch regions. It is furthermore assumed that the switch region interface can only serve as a binding site for one protein at a time. Therefore, the formation of multi-protein signalling complexes including interaction of a central active Rho GTPases with both scaffolding and effector binding partners is unlikely. However, effector proteins could, in principle, serve as both immobilising factor and downstream signalling transducer at the same time. Selective tethering of Rho GTPases by protein-protein interaction has only been shown once so far. As discussed above, Rac1 is recruited to focal adhesions by an interaction with ARHGEF7 through a C-terminal proline region. To my knowledge this is the only known case of Rho signalling that would allow the concerted immobilisation, activation and effector signalling of a Rho GTPase. This is further supported by the fact that constitutively active Rac1 was shown to exhibit temporary immobilisation at focal adhesions (Shibata *et al.*, 2013).

In contrast, seminal studies by William Bement and colleagues on single cell wound closure in *Xenopus laevis* oocytes showed that the Rho GTPases RhoA and Cdc42 cycle even more rapidly between the active GTP-bound state and the inactive GDP-bound state within zones of high activity than outside (Burkel *et al.*, 2012). It was furthermore shown in the same study that GTP-GDP turnover rates differed spatially even within the zone of high activity. This clearly contradicts a model of Rho signalling by local immobilisation and led, together with other findings, to the formulation of a reaction-diffusion-based model of Rho GTPase signalling (Bement *et al.*, 2006; Fritz and Pertz, 2016).

The principle of spatial symmetry breaking in homogeneous media through reaction-

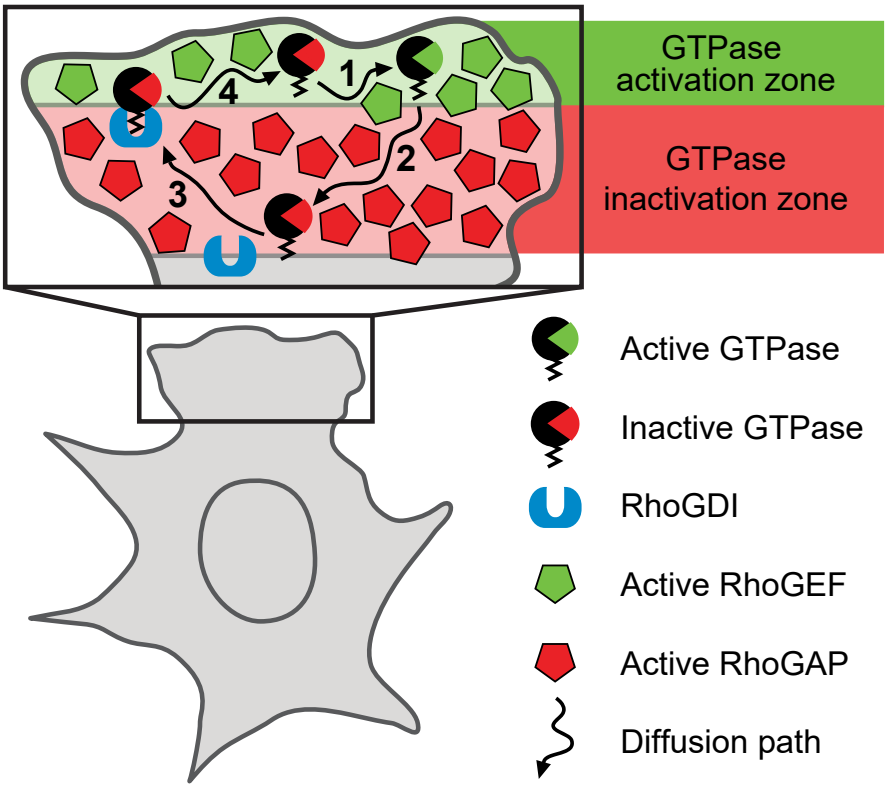

Figure 6.1 Reaction-diffusion system hypothesis of Rho GTPase signalling. Scheme of Rho GTPase activation/inactivation cycle as a reaction-diffusion system. Spatial subcellular separation of RhoGEFs and RhoGAPs may determine distinct activation and deactivation zones, which shape and maintain the Rho GTPase activity gradient. (1) Local activation of a GTPase by a RhoGEF in the activation zone, (2) lateral diffusion into the inactivation zone, local inactivation by a RhoGAP, (3) membrane extraction of the GTPase by RhoGDI and rapid recycling, (4) unloading from RhoGDI and lateral diffusion into the activation zone. Figure modified from Fritz and Pertz (2016).

diffusion processes has first been described by the mathematician Alan Turing (Turing, 1952). In contrast to the model suggested by Turing the intracellular environment for reactions and diffusion is initially inhomogeneous as mostly activating and deactivating enzymes differentially localise to distinct cellular structures. This principle allows the formation of steep gradients of active signalling molecules within confined regions of cells (Kholodenko, 2009).

Accordingly, a reaction-diffusion-based model of Rho signalling is based on the assumption of discrete confined zones of activation by RhoGEFs and inactivation by RhoGAPs combined with mobile Rho GTPases. In this dynamic system Rho GTPase passively cycle between local activation, plasma membrane diffusion, and local inactivation probably supported by RhoGDI-mediated membrane desorption and delivery. Spatial restriction is maintained by formation of local "GAP barriers" which avoid signal leakage into the cell volume. This system is independent of stable Rho GTPase residence and only requires high local activities of RhoGEFs and RhoGAPs that shape Rho GTPase activity patterns.

The interplay of local pools of Rho GTPase activity and its shape by localised RhoGEFs and RhoGAPs has been thoroughly studied at the example of invadopodia formation. RhoC is a critical Rho GTPase for the formation of invadopodia and John Condeelis and colleagues found that RhoC activity is high in a concentric region around invadopodia with a minimum at the centre of invadopodia (Bravo-Cordero *et al.*, 2011). The RhoGEF and the RhoGAP responsible for this RhoC activity pattern during invadopodia formation have been identified as ARHGEF28 (also known as p190RhoGEF) and ARHGAP35 (also known as p190RhoGAP). Whereas ARHGAP35 was shown to localise at invadopodia being responsible for inhibition of RhoC within invadopodia, ARHGEF28 was enriched in areas around invadopodia, correlating with regions of high activity. Together, the authors showed that ARHGEF28 and ARHGAP35 were responsible for the formation of a micrometer scaled highly localised activity gradient by functional cooperation.

The reaction-diffusion hypothesis of Rho GTPase signalling is in agreement with several aspects of my work. I showed that RhoGEFs and RhoGAPs in principle localise to very defined structures and regions, such as focal adhesions (Figure 5.24 and Figure 5.25). Intriguingly, I found that some of the regulators did not localise directly at focal adhesions but in a concentric region around them (Figure 5.26), potentially giving rise the formation of localised Rho activity patterns at these structures, similar as reported for invadopodia (Bravo-Cordero *et al.*, 2011). This is especially interesting, because micrometre to submicrometre organisation of RhoGEF and RhoGAP localisation potentially shapes highly localised Rho activity gradients and has so far rarely been reported.

Furthermore, the systematic analysis of RhoGEF and RhoGAP substrate activities in my work provides an other interesting insight in the potential role of the regulators in a

reaction-diffusion-based signalling system. Most RhoGEFs showed an exclusive predominant substrate specificity. Therefore, they probably activate specific Rho GTPases in a context-dependent manner. However, two classes of RhoGAPs exist: Those with exclusive activity might inactive Rho GTPases in a context-specific manner, to shape highly specific and localised Rho activity gradients, whereas, those RhoGAPs with promiscuous activity might form general Rho activity barriers and downregulate global levels of Rho GTPase activity throughout the cell and by this avoid Rho activity leakage by highly diffusive Rho GTPases.

Together, my experiments provide evidence that the classical static GTPase-centric model of Rho signalling at membranes is outdated and instead support the hypothesis of a reaction-diffusion system-controlled mechanism where Rho signals are orchestrated by localised RhoGEFs and RhoGAPs in a context-dependent manner. Furthermore, the family-wide systematic characterization of the RhoGEF and RhoGAP substrate specificities and localisation yielded valuable datasets that place the regulators into their downstream functional contexts. These datasets will serve as a reference resource and provide the framework for future targeted studies on individual regulators as well for research at the systems-level.

7 References

Abdul-Manan, N., Aghazadeh, B., Liu, G.A., Majumdar, A., Ouerfelli, O., Siminovitch, K.A. and Rosen, M.K. (1999). Structure of Cdc42 in complex with the GTPase-binding domain of the 'Wiskott-Aldrich syndrome' protein. *Nature*, **399**:379–83.

Adra, C.N., Manor, D., Ko, J.L., Zhu, S., Horiuchi, T., Van Aelst, L., Cerione, R.A. and Lim, B. (1997). RhoGDIgamma: a GDP-dissociation inhibitor for Rho proteins with preferential expression in brain and pancreas. *Proc. Natl. Acad. Sci. U. S. A.*, **94**:4279–84.

Ahmadian, M.R., Zor, T., Vogt, D., Kabsch, W., Selinger, Z., Wittinghofer, A. and Scheffzek, K. (1999). Guanosine triphosphatase stimulation of oncogenic Ras mutants. *Proc. Natl. Acad. Sci. U. S. A.*, **96**:7065–70.

Aittaleb, M., Nishimura, A., Linder, M.E. and Tesmer, J.J.G. (2011). Plasma membrane association of p63 Rho guanine nucleotide exchange factor (p63RhoGEF) is mediated by palmitoylation and is required for basal activity in cells. *J. Biol. Chem.*, **286**:34448–56.

Alberts, A.S., Qin, H., Carr, H.S. and Frost, J.A. (2005). PAK1 negatively regulates the activity of the Rho exchange factor NET1. *J. Biol. Chem.*, **280**:12152–61.

Amano, M., Mukai, H., Ono, Y., Chihara, K., Matsui, T., Hamajima, Y., Okawa, K., Iwamatsu, A. and Kaibuchi, K. (1996). Identification of a putative target for Rho as the serine-threonine kinase protein kinase N. *Science*, **271**:648–50.

Amin, E., Jaiswal, M., Derewenda, U., Reis, K., Nouri, K., Koessmeier, K.T., Aspenström, P., Somlyo, A.V., Dvorsky, R. and Ahmadian, M.R. (2016). Deciphering the Molecular and Functional Basis of RHOGAP Family Proteins: A SYSTEMATIC APPROACH TOWARD SELECTIVE INACTIVATION OF RHO FAMILY PROTEINS. *J. Biol. Chem.*, **291**:20353–71.

Asiedu, M., Wu, D., Matsumura, F. and Wei, Q. (2008). Phosphorylation of MyoGEF on Thr-574 by Plk1 promotes MyoGEF localization to the central spindle. *J. Biol. Chem.*, **283**:28392–400.

Aspenström, P., Ruusala, A. and Pacholsky, D. (2007). Taking Rho GTPases to the next level: the cellular functions of atypical Rho GTPases. *Exp. Cell Res.*, **313**:3673–9.

Bacon, D.J. and Sedegah, M. (2007). Reduced production of RNA transcripts from individual DNA plasmids given in a multivalent DNA vaccine formula. *Hum. Vaccin.*, **3**:48–53.

Bement, W.M., Benink, H.A. and von Dassow, G. (2005). A microtubule-dependent zone of active RhoA during cleavage plane specification. *J. Cell Biol.*, **170**:91–101.

Bement, W.M., Miller, A.L. and von Dassow, G. (2006). Rho GTPase activity zones and transient contractile arrays. *Bioessays*, **28**:983–93.

Benard, V. and Bokoch, G.M. (2002). Assay of Cdc42, Rac, and Rho GTPase activation by affinity methods. *Methods Enzymol.*, **345**:349–59.

Benink, H.A. and Bement, W.M. (2005). Concentric zones of active RhoA and Cdc42 around single cell wounds. *J. Cell Biol.*, **168**:429–39.

Benson, D.M., Bryan, J., Plant, A.L., Gotto, A.M. and Smith, L.C. (1985). Digital imaging fluorescence microscopy: spatial heterogeneity of photobleaching rate constants in individual cells. *J. Cell Biol.*, **100**:1309–23.

Bernards, A. and Settleman, J. (2004). GAP control: regulating the regulators of small GTPases. *Trends Cell Biol.*, **14**:377–85.

Bishop, a.L. and Hall, A. (2000). Rho GTPases and their effector proteins. *Biochem. J.*, **348 Pt 2**:241–55.

Bolte, S. and Cordelières, F.P. (2006). A guided tour into subcellular colocalization analysis in light microscopy. *J. Microsc.*, **224**:213–32.

Bos, J.L., Rehmann, H. and Wittinghofer, A. (2007). GEFs and GAPs: critical elements in the control of small G proteins. *Cell*, **129**:865–77.

Boshart, M., Weber, F., Jahn, G., Dorsch-Häsler, K., Fleckenstein, B. and Schaffner, W. (1985). A very strong enhancer is located upstream of an immediate early gene of human cytomegalovirus. *Cell*, **41**:521–30.

Boulter, E., Garcia-Mata, R., Guilluy, C., Dubash, A., Rossi, G., Brennwald, P.J. and Burridge, K. (2010). Regulation of Rho GTPase crosstalk, degradation and activity by RhoGDI1. *Nat. Cell Biol.*, **12**:477–83.

Boureux, A., Vignal, E., Faure, S. and Fort, P. (2007). Evolution of the Rho family of ras-like GTPases in eukaryotes. *Mol. Biol. Evol.*, **24**:203–16.

Bravo-Cordero, J.J., Oser, M., Chen, X., Eddy, R., Hodgson, L. and Condeelis, J. (2011). A novel spatiotemporal RhoC activation pathway locally regulates cofilin activity at invadopodia. *Curr. Biol.*, **21**:635–44.

Breznau, E.B., Semack, A.C., Higashi, T. and Miller, A.L. (2015). MgcRacGAP restricts active RhoA at the cytokinetic furrow and both RhoA and Rac1 at cell-cell junctions in epithelial cells. *Mol. Biol. Cell*, **26**:2439–55.

Buchsbaum, R.J. (2007). Rho activation at a glance. *J. Cell Sci.*, **120**:1149–52.

Burkel, B.M., Benink, H.A., Vaughan, E.M., von Dassow, G. and Bement, W.M. (2012). A Rho GTPase signal treadmill backs a contractile array. *Dev. Cell*, **23**:384–96.

Burridge, K. and Guilluy, C. (2016). Focal adhesions, stress fibers and mechanical tension. *Exp. Cell Res.*, **343**:14–20.

Bustelo, X.R., Sauzeau, V. and Berenjeno, I.M. (2007). GTP-binding proteins of the Rho/Rac family: regulation, effectors and functions in vivo. *Bioessays*, **29**:356–70.

van Buul, J.D., Geerts, D. and Huveneers, S. (2014). Rho GAPs and GEFs: controling switches in endothelial cell adhesion. *Cell Adh. Migr.*, **8**:108–24.

Campellone, K.G. and Welch, M.D. (2010). A nucleator arms race: cellular control of actin assembly. *Nat. Rev. Mol. Cell Biol.*, **11**:237–51.

Canagarajah, B., Leskow, F.C., Ho, J.Y.S., Mischak, H., Saidi, L.F., Kazanietz, M.G. and Hurley, J.H. (2004). Structural mechanism for lipid activation of the Rac-specific GAP, beta2-chimaerin. *Cell*, **119**:407–18.

Chandra, A., Grecco, H.E., Pisupati, V., Perera, D., Cassidy, L., Skoulidis, F., Ismail, S.a., Hedberg, C., Hanzal-Bayer, M., Venkitaraman, A.R., Wittinghofer, A. and Bastiaens, P.I.H. (2012). The GDI-like solubilizing factor PDEδ sustains the spatial organization and signalling of Ras family proteins. *Nat. Cell Biol.*, **14**:148–58.

Chang, F., Lemmon, C.A., Park, D. and Romer, L.H. (2007). FAK potentiates Rac1 activation and localization to matrix adhesion sites: a role for betaPIX. *Mol. Biol. Cell*, **18**:253–64.

Chardin, P. (2006). Function and regulation of Rnd proteins. *Nat. Rev. Mol. Cell Biol.*, **7**:54–62.

Chauhan, B.K., Lou, M., Zheng, Y. and Lang, R.A. (2011). Balanced Rac1 and RhoA activities regulate cell shape and drive invagination morphogenesis in epithelia. *Proc. Natl. Acad. Sci. U. S. A.*, **108**:18289–94.

Cheezum, M.K., Walker, W.F. and Guilford, W.H. (2001). Quantitative comparison of algorithms for tracking single fluorescent particles. *Biophys. J.*, **81**:2378–88.

Chenouard, N., Smal, I., de Chaumont, F., Maška, M., Sbalzarini, I.F., Gong, Y., Cardinale, J., Carthel, C., Coraluppi, S., Winter, M., Cohen, A.R., Godinez, W.J., Rohr, K., Kalaidzidis, Y., Liang, L., Duncan, J., Shen, H., Xu, Y., Magnusson, K.E.G., Jaldén, J., Blau, H.M., Paul-Gilloteaux, P., Roudot, P., Kervrann, C., Waharte, F., Tinevez, J.Y., Shorte, S.L., Willemse, J., Celler, K., van Wezel, G.P., Dan, H.W., Tsai, Y.S., Ortiz de Solórzano, C., Olivo-Marin, J.C. and Meijering, E. (2014). Objective comparison of particle tracking methods. *Nat. Methods*, **11**:281–9.

Cherfils, J. and Chardin, P. (1999). GEFs: structural basis for their activation of small GTP-binding proteins. *Trends Biochem. Sci.*, **24**:306–11.

Cherfils, J. and Zeghouf, M. (2013). Regulation of small GTPases by GEFs, GAPs, and GDIs. *Physiol. Rev.*, **93**:269–309.

Chikumi, H., Barac, A., Behbahani, B., Gao, Y., Teramoto, H., Zheng, Y. and Gutkind, J.S. (2004). Homo- and hetero-oligomerization of PDZ-RhoGEF, LARG and p115RhoGEF by their C-terminal region regulates their in vivo Rho GEF activity and transforming potential. *Oncogene*, **23**:233–40.

Cocucci, E., Aguet, F., Boulant, S. and Kirchhausen, T. (2012). The first five seconds in the life of a clathrin-coated pit. *Cell*, **150**:495–507.

Colón-González, F., Leskow, F.C. and Kazanietz, M.G. (2008). Identification of an autoinhibitory mechanism that restricts C1 domain-mediated activation of the Rac-GAP alpha2-chimaerin. *J. Biol. Chem.*, **283**:35247–57.

Colwill, K., Wells, C.D., Elder, K., Goudreault, M., Hersi, K., Kulkarni, S., Hardy, W.R., Pawson, T. and Morin, G.B. (2006). Modification of the Creator recombination system for proteomics applications–improved expression by addition of splice sites. *BMC Biotechnol.*, **6**:13.

Cook, D.R., Rossman, K.L. and Der, C.J. (2013). Rho guanine nucleotide exchange factors: regulators of Rho GTPase activity in development and disease. *Oncogene*, pages 1–15.

Das, S., Yin, T., Yang, Q., Zhang, J., Wu, Y.I. and Yu, J. (2015). Single-molecule tracking of small GTPase Rac1 uncovers spatial regulation of membrane translocation and mechanism for polarized signaling. *Proc. Natl. Acad. Sci. U. S. A.*

Deakin, N.O. and Turner, C.E. (2008). Paxillin comes of age. *J. Cell Sci.*, **121**:2435–44.

DeGeer, J. and Lamarche-Vane, N. (2013). Rho GTPases in neurodegeneration diseases. *Exp. Cell Res.*, **319**:2384–94.

DerMardirossian, C. and Bokoch, G.M. (2005). GDIs: central regulatory molecules in Rho GTPase activation. *Trends Cell Biol.*, **15**:356–63.

DerMardirossian, C., Schnelzer, A. and Bokoch, G.M. (2004). Phosphorylation of RhoGDI by Pak1 mediates dissociation of Rac GTPase. *Mol. Cell*, **15**:117–27.

Diaspro, A., Chirico, G., Usai, C., Ramoino, P. and Dobrucki, J. (2006). Photobleaching. *Handb. Biol. Confocal Microsc.*, pages 690–702.

Didsbury, J., Weber, R.F., Bokoch, G.M., Evans, T. and Snyderman, R. (1989). rac, a novel ras-related family of proteins that are botulinum toxin substrates. *J. Biol. Chem.*, **264**:16378–82.

Donnelly, S.K., Bravo-Cordero, J.J. and Hodgson, L. (2014). Rho GTPase isoforms in cell motility: Don't fret, we have FRET. *Cell Adh. Migr.*, **8**:37–41.

Dovas, A. and Couchman, J.R. (2005). RhoGDI: multiple functions in the regulation of Rho family GTPase activities. *Biochem. J.*, **390**:1–9.

Dvorsky, R. and Ahmadian, M.R. (2004). Always look on the bright site of Rho: structural implications for a conserved intermolecular interface. *EMBO Rep.*, **5**:1130–6.

Eberth, A. and Ahmadian, M.R. (2009). In vitro GEF and GAP assays. *Curr. Protoc. cell Biol.*, **Chapter 14**:Unit 14.9.

Eberth, A., Dvorsky, R., Becker, C.F.W., Beste, A., Goody, R.S. and Ahmadian, M.R. (2005). Monitoring the real-time kinetics of the hydrolysis reaction of guanine nucleotide-binding proteins. *Biol. Chem.*, **386**:1105–14.

Endris, V., Haussmann, L., Buss, E., Bacon, C., Bartsch, D. and Rappold, G. (2011). SrGAP3 interacts with lamellipodin at the cell membrane and regulates Rac-dependent cellular protrusions. *J. Cell Sci.*, **124**:3941–55.

Etienne-Manneville, S. and Hall, A. (2002). Rho GTPases in cell biology. *Nature*, **420**:629–35.

Feig, L.A. (1999). Tools of the trade: use of dominant-inhibitory mutants of Ras-family GTPases. *Nat. Cell Biol.*, **1**:E25–7.

Filippi, M.D., Harris, C.E., Meller, J., Gu, Y., Zheng, Y. and Williams, D.A. (2004). Localization of Rac2 via the C terminus and aspartic acid 150 specifies superoxide generation, actin polarity and chemotaxis in neutrophils. *Nat. Immunol.*, **5**:744–51.

Flynn, P., Mellor, H., Palmer, R., Panayotou, G. and Parker, P.J. (1998). Multiple interactions of PRK1 with RhoA. Functional assignment of the Hr1 repeat motif. *J. Biol. Chem.*, **273**:2698–705.

Forget, M.A., Desrosiers, R.R., Gingras, D. and Béliveau, R. (2002). Phosphorylation states of Cdc42 and RhoA regulate their interactions with Rho GDP dissociation inhibitor and their extraction from biological membranes. *Biochem. J.*, **361**:243–54.

Förster, T. (1948). Zwischenmolekulare Energiewanderung und Fluoreszenz. *Ann. Phys.*, **437**:55–75.

Frank, S.R., Köllmann, C.P., van Lidth de Jeude, J.F., Thiagarajah, J.R., Engelholm, L.H., Frödin, M. and Hansen, S.H. (2017). The focal adhesion-associated proteins DOCK5 and GIT2 comprise a rheostat in control of epithelial invasion. *Oncogene*, **36**:1816–1828.

Fritz, R.D., Letzelter, M., Reimann, A., Martin, K., Fusco, L., Ritsma, L., Ponsioen, B., Fluri, E., Schulte-Merker, S., van Rheenen, J. and Pertz, O. (2013). A Versatile Toolkit to Produce Sensitive FRET Biosensors to Visualize Signaling in Time and Space. *Sci. Signal.*, **6**:rs12.

Fritz, R.D., Menshykau, D., Martin, K., Reimann, A., Pontelli, V. and Pertz, O. (2015). SrGAP2-Dependent Integration of Membrane Geometry and Slit-Robo-Repulsive Cues Regulates Fibroblast Contact Inhibition of Locomotion. *Dev. Cell*, pages 1–15.

Fritz, R.D. and Pertz, O. (2016). The dynamics of spatio-temporal Rho GTPase signaling: formation of signaling patterns. *F1000Research*, **5**:749.

Fukumoto, Y., Kaibuchi, K., Hori, Y., Fujioka, H., Araki, S., Ueda, T., Kikuchi, A. and Takai, Y. (1990). Molecular cloning and characterization of a novel type of regulatory protein (GDI) for the rho proteins, ras p21-like small GTP-binding proteins. *Oncogene*, **5**:1321–8.

Gandhi, P.N., Gibson, R.M., Tong, X., Miyoshi, J., Takai, Y., Konieczkowski, M., Sedor, J.R. and Wilson-Delfosse, A.L. (2004). An activating mutant of Rac1 that fails to interact with Rho GDP-dissociation inhibitor stimulates membrane ruffling in mammalian cells. *Biochem. J.*, **378**:409–19.

Garcia-Mata, R., Boulter, E. and Burridge, K. (2011). The 'invisible hand': regulation of RHO GTPases by RHOGDIs. *Nat. Rev. Mol. Cell Biol.*, **12**:493–504.

Geiger, B., Bershadsky, A., Pankov, R. and Yamada, K.M. (2001). Transmembrane crosstalk between the extracellular matrix–cytoskeleton crosstalk. *Nat. Rev. Mol. Cell Biol.*, **2**:793–805.

Geiger, B. and Bershadsky, A. (2002). Exploring the neighborhood: adhesion-coupled cell mechanosensors. *Cell*, **110**:139–42.

Geiger, B., Spatz, J.P. and Bershadsky, A.D. (2009). Environmental sensing through focal adhesions. *Nat. Rev. Mol. Cell Biol.*, **10**:21–33.

Gibson, R.M. and Wilson-Delfosse, a.L. (2001). RhoGDI-binding-defective mutant of Cdc42Hs targets to membranes and activates filopodia formation but does not cycle with the cytosol of mammalian cells. *Biochem. J.*, **359**:285–94.

Gibson, R.M., Gandhi, P.N., Tong, X., Miyoshi, J., Takai, Y., Konieczkowski, M., Sedor, J.R. and Wilson-Delfosse, A.L. (2004). An activating mutant of Cdc42 that fails to interact with Rho GDP-dissociation inhibitor localizes to the plasma membrane and mediates actin reorganization. *Exp. Cell Res.*, **301**:211–22.

Gillham, H., Golding, M.C., Pepperkok, R. and Gullick, W.J. (1999). Intracellular movement of green fluorescent protein-tagged phosphatidylinositol 3-kinase in response to growth factor receptor signaling. *J. Cell Biol.*, **146**:869–80.

Gossen, M., Freundlieb, S., Bender, G., Müller, G., Hillen, W. and Bujard, H. (1995). Transcriptional activation by tetracyclines in mammalian cells. *Science*, **268**:1766–9.

Graham, D.L., Eccleston, J.F. and Lowe, P.N. (1999). The conserved arginine in rho-GTPase-activating protein is essential for efficient catalysis but not for complex formation with Rho.GDP and aluminum fluoride. *Biochemistry*, **38**:985–91.

Griesbeck, O., Baird, G.S., Campbell, R.E., Zacharias, D.A. and Tsien, R.Y. (2001). Reducing the environmental sensitivity of yellow fluorescent protein. Mechanism and applications. *J. Biol. Chem.*, **276**:29188–94.

Grimm, J.B., English, B.P., Chen, J., Slaughter, J.P., Zhang, Z., Revyakin, A., Patel, R., Macklin, J.J., Normanno, D., Singer, R.H., Lionnet, T. and Lavis, L.D. (2015). A general method to improve fluorophores for live-cell and single-molecule microscopy. *Nat. Methods*.

Grimm, J.B., Muthusamy, A.K., Liang, Y., Brown, T.A., Lemon, W.C., Patel, R., Lu, R., Macklin, J.J., Keller, P.J., Ji, N. and Lavis, L.D. (2017). A general method to fine-tune fluorophores for live-cell and in vivo imaging. *Nat. Methods*, **14**:987–994.

Grimsley, C.M., Kinchen, J.M., Tosello-Trampont, A.C., Brugnera, E., Haney, L.B., Lu, M., Chen, Q., Klingele, D., Hengartner, M.O. and Ravichandran, K.S. (2004). Dock180 and ELMO1 proteins cooperate to promote evolutionarily conserved Rac-dependent cell migration. *J. Biol. Chem.*, **279**:6087–97.

Guilluy, C., Garcia-Mata, R. and Burridge, K. (2011*a*). Rho protein crosstalk: another social network? *Trends Cell Biol.*, **21**:718–26.

Guilluy, C., Swaminathan, V., Garcia-Mata, R., O'Brien, E.T., Superfine, R. and Burridge, K. (2011*b*). The Rho GEFs LARG and GEF-H1 regulate the mechanical response to force on integrins. *Nat. Cell Biol.*, **13**:722–7.

Hamada, K., Shimizu, T., Matsui, T., Tsukita, S. and Hakoshima, T. (2000). Structural basis of the membrane-targeting and unmasking mechanisms of the radixin FERM domain. *EMBO J.*, **19**:4449–62.

Hanawa-Suetsugu, K., Kukimoto-Niino, M., Mishima-Tsumagari, C., Akasaka, R., Ohsawa, N., Sekine, S.i., Ito, T., Tochio, N., Koshiba, S., Kigawa, T., Terada, T., Shirouzu, M., Nishikimi, A., Uruno, T., Katakai, T., Kinashi, T., Kohda, D., Fukui, Y. and Yokoyama, S. (2012). Structural basis for mutual relief of the Rac guanine nucleotide exchange factor DOCK2 and its partner ELMO1 from their autoinhibited forms. *Proc. Natl. Acad. Sci. U. S. A.*, **109**:3305–10.

Hancock, J.F., Cadwallader, K., Paterson, H. and Marshall, C.J. (1991). A CAAX or a CAAL motif and a second signal are sufficient for plasma membrane targeting of ras proteins. *EMBO J.*, **10**:4033–9.

Hancock, J.F. and Hall, A. (1993). A novel role for RhoGDI as an inhibitor of GAP proteins. *EMBO J.*, **12**:1915–21.

Hancock, J.F., Paterson, H. and Marshall, C.J. (1990). A polybasic domain or palmitoylation is required in addition to the CAAX motif to localize p21ras to the plasma membrane. *Cell*, **63**:133–9.

Hanna, S., Miskolci, V., Cox, D. and Hodgson, L. (2014). A New Genetically Encoded Single-Chain Biosensor for Cdc42 Based on FRET, Useful for Live-Cell Imaging. *PLoS One*, **9**:e96469.

Hart, M.J., Eva, A., Evans, T., Aaronson, S.A. and Cerione, R.A. (1991). Catalysis of guanine nucleotide exchange on the CDC42Hs protein by the dbl oncogene product. *Nature*, **354**:311–4.

Heasman, S.J. and Ridley, A.J. (2008). Mammalian Rho GTPases: new insights into their functions from in vivo studies. *Nat. Rev. Mol. Cell Biol.*, **9**:690–701.

Hemsath, L., Dvorsky, R., Fiegen, D., Carlier, M.F. and Ahmadian, M.R. (2005). An electrostatic steering mechanism of Cdc42 recognition by Wiskott-Aldrich syndrome proteins. *Mol. Cell*, **20**:313–24.

Heo, W.D., Inoue, T., Park, W.S., Kim, M.L., Park, B.O., Wandless, T.J. and Meyer, T. (2006). PI(3,4,5)P3 and PI(4,5)P2 lipids target proteins with polybasic clusters to the plasma membrane. *Science*, **314**:1458–61.

Hiramoto, K., Negishi, M. and Katoh, H. (2006). Dock4 is regulated by RhoG and promotes Rac-dependent cell migration. *Exp. Cell Res.*, **312**:4205–16.

Hoffman, G.R., Nassar, N. and Cerione, R.a. (2000). Structure of the Rho family GTP-binding protein Cdc42 in complex with the multifunctional regulator RhoGDI. *Cell*, **100**:345–56.

Hoppe, A.D. and Swanson, J.A. (2004). Cdc42, Rac1, and Rac2 display distinct patterns of activation during phagocytosis. *Mol. Biol. Cell*, **15**:3509–19.

Horton, E.R., Byron, A., Askari, J.A., Ng, D.H.J., Millon-Frémillon, A., Robertson, J., Koper, E.J., Paul, N.R., Warwood, S., Knight, D., Humphries, J.D. and Humphries, M.J. (2015). Definition of a consensus integrin adhesome and its dynamics during adhesion complex assembly and disassembly. *Nat. Cell Biol.*, **17**:1577–1587.

Hussain, N.K., Jenna, S., Glogauer, M., Quinn, C.C., Wasiak, S., Guipponi, M., Antonarakis, S.E., Kay, B.K., Stossel, T.P., Lamarche-Vane, N. and McPherson, P.S. (2001). Endocytic protein intersectin-l regulates actin assembly via Cdc42 and N-WASP. *Nat. Cell Biol.*, **3**:927–32.

Huttenlocher, A. and Horwitz, A.R. (2011). Integrins in cell migration. *Cold Spring Harb. Perspect. Biol.*, **3**:a005074.

Huveneers, S. and Danen, E.H.J. (2009). Adhesion signaling - crosstalk between integrins, Src and Rho. *J. Cell Sci.*, **122**:1059–69.

Hynes, R.O. (2002). Integrins: bidirectional, allosteric signaling machines. *Cell*, **110**:673–87.

Innocenti, M., Frittoli, E., Ponzanelli, I., Falck, J.R., Brachmann, S.M., Di Fiore, P.P. and Scita, G. (2003). Phosphoinositide 3-kinase activates Rac by entering in a complex with Eps8, Abi1, and Sos-1. *J. Cell Biol.*, **160**:17–23.

Ishikawa-Ankerhold, H.C., Ankerhold, R. and Drummen, G.P.C. (2012). Advanced fluorescence microscopy techniques–FRAP, FLIP, FLAP, FRET and FLIM. *Molecules*, **17**:4047–132.

Itoh, R.E., Kurokawa, K., Ohba, Y., Yoshizaki, H., Mochizuki, N. and Matsuda, M. (2002). Activation of rac and cdc42 video imaged by fluorescent resonance energy transfer-based single-molecule probes in the membrane of living cells. *Mol. Cell. Biol.*, **22**:6582–91.

Itoh, T. and De Camilli, P. (2006). BAR, F-BAR (EFC) and ENTH/ANTH domains in the regulation of membrane-cytosol interfaces and membrane curvature. *Biochim. Biophys. Acta*, **1761**:897–912.

Jaffe, A.B. and Hall, A. (2005). Rho GTPases: biochemistry and biology. *Annu. Rev. Cell Dev. Biol.*, **21**:247–69.

Jaiswal, M., Dvorsky, R. and Ahmadian, M.R. (2013). Deciphering the molecular and functional basis of Dbl family proteins: a novel systematic approach toward classification of selective activation of the Rho family proteins. *J. Biol. Chem.*, **288**:4486–500.

Jaqaman, K., Loerke, D., Mettlen, M., Kuwata, H., Grinstein, S., Schmid, S.L. and Danuser, G. (2008). Robust single-particle tracking in live-cell time-lapse sequences. *Nat. Methods*, **5**:695–702.

Jares-Erijman, E.a. and Jovin, T.M. (2003). FRET imaging. *Nat. Biotechnol.*, **21**:1387–95.

John, J., Sohmen, R., Feuerstein, J., Linke, R., Wittinghofer, A. and Goody, R.S. (1990). Kinetics of interaction of nucleotides with nucleotide-free H-ras p21. *Biochemistry*, **29**:6058–65.

Johnson, J.L., Erickson, J.W. and Cerione, R.a. (2009). New insights into how the Rho guanine nucleotide dissociation inhibitor regulates the interaction of Cdc42 with membranes. *J. Biol. Chem.*, **284**:23860–71.

Justilien, V., Jameison, L., Der, C.J., Rossman, K.L. and Fields, A.P. (2011). Oncogenic activity of Ect2 is regulated through protein kinase C iota-mediated phosphorylation. *J. Biol. Chem.*, **286**:8149–57.

Kanchanawong, P., Shtengel, G., Pasapera, A.M., Ramko, E.B., Davidson, M.W., Hess, H.F. and Waterman, C.M. (2010). Nanoscale architecture of integrin-based cell adhesions. *Nature*, **468**:580–4.

Karnoub, A.E., Worthylake, D.K., Rossman, K.L., Pruitt, W.M., Campbell, S.L., Sondek, J. and Der, C.J. (2001). Molecular basis for Rac1 recognition by guanine nucleotide exchange factors. *Nat. Struct. Biol.*, **8**:1037–41.

Katsumi, A., Milanini, J., Kiosses, W.B., del Pozo, M.A., Kaunas, R., Chien, S., Hahn, K.M. and Schwartz, M.A. (2002). Effects of cell tension on the small GTPase Rac. *J. Cell Biol.*, **158**:153–64.

Kaverina, I., Krylyshkina, O. and Small, J.V. (2002). Regulation of substrate adhesion dynamics during cell motility. *Int. J. Biochem. Cell Biol.*, **34**:746–61.

Kawai, K., Iwamae, Y., Yamaga, M., Kiyota, M., Ishii, H., Hirata, H., Homma, Y. and Yagisawa, H. (2009*a*). Focal adhesion-localization of START-GAP1/DLC1 is essential for cell motility and morphology. *Genes Cells*, **14**:227–41.

Kawai, K., Kiyota, M., Seike, J., Deki, Y. and Yagisawa, H. (2007). START-GAP3/DLC3 is a GAP for RhoA and Cdc42 and is localized in focal adhesions regulating cell morphology. *Biochem. Biophys. Res. Commun.*, **364**:783–9.

Kawai, K., Seike, J.i., Iino, T., Kiyota, M., Iwamae, Y., Nishitani, H. and Yagisawa, H. (2009*b*). START-GAP2/DLC2 is localized in focal adhesions via its N-terminal region. *Biochem. Biophys. Res. Commun.*, **380**:736–41.

Kawase, K., Nakamura, T., Takaya, A., Aoki, K., Namikawa, K., Kiyama, H., Inagaki, S., Takemoto, H., Saltiel, A.R. and Matsuda, M. (2006). GTP Hydrolysis by the Rho Family GTPase TC10 Promotes Exocytic Vesicle Fusion. *Dev. Cell*, **11**:411–421.

Keppler, A., Gendreizig, S., Gronemeyer, T., Pick, H., Vogel, H. and Johnsson, K. (2003). A general method for the covalent labeling of fusion proteins with small molecules in vivo. *Nat. Biotechnol.*, **21**:86–9.

Kholodenko, B.N. (2009). Spatially distributed cell signalling. *FEBS Lett.*, **583**:4006–12.

Kim, D.W., Uetsuki, T., Kaziro, Y., Yamaguchi, N. and Sugano, S. (1990). Use of the human elongation factor 1 alpha promoter as a versatile and efficient expression system. *Gene*, **91**:217–23.

Kitzing, T.M., Wang, Y., Pertz, O., Copeland, J.W. and Grosse, R. (2010). Formin-like 2 drives amoeboid invasive cell motility downstream of RhoC. *Oncogene*, **29**:2441–8.

Klein, T., Löschberger, A., Proppert, S., Wolter, S., van de Linde, S. and Sauer, M. (2011). Live-cell dSTORM with SNAP-tag fusion proteins. *Nat. Methods*, **8**:7–9.

ten Klooster, J.P., Jaffer, Z.M., Chernoff, J. and Hordijk, P.L. (2006). Targeting and activation of Rac1 are mediated by the exchange factor beta-Pix. *J. Cell Biol.*, **172**:759–69.

Koo, T.H., Eipper, B.A. and Donaldson, J.G. (2007). Arf6 recruits the Rac GEF Kalirin to the plasma membrane facilitating Rac activation. *BMC Cell Biol.*, **8**:29.

Kozma, R., Ahmed, S., Best, A. and Lim, L. (1995). The Ras-related protein Cdc42Hs and bradykinin promote formation of peripheral actin microspikes and filopodia in Swiss 3T3 fibroblasts. *Mol. Cell. Biol.*, **15**:1942–52.

Krauss, M. and Haucke, V. (2007). Phosphoinositides: regulators of membrane traffic and protein function. *FEBS Lett.*, **581**:2105–11.

de Kreuk, B.J., Schaefer, A., Anthony, E.C., Tol, S., Fernandez-Borja, M., Geerts, D., Pool, J., Hambach, L., Goulmy, E. and Hordijk, P.L. (2013). The human minor histocompatibility antigen 1 is a RhoGAP. *PLoS One*, **8**:e73962.

Kurokawa, K., Itoh, R.E., Yoshizaki, H., Nakamura, Y.O.T. and Matsuda, M. (2004). Coactivation of Rac1 and Cdc42 at lamellipodia and membrane ruffles induced by epidermal growth factor. *Mol. Biol. Cell*, **15**:1003–10.

Kurooka, T., Yamamoto, Y., Takai, Y. and Sakisaka, T. (2011). Dual regulation of RA-RhoGAP activity by phosphatidic acid and Rap1 during neurite outgrowth. *J. Biol. Chem.*, **286**:6832–43.

Lai, C.C., Boguski, M., Broek, D. and Powers, S. (1993). Influence of guanine nucleotides on complex formation between Ras and CDC25 proteins. *Mol. Cell. Biol.*, **13**:1345–52.

LaLonde, D.P., Grubinger, M., Lamarche-Vane, N. and Turner, C.E. (2006). CdGAP associates with actopaxin to regulate integrin-dependent changes in cell morphology and motility. *Curr. Biol.*, **16**:1375–85.

Lamarche-Vane, N. and Hall, A. (1998). CdGAP, a novel proline-rich GTPase-activating protein for Cdc42 and Rac. *J. Biol. Chem.*, **273**:29172–7.

Lammers, M., Meyer, S., Kühlmann, D. and Wittinghofer, A. (2008). Specificity of interactions between mDia isoforms and Rho proteins. *J. Biol. Chem.*, **283**:35236–46.

Laurin, M. and Côté, J.F. (2014). Insights into the biological functions of Dock family guanine nucleotide exchange factors. *Genes Dev.*, **28**:533–47.

Lavelin, I. and Geiger, B. (2005). Characterization of a novel GTPase-activating protein associated with focal adhesions and the actin cytoskeleton. *J. Biol. Chem.*, **280**:7178–85.

Lawson, C.D. and Burridge, K. (2014). The on-off relationship of Rho and Rac during integrin-mediated adhesion and cell migration. *Small GTPases*, **5**:e27958.

Lee, J., Park, B., Kim, G., Kim, K., Pak, J., Kim, K., Ye, M.B., Park, S.G. and Park, D. (2014). Arhgef16, a novel Elmo1 binding partner, promotes clearance of apoptotic cells via RhoG-dependent Rac1 activation. *Biochim. Biophys. Acta*, **1843**:2438–47.

Lemmon, M.A. (2008). Membrane recognition by phospholipid-binding domains. *Nat. Rev. Mol. Cell Biol.*, **9**:99–111.

Leonard, D.A., Evans, T., Hart, M., Cerione, R.A. and Manor, D. (1994). Investigation of the GTP-binding/GTPase cycle of Cdc42Hs using fluorescence spectroscopy. *Biochemistry*, **33**:12323–8.

Leonard, D.A., Lin, R., Cerione, R.A. and Manor, D. (1998). Biochemical studies of the mechanism of action of the Cdc42-GTPase-activating protein. *J. Biol. Chem.*, **273**:16210–5.

Leonard, D., Hart, M.J., Platko, J.V., Eva, A., Henzel, W., Evans, T. and Cerione, R.A. (1992). The identification and characterization of a GDP-dissociation inhibitor (GDI) for the CDC42Hs protein. *J. Biol. Chem.*, **267**:22860–8.

Lim, Y., Lim, S.T., Tomar, A., Gardel, M., Bernard-Trifilo, J.A., Chen, X.L., Uryu, S.A., Canete-Soler, R., Zhai, J., Lin, H., Schlaepfer, W.W., Nalbant, P., Bokoch, G., Ilic, D., Waterman-Storer, C. and Schlaepfer, D.D. (2008). PyK2 and FAK connections to p190Rho guanine nucleotide exchange factor regulate RhoA activity, focal adhesion formation, and cell motility. *J. Cell Biol.*, **180**:187–203.

Lin, Q., Fuji, R.N., Yang, W. and Cerione, R.A. (2003). RhoGDI is required for Cdc42-mediated cellular transformation. *Curr. Biol.*, **13**:1469–79.

Lin, Q., Yang, W., Baird, D., Feng, Q. and Cerione, R.A. (2006). Identification of a DOCK180-related guanine nucleotide exchange factor that is capable of mediating a positive feedback activation of Cdc42. *J. Biol. Chem.*, **281**:35253–62.

Lingwood, D. and Simons, K. (2010). Lipid rafts as a membrane-organizing principle. *Science*, **327**:46–50.

Liu, P., Cheng, H., Roberts, T.M. and Zhao, J.J. (2009). Targeting the phosphoinositide 3-kinase pathway in cancer. *Nat. Rev. Drug Discov.*, **8**:627–44.

Loew, R., Heinz, N., Hampf, M., Bujard, H. and Gossen, M. (2010). Improved Tet-responsive promoters with minimized background expression. *BMC Biotechnol.*, **10**:81.

Lommerse, P.H.M., Blab, G.a., Cognet, L., Harms, G.S., Snaar-Jagalska, B.E., Spaink, H.P. and Schmidt, T. (2004). Single-molecule imaging of the H-ras membrane-anchor reveals domains in the cytoplasmic leaflet of the cell membrane. *Biophys. J.*, **86**:609–16.

Lommerse, P.H.M., Snaar-Jagalska, B.E., Spaink, H.P. and Schmidt, T. (2005). Single-molecule diffusion measurements of H-Ras at the plasma membrane of live cells reveal microdomain localization upon activation. *J. Cell Sci.*, **118**:1799–809.

Lommerse, P.H.M., Vastenhoud, K., Pirinen, N.J., Magee, A.I., Spaink, H.P. and Schmidt, T. (2006). Single-molecule diffusion reveals similar mobility for the Lck, H-ras, and K-ras membrane anchors. *Biophys. J.*, **91**:1090–7.

Lu, M., Kinchen, J.M., Rossman, K.L., Grimsley, C., DeBakker, C., Brugnera, E., Tosello-Trampont, A.C., Haney, L.B., Klingele, D., Sondek, J., Hengartner, M.O. and Ravichandran, K.S. (2004). PH domain of ELMO functions in trans to regulate Rac activation via Dock180. *Nat. Struct. Mol. Biol.*, **11**:756–62.

Lu, M., Kinchen, J.M., Rossman, K.L., Grimsley, C., Hall, M., Sondek, J., Hengartner, M.O., Yajnik, V. and Ravichandran, K.S. (2005). A Steric-inhibition model for regulation of nucleotide exchange via the Dock180 family of GEFs. *Curr. Biol.*, **15**:371–7.

Lukinavičius, G., Reymond, L. and Johnsson, K. (2015). Fluorescent Labeling of SNAP-Tagged Proteins in Cells. *Methods Mol. Biol.*, **1266**:107–18.

Lukinavičius, G., Umezawa, K., Olivier, N., Honigmann, A., Yang, G., Plass, T., Mueller, V., Reymond, L., Corrêa, I.R., Luo, Z.G., Schultz, C., Lemke, E.a., Heppenstall, P., Eggeling, C., Manley, S. and Johnsson, K. (2013). A near-infrared fluorophore for live-cell super-resolution microscopy of cellular proteins. *Nat. Chem.*, **5**:132–9.

Machacek, M., Hodgson, L., Welch, C., Elliott, H., Pertz, O., Nalbant, P., Abell, A., Johnson, G.L., Hahn, K.M. and Danuser, G. (2009). Coordination of Rho GTPase activities during cell protrusion. *Nature*, **461**:99–103.

Madaule, P. and Axel, R. (1985). A novel ras-related gene family. *Cell*, **41**:31–40.

Manser, E., Loo, T.H., Koh, C.G., Zhao, Z.S., Chen, X.Q., Tan, L., Tan, I., Leung, T. and Lim, L. (1998). PAK kinases are directly coupled to the PIX family of nucleotide exchange factors. *Mol. Cell*, **1**:183–92.

Martin, K., Reimann, A., Fritz, R.D., Ryu, H., Jeon, N.L. and Pertz, O. (2016). Spatio-temporal co-ordination of RhoA, Rac1 and Cdc42 activation during prototypical edge protrusion and retraction dynamics. *Sci. Rep.*, **6**:21901.

Mazhab-Jafari, M.T., Marshall, C.B., Smith, M., Gasmi-Seabrook, G.M.C., Stambolic, V., Rottapel, R., Neel, B.G. and Ikura, M. (2010). Real-time NMR study of three small GTPases reveals that fluorescent 2'(3')-O-(N-methylanthraniloyl)-tagged nucleotides alter hydrolysis and exchange kinetics. *J. Biol. Chem.*, **285**:5132–6.

McTaggart, S.J. (2006). Isoprenylated proteins. *Cell. Mol. Life Sci.*, **63**:255–67.

Medalia, O. and Geiger, B. (2010). Frontiers of microscopy-based research into cell-matrix adhesions. *Curr. Opin. Cell Biol.*, **22**:659–68.

Meder, D., Moreno, M.J., Verkade, P., Vaz, W.L.C. and Simons, K. (2006). Phase coexistence and connectivity in the apical membrane of polarized epithelial cells. *Proc. Natl. Acad. Sci. U. S. A.*, **103**:329–34.

Meller, N., Westbrook, M.J., Shannon, J.D., Guda, C. and Schwartz, M.A. (2008). Function of the N-terminus of zizimin1: autoinhibition and membrane targeting. *Biochem. J.*, **409**:525–33.

Michaelson, D., Silletti, J., Murphy, G., D'Eustachio, P., Rush, M. and Philips, M.R. (2001). Differential localization of Rho GTPases in live cells: regulation by hypervariable regions and RhoGDI binding. *J. Cell Biol.*, **152**:111–26.

Miesenböck, G., De Angelis, D.A. and Rothman, J.E. (1998). Visualizing secretion and synaptic transmission with pH-sensitive green fluorescent proteins. *Nature*, **394**:192–5.

Minoshima, Y., Kawashima, T., Hirose, K., Tonozuka, Y., Kawajiri, A., Bao, Y.C., Deng, X., Tatsuka, M., Narumiya, S., May, W.S., Nosaka, T., Semba, K., Inoue, T., Satoh, T., Inagaki, M. and Kitamura, T. (2003). Phosphorylation by aurora B converts MgcRacGAP to a RhoGAP during cytokinesis. *Dev. Cell*, **4**:549–60.

Mitin, N., Roberts, P.J., Chenette, E.J. and Der, C.J. (2012). Posttranslational lipid modification of Rho family small GTPases. *Methods Mol. Biol.*, **827**:87–95.

Miyamoto, Y., Torii, T., Yamamori, N., Ogata, T., Tanoue, A. and Yamauchi, J. (2013). Akt and PP2A reciprocally regulate the guanine nucleotide exchange factor Dock6 to control axon growth of sensory neurons. *Sci. Signal.*, **6**:ra15.

Moffat, J., Grueneberg, D.A., Yang, X., Kim, S.Y., Kloepfer, A.M., Hinkle, G., Piqani, B., Eisenhaure, T.M., Luo, B., Grenier, J.K., Carpenter, A.E., Foo, S.Y., Stewart, S.A., Stockwell, B.R., Hacohen, N., Hahn, W.C., Lander, E.S., Sabatini, D.M. and Root, D.E. (2006). A lentiviral RNAi library for human and mouse genes applied to an arrayed viral high-content screen. *Cell*, **124**:1283–98.

Moissoglu, K., Kiessling, V., Wan, C., Hoffman, B.D., Norambuena, A., Tamm, L.K. and Schwartz, M.A. (2014). Regulation of Rac1 translocation and activation by membrane domains and their boundaries. *J. Cell Sci.*, **127**:2565–76.

Moshfegh, Y., Bravo-Cordero, J.J., Miskolci, V., Condeelis, J. and Hodgson, L. (2014). A Trio-Rac1-Pak1 signalling axis drives invadopodia disassembly. *Nat. Cell Biol.*, **16**:571–585.

Mou, F., Praskova, M., Xia, F., Van Buren, D., Hock, H., Avruch, J. and Zhou, D. (2012). The Mst1 and Mst2 kinases control activation of rho family GTPases and thymic egress of mature thymocytes. *J. Exp. Med.*, **209**:741–59.

Mukaka, M.M. (2012). Statistics corner: A guide to appropriate use of correlation coefficient in medical research. *Malawi Med. J.*, **24**:69–71.

Munemitsu, S., Innis, M.A., Clark, R., McCormick, F., Ullrich, A. and Polakis, P. (1990). Molecular cloning and expression of a G25K cDNA, the human homolog of the yeast cell cycle gene CDC42. *Mol. Cell. Biol.*, **10**:5977–82.

Murphy, D.A. and Courtneidge, S.A. (2011). The 'ins' and 'outs' of podosomes and invadopodia: characteristics, formation and function. *Nat. Rev. Mol. Cell Biol.*, **12**:413–26.

Namekata, K., Kimura, A., Kawamura, K., Harada, C. and Harada, T. (2014). Dock GEFs and their therapeutic potential: neuroprotection and axon regeneration. *Prog. Retin. Eye Res.*, **43**:1–16.

Nimnual, A.S., Yatsula, B.A. and Bar-Sagi, D. (1998). Coupling of Ras and Rac guanosine triphosphatases through the Ras exchanger Sos. *Science*, **279**:560–3.

Nimnual, A.S., Taylor, L.J. and Bar-Sagi, D. (2003). Redox-dependent downregulation of Rho by Rac. *Nat. Cell Biol.*, **5**:236–41.

Nishimura, T., Yamaguchi, T., Tokunaga, A., Hara, A., Hamaguchi, T., Kato, K., Iwamatsu, A., Okano, H. and Kaibuchi, K. (2006). Role of numb in dendritic spine development with a Cdc42 GEF intersectin and EphB2. *Mol. Biol. Cell*, **17**:1273–85.

Nobes, C.D. and Hall, A. (1995). Rho, rac, and cdc42 GTPases regulate the assembly of multimolecular focal complexes associated with actin stress fibers, lamellipodia, and filopodia. *Cell*, **81**:53–62.

Nomanbhoy, T.K., Erickson, J.W. and Cerione, R.a. (1999). Kinetics of Cdc42 membrane extraction by Rho-GDI monitored by real-time fluorescence resonance energy transfer. *Biochemistry*, **38**:1744–50.

Ohta, Y., Hartwig, J.H. and Stossel, T.P. (2006). FilGAP, a Rho- and ROCK-regulated GAP for Rac binds filamin A to control actin remodelling. *Nat. Cell Biol.*, **8**:803–14.

Okabe, T., Nakamura, T., Nishimura, Y.N., Kohu, K., Ohwada, S., Morishita, Y. and Akiyama, T. (2003). RICS, a novel GTPase-activating protein for Cdc42 and Rac1, is involved in the beta-catenin-N-cadherin and N-methyl-D-aspartate receptor signaling. *J. Biol. Chem.*, **278**:9920–7.

Pai, S.Y., Kim, C. and Williams, D.A. (2010). Rac GTPases in human diseases. *Dis. Markers*, **29**:177–87.

Pan, Q., Shai, O., Lee, L.J., Frey, B.J. and Blencowe, B.J. (2008). Deep surveying of alternative splicing complexity in the human transcriptome by high-throughput sequencing. *Nat. Genet.*, **40**:1413–5.

Parker, J.A. and Mattos, C. (2015). The Ras-Membrane Interface: Isoform-specific Differences in The Catalytic Domain. *Mol. Cancer Res.*, **13**:595–603.

Paroutis, P., Touret, N. and Grinstein, S. (2004). The pH of the secretory pathway: measurement, determinants, and regulation. *Physiology (Bethesda).*, **19**:207–15.

Parsons, J.T., Horwitz, A.R. and Schwartz, M.A. (2010). Cell adhesion: integrating cytoskeletal dynamics and cellular tension. *Nat. Rev. Mol. Cell Biol.*, **11**:633–43.

Paul, F., Zauber, H., von Berg, L., Rocks, O., Daumke, O. and Selbach, M. (2017). Quantitative GTPase Affinity Purification Identifies Rho Family Protein Interaction Partners. *Mol. Cell. Proteomics*, **16**:73–85.

Pechstein, A., Shupliakov, O. and Haucke, V. (2010). Intersectin 1: a versatile actor in the synaptic vesicle cycle. *Biochem. Soc. Trans.*, **38**:181–6.

Pertz, O. (2010). Spatio-temporal Rho GTPase signaling - where are we now? *J. Cell Sci.*, **123**:1841–50.

Pertz, O., Hodgson, L., Klemke, R.L. and Hahn, K.M. (2006). Spatiotemporal dynamics of RhoA activity in migrating cells. *Nature*, **440**:1069–72.

Pietraszewska-Bogiel, A. and Gadella, T.W.J. (2011). FRET microscopy: from principle to routine technology in cell biology. *J. Microsc.*, **241**:111–8.

Platko, J.V., Leonard, D.A., Adra, C.N., Shaw, R.J., Cerione, R.A. and Lim, B. (1995). A single residue can modify target-binding affinity and activity of the functional domain of the Rho-subfamily GDP dissociation inhibitors. *Proc. Natl. Acad. Sci. U. S. A.*, **92**:2974–8.

Reid, T., Furuyashiki, T., Ishizaki, T., Watanabe, G., Watanabe, N., Fujisawa, K., Morii, N., Madaule, P. and Narumiya, S. (1996). Rhotekin, a new putative target for Rho bearing homology to a serine/threonine kinase, PKN, and rhophilin in the rho-binding domain. *J. Biol. Chem.*, **271**:13556–60.

Ren, X.D. and Schwartz, M.A. (2000). Determination of GTP loading on Rho. *Methods Enzymol.*, **325**:264–72.

Ren, X.D., Kiosses, W.B. and Schwartz, M.A. (1999). Regulation of the small GTP-binding protein Rho by cell adhesion and the cytoskeleton. *EMBO J.*, **18**:578–85.

Ridley, A.J. (2013). RhoA, RhoB and RhoC have different roles in cancer cell migration. *J. Microsc.*, **251**:242–9.

Ridley, A.J. and Hall, A. (1992). The small GTP-binding protein rho regulates the assembly of focal adhesions and actin stress fibers in response to growth factors. *Cell*, **70**:389–99.

Ridley, A.J., Paterson, H.F., Johnston, C.L., Diekmann, D. and Hall, A. (1992). The small GTP-binding protein rac regulates growth factor-induced membrane ruffling. *Cell*, **70**:401–10.

Ridley, A.J. (2011). Life at the leading edge. *Cell*, **145**:1012–22.

Ridley, A.J. (2015). Rho GTPase signalling in cell migration. *Curr. Opin. Cell Biol.*, **36**:103–112.

Rocks, O., Gerauer, M., Vartak, N., Koch, S., Huang, Z.P., Pechlivanis, M., Kuhlmann, J., Brunsveld, L., Chandra, A., Ellinger, B., Waldmann, H. and Bastiaens, P.I.H. (2010). The palmitoylation machinery is a spatially organizing system for peripheral membrane proteins. *Cell*, **141**:458–71.

Rocks, O., Peyker, A. and Bastiaens, P.I.H. (2006). Spatio-temporal segregation of Ras signals: one ship, three anchors, many harbors. *Curr. Opin. Cell Biol.*, **18**:351–7.

Rocks, O., Peyker, A., Kahms, M., Verveer, P.J., Koerner, C., Lumbierres, M., Kuhlmann, J., Waldmann, H., Wittinghofer, A. and Bastiaens, P.I.H. (2005). An acylation cycle regulates localization and activity of palmitoylated Ras isoforms. *Science*, **307**:1746–52.

Ron, D., Graziani, G., Aaronson, S.A. and Eva, A. (1989). The N-terminal region of proto-dbl down regulates its transforming activity. *Oncogene*, **4**:1067–72.

Rosenberger, G. and Kutsche, K. (2006). AlphaPIX and betaPIX and their role in focal adhesion formation. *Eur. J. Cell Biol.*, **85**:265–74.

Rossier, O., Octeau, V., Sibarita, J.B., Leduc, C., Tessier, B., Nair, D., Gatterdam, V., Destaing, O., Albigès-Rizo, C., Tampé, R., Cognet, L., Choquet, D., Lounis, B. and Giannone, G. (2012). Integrins $\beta 1$ and $\beta 3$ exhibit distinct dynamic nanoscale organizations inside focal adhesions. *Nat. Cell Biol.*, **14**:1057–67.

Rossman, K.L., Der, C.J. and Sondek, J. (2005). GEF means go: turning on RHO GTPases with guanine nucleotide-exchange factors. *Nat. Rev. Mol. Cell Biol.*, **6**:167–80.

Rowland, A.F., Larance, M., Hughes, W.E. and James, D.E. (2011). Identification of RhoGAP22 as an Akt-dependent regulator of cell motility in response to insulin. *Mol. Cell. Biol.*, **31**:4789–800.

Roy, M.O., Leventis, R. and Silvius, J.R. (2000). Mutational and biochemical analysis of plasma membrane targeting mediated by the farnesylated, polybasic carboxy terminus of K-ras4B. *Biochemistry*, **39**:8298–307.

Rümenapp, U., Freichel-Blomquist, A., Wittinghofer, B., Jakobs, K.H. and Wieland, T. (2002). A mammalian Rho-specific guanine-nucleotide exchange factor (p164-RhoGEF) without a pleckstrin homology domain. *Biochem. J.*, **366**:721–8.

Runne, C. and Chen, S. (2013*a*). PLEKHG2 promotes heterotrimeric G protein $\beta\gamma$-stimulated lymphocyte migration via Rac and Cdc42 activation and actin polymerization. *Mol. Cell. Biol.*, **33**:4294–307.

Runne, C. and Chen, S. (2013*b*). PLEKHG2 promotes heterotrimeric G protein $\beta\gamma$-stimulated lymphocyte migration via Rac and Cdc42 activation and actin polymerization. *Mol. Cell. Biol.*, **33**:4294–307.

Sander, E.E., ten Klooster, J.P., van Delft, S., van der Kammen, R.A. and Collard, J.G. (1999). Rac downregulates Rho activity: reciprocal balance between both GTPases determines cellular morphology and migratory behavior. *J. Cell Biol.*, **147**:1009–22.

Sanz-Moreno, V., Gadea, G., Ahn, J., Paterson, H., Marra, P., Pinner, S., Sahai, E. and Marshall, C.J. (2008). Rac activation and inactivation control plasticity of tumor cell movement. *Cell*, **135**:510–23.

Schmick, M., Vartak, N., Papke, B., Kovacevic, M., Truxius, D.C., Rossmannek, L. and Bastiaens, P.I.H. (2014). KRas Localizes to the Plasma Membrane by Spatial Cycles of Solubilization, Trapping and Vesicular Transport. *Cell*, **157**:459–71.

Schmidt, A. and Hall, A. (2002). Guanine nucleotide exchange factors for Rho GTPases: turning on the switch. *Genes Dev.*, **16**:1587–1609.

Schwanhäusser, B., Busse, D., Li, N., Dittmar, G., Schuchhardt, J., Wolf, J., Chen, W. and Selbach, M. (2011). Global quantification of mammalian gene expression control. *Nature*, **473**:337–42.

Self, A.J. and Hall, A. (1995). Measurement of intrinsic nucleotide exchange and GTP hydrolysis rates. *Methods Enzymol.*, **256**:67–76.

Shaner, N.C., Campbell, R.E., Steinbach, P.a., Giepmans, B.N.G., Palmer, A.E. and Tsien, R.Y. (2004). Improved monomeric red, orange and yellow fluorescent proteins derived from Discosoma sp. red fluorescent protein. *Nat. Biotechnol.*, **22**:1567–72.

Shang, X., Zhou, Y.T. and Low, B.C. (2003). Concerted regulation of cell dynamics by BNIP-2 and Cdc42GAP homology/Sec14p-like, proline-rich, and GTPase-activating protein domains of a novel Rho GTPase-activating protein, BPGAP1. *J. Biol. Chem.*, **278**:45903–14.

Sharma, P., Varma, R., Sarasij, R.C., Ira, Gousset, K., Krishnamoorthy, G., Rao, M. and Mayor, S. (2004). Nanoscale organization of multiple GPI-anchored proteins in living cell membranes. *Cell*, **116**:577–89.

Shibata, A.C.E., Fujiwara, T.K., Chen, L., Suzuki, K.G.N., Ishikawa, Y., Nemoto, Y.L., Miwa, Y., Kalay, Z., Chadda, R., Naruse, K. and Kusumi, A. (2012). Archipelago architecture of the focal adhesion: membrane molecules freely enter and exit from the focal adhesion zone. *Cytoskeleton (Hoboken).*, **69**:380–92.

Shibata, A.C.E., Chen, L.H., Nagai, R., Ishidate, F., Chadda, R., Miwa, Y., Naruse, K., Shirai, Y.M., Fujiwara, T.K. and Kusumi, A. (2013). Rac1 recruitment to the archipelago structure of the focal adhesion through the fluid membrane as revealed by single-molecule analysis. *Cytoskeleton (Hoboken).*, **70**:161–77.

Shibata, S., Nagase, M., Yoshida, S., Kawarazaki, W., Kurihara, H., Tanaka, H., Miyoshi, J., Takai, Y. and Fujita, T. (2008). Modification of mineralocorticoid receptor function by Rac1 GTPase: implication in proteinuric kidney disease. *Nat. Med.*, **14**:1370–6.

Sivars, U., Aivazian, D. and Pfeffer, S.R. (2003). Yip3 catalyses the dissociation of endosomal Rab-GDI complexes. *Nature*, **425**:856–9.

Slaughter, B.D., Das, A., Schwartz, J.W., Rubinstein, B. and Li, R. (2009). Dual modes of cdc42 recycling fine-tune polarized morphogenesis. *Dev. Cell*, **17**:823–35.

Snyder, J.T., Worthylake, D.K., Rossman, K.L., Betts, L., Pruitt, W.M., Siderovski, D.P., Der, C.J. and Sondek, J. (2002). Structural basis for the selective activation of Rho GTPases by Dbl exchange factors. *Nat. Struct. Biol.*, **9**:468–75.

Southgate, L., Machado, R.D., Snape, K.M., Primeau, M., Dafou, D., Ruddy, D.M., Branney, P.a., Fisher, M., Lee, G.J., Simpson, M.a., He, Y., Bradshaw, T.Y., Blaumeiser, B., Winship, W.S., Reardon, W., Maher, E.R., FitzPatrick, D.R., Wuyts, W., Zenker, M., Lamarche-Vane, N. and Trembath, R.C. (2011). Gain-of-function mutations of ARHGAP31, a Cdc42/Rac1 GTPase regulator, cause syndromic cutis aplasia and limb anomalies. *Am. J. Hum. Genet.*, **88**:574–85.

Spiering, D. and Hodgson, L. (2011). Dynamics of the Rho-family small GTPases in actin regulation and motility. *Cell Adh. Migr.*, **5**:170–80.

Stankiewicz, T.R. and Linseman, D.A. (2014). Rho family GTPases: key players in neuronal development, neuronal survival, and neurodegeneration. *Front. Cell. Neurosci.*, **8**:314.

Stastna, M. and Van Eyk, J.E. (2012). Analysis of protein isoforms: can we do it better? *Proteomics*, **12**:2937–48.

Sternberg, N., Hamilton, D., Austin, S., Yarmolinsky, M. and Hoess, R. (1981). Site-specific recombination and its role in the life cycle of bacteriophage P1. *Cold Spring Harb. Symp. Quant. Biol.*, **45 Pt 1**:297–309.

Sun, X., Zhang, A., Baker, B., Sun, L., Howard, A., Buswell, J., Maurel, D., Masharina, A., Johnsson, K., Noren, C.J., Xu, M.Q. and Corrêa, I.R. (2011). Development of SNAP-tag fluorogenic probes for wash-free fluorescence imaging. *Chembiochem*, **12**:2217–26.

Takahashi, K., Sasaki, T., Mammoto, A., Takaishi, K., Kameyama, T., Tsukita, S. and Takai, Y. (1997). Direct interaction of the Rho GDP dissociation inhibitor with ezrin/radixin/moesin initiates the activation of the Rho small G protein. *J. Biol. Chem.*, **272**:23371–5.

Takai, Y., Sasaki, T. and Matozaki, T. (2001). Small GTP-binding proteins. *Physiol. Rev.*, **81**:153–208.

Tcherkezian, J. and Lamarche-Vane, N. (2007). Current knowledge of the large RhoGAP family of proteins. *Biol. Cell*, **99**:67–86.

Thompson, G., Owen, D., Chalk, P.A. and Lowe, P.N. (1998). Delineation of the Cdc42/Rac-binding domain of p21-activated kinase. *Biochemistry*, **37**:7885–91.

Tinevez, J.Y., Perry, N., Schindelin, J., Hoopes, G.M., Reynolds, G.D., Laplantine, E., Bednarek, S.Y., Shorte, S.L. and Eliceiri, K.W. (2017). TrackMate: An open and extensible platform for single-particle tracking. *Methods*, **115**:80–90.

Tkachenko, E., Sabouri-Ghomi, M., Pertz, O., Kim, C., Gutierrez, E., Machacek, M., Groisman, A., Danuser, G. and Ginsberg, M.H. (2011). Protein kinase A governs a RhoA-RhoGDI protrusion-retraction pacemaker in migrating cells. *Nat. Cell Biol.*, **13**:660–7.

Tnimov, Z., Guo, Z., Gambin, Y., Nguyen, T.T., Wu, Y.W., Abankwa, D., Stigter, A., Collins, B., Waldmann, H., Goody, R.S. and Alexandrov, K. (2012). Quantitative analysis of prenylated RhoA interaction with its chaperone, RhoGDI. *J. Biol. Chem.*, pages 1–25.

Togawa, A., Miyoshi, J., Ishizaki, H., Tanaka, M., Takakura, A., Nishioka, H., Yoshida, H., Doi, T., Mizoguchi, A., Matsuura, N., Niho, Y., Nishimune, Y., Nishikawa, S.i. and Takai, Y. (1999). Progressive impairment of kidneys and reproductive organs in mice lacking Rho GDIalpha. *Oncogene*, **18**:5373–80.

Tomar, A., Lim, S.T., Lim, Y. and Schlaepfer, D.D. (2009). A FAK-p120RasGAP-p190RhoGAP complex regulates polarity in migrating cells. *J. Cell Sci.*, **122**:1852–62.

Toret, C.P., Collins, C. and Nelson, W.J. (2014). An Elmo-Dock complex locally controls Rho GTPases and actin remodeling during cadherin-mediated adhesion. *J. Cell Biol.*, **207**:577–87.

Toseland, C.P. (2013). Fluorescent labeling and modification of proteins. *J. Chem. Biol.*, **6**:85–95.

Touré, A., Dorseuil, O., Morin, L., Timmons, P., Jégou, B., Reibel, L. and Gacon, G. (1998). MgcRacGAP, a new human GTPase-activating protein for Rac and Cdc42 similar to Drosophila rotundRacGAP gene product, is expressed in male germ cells. *J. Biol. Chem.*, **273**:6019–23.

Tsyba, L., Nikolaienko, O., Dergai, O., Dergai, M., Novokhatska, O., Skrypkina, I. and Rynditch, A. (2011). Intersectin multidomain adaptor proteins: regulation of functional diversity. *Gene*, **473**:67–75.

Turing, A.M. (1952). The chemical basis of morphogenesis. 1953. *Philos. Trans. R. Soc. Lond. B. Biol. Sci.*, **237**:37–72.

Ueda, H., Nagae, R., Kozawa, M., Morishita, R., Kimura, S., Nagase, T., Ohara, O., Yoshida, S. and Asano, T. (2008). Heterotrimeric G protein betagamma subunits stimulate FLJ00018, a guanine nucleotide exchange factor for Rac1 and Cdc42. *J. Biol. Chem.*, **283**:1946–53.

Ueda, T., Kikuchi, A., Ohga, N., Yamamoto, J. and Takai, Y. (1990). Purification and characterization from bovine brain cytosol of a novel regulatory protein inhibiting the dissociation of GDP from and the subsequent binding of GTP to rhoB p20, a ras p21-like GTP-binding protein. *J. Biol. Chem.*, **265**:9373–80.

Ugolev, Y., Berdichevsky, Y., Weinbaum, C. and Pick, E. (2008). Dissociation of Rac1(GDP).RhoGDI complexes by the cooperative action of anionic liposomes containing phosphatidylinositol 3,4,5-trisphosphate, Rac guanine nucleotide exchange factor, and GTP. *J. Biol. Chem.*, **283**:22257–22271.

van Unen, J., Reinhard, N.R., Yin, T., Wu, Y.I., Postma, M., Gadella, T.W.J. and Goedhart, J. (2015). Plasma membrane restricted RhoGEF activity is sufficient for RhoA-mediated actin polymerization. *Sci. Rep.*, **5**:14693.

Vega, F.M., Fruhwirth, G., Ng, T. and Ridley, A.J. (2011). RhoA and RhoC have distinct roles in migration and invasion by acting through different targets. *J. Cell Biol.*, **193**:655–65.

Vega, F.M. and Ridley, A.J. (2008). Rho GTPases in cancer cell biology. *FEBS Lett.*, **582**:2093–101.

Vetter, I.R. and Wittinghofer, A. (2001). The guanine nucleotide-binding switch in three dimensions. *Science*, **294**:1299–304.

Vetter, I.R. (2014). The Structure of the G Domain of the Ras Superfamily. In Ras Superfamily Small G Proteins Biol. Mech. 1, pages 25–50. Springer Vienna, Vienna. ISBN 978-3-7091-1805-4.

Walzl, A., Kramer, N., Mazza, G., Rosner, M., Falkenhagen, D. and Hengstschläger, M. (2012). A Simple and Cost Efficient Method to Avoid Unequal Evaporation in Cellular Screening Assays , Which Restores Cellular Metabolic Activity. *Int. J. Appl. Sci. Technol.*, **2**:17–22.

Wang, G.S. and Cooper, T.A. (2007). Splicing in disease: disruption of the splicing code and the decoding machinery. *Nat. Rev. Genet.*, **8**:749–61.

Wang, J. and Richards, D.A. (2012). Segregation of PIP2 and PIP3 into distinct nanoscale regions within the plasma membrane. *Biol. Open*, **1**:857–62.

Wang, S., Watanabe, T., Matsuzawa, K., Katsumi, A., Kakeno, M., Matsui, T., Ye, F., Sato, K., Murase, K., Sugiyama, I., Kimura, K., Mizoguchi, A., Ginsberg, M.H., Collard, J.G. and Kaibuchi, K. (2012). Tiam1 interaction with the PAR complex promotes talin-mediated Rac1 activation during polarized cell migration. *J. Cell Biol.*, **199**:331–45.

Weber, G.F., Bjerke, M.A. and DeSimone, D.W. (2011). Integrins and cadherins join forces to form adhesive networks. *J. Cell Sci.*, **124**:1183–93.

Wehrle-Haller, B. and Imhof, B.a. (2003). Actin, microtubules and focal adhesion dynamics during cell migration. *Int. J. Biochem. Cell Biol.*, **35**:39–50.

Weidenfeld, I., Gossen, M., Löw, R., Kentner, D., Berger, S., Görlich, D., Bartsch, D., Bujard, H. and Schönig, K. (2009). Inducible expression of coding and inhibitory RNAs from retargetable genomic loci. *Nucleic Acids Res.*, **37**:e50.

Welch, H.C.E., Coadwell, W.J., Ellson, C.D., Ferguson, G.J., Andrews, S.R., Erdjument-Bromage, H., Tempst, P., Hawkins, P.T. and Stephens, L.R. (2002*a*). P-Rex1, a PtdIns(3,4,5)P3- and Gbetagamma-regulated guanine-nucleotide exchange factor for Rac. *Cell*, **108**:809–21.

Welch, H.C.E., Coadwell, W.J., Ellson, C.D., Ferguson, G.J., Andrews, S.R., Erdjument-Bromage, H., Tempst, P., Hawkins, P.T. and Stephens, L.R. (2002*b*). P-Rex1, a PtdIns(3,4,5)P3- and Gbetagamma-regulated guanine-nucleotide exchange factor for Rac. *Cell*, **108**:809–21.

Wennerberg, K. and Der, C.J. (2004). Rho-family GTPases: it's not only Rac and Rho (and I like it). *J. Cell Sci.*, **117**:1301–12.

Wentzel, C., Sommer, J.E., Nair, R., Stiefvater, A., Sibarita, J.B. and Scheiffele, P. (2013). mSYD1A, a mammalian synapse-defective-1 protein, regulates synaptogenic signaling and vesicle docking. *Neuron*, **78**:1012–23.

Wiborg, O., Pedersen, M.S., Wind, A., Berglund, L.E., Marcker, K.A. and Vuust, J. (1985). The human ubiquitin multigene family: some genes contain multiple directly repeated ubiquitin coding sequences. *EMBO J.*, **4**:755–9.

Winograd-Katz, S.E., Fässler, R., Geiger, B. and Legate, K.R. (2014). The integrin adhesome: from genes and proteins to human disease. *Nat. Rev. Mol. Cell Biol.*, **15**:273–88.

Worthylake, D.K., Rossman, K.L. and Sondek, J. (2000). Crystal structure of Rac1 in complex with the guanine nucleotide exchange region of Tiam1. *Nature*, **408**:682–8.

Wright, L.P. and Philips, M.R. (2006). Thematic review series: lipid posttranslational modifications. CAAX modification and membrane targeting of Ras. *J. Lipid Res.*, **47**:883–91.

Wu, D., Asiedu, M. and Wei, Q. (2009). Myosin-interacting guanine exchange factor (MyoGEF) regulates the invasion activity of MDA-MB-231 breast cancer cells through activation of RhoA and RhoC. *Oncogene*, **28**:2219–30.

Xu, X., Han, L., Zhao, G., Xue, S., Gao, Y., Xiao, J., Zhang, S., Chen, P., Wu, Z.Y., Ding, J., Hu, R., Wei, B. and Wang, H. (2017). LRCH1 interferes with DOCK8-Cdc42-induced T cell migration and ameliorates experimental autoimmune encephalomyelitis. *J. Exp. Med.*, **214**:209–226.

Yamashita, T. and Tohyama, M. (2003). The p75 receptor acts as a displacement factor that releases Rho from Rho-GDI. *Nat. Neurosci.*, **6**:461–7.

Yang, H.W., Collins, S.R. and Meyer, T. (2016). Locally excitable Cdc42 signals steer cells during chemotaxis. *Nat. Cell Biol.*, **18**:191–201.

Yeung, T., Gilbert, G.E., Shi, J., Silvius, J., Kapus, A. and Grinstein, S. (2008). Membrane phosphatidylserine regulates surface charge and protein localization. *Science*, **319**:210–213.

Yohe, M.E., Rossman, K.L., Gardner, O.S., Karnoub, A.E., Snyder, J.T., Gershburg, S., Graves, L.M., Der, C.J. and Sondek, J. (2007). Auto-inhibition of the Dbl family protein Tim by an N-terminal helical motif. *J. Biol. Chem.*, **282**:13813–23.

Yokoe, H. and Meyer, T. (1996). Spatial dynamics of GFP-tagged proteins investigated by local fluorescence enhancement. *Nat. Biotechnol.*, **14**:1252–6.

Yoon, H.Y., Miura, K., Cuthbert, E.J., Davis, K.K., Ahvazi, B., Casanova, J.E. and Randazzo, P.A. (2006). ARAP2 effects on the actin cytoskeleton are dependent on Arf6-specific GTPase-activating-protein activity and binding to RhoA-GTP. *J. Cell Sci.*, **119**:4650–66.

Yoshida, S., Hoppe, A.D., Araki, N. and Swanson, J.A. (2009). Sequential signaling in plasma-membrane domains during macropinosome formation in macrophages. *J. Cell Sci.*, **122**:3250–61.

Yoshizaki, H., Ohba, Y., Kurokawa, K., Itoh, R.E., Nakamura, T., Mochizuki, N., Nagashima, K. and Matsuda, M. (2003). Activity of Rho-family GTPases during cell division as visualized with FRET-based probes. *J. Cell Biol.*, **162**:223–32.

Yu, B., Martins, I.R.S., Li, P., Amarasinghe, G.K., Umetani, J., Fernandez-Zapico, M.E., Billadeau, D.D., Machius, M., Tomchick, D.R. and Rosen, M.K. (2010). Structural and energetic mechanisms of cooperative autoinhibition and activation of Vav1. *Cell*, **140**:246–56.

Zacharias, D.a., Violin, J.D., Newton, A.C. and Tsien, R.Y. (2002). Partitioning of lipid-modified monomeric GFPs into membrane microdomains of live cells. *Science*, **296**:913–6.

Zaidel-Bar, R. and Geiger, B. (2010). The switchable integrin adhesome. *J. Cell Sci.*, **123**:1385–8.

Zaidel-Bar, R., Itzkovitz, S., Ma'ayan, A., Iyengar, R. and Geiger, B. (2007). Functional atlas of the integrin adhesome. *Nat. Cell Biol.*, **9**:858–67.

Zamanian, J.L. and Kelly, R.B. (2003). Intersectin 1L guanine nucleotide exchange activity is regulated by adjacent src homology 3 domains that are also involved in endocytosis. *Mol. Biol. Cell*, **14**:1624–37.

Zawistowski, J.S., Sabouri-Ghomi, M., Danuser, G., Hahn, K.M. and Hodgson, L. (2013). A RhoC biosensor reveals differences in the activation kinetics of RhoA and RhoC in migrating cells. *PLoS One*, **8**:1–9.

Zhang, B., Chernoff, J. and Zheng, Y. (1998). Interaction of Rac1 with GTPase-activating proteins and putative effectors. A comparison with Cdc42 and RhoA. *J. Biol. Chem.*, **273**:8776–82.

Zhang, Y., Sawada, T., Jing, X., Yokote, H., Yan, X. and Sakaguchi, K. (2007). Regulation of ephexin1, a guanine nucleotide exchange factor of Rho family GTPases, by fibroblast growth factor receptor-mediated tyrosine phosphorylation. *J. Biol. Chem.*, **282**:31103–12.

Zhang, Y., Sukthankar, P., Tomich, J.M. and Conrad, G.W. (2012). Effect of the synthetic NC-1059 peptide on diffusion of riboflavin across an intact corneal epithelium. *Invest. Ophthalmol. Vis. Sci.*, **53**:2620–9.

Zhao, C., Ma, H., Bossy-Wetzel, E., Lipton, S.A., Zhang, Z. and Feng, G.S. (2003). GC-GAP, a Rho family GTPase-activating protein that interacts with signaling adapters Gab1 and Gab2. *J. Biol. Chem.*, **278**:34641–53.

Zheng, Y., Hart, M.J. and Cerione, R.A. (1995). Guanine nucleotide exchange catalyzed by dbl oncogene product. *Methods Enzymol.*, **256**:77–84.

Zhou, Y., Prakash, P., Liang, H., Cho, K.J., Gorfe, A.A. and Hancock, J.F. (2017). Lipid-Sorting Specificity Encoded in K-Ras Membrane Anchor Regulates Signal Output. *Cell*, **168**:239–251.e16.

Zhu, B., Cai, G., Hall, E.O. and Freeman, G.J. (2007). In-fusion assembly: seamless engineering of multidomain fusion proteins, modular vectors, and mutations. *Biotechniques*, **43**:354–9.

Appendix

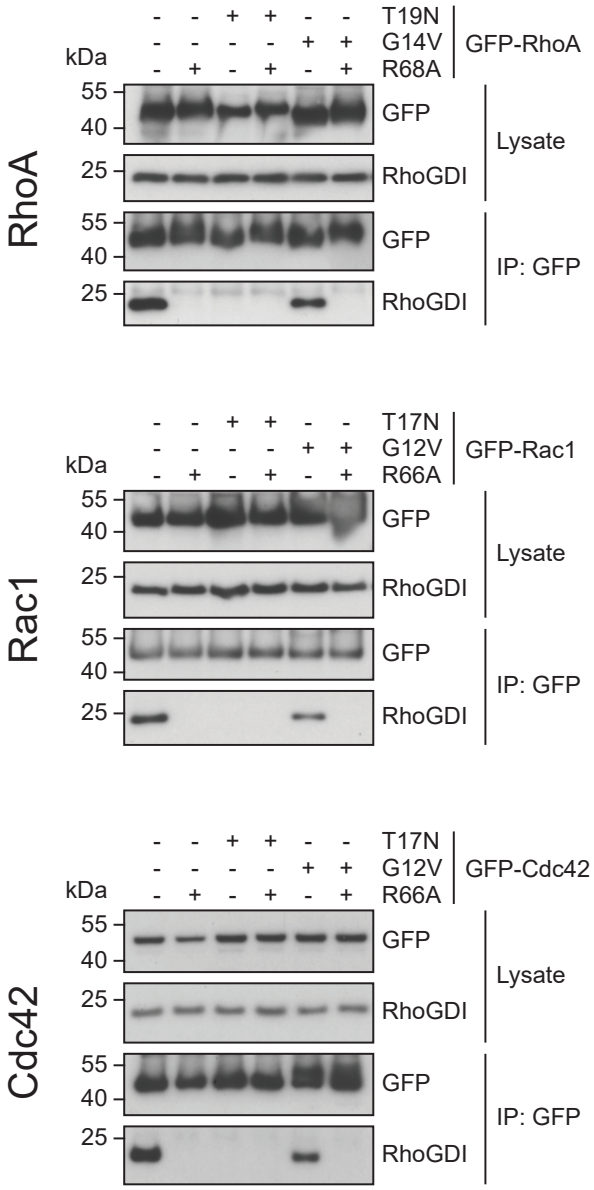

Figure 7.1 Point mutations on Rho GTPases abolish the interaction with RhoGDI. HEK293T cells were transfected with mEGFP-RhoA, mEGFP-Rac1, and mEGFP-Cdc42 containing combinations of dominant negative (T17N or T19N), constitutively active (G12v or G14V) and RhoGDI-binding deficient mutations (R66A or R68A). Lysates were immunoprecipitated using a anti-GFP antibody, and immunoblotted with anti-GFP or anti-RhoGDI antibodies.

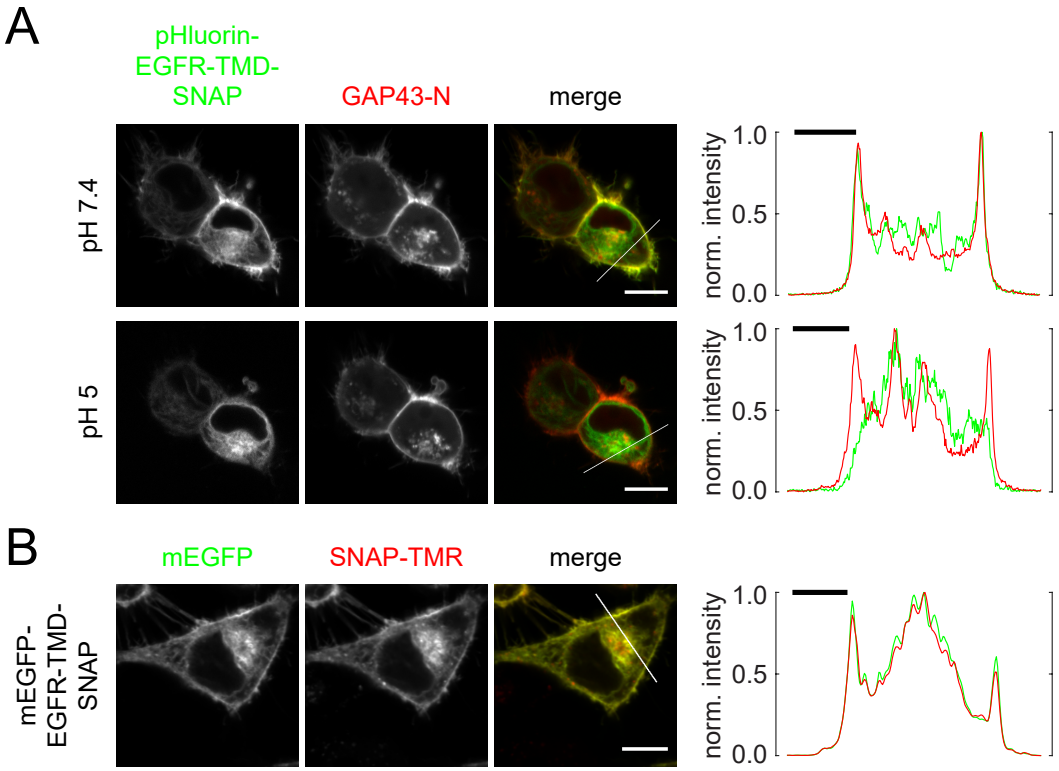

Figure 7.2 The "artificial receptor" localises at the plasma membrane. (**A**) HeLa cells were transfected with unlabelled e-pHluorin-EGFR-TMD-SNAP and an N-terminal truncation of GAP43 fused to mCherry as a marker for plasma membrane and Golgi complex (GAP43-N) (Rocks *et al.*, 2005). 16 h post transfection images were collected by live cell confocal microscopy at physiologic pH 7.4 and at acidified pH 5. Line scan fluorescence intensity profiles on the right show normalised intensities across the white lines in the merged images. White scale bars in images: 10 μm. Black scale bars in graphs: 5 μm. (**B**) HeLa Tet-On cells were transfected with mEGFP-EGFR-TMD-SNAP and expression was induced with 300 ng/ml doxycyclin. 16 h post transfection cells were labelled with 0.1 μM SNAP-Cell TMR-Star for 1 h and images were were collected by live cell confocal microscopy. Line scan fluorescence intensity profile on the right show normalised intensities across the white line in the merged image. White scale bar in image: 10 μm. Black scale bar in graph: 5 μm.

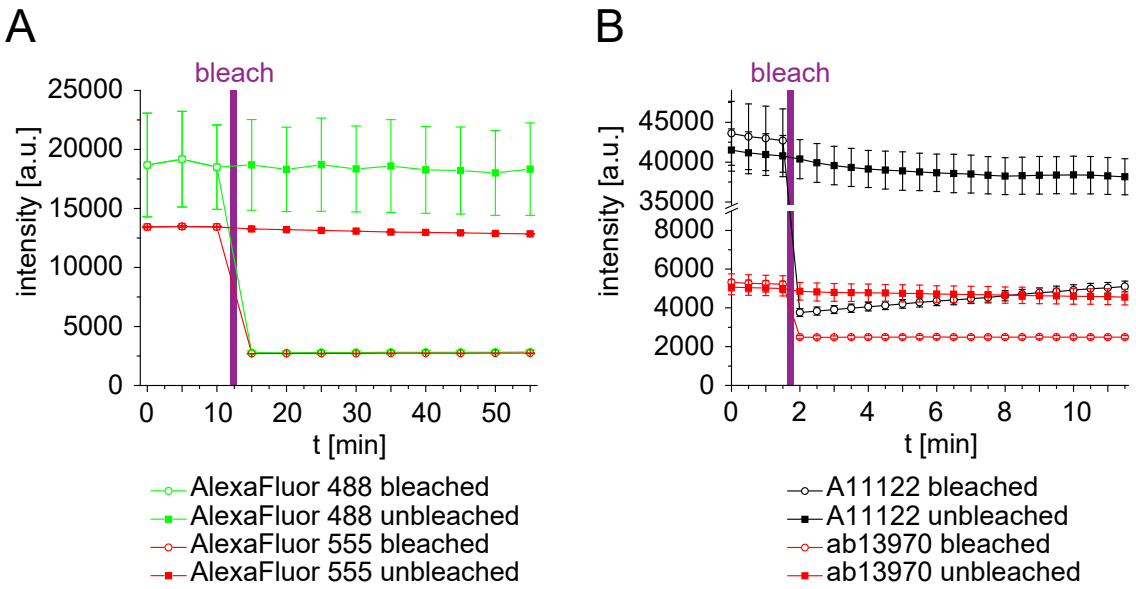

Figure 7.3 Antibody immobilisation and antibody-mediated GFP immobilisation on epoxysilan-coated glass slides is stable. (**A**) Epoxysilan-coated glass slides were loaded with 20 μg/ml goat anti-rabbit IgG labelled with AlexaFluor 555 or AlexaFluor 488 for 1 h at RT and blocked with 1 % BSA for 1 h at RT. Glass slides were mounted in a microscopic mounting chamber and antibody immobilisation was observed by FRAP experiments comparing fluorescence intensity of a bleached with an unbleached region by TIRF microscopic time-lapse imaging. (**B**) Epoxysilan-coated glass slides were loaded with two different anti-GFP antibodies (20 μg/ml A11122 (Thermo Fisher Scientific) and 20 μg/ml ab13970 (abcam)) for 1 h at RT and afterwards blocked with 1 % BSA for 1 h at RT. Antibodies on glass slides were then decorated with mEGFP from HEK293T cell lysate for for 1 h at RT. Glass slides were mounted in a microscopic mounting chamber and mEGFP immobilisation was observed by epifluorescence intensity time-lapse imaging (unbleached) and FRAP experiments (bleached). Data for two more antibodies not shown.

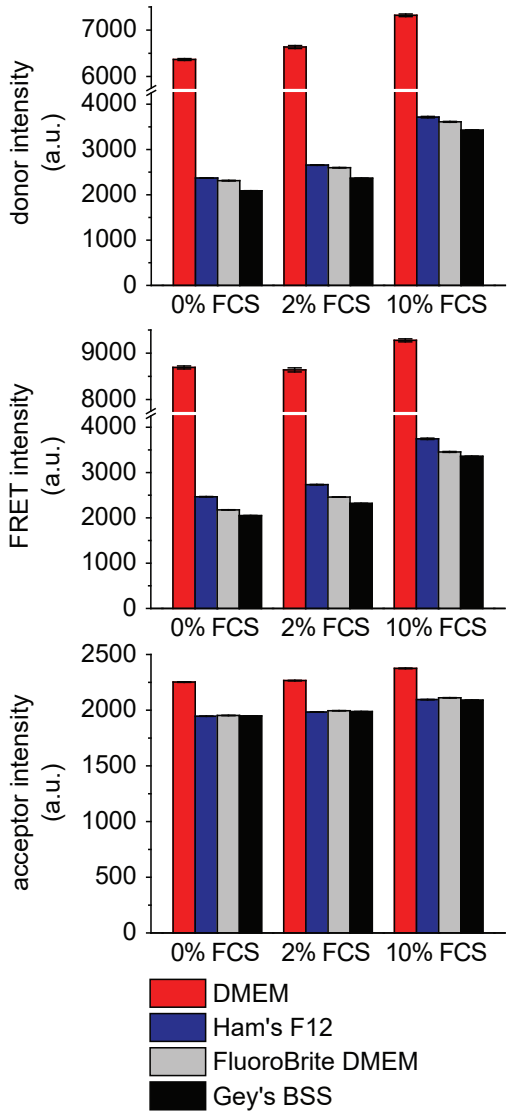

Figure 7.4 Background signal of different cell culture media. Untransfected HEK293T cells were incubated in different Phenol Red free media (DMEM, Ham's F12, FluoroBrite DMEM and Gey's balanced salt solution) with 0 %, 2 %, and 10 % FCS. Background intensity levels were microscopically measured in donor, FRET, and acceptor channel. Graphs show average of ten fields of view, error bars indicate standard deviation.

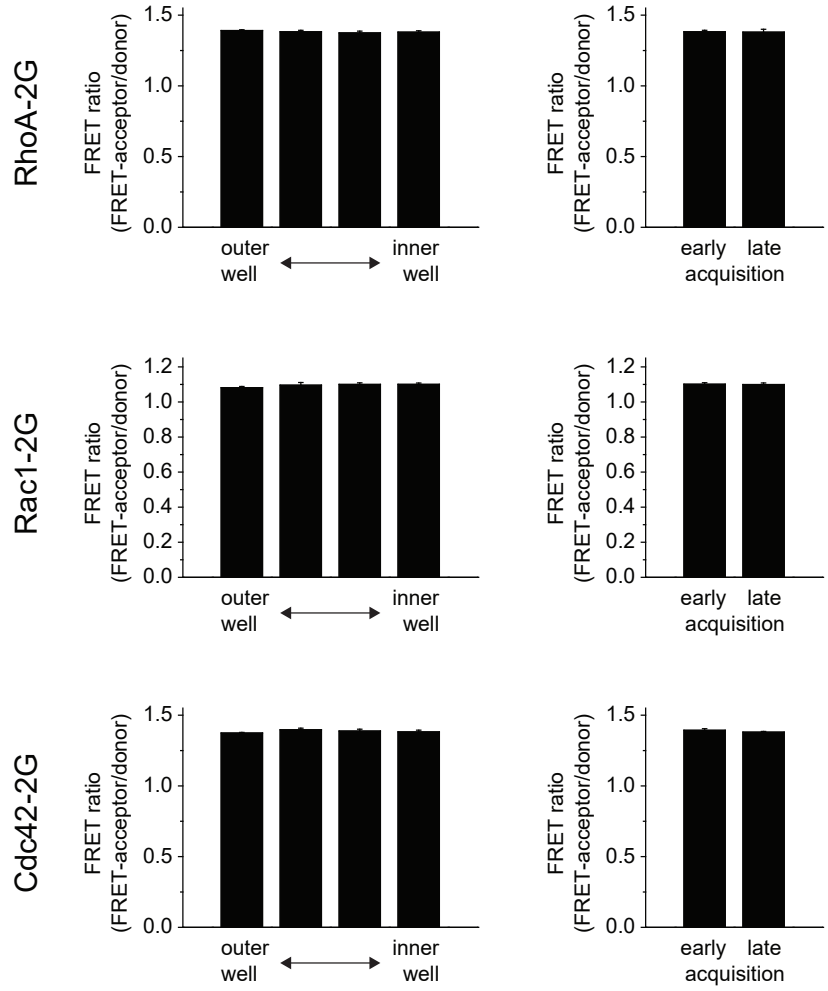

Figure 7.5 FRET ratio of sensors is highly consistent throughout 96 well plates. HEK293T cells were transfected with RhoA-2G, Rac1-2G, and Cdc42-2G FRET sensors. FRET-ratio was measured across four wells from outer to inner positions on a 96 well plate (left panels). FRET ratios recorded at the beginning of the measurement (early) were compared to those recorded at the end of a measurement (late) of a 96 well plate with a time interval of 45-90 min (right panels). FRET ratio was calculated as FRET-acceptor channel intensity divided by donor channel intensity. Graphs show average of five fields of view, error bars indicate standard deviation.

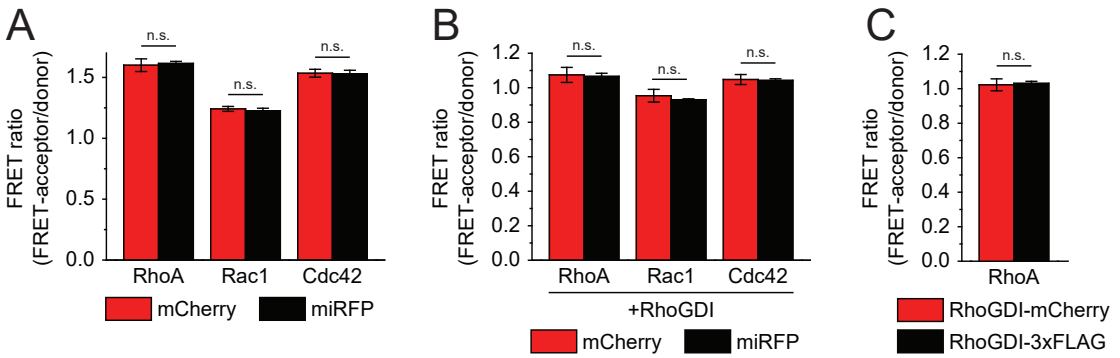

Figure 7.6 mCherry does not interfere with mTFP1 to mVenus FRET measurement. HEK293T cells were transfected with RhoA-2G, Rac1-2G, and Cdc42-2G FRET sensors as indicated together with excess mCherry or miRFP670 in the absence (**A**) or in the presence (**B**) of RhoGDI. (**C**) RhoA FRET sensor was expressed in HEK293T cells together with either mCherry-labelled RhoGDI or with triple-FLAG-labelled RhoGDI. Sensitised FRET ratio was calculated from microscopic images. FRET ratio was calculated as FRET-acceptor channel intensity divided by donor channel intensity. Graphs show average of five fields of view (A+B) or average of four different wells with five fields of view each (C) , error bars indicate standard deviation. Significance levels were calculated by unpaired t-test as indicated by lines: n.s.=not significant.

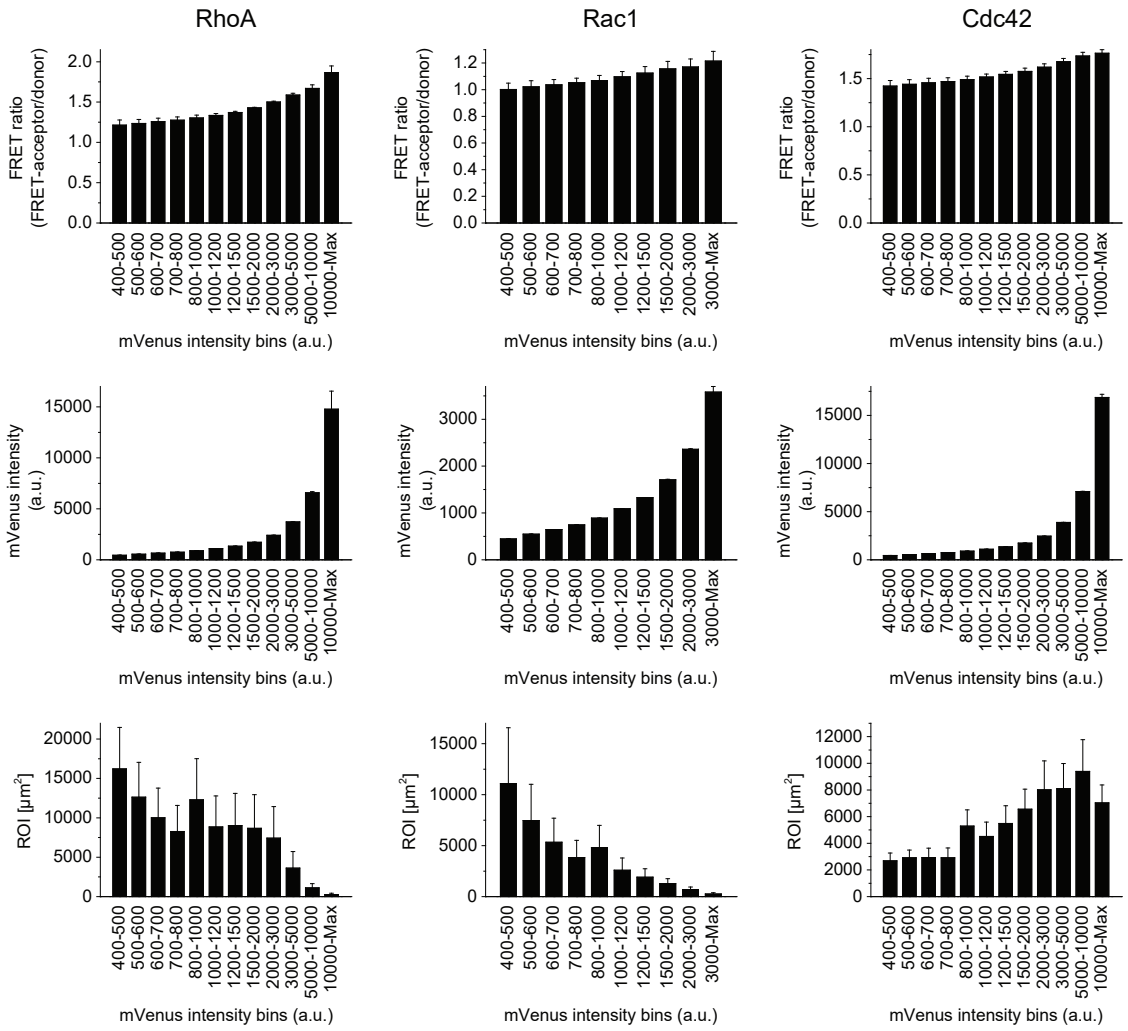

Figure 7.7 Regions of high FRET sensor expression show higher FRET ratio. HEK293T cells were transfected with RhoA-2G, Rac1-2G and Cdc42-2G FRET sensors. FRET ratio, mVenus intensity and area were measured in regions of interest defined by mVenus intensity bins as indicated. FRET ratio was calculated as FRET channel intensity divided by donor channel intensity. Graphs show average of three different wells, error bars indicate standard deviation.

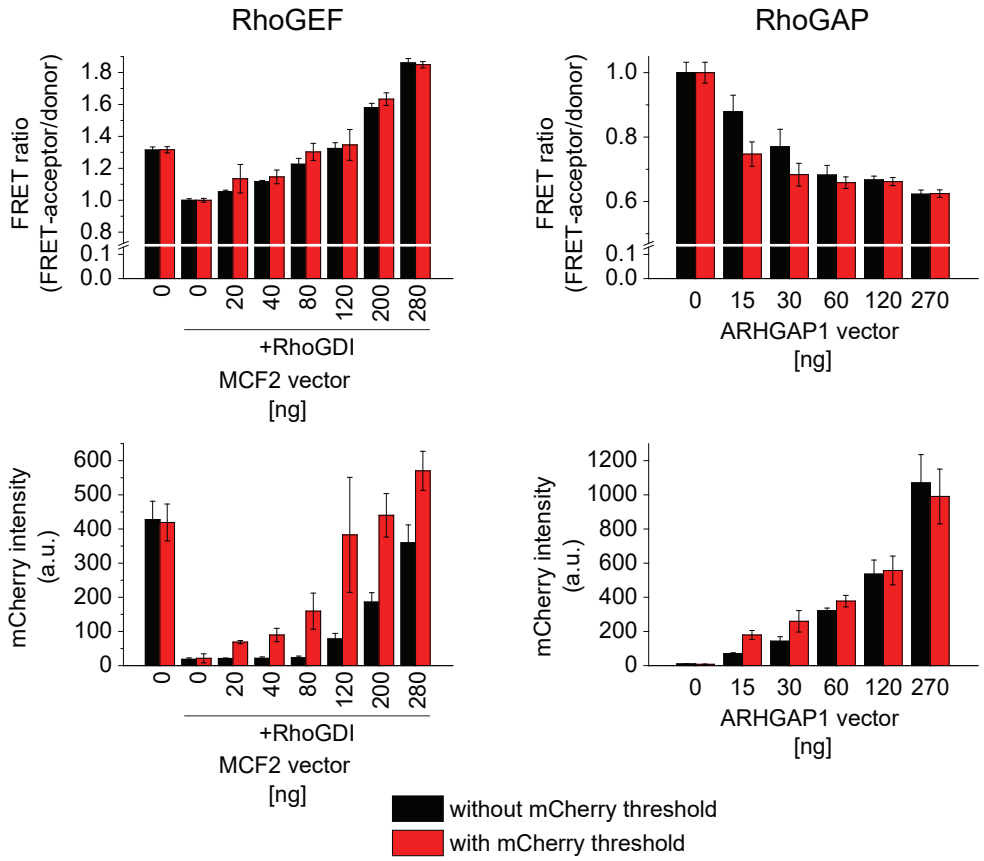

Figure 7.8 Selection of RhoGEF and RhoGAP expressing cells increases sensitivity of the FRET assay. HEK293T cells were transfected as described in Figure 5.12 and 5.13. Only data for RhoA-2G is shown in the figure. Black bars show the analysis of the FRET ratio without selection for RhoGEF and RhoGAP expressing cells by thresholding the mCherry channel. Red bars show the same analysis with the only difference that only mCherry-positive cells were included in the region of interest by thresholding. All data represent the mean of five fields of view, error bars indicate standard deviation.

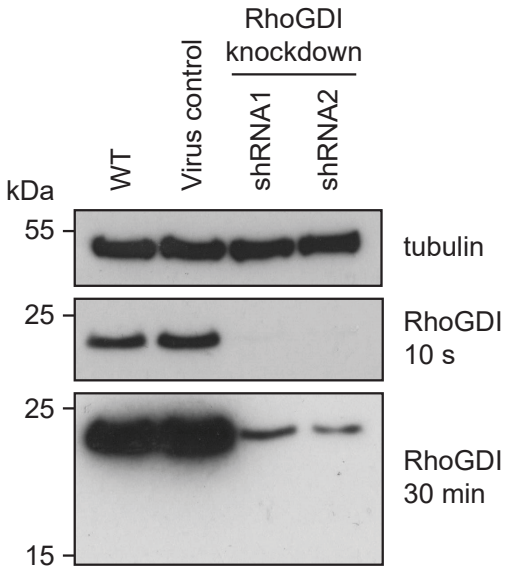

Figure 7.9 Efficient shRNA-mediated knockdown of RhoGDI. Stable RhoGDI knockdown cell lines were created by lentiviral infection of HEK293T cells with two different shRNA vectors (shRNA1 and shRNA2) and subsequent antibiotic selection. Cells stably transduced with stuffer pLKO.1 vector served as control together with non-infected WT HEK293T cells. 15 μg total cell lysates were immunoblotted with antibodies against RhoGDI and tubulin. For RhoGDI, a short and a long exposure is shown (10 s and 30 min).

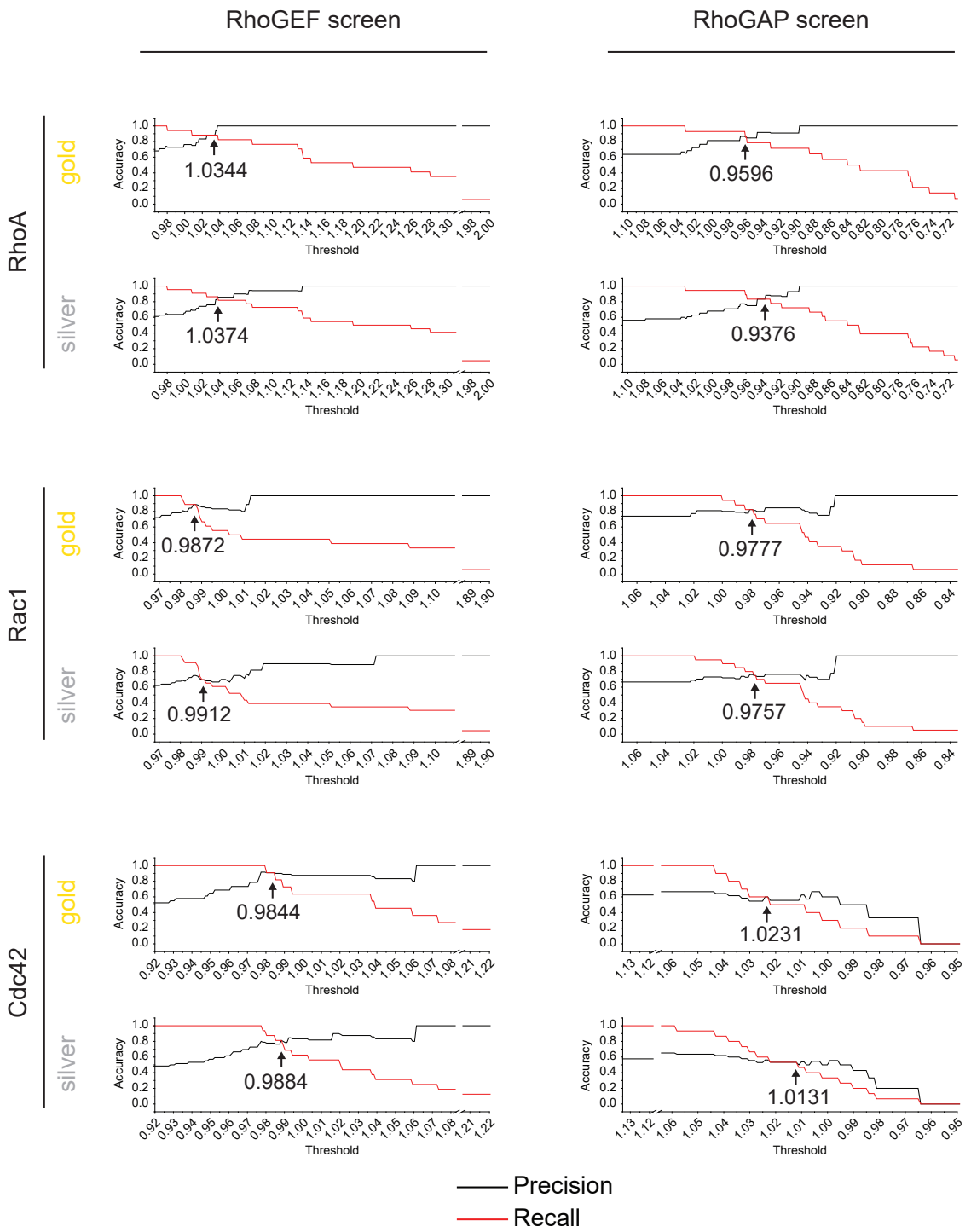

Figure 7.10 Precision and recall analysis for estimation of threshold benchmarks. Precision and recall analysis was performed with the results of the individual screens as an objective measure to obtain benchmarks for the threshold. The meta-analysis silver and gold lists served as ground truth as indicated. The accuracy of precision and recall are plotted against the threshold. The objective benchmark for the threshold is obtained from the graphs where the accuracy of the precision (black) and recall (red) curves intersect (break-even point, indicated by arrow and number).

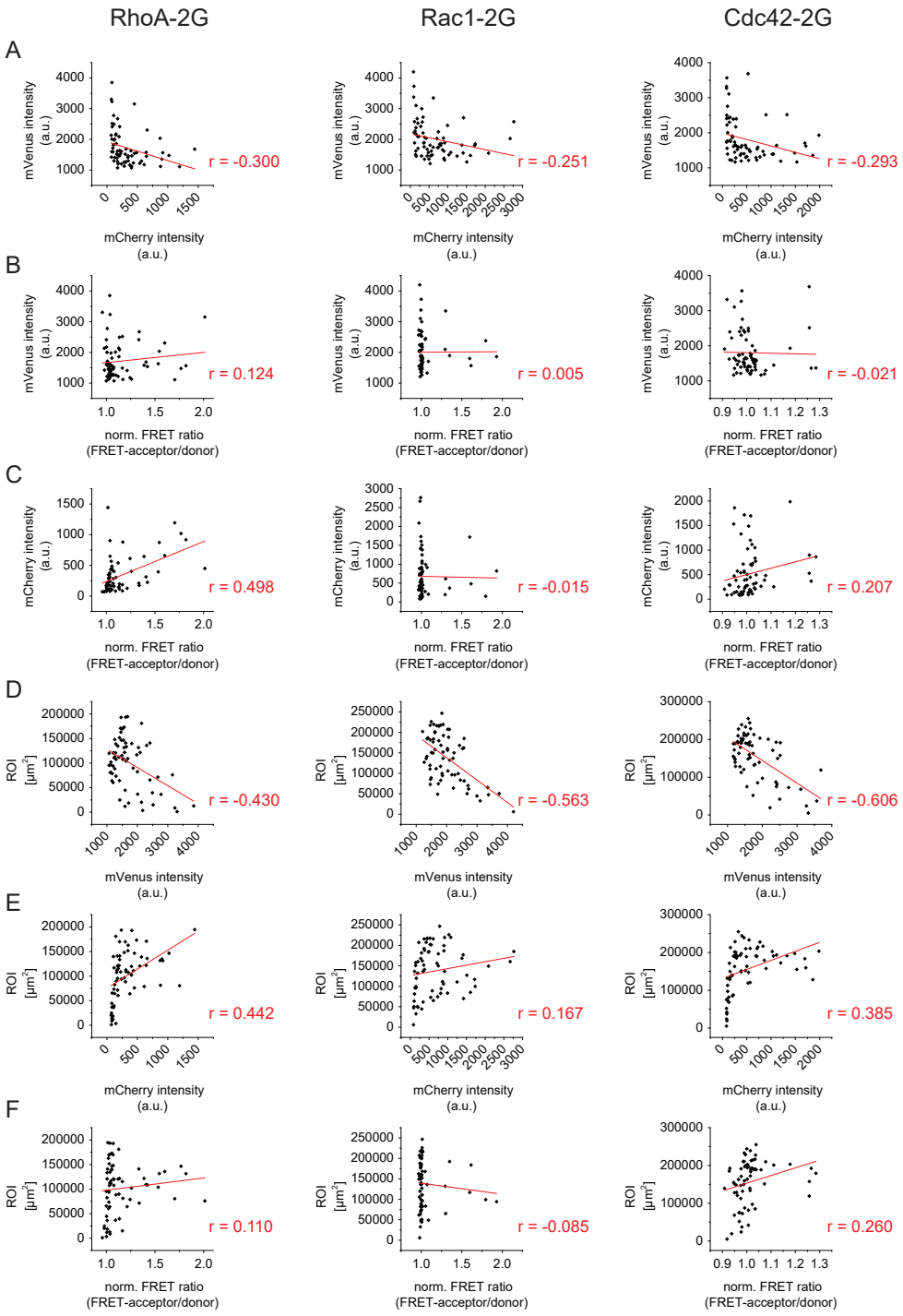

Figure 7.11 Correlation analysis of RhoGEF FRET screen control readout data. FRET-ratio, mVenus intensity, mCherry intensity and the area of the region of interest (ROI) were acquired by automated image analysis from RhoGEF substrate specificity FRET screen data for RhoA-2G, Rac1-2G, and Cdc42-2G FRET sensors. (**A**) mVenus intensity (from acceptor channel) was plotted against mCherry intensity; (**B**) mVenus intensity was plotted against normalised FRET-ratio; (**C**) mCherry intensity was plotted against normalised FRET-ratio; (**D**) ROI was plotted against mVenus intensity; (**E**) ROI was plotted against mCherry intensity; (**F**) ROI was plotted against normalised FRET-ratio. (**A**-**F**) Red line indicates linear regression analysis, r indicates Pearson's correlation coefficient.

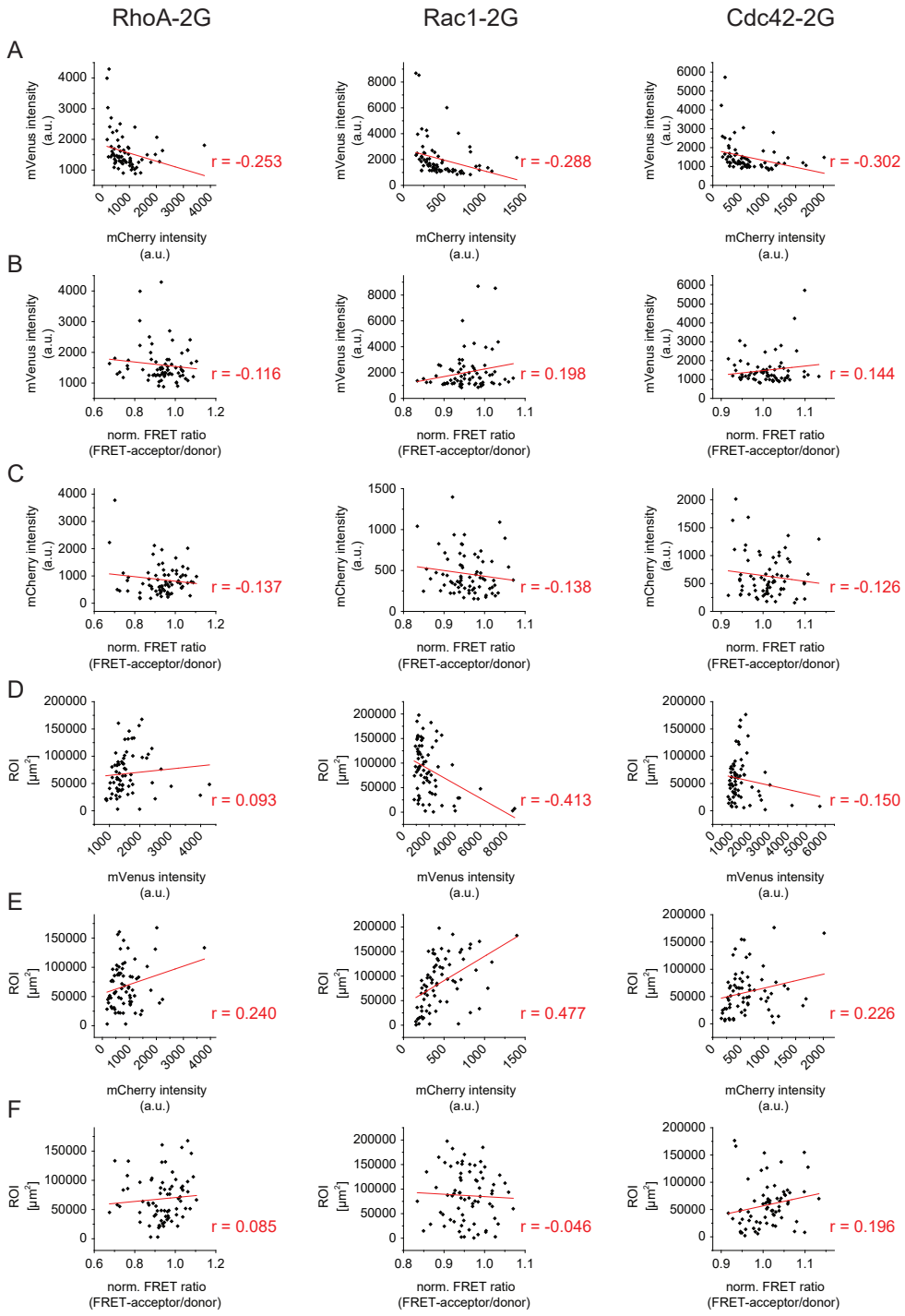

Figure 7.12 Correlation analysis of RhoGAP FRET screen control readout data. FRET-ratio, mVenus intensity, mCherry intensity and the area of the region of interest (ROI) were acquired by automated image analysis from RhoGAP substrate specificity FRET screen data for RhoA-2G, Rac1-2G, and Cdc42-2G FRET sensors. (**A**) mVenus intensity (from acceptor channel) was plotted against mCherry intensity; (**B**) mVenus intensity was plotted against normalised FRET-ratio; (**C**) mCherry intensity was plotted against normalised FRET-ratio; (**D**) ROI was plotted against mVenus intensity; (**E**) ROI was plotted against mCherry intensity; (**F**) ROI was plotted against normalised FRET-ratio. (**A**-**F**) Red line indicates linear regression analysis, r indicates Pearson's correlation coefficient.

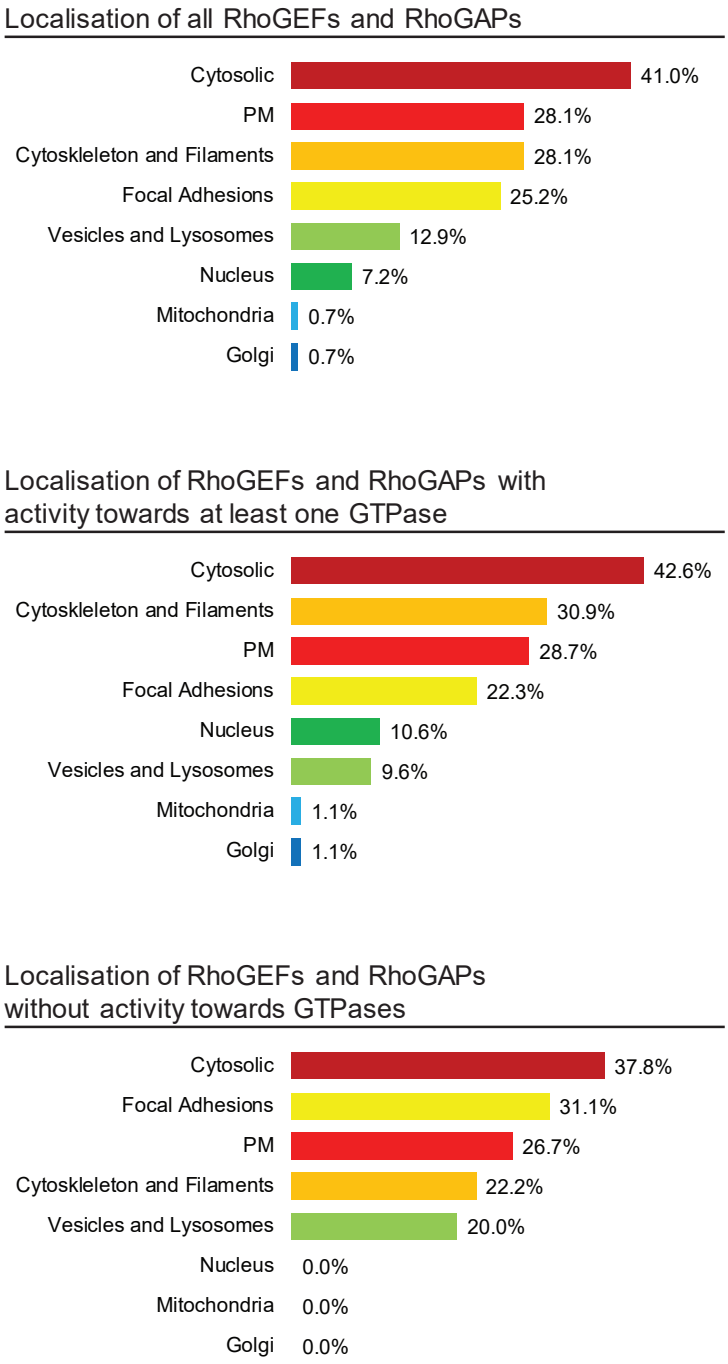

Figure 7.13 RhoGEF and RhoGAP activity is independent of their subcellular localisation. Bar diagram of percentages of subcellular localisations of RhoGEFs and RhoGAPs: All RhoGEFs and RhoGAPs (above), RhoGEFs and RhoGAPs which were active towards at least one Rho GTPase in the screen (middle), and RhoGEFs and RhoGAPs that did not show any activity towards RhoA, Rac1, and Cdc42 in the screen (bottom). Some RhoGEFs and RhoGAPs localised on multiple cellular compartments and structures.

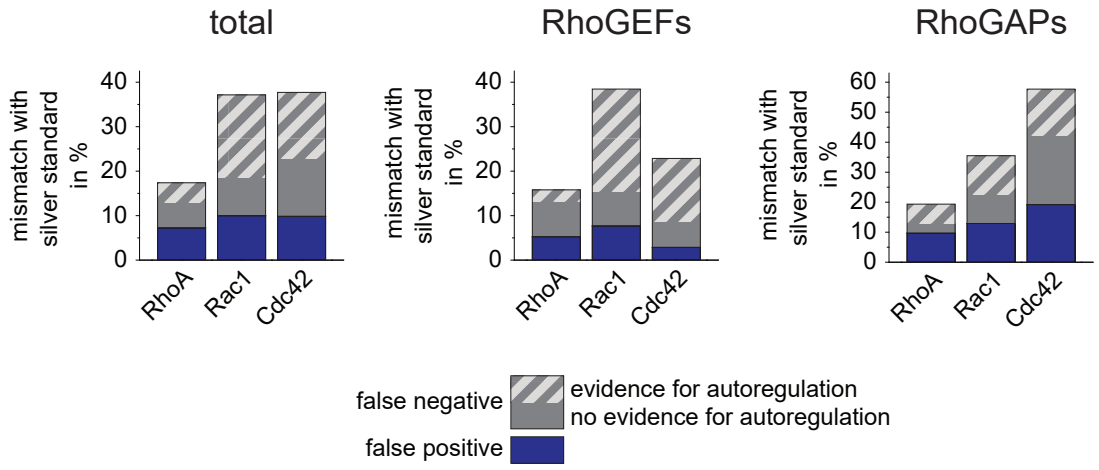

Figure 7.14 RhoGEF and RhoGAP activities identified by screen and by meta-analysis coincide well. RhoGEF and RhoGAP activities from the screen were compared to activities from the meta-analysis silver standard list. Results are shown as % of total number of activities included in the silver standard list. "False positive" (blue) and "false negative" (grey) results of the FRET screen were defined with regard to silver standard list. "False negative" results are shown as sum of results for which autoinhibition of activity has been suggested (striped grey) and for which it has not been described yet (uniform grey). The combined results are shown on the left (total), the two graphs in the centre and on the right show the individual results of the RhoGEF screen and the RhoGAP screen.

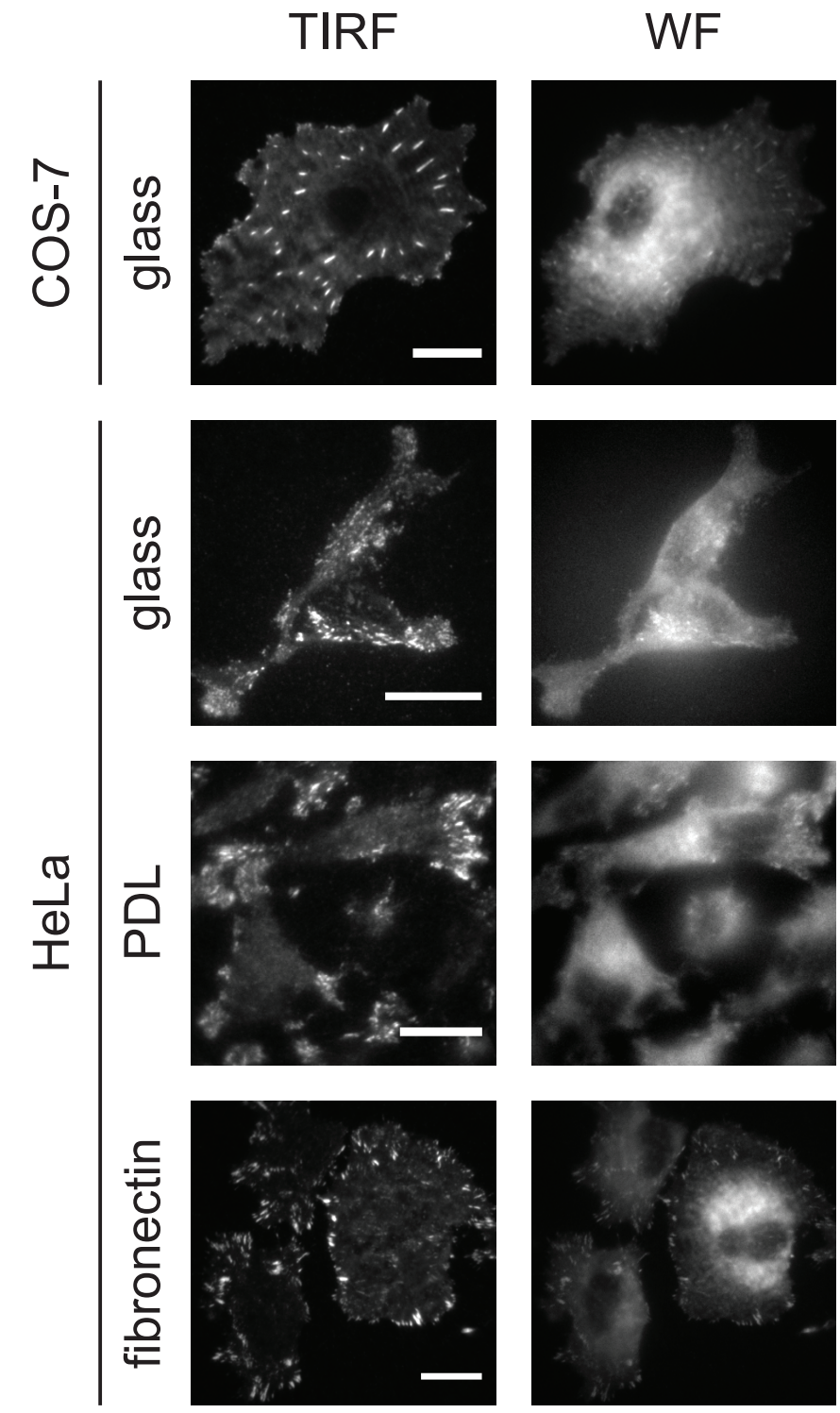

Figure 7.15 COS-7 cells display distinct and evenly distributed focal adhesions. COS-7 cells and HeLa cells were stably transfected with mCherry-paxillin using lentiviral transduction. Focal adhesion morphology and distribution was visualised by TIRF microscopy. Cells were seeded on substrate as indicated (no substrate = glass; PDL = poly-D-Lysine; Fibronectin). Images were acquired in TIRF illumination and in WF illumination. Scale bars: 20 μm.

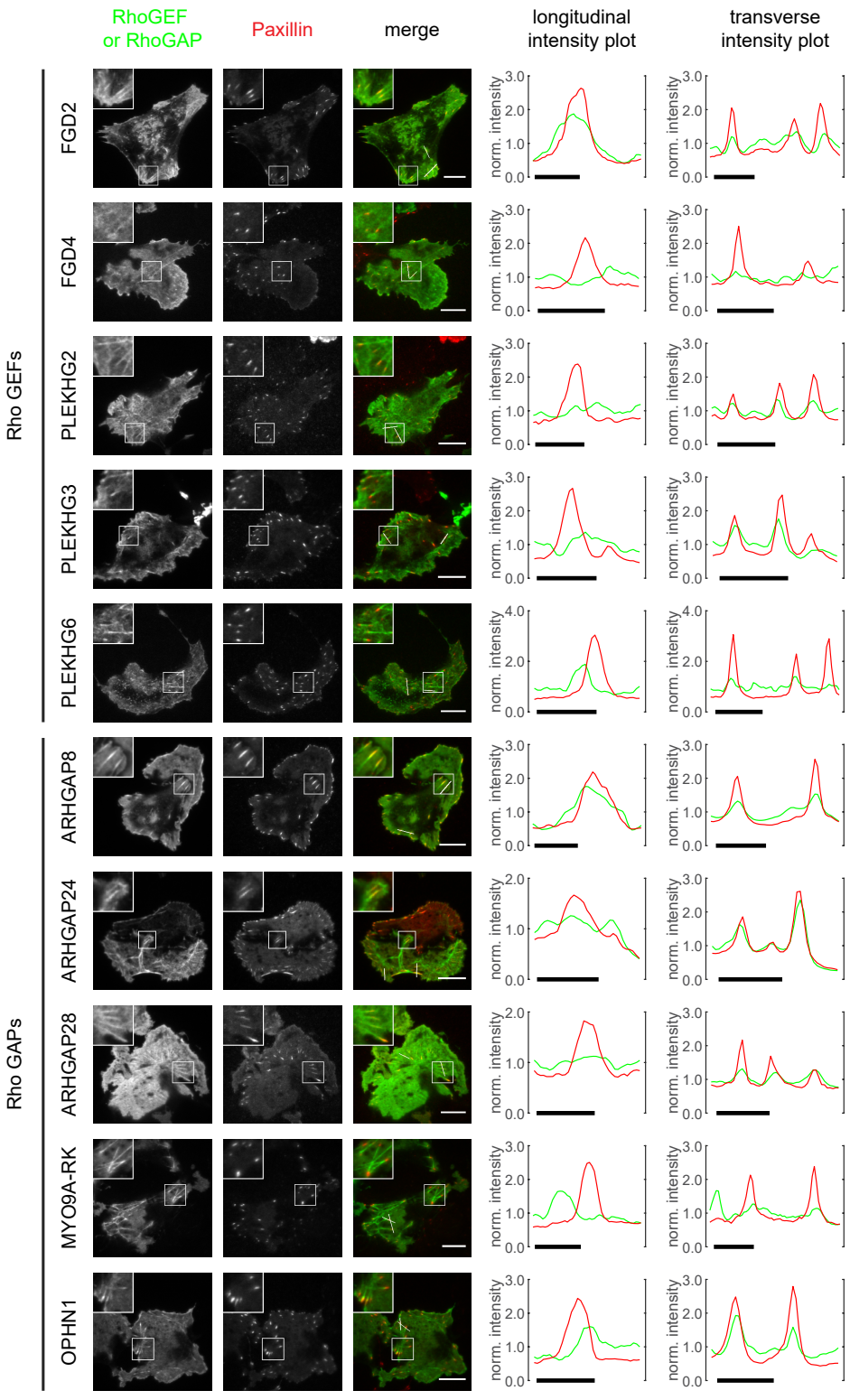

Figure 7.16 10 RhoGEFs and RhoGAPs showed an actin- or actinin-like localisation. YFP-tagged RhoGEFs and RhoGAPs were expressed in COS-7 cells stably expressing mCherry-paxillin. Images were collected by live cell TIRF microscopy. Fluorescence intensity profiles of longitudinal and transverse sections through focal adhesions are shown on the right and indicated by white lines in the merged images. Intensity plots were normalised to the average intensity over the whole line to maintain relative intensity proportions. Insets on the upper left of each image represents an approximately two-fold magnification of the area indicated by a box. White scale bars in images: 20 μm. Black scale bars in graphs: 5 μm.

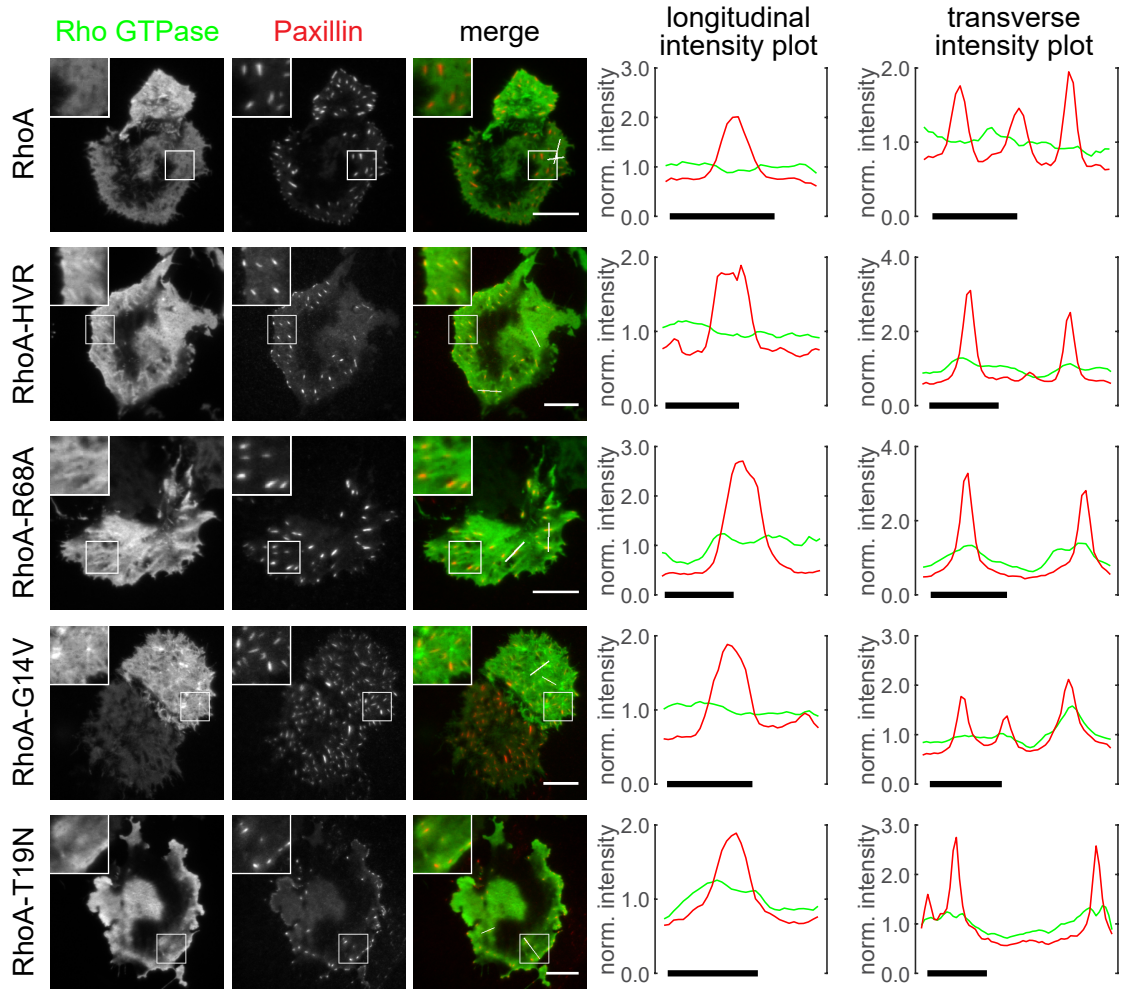

Figure 7.17 RhoA does not localise at focal adhesions. mCitrine-tagged RhoA and mutated versions of Rac1 were expressed in COS-7 cells stably expressing mCherry-paxillin. Images were collected by live cell TIRF microscopy. Fluorescence intensity profiles of longitudinal and transverse sections through focal adhesions are shown on the right and indicated by white lines in the merged images. Intensity plots were normalised to the average intensity over the whole line to maintain relative intensity proportions. Insets on the upper left of each image represents an approximately two-fold magnification of the area indicated by a box. White scale bars in images: 20 μm. Black scale bars in graphs: 5 μm.

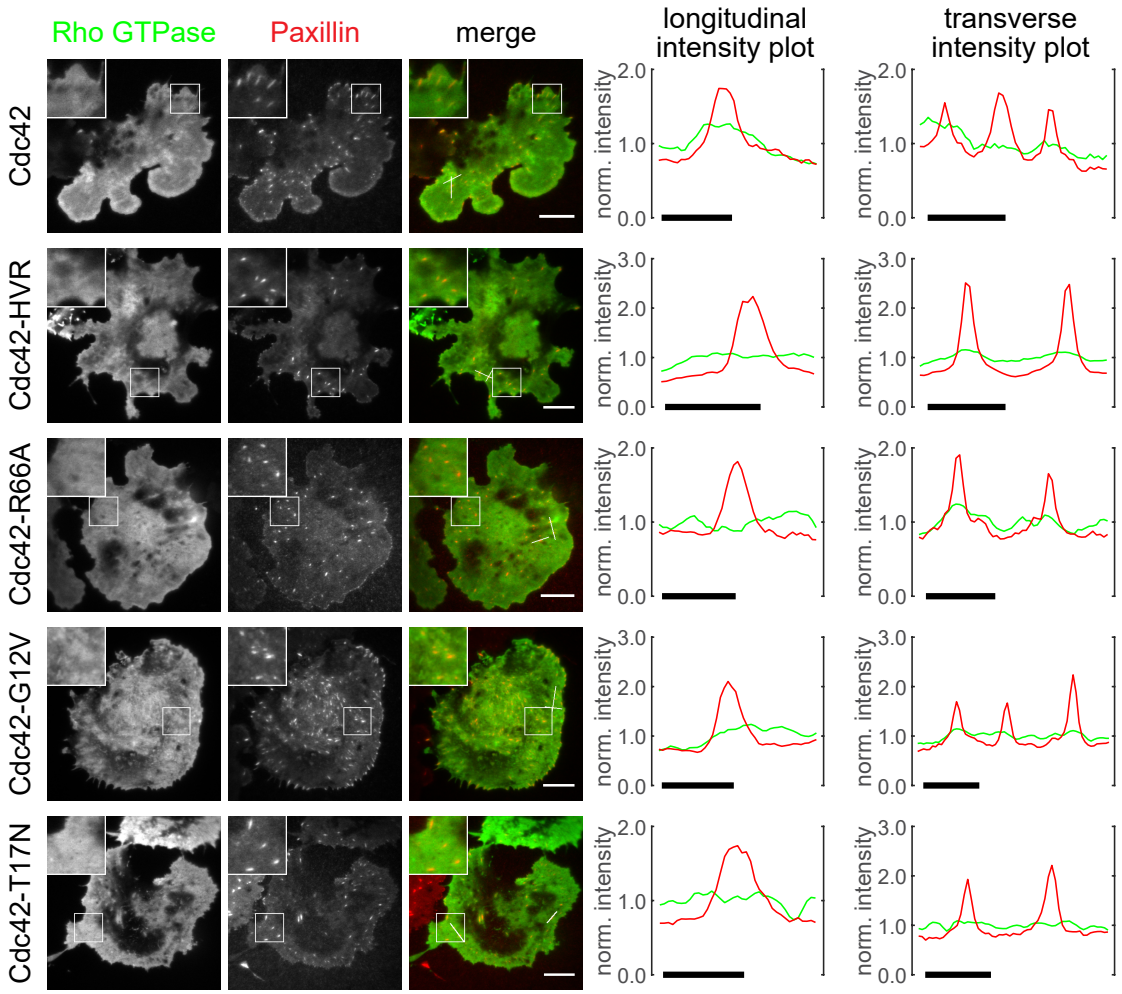

Figure 7.18 Cdc42 does not localise at focal adhesions. mCitrine-tagged Cdc42 and mutated versions of Rac1 were expressed in COS-7 cells stably expressing mCherry-paxillin. Images were collected by live cell TIRF microscopy. Fluorescence intensity profiles of longitudinal and transverse sections through focal adhesions are shown on the right and indicated by white lines in the merged images. Intensity plots were normalised to the average intensity over the whole line to maintain relative intensity proportions. Insets on the upper left of each image represents an approximately two-fold magnification of the area indicated by a box. White scale bars in images: 20 μm. Black scale bars in graphs: 5 μm.

Table 7.1 Substrate specificity of RhoGEFs and RhoGAPs that localise at focal adhesions. Substrate specificities of RhoGEFs and RhoGAPs that localised on focal adhesion were summarised as follows: all specificities from the curated screen results (curated screen all specificities); only RhoGEFs and RhoGAPs with exclusive specificity towards one Rho GTPase (curated screen single specificities); all specificities from the meta-analysis gold list (meta-analysis all specificities).

	Rho GTPase	curated screen all specificities	curated screen exclusive specificity	meta-analysis all specificities
RhoGEFs	**RhoA**	4	2	1
	Rac1	5	3	6
	Cdc42	2	1	2
RhoGAPs	**RhoA**	7	2	3
	Rac1	12	5	5
	Cdc42	6	0	2

Table 7.2 Expression plasmid list.

Name/cDNA	Promoter	Fluorophores/Tags	Vector backbone	Source
Actinin	CMV	3'-mEYFP	N1	Danijela Vignjevic
EGFR-TMD	CMV	3'-mPAGFP	N1	Kai Simons
EGFR-TMD	Tet-On-T6	5'-mEGFP and 3'-SNAP, 5'-pHluorin and 3'-SNAP	C1	This work
GAP43-N	CMV	3'-mEGFP, 3'-mCherry	C1	AG Rocks
GPI	CMV	3'-mPAGFP	N1	AG Rocks
KRas-HVR	Tet-On-T6	5'-SNAP	C1	This work
KRas-HVR	CMV	5'-mCherry, 5'-mPAGFP, 5'-miRFP670	C1	This work
Lifeact	CMV	3'-mEGFP	N1	AG Rocks
Rho GTPase FRET sensors	CMV		pTriEx	Olivier Pertz
Rho GTPase FRET sensors	CMV		pcDNA3.1(-)	This work
Rho GTPase FRET sensors	EF1a		pcDNA3.1(-)	This work
Rho GTPase FRET sensors	UbC		pcDNA3.1(-)	This work
Rho GTPase HVR	CMV	5'-mCitrine, 5'-mCherry, 5'-mPAGFP	C1	This work
Rho GTPases	CMV	5'-mCitrine, 5'-mCherry, 5'-mPAGFP	C1	AG Rocks
RhoGAPs	CMV	5'-mCitrine, 5'-mCherry	Creator	AG Rocks
RhoGDI	CMV	3'-tripleFLAG, 3'-mCherry	Creator	This work
RhoGEFs	CMV	5'-mCitrine, 5'-mCherry	Creator	AG Rocks
Talin	CMV	5'-mEYFP		Harvard clone: MmCD00292816
Tensin	CMV	5'-mEGFP		Harvard clone: GgCD00292841
VASP	CMV	5'-mEGFP	C2	Theresia Stradal/Clemens Rottner
Vinculin	CMV	5'-mEGFP	C1	Theresia Stradal/Clemens Rottner
Zyxin	CMV	5'-mEGFP	C1	Theresia Stradal/Clemens Rottner
β-Actin	CMV	3'-mCitrine	Creator	AG Rocks

Table 7.3 Oligonucleotides and primer for molecular cloning.

Oligonucleotides and primer
Oligonucleotides for generation of HVR constructs
Oligonucleotides were annealed and ligated into pEGFP-C1-derived destination vectors via BsrGI and EcoRI
RhoA-HVR sense
GTACAAGTCCGGACAAGCTAGACGTGGGAAGAAAAAATCTGGGTGCCTTGTCTTGTAAGGCGCGCCG
RhoA-HVR antisense
AATTCGGCGCGCCTTACAAGACAAGGCACCCAGATTTTTTCTTCCCACGTCTAGCTTGTCCGGACTT
Rac1-HVR sense
GTACAAGTCCGGATGCCCGCCTCCCGTGAAGAAGAGGAAGAGAAAATGCCTGCTGTTGTAAGGCGCGCCG
Rac1-HVR antisense
AATTCGGCGCGCCTTACAACAGCAGGCATTTTCTCTTCCTCTTCTTCACGGGAGGCGGGCATCCGGACTT
Cdc42-HVR sense
GTACAAGTCCGGAGAGCCTCCAGAACCGAAGAAGAGCCGCAGGTGTGTGCTGCTATAAGGCGCGCCG
Cdc42-HVR antisense
AATTCGGCGCGCCTTATAGCAGCACACACCTGCGGCTCTTCTTCGGTTCTGGAGGCTCTCCGGACTT
KRas-HVR sense
GTACAAGTCCGGAGGTAAAAAGAAGAAAAAGAAGTCAAAGACAAAGTGTGTAATTATGTAAGGCGCGCCG
KRas-HVR antisense
AATTCGGCGCGCCTTACATAATTACACACTTTGTCTTTGACTTCTTTTTCTTCTTTTTACCTCCGGACTT
Oligonucleotides for site directed mutagenesis
RhoA-R68A for
TGGGCAGGAAGATTATGATGCCCTGAGGCCCCT
RhoA-R68A rev
AGGGGCCTCAGGGCATCATAATCTTCCTGCCCA
Rac1-R66A for
CAGCTGGACAAGAAGATTATGACGCATTACGCCCCCTATCC
Rac1-R66A rev
GGATAGGGGGCGTAATGCGTCATAATCTTCTTGTCCAGCTG
Cdc42-R66A for
AGGGCAAGAGGATTATGACGCATTACGACCGCTGAGTTAT
Cdc42-R66A rev
ATAACTCAGCGGTCGTAATGCGTCATAATCCTCTTGCCCT
Primer for PCR-based amplification of SNAP
PCR products were cloned into mEGFP-C1 via NheI and BsrGI
SNAP-C1 for
GCGCCGCTAGCGCTACCGGTCGCCACCATGGACAAAGACTGCG
SNAP-C1 rev
CGCGCTGTACAGACCCAGCCCAGGCTTG

Table 7.3 Oligonucleotides and primer for molecular cloning (continued).

Oligonucleotides and primer
Primer for PCR-based amplification of EGFR-TMD-SNAP including backbone
PCR products were used for In-Fusion reaction with mEGFP and pHluorin
IF EGFR-TMD bb for
CAGTGTGCCCACTACATTGAC
IF EGFR-TMD bb rev
TTTCTTTTCCTCCAGAGCCC
Primer for PCR-based amplification of mEGFP
PCR products were used for In-Fusion reaction with EGFR-TMD-SNAP including backbone
IF GFP for
CTGGAGGAAAAGAAAATGGTGAGCAAGGGCGAG
IF GFP rev
GTAGTGGGCACACTGGTACAGCTCGTCCATGCCG
Primer for PCR-based amplification of pHluorin
PCR products were used for In-Fusion reaction with EGFR-TMD-SNAP including backbone
IF pHluorin for
CTGGAGGAAAAGAAAATGGTGAGTAAAGGAGAAGAACTTTTCACTG
IF pHluorin rev
GTAGTGGGCACACTGTTTGTATAGTTCATCCATGCC
Oligonucleotides for the generation of a promoter cloning site in pEGFP-C1 derived backbones
Oligonucleotides were annealed and ligated into pEGFP-C1 via AseI and SalI
Tet-On cloning site sense
TAATGAATTCCTCGAGGCAAGCGTCGACGCTAGCGCTACCGGTC
Tet-On cloning site antisense
TCGAGACCGGTAGCGCTAGCGTCGACGCTTGCCTCGAGGAATTCAT

Table 7.3 Oligonucleotides and primer for molecular cloning (continued).

Oligonucleotides and primer
Oligonucleotides for the generation of a promoter and ORF cloning site in pcDNA3.1(-)
Oligonucleotides were annealed and ligated into pcDNA3.1(-) via BsrGI and EcoRI
FRET 3.1 CS sense
CGCGTGGCGCGCCAGCTGCTCGTAAGCTTGGTTAATTAAGCGGATCCG
FRET 3.1 CS antisense
AGCTCGGATCCGCTTAATTAACCAAGCTTACGAGCAGCTGGCGCGCCA
Primer for PCR-based amplification of Rho GTPase FRET sensors
PCR products were cloned into pcDNA3.1(-) cloning site via HindIII and BamHI
RhoA-2G 3.1 for
GCGCAAGCTTGCCACCATGGGCGGCCACCACCG
RhoA-2G rev
GCGCGGATCCTCACAAGACAAGGCAACC
Rac1-2G 3.1 for
GCGCAAGCTTGCCACCATGTCCACCGACGGCATG
Rac1-2G rev
GCGCGGATCCTCACAACAGCAGGCATT
Cdc42-2G 3.1 for
GCGCAAGCTTGCCACCATGTCCACCGACGGCATG
Cdc42-2G rev
GCGCGGATCCTCATAGCAGCACACACCT
Primer for PCR-based amplification of promoters
PCR products were cloned into pcDNA3.1(-) cloning site via AscI and HindIII
EF1a 3.1 for
GCAAGGCGCGCCGCTCCGGTGCCCGTC
EF1a 3.1 rev
GCGCAAGCTTTCACGACACCTGAAATGGAAG
UbC 3.1 for
GCAAGGCGCGCCGTATAGAAAAGTTGGGCCTCCG
UbC 3.1 rev
GCGCAAGCTTAAACTTGTGTCTAACAAAAAAGCCA
CMV 3.1 for
GCAAGGCGCGCCATAGTAATCAATTACGGGGTCATTAGTTC
CMV 3.1 rev
GCGCAAGCTTGATCTGACGGTTCACTAAACCAG

Acknowledgements

First, I would like to thank my advisor, Oliver Rocks. He has given me the guidance and the support I needed to pursue my work and the freedom to explore scientific questions into various directions and to develop as a scientist. For this I am very thankful.

Additionally, I would like to thank Volker Haucke for very helpful discussions in my committee meetings and for supervising my thesis at Freie Universität Berlin.

I would like to greatly acknowledge the support from the following people: Olivier Pertz and Rafael Fritz for sharing the FRET-biosensors and helpful discussions; Anje Sporbert, Anca Margineanu, and the team of the Advanced Light Microscopy Facility at the MDC for technical and practical advice; Jan Schmoranzer, Martin Lehmann and the Haucke lab for helpful discussions and constructs; Malte Schmick for his introduction into TIRF microscopy and his help with programming; Martin Falcke for his support with the analysis of the FLAP assay; Evangelia for doing the precision and recall analysis; Manfred Gossen for Tet-On cell lines, promoters and advice.

Thank you to the AG Rocks family, the time I have spent in the lab also would not have been the same without you. First of all, thank you to the Rock stars Rebecca, Caro, Matti, and Juliane. You really made the lab a special place. Thank you to Philipp for help with generation of lentiviral particles, to Lennart for help with generation of stable COS-7 mCherry-Paxillin cell lines, cloning, and the pasta alla norma recipe, and to Juliane and Kiara for great support with cloning the library. Thank you to Marlies, Lisa K., Lisa S., and all Azubis for your diligent daily work to keep the lab running. Thank you to all the past and present members of the Rocks lab, especially Maciej, Celina, Merve, Robert-William, Sebastian, Vicky, Lennart, Philipp, Laura and Moritz for making the lab such a great place to do science and drink coffee.

Thank you to Drazen for carefully reading this thesis, thank you for past and future Colle evenings.

Thank you to my parents, my brother, and my sister for their encouragement, for their belief in me and their support which make this work possible.

Thank you to my beloved daughters Mathilda and Frieda for your constant distraction, for changing every day into a good one, and for being an endless source of genuine happiness.

I am so thankful for my partner, Sarah, who supports me unconditionally. Your patience, your encouragement, and your love mean more to me than I can ever express in simple words, thank you for sharing your life with me.

Declaration

The present thesis "Temporal and Spatial Regulation of Rho GTPase Activity and Specificity" has been composed by myself and describes my own work, unless specifically acknowledged in the text. This thesis is submitted to the Department of Biology, Chemistry and Pharmacy of Freie Universität Berlin to obtain the academic degree Doctor rerum naturalium (Dr. rer. nat.). This work has not been submitted for any other degree.

Berlin, December 2017 Paul Markus Müller